

DETERMINATION OF EFFICIENCIES, LOSS MECHANISMS,
AND PERFORMANCE DEGRADATION FACTORS IN CHOPPER
CONTROLLED DC VEHICLE MOTORS

SECTION I

"TEST PROGRAM RESULTS AND RECOMMENDATIONS"

Prepared for: NASA - Lewis Research Center and The Department of Energy

by: Electrical Engineering Department
University of Pittsburgh
Pittsburgh, PA 15139

Howard B. Hamilton, Principal Investigator
Elias Strangas, Research Assistant

FINAL REPORT

GRANT NSG #3163

DECEMBER 30, 1980

- INDEX -

	<u>Page</u>
<u>EXECUTIVE SUMMARY</u>	1
<u>CHAPTER 1. INTRODUCTION</u>	8
Project Objective	8
Historical Background	8
Scope of the Investigation.	13
<u>CHAPTER 2. THE CONVENTIONAL MOTOR MODEL.</u>	15
Parameter Measurement	17
<u>CHAPTER 3. LOSSES.</u>	35
I.....Loss Classification	35
II.....Joule Losses.	36
II,1.....Load Current.	36
II,2.....Eddy Current Losses	41
II,2A.....In the Armature Due to Distorted Pole Face Flux	41
II,2B.....In the Armature Due to Tooth Saturation	42
II,2C.....In the Armature Due to Cross Slot Leakage Flux.	44
II,2D.....In Pole Face Iron Due to Slot Effect.	53
II,2E.....In the Magnetic Circuit Due to Harmonics Resulting From Chopper Action	54
II,2F.....In Steel Banding Wire Used to Secure Armature Winding	55
II,3.....Losses In the Equalizer Connection.	55
II,4.....Losses in Commutated Coils.	56
II,5.....Losses Due to Brush Resistance.	66
II,6.....Losses Due to Free Wheeling Diode	67
II,7.....Losses Due to Shaft, Bearing Housing Current.	69

	<u>Page</u>
III.....Iron Hysteresis Losses.	71
III,8.....In the Magnetic Structure Due to Chopper Harmonics.	71
III,9.....In the Pole Face Due to Flux Variation Due to Slot Openings	74
IV.....Mechanical Losses	74
IV,10,11..Bearing and Brush Friction and Windage.	74
IV,12.....Ventilation Losses.	81
SUMMARY ON LOSSES	87
<u>CHAPTER 4. TORQUE/AMPERE OBSERVATIONS.</u>	90
<u>Paper:</u> "Torque/Ampere Anomalies and The Need For Interpoles In Chopper Controlled DC Series Traction Motors"	94
<u>CHAPTER 5. MODELS.</u>	100
<u>Paper:</u> "A Model For Chopper Controlled DC Series Motors"	104
<u>REFERENCES.</u>	109
<u>APPENDIX A THE TEST FACILITY</u>	A-1
<u>Paper:</u> "A DC Power Source For Testing Battery Powered Electric Vehicle Motors"	A-7
<u>APPENDIX B DESIGN DETAILS OF MOTOR TESTED.</u>	B-1
Red Motor	B-1
Blue Motor.	B-5
<u>APPENDIX C WAVE FORMS AND THEIR HARMONIC CONTENT</u>	C-1
Instrumentation Requirements.	C-25
<u>APPENDIX D MEASUREMENT OF RESISTANCE AND INDUCTANCE.</u>	D-1
<u>Paper:</u> "Series Motor Parameter Variations As A Function of Frequency and Saturation"	D-19
<u>APPENDIX E CURVE FITTING</u>	E-1
<u>APPENDIX F EV MOTOR CHOPPER APPLICATION CRITERIA</u>	F-1

	<u>Page</u>
Motor Rating	F-1
Chopper Consideration.	F-19
<u>APPENDIX G</u> <u>MOTOR DESIGN CONSIDERATIONS.</u>	G-1

- LIST OF FIGURES -

	<u>Page</u>
Figure 1. Schematic of Basic Chopper Drive for Reversible DC Series Motor	10
2. DC Motor Model.	15
3. Circuit Resistance and Brush Drop	17
4. K_t, K_v vs I_f . (Red Motor)	20
5. Saturation Curve (Red Motor).	21
6. K_t, K_v vs I_f . (Blue Motor).	22
7. Speed, Torque vs I. (Blue Motor).	27
8. Power, Efficiency vs I. (Blue Motor).	28
9. Speed, Torque vs I. (Red Motor)	29
10. Power, Efficiency vs I. (Red Motor)	30
11. Effect of Brush Shift and Frequency on the Speed-Current Characteristic (Red Motor).	32
12. Effect of Brush Shift on the Torque-Current Characteristic (Red Motor).	34
13. Efficiency vs Amperes as a Function of Chopper Frequency (Red Motor)	37
14. Inductor Skin Effect.	38
15. Slot Cross Leakage Flux Density	45
16. The Carter Coefficient.	53
17. Loss in Commutated Coils as a Function of Speed and Current (Blue Motor).	58
18. Loss in Commutated Coils as a Function of Brush Shift and Speed (Blue Motor).	59

Figure 19.	Losses In Commutated Coils as a Function of	
	Speed and Current (Red Motor).	60
20.	Losses In Commutated Coils as a Function of Brush	
	Shift and Speed (Red Motor).	61
21.	Losses In Commutated Coils as a Function of Brush	
	Shift and Speed, Chopper Control (Red Motor)	63
22.	Losses In Commutated Coils as a Function of Speed	
	for DC and 77 Hz (Red Motor)	64
23.	Losses In Commutated Coils as a Function of Speed	
	for 15, 33 Hz (50 amperes) and 77, 100 Hz (200 amperes)	
	(Blue Motor)	65
24.	Free Wheeling Diode Current.	68
25.	Core Loss as a Function of Frequency	72
26.	Flux Density Distribution (Red Motor).	73
27.	Rotating Losses (Red Motor).	77
28.	Rotating Losses (Blue Motor)	78
29.	Ventilation Provision (Blue Motor)	82
30.	Ventilating Fan (Red Motor).	82
31.	Torque vs Amperes (Blue Motor)	91
32.	Torque vs Amperes (Red and Blue Motors).	92
33.	K_t vs I, Frequency Dependence.	93
34.	The Ewing Model.	100
A-1	Test Facility Schematic.	A-2
A-2	Chopper/Controller Modification.	A-4
A-3	Schematic For Measuring R, L	A-6

	<u>Page</u>
Figure B-1 Coils Shorted During Commutation (Red Motor)	B-2
B-2 Slot/Conductor and Field Dimensions (Red Motor)	B-3
B-3 Rotor/Stator Dimensions	B-4
B-4 Coils Shorted During Commutation.	B-7
B-5 Frame Dimensions (Blue Motor)	B-8
B-6 Slot/Conductor Details (Blue Motor)	B-9
C-1 Chopper Controlled Motor Voltage Waveform	C-1
C-2 Motor and Line Current Waveform	C-2
C-3 Current Waveforms, Harmonic Spectrums 100 Hz, $T_0/T=0.5$	
I motor = 198a.	C-6
C-4a 200 Hz, $T_0/T=0.5$ I motor = 199a.	C-7
C-4b 200 Hz, $T_0/T=0.5$ I motor - 107a.	C-8
C-5a 400 Hz, $T_0/T=0.5$ I motor - 199a.	C-9
C-5b 400 Hz, $T_0/T=0.5$ I motor = 110a.	C-10
C-6 Typical Voltage Waveform.	C-11
C-7 Current Waveforms	C-13
C-8 Irms vs Harmonic Number $f=100$	C-16
C-9 Irms vs Average Current, 0° , -28°	C-17
C-10 % Ripple vs Average Current as a Function of Frequency.	C-19
C-11 I peak/I average vs Average Current as a Function of Frequency.	C-20
C-12 $\Delta i/I$ average vs Average Current as a Function of Frequency.	C-21
C-13 Variation of I average as a Function of T_0/T . Variation of Δi as a Function of T_0/T	C-22
C-14 P/V average I average vs I average.	C-27

	<u>Page</u>
Figure C-15 % Error vs Highest Harmonic Watt-Meter Response	C-29
D-1 L vs I average as a Function of Frequency	D-8
D-2 L vs f as a Function of I average	D-9
D-3 L vs I average, For Armature and Total as a Function of Brush Shift	D-10
D-4 L vs I average, For Armature and Field at 400 Hz. . . .	D-11
D-5 L vs I average Cu Blocks and Carbon Brushes	D-12
D-6 R, L as a Function of Frequency (Blue Motor).	D-13
D-7 L vs I average as a Function of Frequency (Blue Motor)	D-14
D-8 R vs I average as a Function of Frequency (Red Motor)	D-15
D-9 R vs Frequency (Red Motor).	D-16
D-10 R vs I average (Field and Armature) (Red Motor)	D-17
D-11 R vs I average as a Function of Frequency (Blue Motor)	D-18
F-1 Road Load Ideal 3000 lb Vehicle	F-3
F-2 Typical Motor Duty In Electric Urban Passenger Vehicle	F-4
F-3 SAE EV Duty Cycle Schedules	F-5
F-4 Aerodynamic Drag vs Speed	F-6
F-5 Horsepower vs Speed For Rolling Resistance and % Grade	F-7
F-6 Conversion Factors.	F-8
F-7 Motor Power Required For 3000 lb EV, SAE 227C Schedule	F-11
F-8 "Universal Series Motor" Saturation Curve".	F-13
F-9 Per Unit Speed vs Per Unit Torque as a Function of Voltage.	F-15
F-10 Per Unit Speed vs Per Unit Power as a Function of Voltage/Current.	F-16
G-1 Motor Weight vs Specific Electric Loading	G-3

- LIST OF TABLES -

	<u>Page</u>
TABLE I Losses Due To Harmonic Currents.	40
TABLE II Calculated Loss Due to Slot Cross Leakage Flux	50
TABLE III Free Wheeling Diode Performance.	67
TABLE IV Test and Simulation Results.	102
TABLE C-1 Voltage Harmonics, RMS Values.	C-5
TABLE C-2 Voltage Surges	C-12
TABLE C-3 Irms/I average as a Function of Frequency.	C-15
TABLE C-4 Motor and Line Current Harmonics as a Function of Frequency	C-24
TABLE C-5 Motor Current Fundamental Harmonics.	C-23

EXECUTIVE SUMMARY

Motors for Electric Vehicle (EV) applications must have different features from DC motors designed for industrial applications. The motor application is characterized by:

1. The need for highest possible efficiency from low load to over load, for maximum EV range.
2. Short time overload capability. The ratio of peak power to average power varies from 5/1 in heavy city traffic to 3/1 in suburban driving situations.
3. Operation from power supply voltage levels of 84-144 volts (probably 120 volts maximum).

To meet objective No. 1, the mechanisms that produce losses have been identified and the influence of chopper characteristics on motor efficiency evaluated.

Objective No. 2 necessitates a design approach based on commutation limits, as distinct from design based on thermal constraints (as is the usual limitation in the design of motors for conventional industrial applications).

Characterization No. 3 poses something of a dilemma in that it is a voltage level between which clear cut choice of parallel or series type (lap or wave) windings cannot be made.

This report summarizes the investigative research performed at the University of Pittsburgh by Howard B. Hamilton, Principal Investigator, under the technical guidance and project supervision of Edwin F. McBrien, NASA-Lewis Research Center, during the course of the Grant (NASA/DOE NSG-3163). The objective was design and fabrication of a test facility suitable for conducting tests on EV motors; to develop test procedures, to obtain data which can be used to isolate losses, visualize where motor design changes can and should be made, to indicate problems arising from chopper control, and to make recommendations with respect to test

procedures, instrumentation and chopper operating modes.

APPENDIX A describes the test facility and instrumentation utilized. APPENDIX B gives technical information on the two different types of motors tested - one a solid-frame wave-wound, self-ventilated motor, the other a laminated-frame, non-symmetrical, pole-lap-wound motor requiring external ventilation.

After the introduction and historical background in Chapter 1, Chapter 2 presents a discussion of the conventional series motor model. Procedures for obtaining, by test, the parameters necessary for calculating performance and losses are discussed, and the calculated results for operation from ripple-free DC are compared with observed test results, indicating approximately 5% or less error. Experimental data indicating the influence of brush shift and chopper frequency are also presented. Both factors have a significant effect on the speed and torque relationships.

Chapter 3 presents an in-depth discussion of the losses and loss mechanisms present in a DC series motor and an attempt is made to evaluate the added losses due to harmonic currents and fluxes. The summary of findings with respect to these losses is reproduced here.

-SUMMARY ON LOSSES-

Exact prediction of the magnitude of motor losses is a very difficult task. It is even more complex and difficult if the motor is chopper controlled. However, based on the analysis in this chapter, several important techniques and procedures can be formulated based on the following:

1. Efficiency of a motor is sharply reduced when it is chopper controlled. The higher the chopper frequency, the less the reduction in efficiency.
2. The decrease in efficiency is more pronounced at lower values of average current.

3. Chopper control introduces additional losses not accounted for from consideration of harmonic currents and apparent resistance as measured.
4. Eddy current losses in the armature due to tooth saturation and the main flux can be significant. For example, for the RED motor, at 2000 rev/m. this loss was calculated as 52% of the rated $I^2 R$ value.

This loss can be mitigated by:
 - i) reducing conductor height
 - ii) using deeper slots
 - iii) using more iron (less flux density) in the motor
5. Eddy current losses in the armature due to cross slot leakage flux may be significant. This loss is one of the major components of "stray load" loss. Current harmonics due to chopper control increased this loss about 25% over the loss that exists without the harmonic currents.

This loss can be mitigated and greatly reduced if fine stranded conductors are used, since the loss is proportional to the square of the height of the conductor. Also, increasing the chopper frequency decreases this loss, since harmonic current magnitudes decrease with increasing frequency.

- 6) Losses in the pole face iron due to slot effect are negligible if the poles are laminated, but a major loss if the poles are solid iron.
- 7) Non-conducting banding (such as Kevlar) should be used to secure the armature winding end turns, to eliminating banding losses due to harmonic fluxes.

- 8) Equalizer connection losses are non-existent in a wave wound machine and are minimized in a lap winding if:

$$\frac{\# \text{ of commutator bars}}{\text{parallel paths}/2} = \text{integer}$$

and
$$\frac{\# \text{ of slots}}{\text{parallel paths}/2} = \text{integer}$$

- 9) Losses in the coils undergoing commutation can be substantial if the brushes are located very far (10-15 degrees) off magnetic neutral and increase with chopper frequency. The loss can be reduced by decreasing the number of turns shorted during the commutating process - using a wave winding or by using longer, less wide brushes (increasing commutator length).

Interpoles will eliminate the need for brush shift and are strongly recommended.

- 10) Brush loss can be minimized by utilizing metal graphite brushes with silver if good commutation exists. Again, interpoles are strongly recommended.

- 11) With a FWD diode having 0.86 volt drop, 75 watts diode loss was measured at full load current. It is important to select a low voltage drop diode for this application.

- 12) Losses due to shaft, bearing, housing currents due to shaft induced emf are negligible.

- 13) Hysteresis losses in the magnetic structure due to chopper harmonics are negligible with laminated magnetic circuit. It is recommended that a laminated frame also be utilized (see Figure 26).

- 14) Attempts to secure low brush voltage drop by large brush pressure should be evaluated against increasing brush friction loss.

- 15) For an internally fan ventilated motor of the size for EV, the fan loss is on the order of 0.33% of the output power rating. This type of ventilation is recommended to avoid duct losses. For an externally ventilated motor, the ducting and manifold should be carefully designed to minimize losses. Consideration of the useage of ram air for cooling should also be given in lieu of blower produced ventilation.

Chapter 4 is a discussion of the torque/ampere observations made in the course of the investigation.

Chapter 5 is a discussion of various models and equivalent lumped parameter circuits that have been proposed for chopper controlled series motor analysis. It also briefly discusses the finite element computer simulation developed during

the course of this investigation. This simulation was accepted as a dissertation for Dr. Elias Strangas, Graduate Research Assistant on this grant. Time limitations precluded refinement of this simulation into an easily usable user-oriented program, but it is at a high degree of refinement and can be so developed. Results obtained lack the exact degree of accuracy desired. However, this failure is due to non-exact knowledge of the resistivity and permeability of the frame material, which was found to be a very sensitive parameter in performance calculations. The dissertation is reproduced as SECTION II of this report.

In addition to details on the test facility and the specific motors tested, the various appendices describe other phenomena, engineering data and application information of interest to EV drive train designers and analysts.

APPENDIX C discusses current and voltage wave forms encountered during the various tests. Attempts to correlate observed results with various analytical techniques are discussed. None of the attempted procedures was markedly success-

ful. Data on Root Mean Square values, harmonic current magnitudes, % Ripple current, ratio of peak to average currents, current excursion, etc., are shown in graphic and tabulated form. Instrumentation requirements (theoretical wattmeter band width) are also discussed. For example, if less than 1% error in electric power measurement is desired, it is shown that the wattmeter must respond to the tenth harmonic of the chopper repetition frequency.

APPENDIX D presents a technique and instrumentation for the measurement of resistance and inductance of the motor as a function of frequency and saturation. Curve fit techniques, presented in APPENDIX E, were used to obtain empirical relationships describing these variations and these empirical relationships serve to reinforce this investigator's conviction that no lumped impedance model can be found which will accurately predict motor performance and efficiency. These can only be determined by actual test, to a standard test code. The existing

IEEE #113 "IEEE Standard Test Code for Direct Current Machines" is not adequate in this respect. It does not address the procedures, problems and instrumentation required.

It is a recommendation of this investigator that such a code be drafted.

APPENDIX F discusses EV motor and chopper application criteria. The procedure for selecting a motor rating for an example EV designed to meet SAE 227C cycle requirements is presented. This example graphically illustrates the reduction in size and power rating that can be obtained if a motor capable of commutating a 2.5 per unit overload is available. In the example, if such a motor is available, a 20 Kw, 5000 rev/m motor can be used. If per unit overload is restricted to 1.6 per unit current short time overload, a 30 Kw, 4000 rev/m motor is required. This variation is the basis for the strong recommendation to incorporate interpoles and compensating windings in the motor design and for the recommendation that the design limitation be based on commutation rather than on

thermal limits. The discussion in APPENDIX F with respect to chopper application points up the requirement for designing the motor for high inductance (not normally a requirement in industrial motors).

APPENDIX G presents a discussion on steps the motor designer can take to meet the high commutation ability, high inductance requirement.

CHAPTER 1

INTRODUCTION

This report details the results of an investigation into the behavior of series DC motors, suitable for electric vehicle (EV) applications, powered from a chopper* controlled energy source, commonly referred to as a "chopper drive."

The investigative work was undertaken by the Electrical Engineering Department, University of Pittsburgh, Howard B. Hamilton, Principal Investigator for the Department of Energy under NASA/DOE Grant NSG 3163. Technical guidance and project supervision was by the NASA/Lewis Research Center. Mr. Edwin F. McBrien was the NASA Technical Officer.

-Project Objective-

To design and fabricate a test facility suitable for conducting various tests; to develop test procedures and obtain data which can be analyzed to isolate losses; visualize where motor design changes can, or should, be made; to provide a basis for analytical prediction of motor performance under chopper power situations (model) and to make recommendations on changes to existing standard test procedures and pulse repetition rate/pulse widths used to minimize motor losses.

-Historical Background-

A conventional model of DC motors has been used in theoretical analysis and prediction of efficiency and performance for many years. The model used has yielded acceptable, but not exact results with larger departures from true values for smaller, low voltage motors. Generally, when performance met

* Chopper drive implies the use of a thyristor (or other form of switch) interposed between the source and the motor and alternately applying and removing the source voltage. The applied voltage can be at either constant or variable repetition rate and for either constant or variable duration. The ratio of pulse on time, T_o , to the period of the cycle, T , is referred to as the "duty cycle." Chopper frequency is $1/T$.

minimum requirements, even though efficiencies calculated were quite erroneous, the analysis and design were acceptable since the vast majority of the applications were not dependent upon the power supply being propelled along with the motor or involved motors of such a size that things like cost were deemed more important than efficiency. Further, performance was verified by test from a source of pure DC. Test standards⁽¹⁾ were adopted which enabled the user to evaluate specific test results based on those standards. In many instances, brush losses and so called "stray load" losses were assumed to be fixed values or fixed percentage of the output.

The inherent short comings in the existing standards and procedures has been known for years and accepted for the reasons detailed above. However, the advent of rectified AC for supply (rather than from a DC generator) did cause concern as to the effect of the harmonics on losses and performance. This concern has been expressed mostly (on rectifier drives) as the need to standardize the measuring techniques and test procedures.⁽²⁾

DC series motors have perceived advantages in so far as traction or vehicle propulsion systems are concerned, i.e. they can develop maximum torque at standstill, etc. They have been used for these purposes for many years. However, it should be noted that many EV applications will utilize shunt connected motors which have the capability of being easily connected for regeneration, i.e. pumping energy from the machine back into the supply system during braking or slowing operation.

The advent of the thyristor introduced a new era into the DC controlled motor drive arena. Basically, the use of chopper drives, with power thyristors, increased the efficiency of the overall drive system but probably reduced the efficiency of operation of the motor itself, due to the current wave forms resulting.

Refer to Figure 1 for a simplified schematic of a chopper drive.

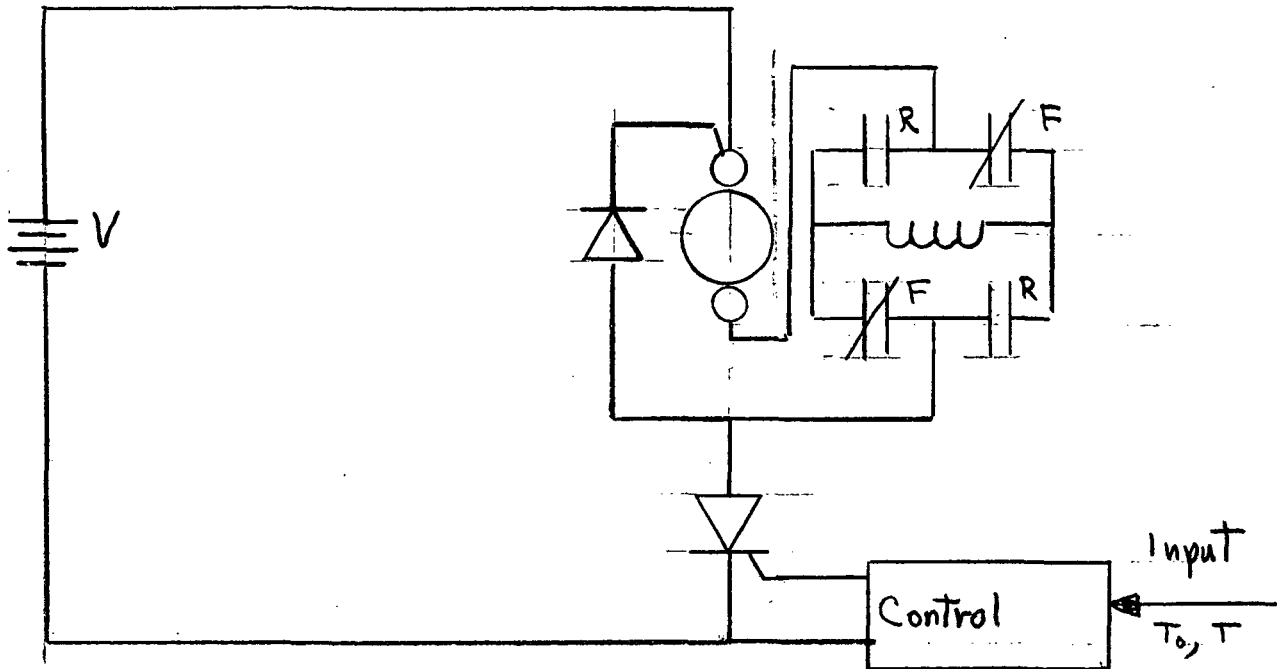


Figure 1. Schematic of Basic Chopper Drive for Reversible DC Series Motor

Attempts to design an electric drive system for battery powered electric vehicles has increased the awareness for the need to develop reliable test and measuring techniques as well as a new model for the DC motor. This is necessary in order to:

1. minimize the losses, i.e., higher efficiency drives;
2. identify the important motor design parameters for a motor to be operated in conjunction with a battery/chopper supply;
3. improve motor performance for a specific weight/size configuration;
4. to have a reliable motor model which permits reliable performance predictions;
5. to have a standardized recognized test procedure so that all concerned agree on the meaning of test results.

With respect to efficiency and weight, a commonly accepted 'rule of thumb' indicates that with present motor designs and battery technology, 1% change in efficiency changes the available EV range 1 mile. 50 lbs. of weight change has the same effect!

Conventionally designed DC motors are usually not designed for high performance at non "design" voltages or for high harmonic content pulsed chopper supplies.

In connection with the use of choppers, it should be noted that the vast majority of chopper applications have dealt with shunt wound motors, (usually from alternating current supplies) and that there is a scarcity of literature on series motor applications; yet the series motor appears to be an attractive type for EV and traction applications.

There is very little information available on how to match motors and controllers (choppers). Guidelines need to be established for each such that off the shelf items can be applied. The chopper designer insists on some minimum inductance, resistance and inductance/resistance ratios in the motor. The motor designer must be cognizant of the additional iron losses due to pulsating fluxes; the skin/proximity effects and additional I^2R losses and the performance degradation due to factors discussed above and the lessened ability of the motor to properly commutate. (Measurements reported in this report indicate a 3.5/1 change in inductance and a 6/1 change in apparent resistance over a frequency range of 30-360 Hz, as measured on a DC Series motor.)

The problem areas discussed above point up the need for a better understanding of the behavior of the DC motor powered from a chopper supply and the need for a more exact model than that presently used, as well as the need for "interface" guidelines.

There are many facets of motor design that warrant investigation. Some of these stem from the fact that the motor power size, for electric vehicles, is normally designed for a higher supply voltage. For example, many of the

motors are rated around 20-30 horsepower. A low voltage machine of this size, or larger, would normally have a parallel (lap) type winding. A regular industrial machine would normally be wound series (wave) for 250 volts, DC, or higher. The power supply for electric vehicles will most probably be in the range 84-144 volts, which is between low and high voltages. Of the two motors examined in this investigation, one was wave; the other lap wound. How the motor is wound and the duty cycle it is designed for will have a large impact on the I^2R losses in the armature circuit. Another problem area for design compromise is in brush, brush spring tension selection. Electrographic or metallic/graphitic brushes plus high spring tension can be utilized to reduce the voltage drop across the brushes - very important in low voltage motors. Yet, this approach often yields increased brush friction (rotating losses). Should the motors be "copper poor" necessitating an internal blower or an external source of cooling air? Heavy conductors, eliminating the need for cooling, face a skin effect/proximity effect when subjected to the harmonics associated with a chopper supply.

A series motor can be partially compensated for the effects of armature reaction upon commutation by a fixed brush shift position. This brush shift can also actually aid commutation (always a problem with a power source containing harmonics). In conventional applications, brush shift (fixed) in a series motor is a self-compensating effect, i.e., one position is suitable for all loads for rotation always in the same direction. However, brush shift degrades performance, because of loss of some active inductors. If the brushes are not on the proper location, "rotating core losses," or losses due to joule heating in the coils undergoing commutations, can be excessive. This is an especially cogent consideration during reverse motor operation. The alternative is the use of interpoles, and possibly compensating windings. Yet these additions increase cost, weight and introduce additional I^2R losses in the motor!

Other aspects of motor design, for electric vehicle applications, that may have different relations than those in conventional applications are as follows:

1. working flux densities - how much saturation should be tolerated in the interest of lightweight but at a sacrifice of performance?
2. the electrical loading - should fan cooling be required?
3. are conventional length/diameter ratios optimum?
4. air gap size and the weight/cost/design life relationships based on field maintenance and expected life realities;
5. are commutator bar-bar voltages consistent with the harmonics involved in armature current?
6. use of solid vs. laminated yokes;
7. insulation levels required - is it possible to reduce weight and cost if not overinsulated?
8. need for maximum efficiency over a wide range of output.
9. need for relatively high values of circuit inductance.
10. the design objective must be based on commutation limit as opposed to thermal constraint.

These questions can only be addressed after an examination of the various loss mechanisms.

Scope of the Investigation

In order to perform the experimental work necessary, a test facility was designed and fabricated, with basic instrumentation easily obtainable. A comprehensive report on an investigation of possible DC power sources for testing DC EV motors was submitted to NASA/Lewis Research Center⁽³⁾ and a summary of the report was presented at the 1979 IEEE-IAS meeting⁽⁴⁾. Details on the test facility and instrumentation are presented in Appendix A of this report. Also included are reports (3) and (4).

Two motors, one lap wound, the other wave wound, were provided for testing. Details on the motor designs are presented in APPENDIX B.

Throughout the test program, the current and voltage waveforms were monitored and analyzed. APPENDIX C presents a detailed discussion of results observed, i.e., shape, harmonic content, instrumentation requirements for current and power measurements and comparison of observed results with those obtained using a "linearized" version of the waveforms and with those utilizing a 'more exact technique' which includes the motor circuit time constant⁽⁵⁾. Suffice to say that the conclusions drawn from the latter effort is that analytical prediction of harmonic current magnitude is not possible with either approach and that accurate values can be obtained only by test and actual measurement.

IEEE Std #113⁽¹⁾ does not address determinations of the resistance and inductance variations with frequency and saturation level and thus it was necessary necessary to make these determinations as an early part of this investigation. A technique suggested by Saunders⁽⁶⁾ was utilized for these measurements. However, instrumentation techniques had to be developed to accomplish this. The procedure and instrumentation technique, as well as the results obtained are detailed in APPENDIX D and papers summarizing the results were prepared and presented at various technical meetings^(7,8). Paper (7) is included in APPENDIX D.

The following chapter presents the results of efficiency and performance calculations based on the conventional DC series motor model and IEEE Std #113⁽¹⁾. The results are compared with observed performance and efficiency, under both "pure" DC, herein after referred to as DC and the chopper controlled situation, herein after denoted by a specific frequency in Hz and by duty cycle, T_o/T .

Subsequent chapters deal with the various loss mechanisms and recommendations with respect to modeling, motor design, suggested test procedures and conclusions.

-CHAPTER 2-

THE CONVENTIONAL MOTOR MODEL

Figure 2 depicts, in circuit form, the model that has been traditionally used for calculating performance and efficiency of DC motors.

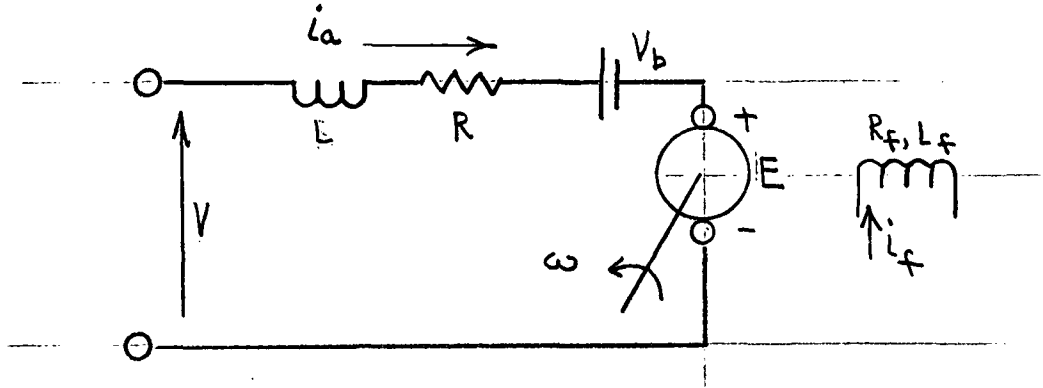


Figure 2. DC Motor Model

For the series motor, $i_f = i_a$ and field and armature resistance and inductance combine as lumped values, R and L . V_b represents voltage drop across the brush system, E is the counter electromotive force and ω the shaft speed in rad/s.

Equations representing electrical performance can be written as follows:

$$V = R i + L \frac{di}{dt} + V_b + E \quad (1)$$

$$E = \frac{Z P}{2\pi a} \phi \omega = K' \phi \omega \quad (2)$$

$$M_e = \frac{E i}{\omega} = K' \phi i_a \quad (3)$$

where: Z = number of inductors

P = number of poles

a = parallel paths in the armature

ϕ = total flux per pole, Wb.

M_e = electrical torque, Nm developed

V = applied voltage.

Since $\phi \propto i$, $K'\phi$ can be expressed as:

$$K'\phi = K i_f \quad (4)$$

if it is understood that K is not a constant, but rather a function of excitation, i_f (saturation).

Efficiency can be expressed as:

$$\eta = \frac{P_{out}}{P_{in}} = 1 - \frac{P_{loss}}{P_{in}} \quad (5)$$

where P_{in} is average power input and P_{loss} is the sum of the losses involved in the energy conversion process.

IEEE Standard #113⁽¹⁾ details procedures for performance determination based on ripple free DC or, to a limited extent, DC from a rectifier type supply. The losses used consist of:

Joule (I^2R) type losses

Brush contact loss ($V_b I$)

Rotational Core loss

Stray Load loss

Friction, Windage and Ventilating Loss.

Losses are discussed in detail in following chapters; however, in this brief overview of the use of the conventional model and in presenting its limitations as applied to the motors investigated in this program, the above listed losses are categorized as follows:

- a) Joule loss is the I^2R loss in the armature and series field, based on measured circuit resistance
- b) Brush contact loss is based on measured voltage drop across the brush-commutator, including the non-linear carbon resistance and is considered constant
- c) The brushes are supposedly on magnetic neutral and no rotational core loss is present
- d) Stray load loss cannot be calculated or measured directly and is, in accordance with IEEE 113⁽¹⁾ taken as 1% of the output power
- e) The Brush and Bearing Friction and Windage are determined experimentally and designated as p_{fw}
- f) Ventilating requirements are not considered.

-Parameter Measurement-

Section 4.2, IEEE 113 specifies various methods of armature and field resistance measurement and Section 5.5.3 provides values for V_b for various brush types. In the motors tested, brush (material) types were not known with certainty and therefore a "non-standard" test was utilized to determine V_b and total circuit resistance.

The test is based on the relationship shown in Figure 3.

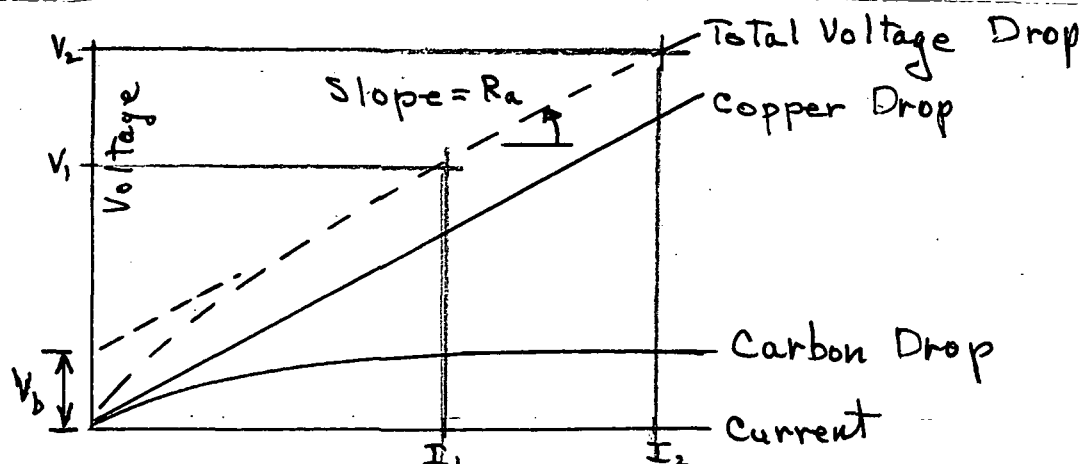


Figure 3. Circuit Resistance and Brush Drop

Armature resistance is, of course, linear (at constant temperature). However, voltage drop across the brushes commences at zero with zero current, rising to a nearly constant value at somewhere between 20 and 40% of rated current in a reasonably designed brush system. The sum of a linear plus constant volt-ampere characteristic is also linear, displaced from the zero intercept. The linear slope is the copper circuit resistance; the zero current intercept of the extended portion of the total is the brush voltage drop, V_b .

This technique yielded the following values:

-Blue Motor-

Armature, Field and Connectors: 0.0301 ohms

Total Brush Voltage Drop: 0.53 volts

(The manufacturer gave a value of 0.029 ohms)

-Red Motor-

Armature, Field and Connectors: 0.0354 ohms

Total Brush Voltage Drop: 0.50 volts

The mechanical loss, $P_{f\omega}$ was measured, for both the Red and Blue motors, using the facility described in APPENDIX A, page 3. Curve fit routines (See APPENDIX E) were used to establish the following relationships (actual test points are shown in the section of this report where rotating losses are discussed).

$$\text{Blue motor: } P_{f\omega} = 0.03 (\text{RPM})^{1.18} = 0.43 \omega^{1.18}$$

$$\text{Red motor: } P_{f\omega} = 0.072 (\text{RPM})^{1.184} = 1.04 \omega^{1.184}$$

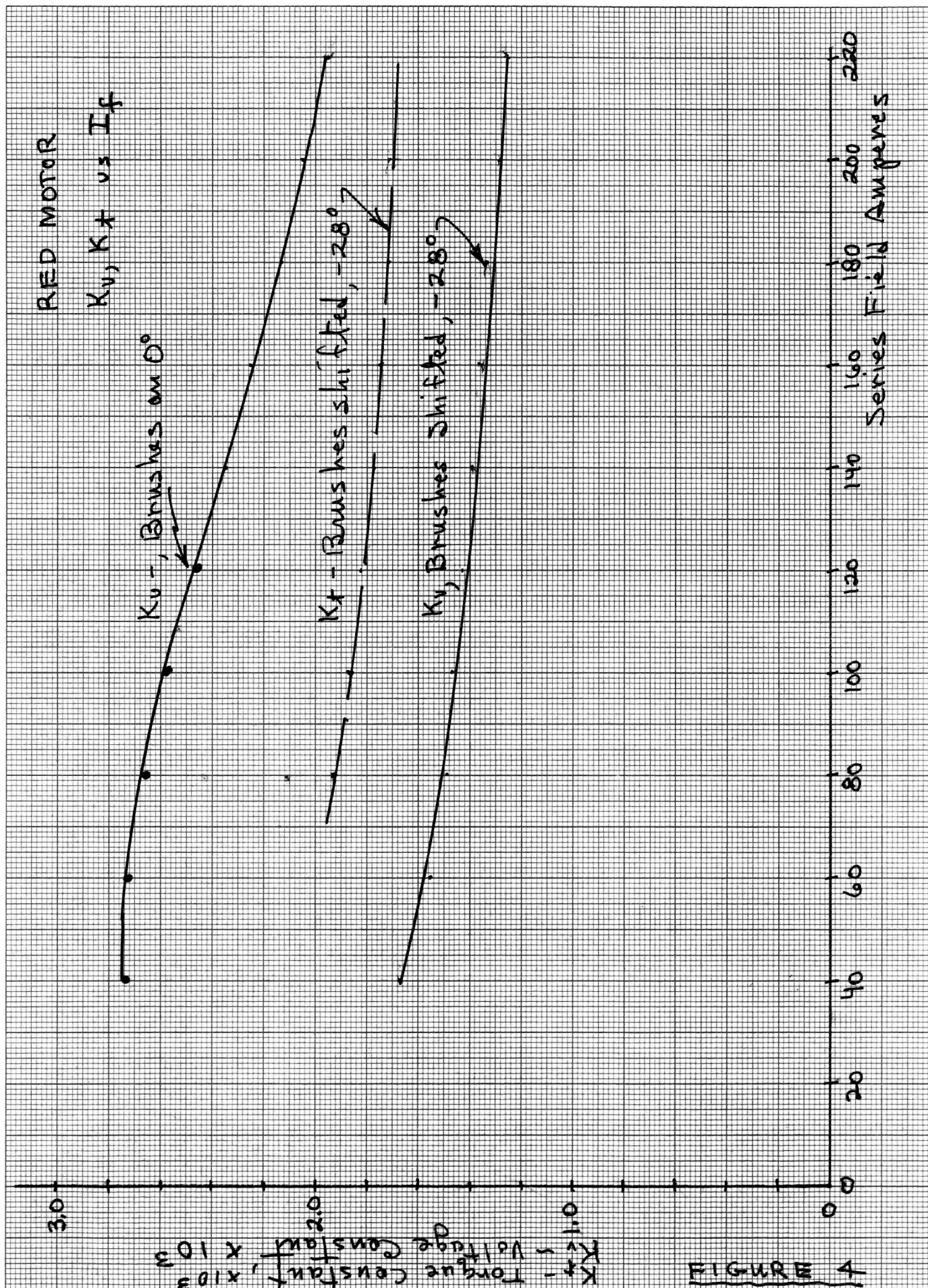
In theory, K can be determined from either torque measurements or from the open circuit saturation (OCS) characteristic, i.e.

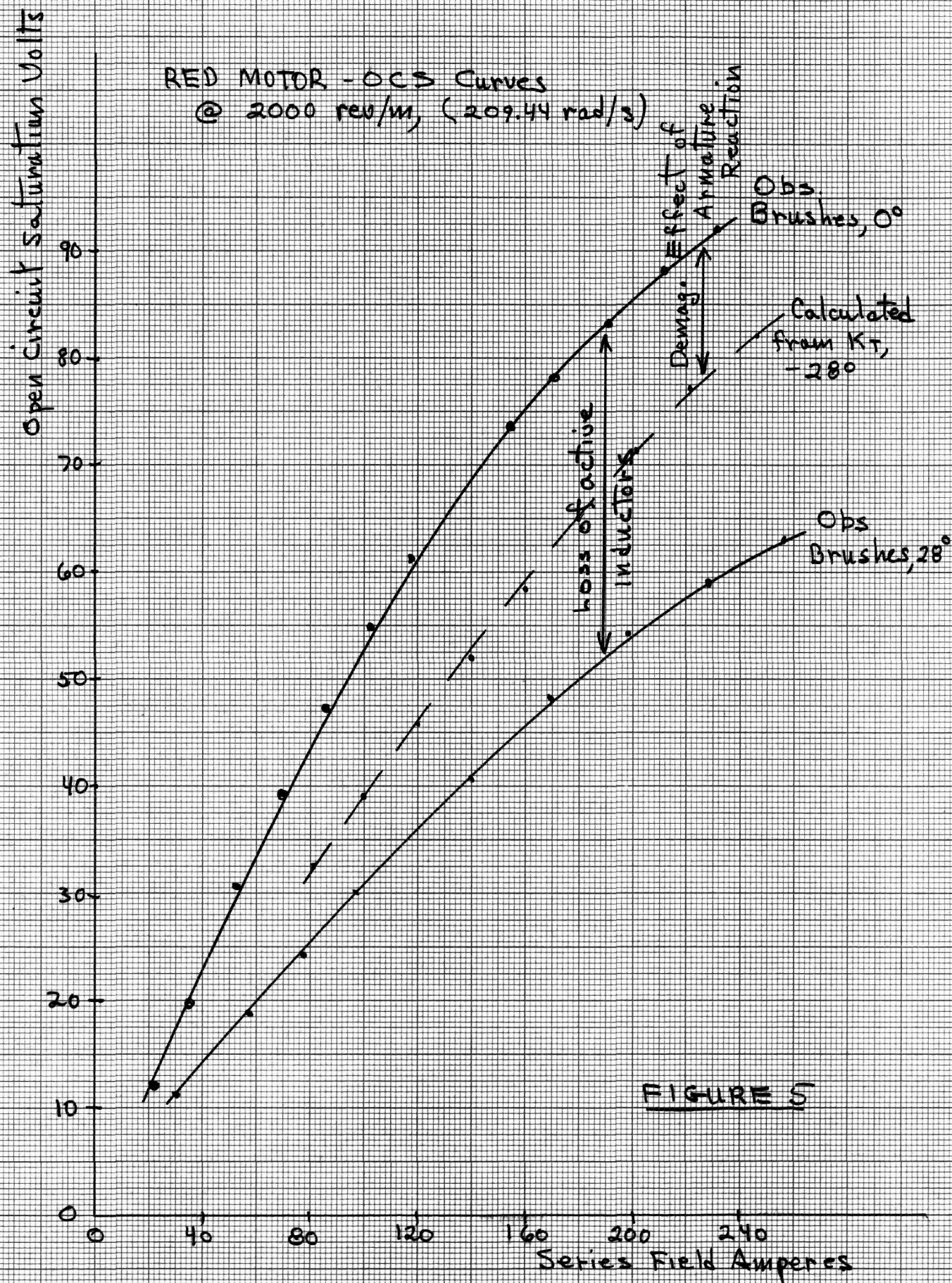
$$K = \frac{E_{oc}}{I_f} \quad \text{or} \quad K = \frac{M}{I_a I_f} \quad (6)$$

If the torque test is made under locked rotor conditions the measured torque is the electrical torque developed. For a motor without interpoles, the locked rotor test should be made with the brushes located near magnetic neutral. If this is done, the brushes are near, or on, the brush location for proper commutation and are in the normal run location. For a series motor, so locating the brushes accounts for the demagnetizing effect of armature reaction and also for the loss of active conductors due to brush shift.

K cannot be determined from the OCS curve for a motor to be operated with brushes shifted. Refer to Figures 4, 5 and 6. In Figure 4, two values of K , designated K_v are shown as calculated from the 2000 rev/m. OCS curves in Figure 5. One curve, yielding the highest values of E and K_v was taken with the brushes on mechanical neutral, i.e. 0° shift. The lower curve is data taken at -28° shift and reflects the loss of active inductors. (Since an open circuit, no armature reaction is present.) If the brushes are shifted an angle β , the inductors in the region $0^\circ - \beta$ and $\pi - (\pi - \beta)$ have opposite induced voltage in them and this voltage subtracts from the total voltage between brushes. If there are Z' inductors between brushes, the net inductors, for β shift from magnetic neutral, is: $Z' - Z'(\frac{2\beta}{180}) = Z'(1 - \frac{2\beta}{180})$ (7) yielding a ratio of:

$$\frac{K_v \text{ (shifted)}}{K_v \text{ (magnetic neutral)}} = 1 - \frac{2\beta}{180} \quad (8)$$





Voltage and Torque Constants
BLUE MOTOR, Brushes Shifted
(DC)

K_v (from DC)

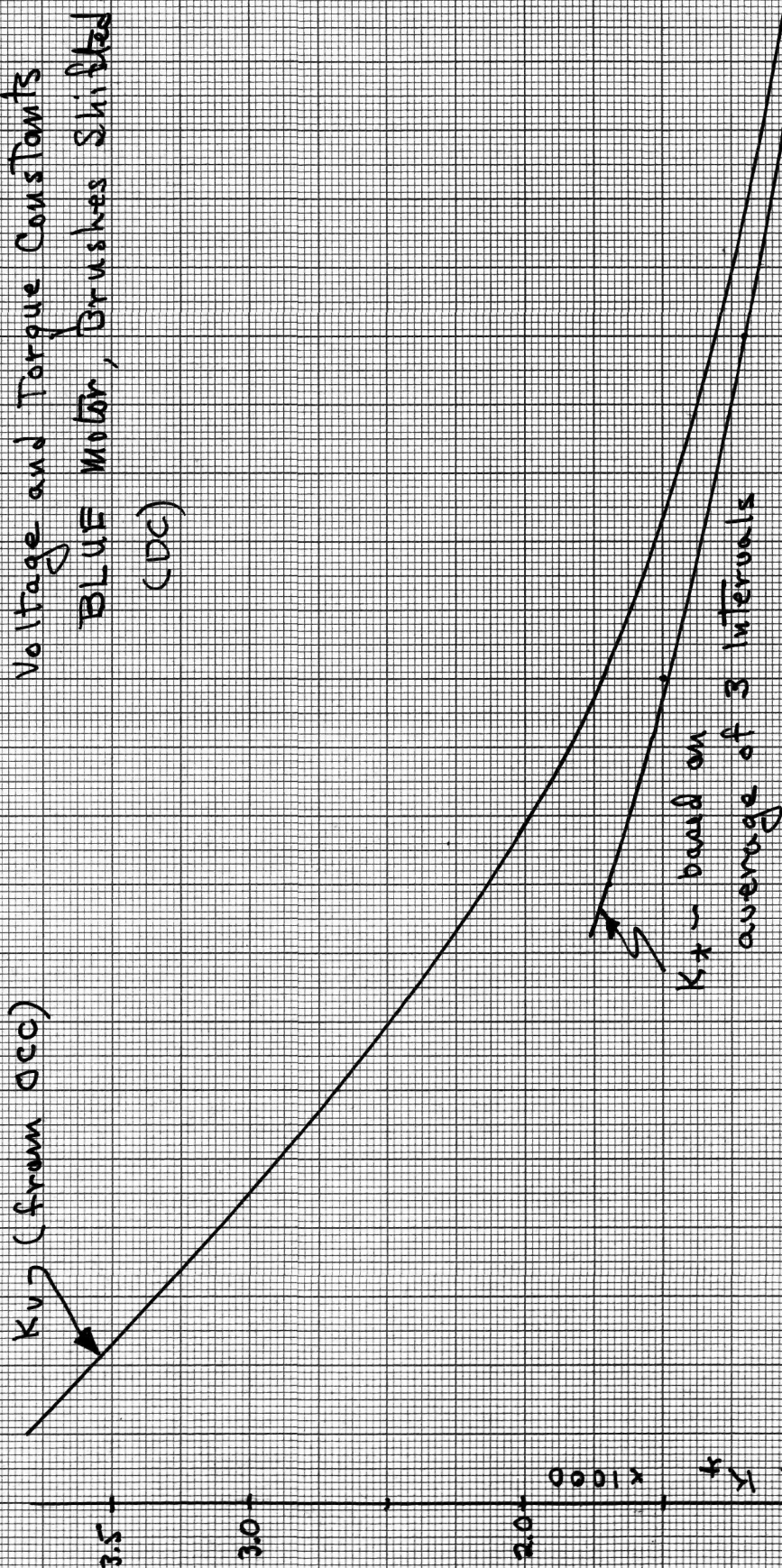


FIGURE 6

In theory, for a 28° shift, this ratio would be 0.68. From Figure 4, the ratio actually observed was between 0.56 and 0.59. The difference is due to inability to precisely determine exact brush position.

If compensating windings, to eliminate the demagnetizing effect of armature reaction, were present, and the brushes were on mechanical neutral, K could be determined from the OCS curve, because magnetic neutral and mechanical neutral coincide.

When the brushes are shifted and the motor loaded, if the brushes are truly on magnetic neutral, there is no loss of active inductors; there is a demagnetizing effect due to armature reaction, however. This is the reason why $K_t = K$ is larger, at 28° brush shift than K_v .

The demagnetizing ampere turns per pole are equal to the inductors in the angle of brush shift times the current per armature path,⁽⁵⁾ or

$$AT_{\text{demag}} = \frac{\beta}{360} Z \frac{I_a}{a} \quad (9)$$

or, demagnetizing field current is:

$$I_{f \text{ demag}} = \frac{\beta}{360} \frac{Z I_a}{N_f a} \quad (10)$$

where N_f = series field turns/pole. For the RED motor, $Z = 162$, $\beta = 28$, $a = 2$, $N_f = 20$ (See APPENDIX B).

Thus,

$$I_{f \text{ demag}} = \frac{(28)(162)}{(360)(20)(2)} I_a = 0.33 I_a \quad (11)$$

This relationship indicates that, for $I_f = I_a$, $K_t = (1-0.33) K_v$ where K_v is calculated from the OCS curve taken with the brushes on mechanical neutral.

From Figure 4, the ratio K_t/K_v varies from 0.73 at 80 amperes to 0.83 at 200 amperes vs. the theoretical value of 0.667.

The OCS curve calculated from measured values of K_t is shown dotted in Figure 5.

For a motor in a saturated (magnetically) condition, there is no demagnetizing effect due to armature reaction if the brushes are not shifted. Similarly, there is no loss of active inductor phenomena. Even in the unsaturated operating condition, it appears that the demagnetizing effect of armature is not as large a factor as loss of active inductors if the brushes are shifted to obtain satisfactory commutation.

Therefore, use of interpoles to avoid brush shift will yield higher torque per ampere, more power output per ampere (higher efficiency) and satisfactory commutation at all speeds, both forward and reverse.

To examine the implications with respect to power, note that for a given current, lower K will yield a higher speed, but a lower torque. If the per unit increase in speed is less than the per unit decrease in torque, the power output per ampere input will be decreased.

From (8) the per unit increase in speed is (approximately) (neglecting voltage drops in the circuit);

$$\frac{1}{1 - \frac{2\beta}{180}} \quad (12)$$

From (10) the per unit decrease in torque:

$$1 - \frac{\beta z}{360} N_f a \quad (13)$$

Therefore, since Power equals (torque)(speed); if

$$\left(1 - \frac{\beta Z}{360} N_f a\right) \left(\frac{1}{1 - \frac{2\beta}{180}}\right) < 1 \quad (14)$$

use of interpoles will yield a higher torque, higher power output per ampere, and a more efficient motor.

For the RED MOTOR, the left hand side of equation (9) is 0.99. For the BLUE MOTOR it is 0.88. Thus, interpoles would improve the performance of these motors.

If interpoles and compensating are not used, armature reaction effects can be partially mitigated by increasing the reluctance of the air gap at the pole tips. This was not done in either of the motors tested.

Two other conclusions are readily drawn, i.e. in any event the brushes must be properly located and K can only be determined from tests involving locked rotor torque as a function of current in the field and armature for a machine without interpoles, requiring brush shift.

In obtaining the torque vs. ampere characteristic, three tests were made for each motor, i.e., runs were made at 120° intervals of the stalled rotor. Approximately 10% variation in torque/ampere² was noted for the 3 positions of the Blue motor rotor; approximately 3% variation for the Red motor. The readings were averaged to calculate K_t used in this section.

Based on measured values of R, V_b , $P_{f\omega}$, and K, steady state torque, speed, power output and efficiency as functions of current, for ripple free DC supply, can be calculated as follows: ($K_t = K$)

Speed

$$N = \frac{60\omega}{2\pi} = \frac{V - V_b - I_a R}{K I_f} \left(\frac{30}{\pi}\right) \text{ rev/min} \quad (15)$$

Mechanical Torque Output

$$M = M_e - \frac{P_{f\omega}}{\omega} = I^2 K - \frac{P_{f\omega}}{\omega} \quad (16)$$

Power Output

$$P_o = M\omega \quad (17)$$

Efficiency

$$\% \eta = \left(1 - \frac{P_{\text{loss}}}{P_{\text{in}}} \right) 100 = \left(1 - \frac{(I^2 R + P_{f\omega} + 0.01 P_o + V_b I)}{VI} \right) 100 \quad (18)$$

also,

$$\% \eta = \frac{M\omega}{VI} 100 \quad (19)$$

Actual load tests were conducted on the Red and the Blue motors in order to evaluate the accuracy of calculated performance equations. Laboratory quality instrumentation, as described in APPENDIX A, including a digital stroboschometer, were used in the determination of the experimental data. Since data is used in later comparisons, the tests were run at nominal 42 volts, corresponding to many of the chopper supplied tests.

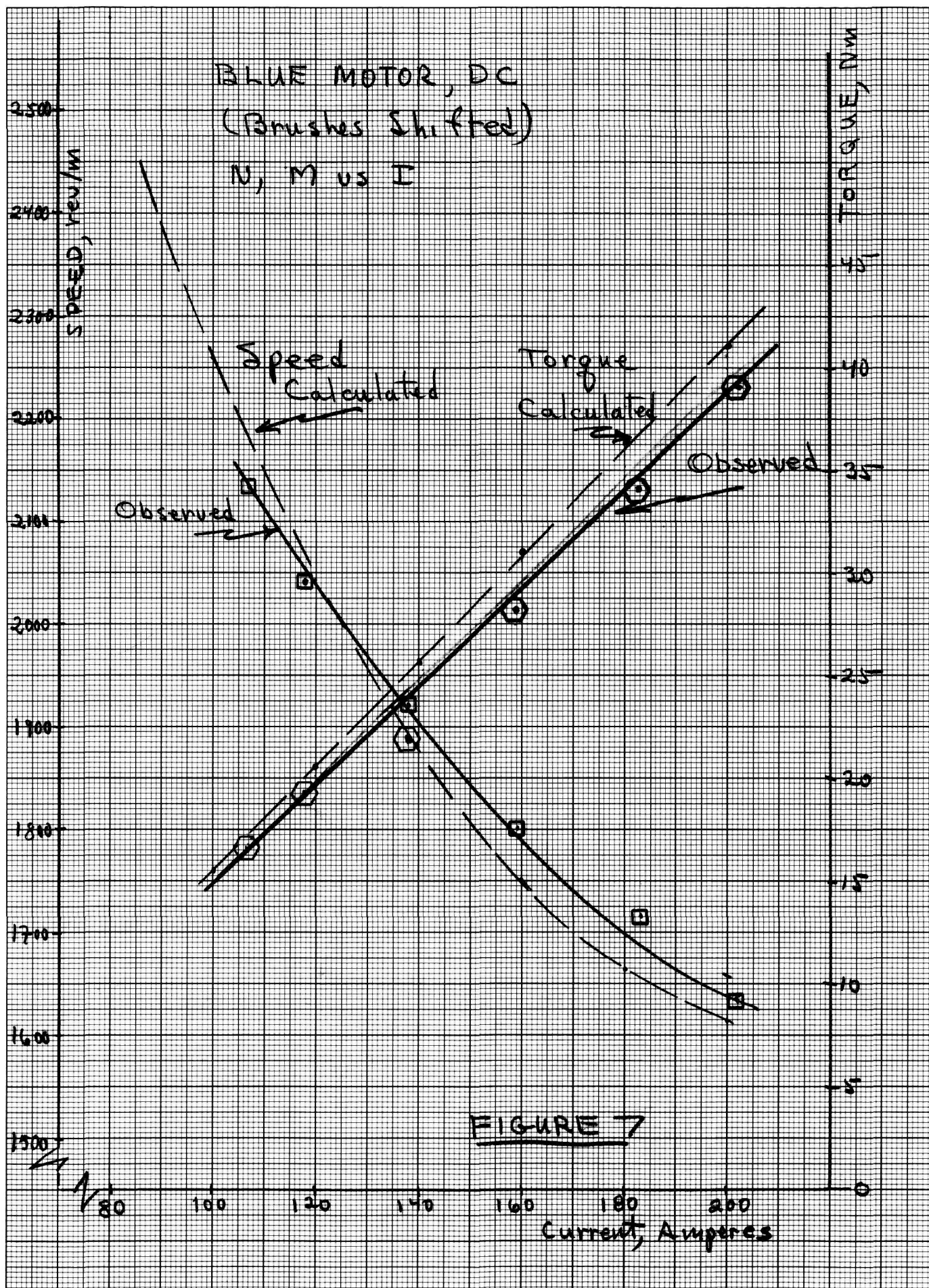
Figures 7, 8, 9, and 10 present the results observed experimentally and as calculated using equations (15) through (19).

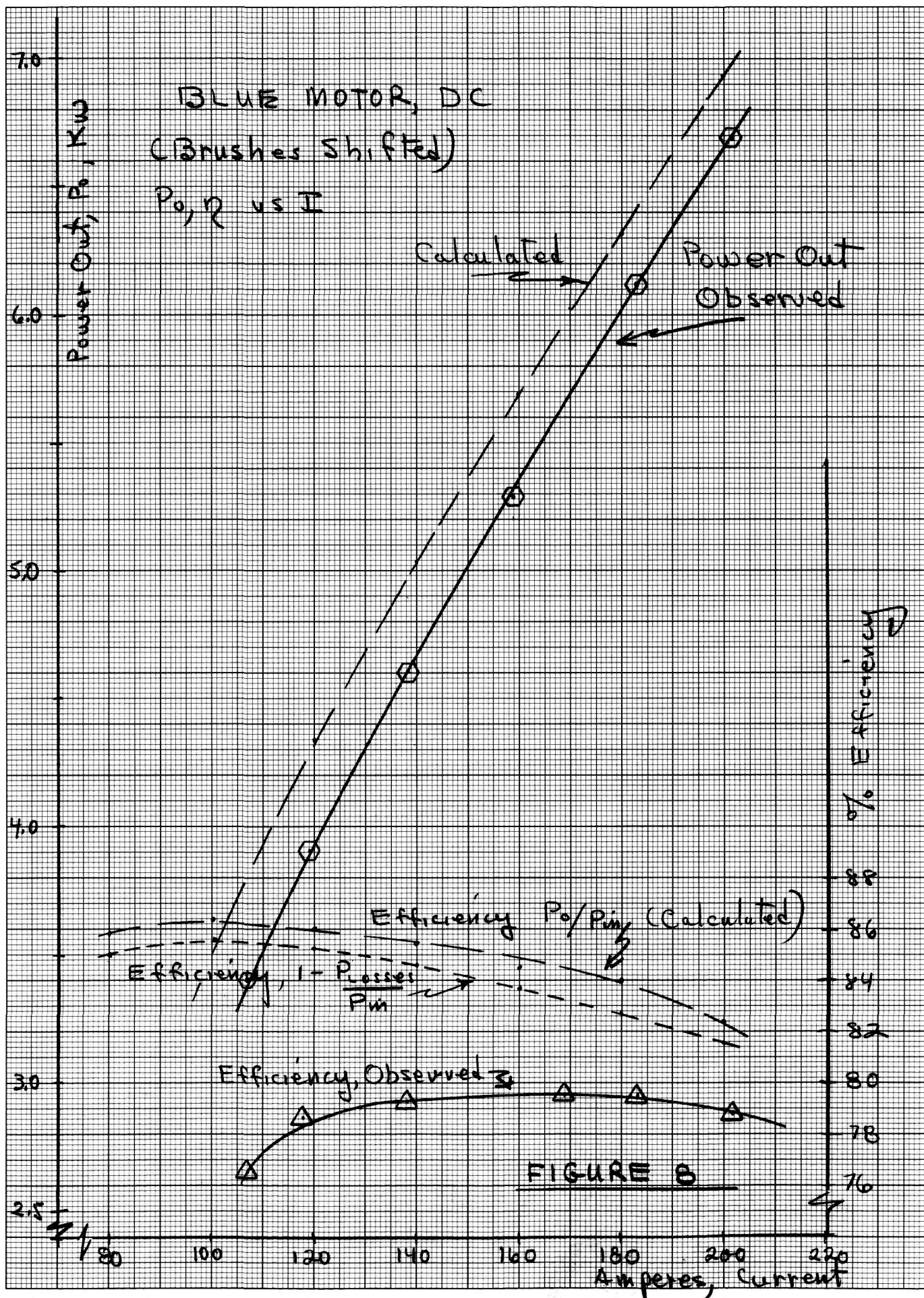
As can be seen, in general, there is very good correlation between observed and calculated results.

In general, calculated results are within 5% of observed experimental results. Because of the hysteresis effects in the magnetic circuit and due to the fact that the value of K is the average of 3 rotor position measurements, 5% error is considered acceptable, since the value of torque, for a given current on stalled rotor varied over a 3-10% range.

For both motors, calculated efficiency was higher than actual efficiency. It is believed that this is due to neglect of "rotating core loss," which

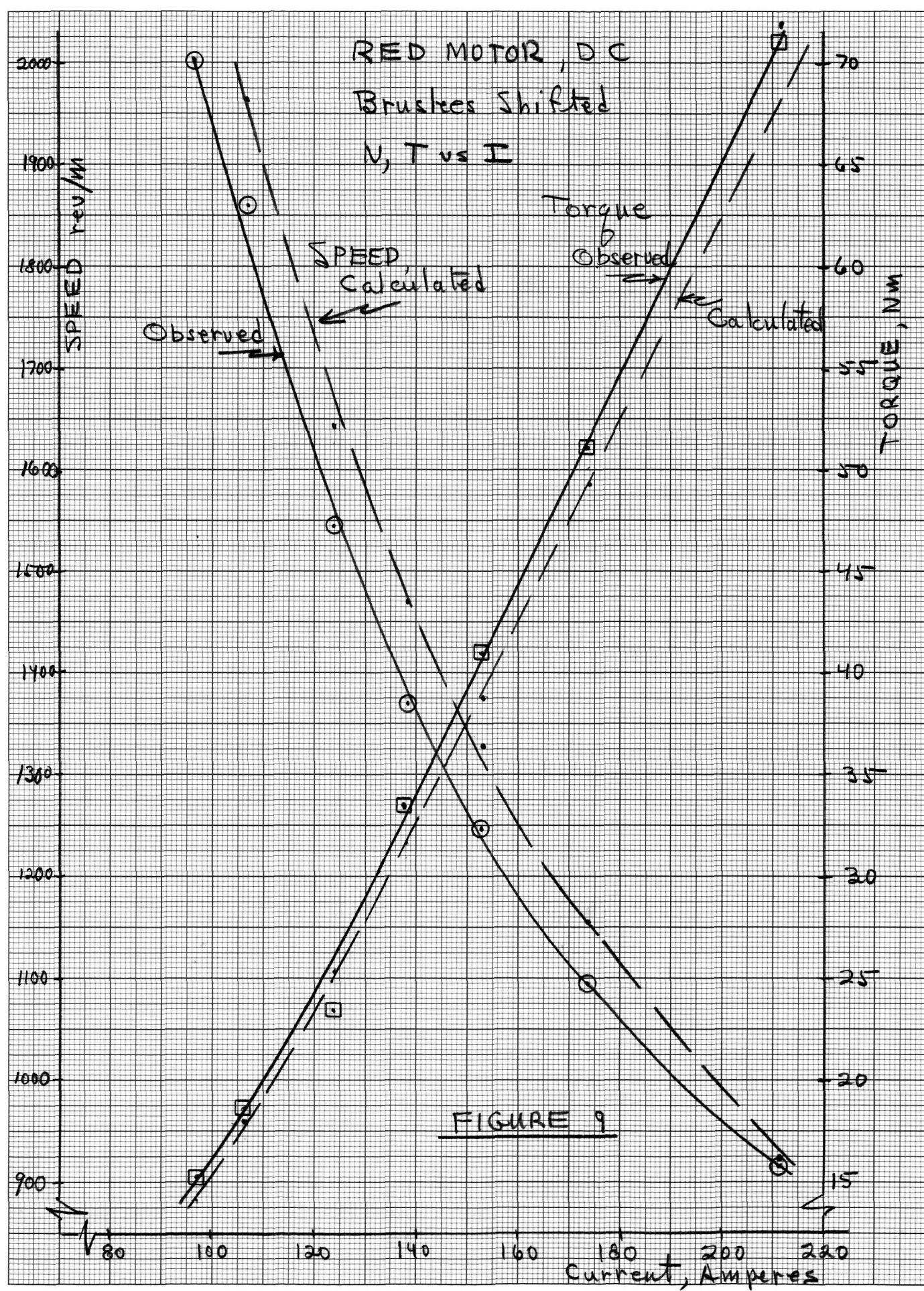
461510

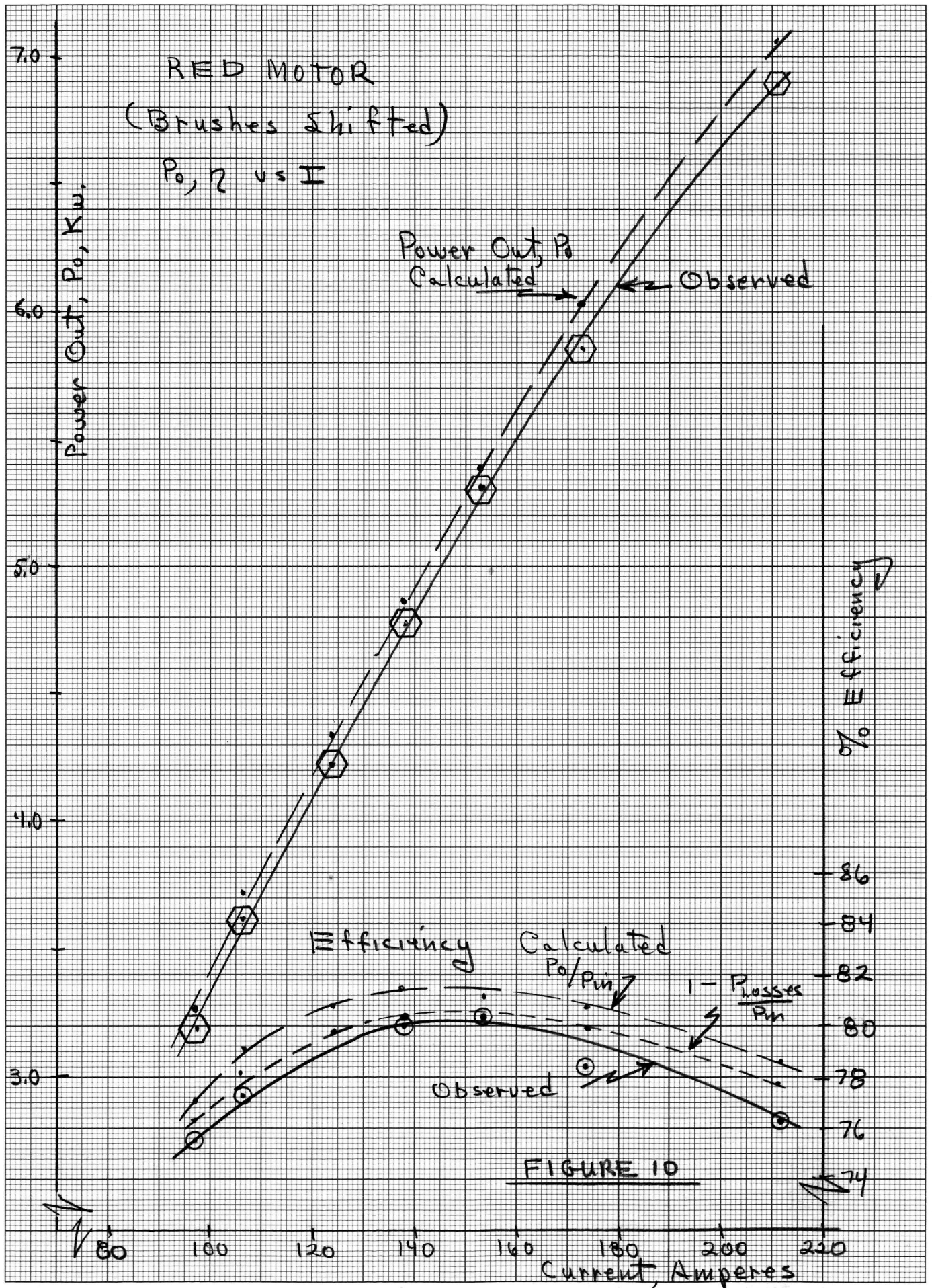
K&E 10 X 10 TO THE CENTIMETER 18 X 25 CM.
KEUFFEL & ESSER CO. MADE IN U.S.A.



46 1510

10 X 10 TO THE CENTIMETER
KEUFFEL & ESSER CO. MADE IN U.S.A.

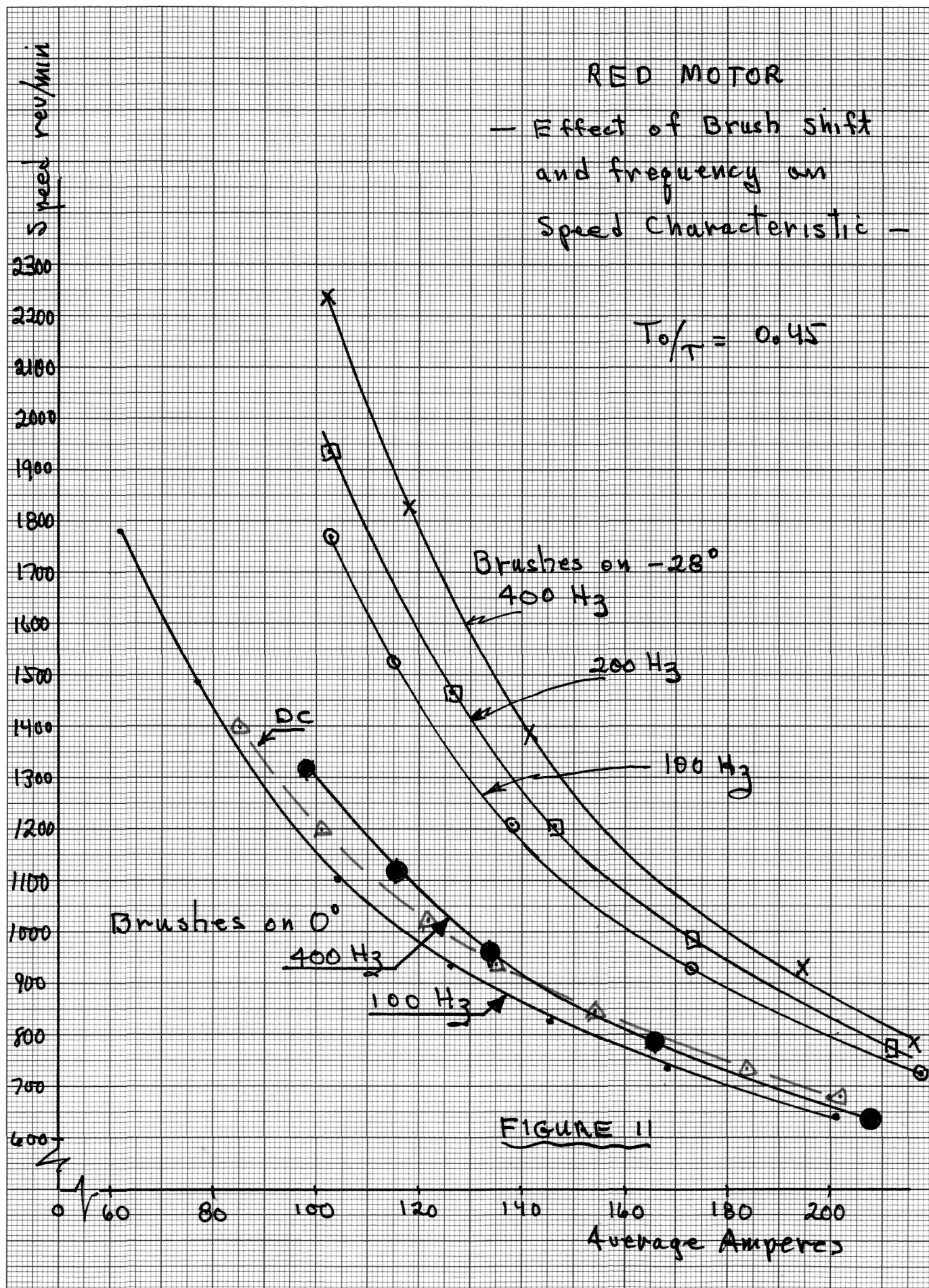




results from joule loss in the conductors undergoing commutation if the conductors are not in a position of zero flux density during the process. (This is discussed in a later chapter.) This is a substantial loss if the brushes are not precisely located or if an excessive number of coils are shorted during the commutation process. The Red motor efficiency calculated was quite close to the observed value; the Blue motor value was much more in error. This can be attributed to the fact that more coils are shorted during commutation in the Blue motor and to the fact that the Blue motor (because it is lap wound) has an equalizer connection which results in a finite joule loss not reckoned with in equation (18).

As will be shown in following chapters, there are additional losses introduced if the current and voltage are other than ripple free DC and it should be noted that the conventional model does not account for these effects which are introduced by virtue of the chopper action.

Also, when the motor is Chopper controlled, the speed-ampere characteristic is altered and is both frequency of chopper action and brush position dependent. If the brushes are shifted for proper commutation, the speed, at a given current is increased significantly over the speed, at the same current, with the brushes on mechanical neutral, i.e. 0° . The reason for this is the decrease in the number of active inductors in the armature. With the brushes on 0° , there is relatively little effect on speed due to frequency. Refer to Figure 11, (approximately a 10% band covering DC, 100, and 400 Hz). However, when the brushes are shifted, the effect of frequency on the characteristic is quite pronounced. For example, at 150 amperes, brushes on -28° , reference to Figure 4 indicates that the value of K_v changes by 11% when the brushes are shifted, when supplied from ripple free DC. However, from Figure 11, if the motor is Chopper controlled, at 400 Hz repetition rate, the speed changes by 48% in shifting brushes from 0° to -28° , and the spread in speed between



100 Hz and 400 Hz is about 18%, with higher speed with higher frequency at a specific current.

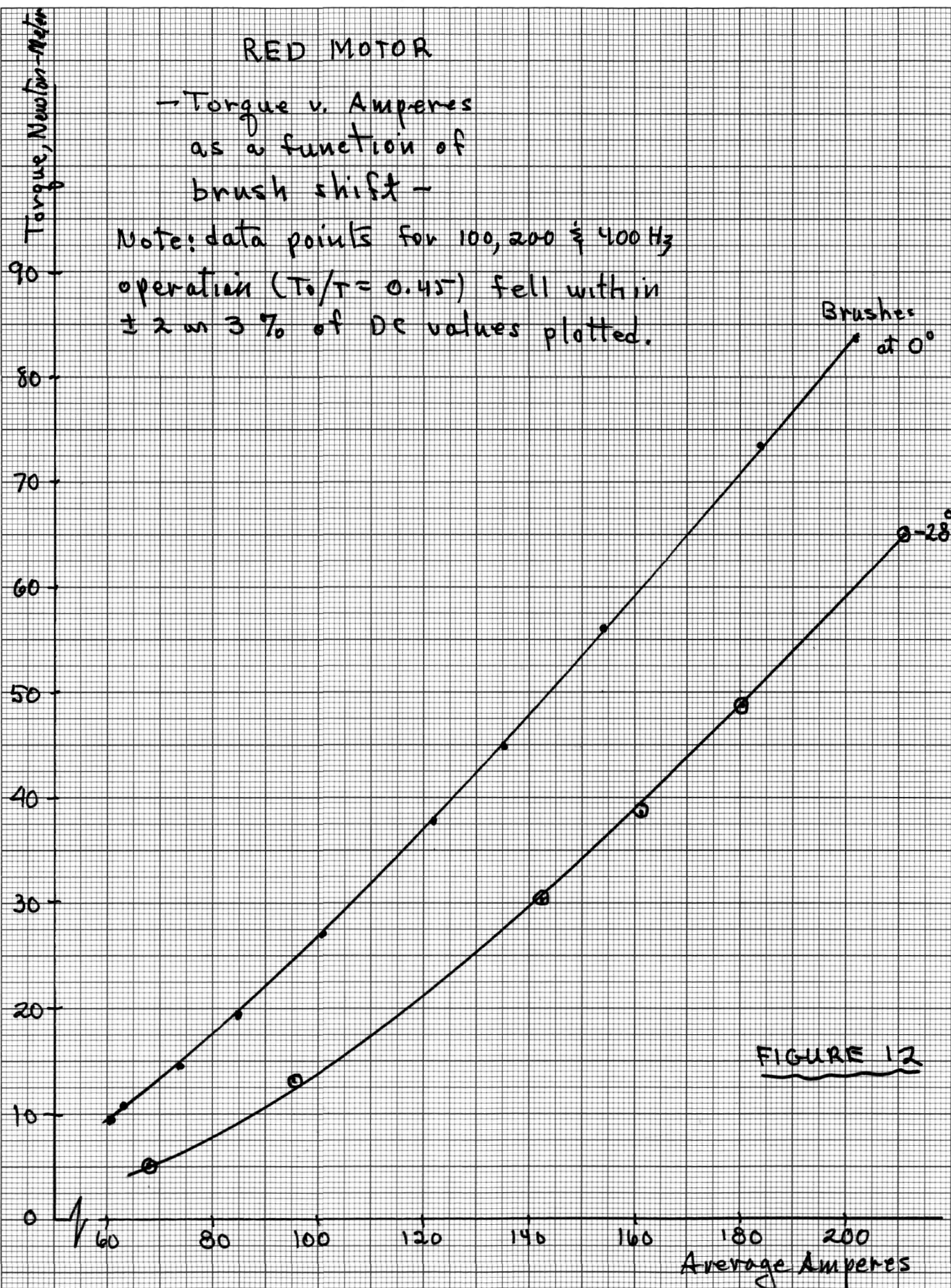
Thus, Chopper control and the repetition frequency of the Chopper have a very marked effect on the speed-current characteristic of the motor. However, reference to Figure 12 verifies that only brush shift affects the torque per ampere characteristic.

As a part of this investigation a time dependent finite element model for modeling the electromagnetic field in electrical machines was developed. It was published as a Ph.D. dissertation⁽¹⁰⁾ and has been reported in technical papers.^(11,12) It is discussed later in this report.

RED MOTOR

→ Torque v. Amperes
as a function of
brush shift -

Note: data points for 100, 200 & 400 Hz
operation ($T_0/r = 0.45$) fell within
 ± 2 or 3 % of DC values plotted.



-CHAPTER 3-LOSSESI Loss Classification

Losses were discussed in a general fashion in the previous chapter. This chapter discusses the losses in a more quantitative manner, presents the results of experimental tests and observations and presents some suggestions as to means to decrease the losses through design methods.

The losses can be classified as follows:

-Joule Losses-

1. Load current losses in the field and armature windings due to normal ohmic resistance and skin effect.
2. Eddy current losses in the following:
 - A) the armature winding, due to flux distortion under the pole faces
 - B) the armature winding, due to tooth saturation and the main flux
 - C) the armature conductors, due to slot leakage flux during commutation
 - D) the iron of the pole face due to variation of air gap flux density due to slot openings
 - E) throughout the magnetic circuit (armature, poles, yoke) due to chopper action.
 - F) in the steel banding wire used to secure the armature winding.
3. Losses in the equalizer connection, if present.
4. Loss in the coils undergoing commutation due to the short circuit current flowing.
5. Loss due to the carbon brush and brush to commutator contact resistance.
6. Loss due to the Free Wheeling Diode, if Chopper controlled.
7. Loss due to current circulating in the shaft, housing and bearings resulting from shaft induced emf due to:
 - A) unsymmetrical distribution of flux between the poles resulting in a net flux encircling the shaft
 - B) capacitive coupling between windings and the magnetic core in conjunction with the current harmonics.

-Iron Hysteresis Losses-

8. Throughout the magnetic structure due to current harmonics resulting from Chopper action
9. In the pole face due to variation of air gap flux due to slot openings.

-Mechanical Losses-

10. Frictional Losses due to:
 - A) bearings
 - B) brushes
11. Losses due to windage, (or drag)
12. Losses due to ventilation requirements.

In performance calculations involving ripple free DC supplied motors, the term "stray-load" loss is applied to 2a, b, c, d, f, 3, 4, 7 and 9, and is commonly taken as 1% of the output power. This is not an appropriate value to use if current harmonics are present, as shown in Figure 13. It should be noted that these types of losses cannot be either measured (except by other loss elimination) or accurately calculated. The method of dealing with these losses is for the motor designer to incorporate design features which minimize these types of losses. The same approach is true for many of the other loss types, also, such as 2e and 8.

II Joule Losses

1. Load Current Losses

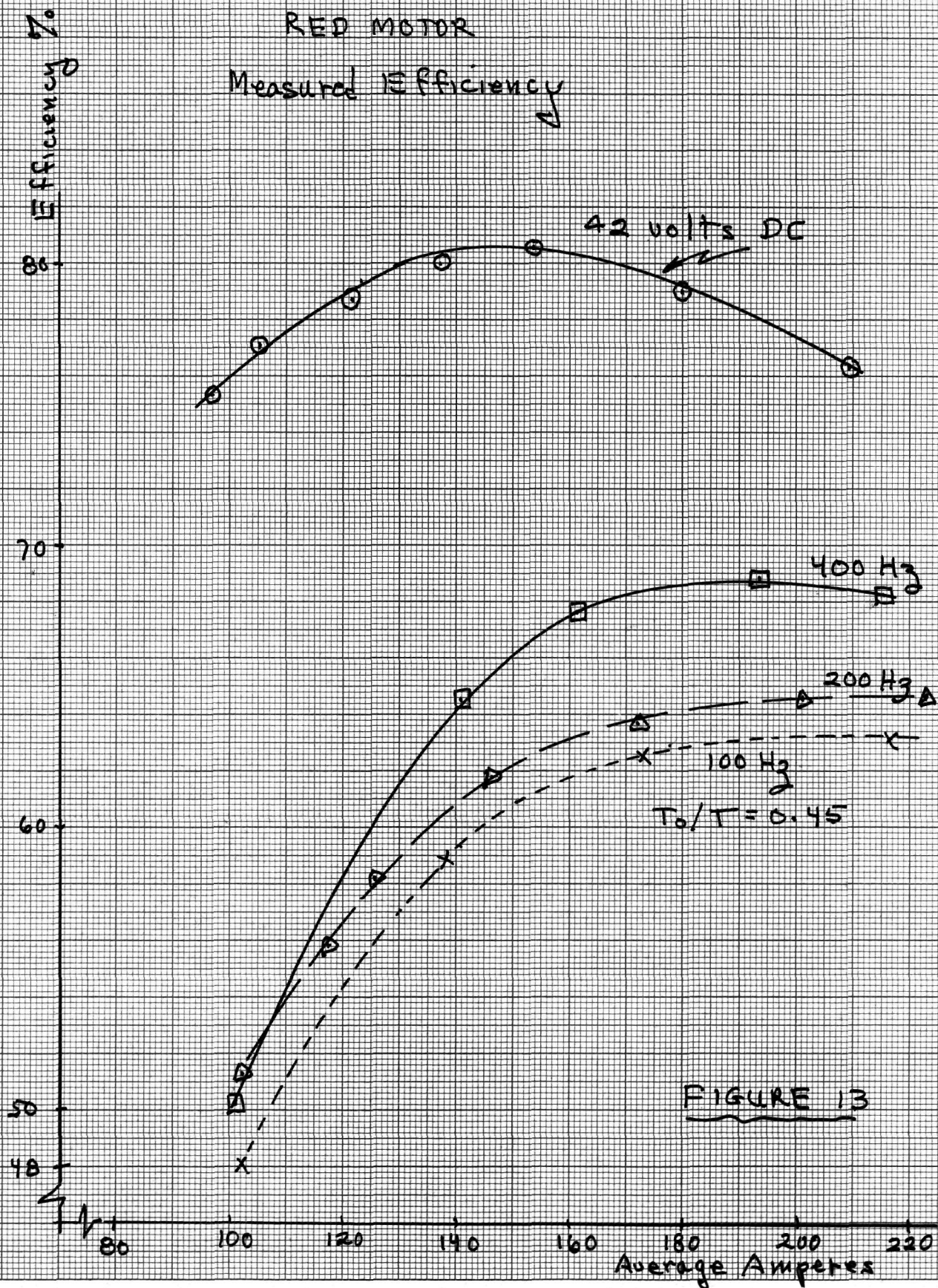
Joule losses occur in the armature and field winding and are typically 3-5% of the rated power output at rated output of the motor, if supplied from ripple free DC. However, if harmonics are present this type of loss is increased substantially due to skin effect and eddy current losses resulting from the current harmonics associated with Chopper action.

It should be noted that even when a motor is supplied from ripple free DC, skin effect in the armature inductors is present, although less than the skin effects resulting from chopper current harmonics. The reason for this skin effect, and steps to take to mitigate it, can be visualized if it is noted that armature inductor current is alternating in nature (prior to commutation) at a frequency:

$$f = \frac{np}{120} \quad (20)$$

where n = rev/m; p = number of poles.

There is a cross slot leakage flux associated with each conductor and the current which flows therein. The slot leakage flux passes across the slot, through the teeth and around the bottom of the slot, as shown in Figure 14.



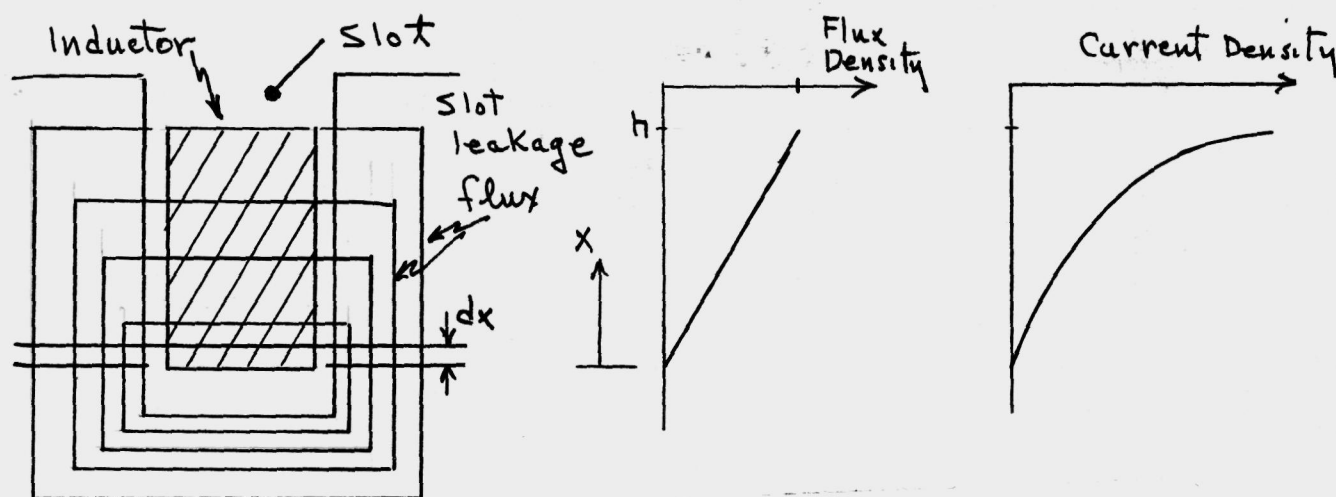


Figure 14. Inductor Skin Effect

Applying Amperes law, it can be seen that the magnetizing force increases as x increases, thus the flux density of the cross flux increases linearly (if $\mu_{\text{iron}} \gg \mu_0$) toward the top of the slot. However, the bottom element (shown as dx) is linked by all of the flux; the uppermost element element by only the flux due to current in that element. Thus, the inductance of the elements decrease with increasing x . The voltage drop in all elements must be the same; therefore, because of the $L \frac{di}{dt}$ voltage drop, the current is crowded into the upper portion of the conductor and the current density is as shown in Figure 14, reaching a maximum at the top of the inductor. Thus, a skin effect phenomena, even with ripple free DC exists. This skin effect can be reduced if multiple strands, insulated from each other are used, since the skin effect increases with the square of the height of the conductor.

The skin effect loss in the armature is estimated⁽¹⁰⁾ at 5-25% of the "DC" chopper loss, based on the DC ohmic resistance, depending upon how finely the inductors are stranded. Formulas for estimating this loss are presented in Section II, 2, c.

APPENDIX D details static tests made to determine the variation of resistance and inductance with frequency. The apparent resistance measured accounts for skin effect in the conductors (loss #1) and for eddy current loss effects due to harmonic currents, loss #2e, but does not account for other eddy and hysteresis effects present when the motor is loaded and running.

Based on R,L tests made on the BLUE and RED motors⁽⁷⁾, (APPENDIX D), it was established that R and L, as functions of frequency and saturation, varied in an identical fashion, for the two motors, although actual values for the motors were different. The curve fit routine (APPENDIX E), applied to the RED motor yielded (with the two field windings in series with the armature) the following apparent resistance and inductance as seen by harmonic currents:

$$R = 0.0167 f^{0.7} I^{-0.07} \text{ ohms} \quad (21)$$

$$L = 3.8 f^{-0.24} I^{-0.063} \text{ mH} \quad (22)$$

(These expressions point up the difficulty of applying a model, consisting of R,L,C components to the analysis of the behavior of the motor when subjected to Chopper control and the resulting current voltage harmonics.

TABLE I presents calculated losses due to observed harmonic currents for conditions of approximately 100 amperes and 200 amperes for Chopper frequencies of 100 and 400 Hz and using the values of apparent resistance measured for those frequencies and currents.

Figure 14 compares the efficiency calculated from test results on the RED motor for conditions of ripple free DC and Chopper controlled at chopper frequencies of 100, 200 and 400 Hz. Efficiencies from these curves are utilized in TABLE I to determine total losses for the conditions presented. Data tabulated includes:

- A) the increase in losses using the Chopper control over the ripple free DC
- B) the calculated sum of the losses due to the harmonic currents
- C) the difference between a) and b), denoted as "non-accounted for increase"
- D) the joule loss due to a ripple free DC current and the measured DC resistance.
- E) in condition A, the values of L and $\omega L/R$ were calculated to verify the near constant ratio discussed in APPENDIX D.

TABLE I (RED Motor, $T_o/T = 0.145$)- Calculated $I^2 R$ Losses -A. - Condition: $T = 0.01$, $f = 100$, $I_m = 103$ amperes, $P_o = 3500$ watts (DC supplied)

<u>I(Harmonic)</u>	<u>f</u>	<u>R</u>	<u>$I^2 R$</u>	<u>LmH</u>	<u>wL/R</u>
29.6	100	.303	265.5	0.94	1.95
4.3	200	.492	9.1	0.8	2.03
5.9	300	.654	22.8	0.72	2.08
2.8	400	.8	6.3	0.67	2.11
3.2	500	.935	9.6	0.64	2.14
1.9	600	1.062	3.8	0.61	2.3
Total			317		

$$I_{DC}^2 R_{DC} = 371 \text{ (calculated)}$$

From Figure 10, 12, For same Pin

$$100 \text{ Hz Eff: } 48.2\%, P_{Loss} = 2367 \text{ watt}$$

$$DC \text{ Eff: } 76.6\%, P_{Loss} = 1069 \text{ watt}$$

$$\text{Increase: } 1298$$

$$\text{- Harmonic Calc: } -317$$

$$\text{non accounted for increase} = 981 \text{ watts}$$

B. - Condition: $T = 0.01$, $f = 100$, $I_m = 201$ amperes, $P_o = 6660$ watts

36.4	100	.289	383.1
6.5	200	.470	19.8
6.6	300	.624	27.2
3.1	400	.763	7.4
3.4	500	.892	10.3
2.3	600	1.013	5.4
1.7	700	1.13	3.3
Total			457

$$I_{DC}^2 R_{DC} = 1414 \text{ (Calculated)}$$

$$100 \text{ Hz Eff: } 63.2\%, P_{Loss} = 3167 \text{ watts}$$

$$DC \text{ Eff: } 77.4\%, P_{Loss} = 1945 \text{ watts}$$

$$\text{Increase} = 1222$$

$$\text{- Harmonic Calc} = -457$$

$$\text{non accounted for increase} = 765 \text{ watts}$$

C. - Condition: $T = 0.0025$, $f = 400$, $I_m = 98$ amps, $P_o = 3393$ watts

11.9	400	.762	107.9
.91	800	1.238	1.0
2.4	1200	1.644	9.5
.4	1600	2.01	0.3
1.5	2000	2.351	5.3
.7	2400	2.671	1.3
Total			125

$$I_{DC}^2 R_{DC} = 336 \text{ (Calculated)}$$

$$400 \text{ Hz Eff: } 49\%, P_{Loss} = 2289 \text{ watts}$$

$$DC \text{ Eff: } 75.6\%, P_{Loss} = 1095$$

$$\text{Increase} = 1194$$

$$\text{- Harmonic Calc} = -125$$

$$\text{non accounted for increase} = 1068$$

D. - Condition: $T = 0.0025$, $f = 400$, $I_m = 208$, $P_o = 6840$ watts

13.9	400	.723	139.7
1.7	800	1.174	3.4
2.4	1200	1.56	9.0
1.3	1600	1.907	3.2
1.1	2000	2.23	2.7
.9	2400	2.534	2.0
Total			160

$$I_{DC}^2 R_{DC} = 1514$$

$$400 \text{ Hz Eff: } 68.5\%, P_{Loss} = 2805$$

$$DC \text{ Eff: } 76.8\%, P_{Loss} = 2066$$

$$\text{Increase} = 739$$

$$\text{- Harmonic Calc.} = 160$$

$$\text{non accounted for increase} = 579$$

For each condition, the observed power output, P_o is shown. Using the DC efficiency, power input is calculated and the losses under Chopper operation are calculated from this same input power and the efficiency from Figure 14.

Observations and Conclusions

i) Efficiency of a conventional motor is sharply reduced when Chopper controlled. The higher the Chopper frequency, the less the reduction in efficiency.

ii) The decrease in efficiency is more pronounced at lower values of average current, because the ripple (and magnitude of the harmonics) is a higher percentage of the average current, I_m . For example, refer to Figures C-11, C-12, APPENDIX C which show an increase of $\Delta i/I_{\text{average}}$ as I_{average} decreases and as frequency decreases.

iii) Chopper control introduces additional losses not accounted for by consideration of harmonic currents and apparent resistance as measured.

2. EDDY CURRENT LOSSES

A. In Armature Due to Distorted Pole Face Flux

Eddy current losses occur in the armature inductors as they pass under the pole face if the flux density is not uniform. Non-uniformity results from the cross field component of armature reaction. The armature mmf is triangular in shape, with zero crossing midway between the brushes. If the brushes are on mechanical neutral, the flux density resulting from the armature mmf can be decreased by increasing the reluctance of the air gap under the pole tips. This is accomplished by designing the arc of the pole face with a radius much larger than the radius of the armature (chamfered pole shape), causing armature and pole face to be non-concentric, with air gap length at the pole tips larger than at mid pole. Another approach, if laminated poles are used, is to have the laminations with only one tip at each pole and stack the laminations such that the tip is in the opposite directions for adjoining laminations. The effect here is to decrease the permeability by decreasing the area of pole tip iron.

The above approaches merely modify (decrease) the magnitude of the loss. The armature reaction effect can be (theoretically) completely suppressed by the use of compensating windings embedded in the pole face.

The magnitude of this loss cannot be ascertained by measurement nor accurately calculated. In a motor operated on ripple free DC, it is estimated⁽¹⁰⁾ to be 0.05-0.06% of the power output in a non-compensated motor and to be negligible

if compensating windings are present. If the motor is supplied from a chopper source, the losses will most certainly be considerably higher because of the pulsations of the armature current due to the Chopper action and resulting harmonics.

Compensating Winding Design

If armature current is to be passed through the compensating winding, the cross sectional area of the compensating winding must be "a" times greater than that of the armature conductors which carry a current of I/a amperes (a is the number of parallel paths in the motor). If Z_c is the number of compensating conductors per pole and the compensating winding is to provide the same mmf as that of the armature:

$$Z_c I_a = \lambda \left(\frac{Z}{P} \right) \left(\frac{I_a}{a} \right) \quad (23)$$

$$\text{or} \quad Z_c = \frac{\lambda Z}{ap} \quad (24)$$

where Z = total inductors
 λ = pole arc/pole pitch

For the BLUE motor, with $Z = 256$, $a = 4$, $p = 4$, $\lambda = 53/90$ and 4 - #15 wire coils,

$$Z_c = 9^+ = 10$$

The cross sectional area required, for Z_c , is calculated as 0.01 square inches. Based on each Z_c equal to three times armature length (4 3/4 inches). This would add 1.83 lbs copper to the weight of the motor.

For the RED motor, $Z_c = 5$, of area 0.023 square inches, yielding an added weight of copper of 1.67 lbs.

The conductor Z_c should be stranded, to reduce eddy current losses. It appears that the increase in efficiency would offset the added weight of the winding.

B. In Armature Due to Tooth Saturation

Eddy losses occur in the armature inductors due to tooth saturation and the main flux. Most DC machines are highly saturated, magnetically, (refer to the nearly linear torque vs. ampere curves, Figures 7 and 9) with the armature teeth being the most saturated. A portion of the main flux passes

through the slots and conductors. As the armature rotates, and a tooth passes under a pole tip, the saturation level changes and the flux linking the conductors changes, eddy currents are induced in the conductors, especially those conductors lying in the top part of the slot, and losses result. The losses have been estimated⁽¹⁰⁾ to be on the order of 10-30% of the copper losses due to armature current in a motor supplied from ripple free DC.

Liwschitz-Garik⁽¹⁰⁾ presents an empirical method of calculating these losses by expressing them as equivalent losses produced by a current flowing in the embedded part of the total winding. The current density, corresponding to this current is:

$$J_m = 16 \frac{hf}{\rho} \left(\frac{B'}{6450} - 16 \right) \text{ amps/in}^2 \quad (25)$$

Where: h = conductor height, inches
 ρ = resistivity, micro ohm inches = 0.825
 $f = \frac{Np}{120}$, N = rev/min, p = # poles
 B' = flux density at tooth root (taken as saturation level \approx 120,000 lines/in²).

Let: K_1 = this loss as a % of DC copper loss at rated current
 J = Current density at rated load
 λ = net core length/1/2 mean turn length

Then:
$$K_1 = \left(\frac{J_m^2}{J^2} \lambda \right) 100 \quad (26)$$

For the RED motor:

$$J = 1448 \text{ amps/in}^2$$

$$\lambda = 0.325$$

$$f = \frac{N}{30} \quad h = 0.31$$

$$J_m = 0.52 N$$

$$K_1 = \frac{1.3}{10^5} N^2 \%$$

For $N = 2000$

$$K_1 = 52\%$$

of rated I^2R loss

$N = 1000$

$$K_1 = 13\%$$

For the BLUE motor, this loss is negligible because of the relatively small height of the conductor (0.057 inches, 18% of height of RED motor conductor) and K_1 is proportional to the square of the height.

Observations and Conclusions

These losses can be mitigated by:

- a. reducing conductor height
- b. using deeper slots (with the top inductors further from the air gap
- c. by using more iron in the motor (less saturation) which will improve the torque/ampere characteristic also but which adds weight and cost to the motor.

C. In Armature Due to Cross Slot Leakage Flux

Eddy current losses are present in the conductors undergoing commutation (current reversal). The current reversal causes the slot cross leakage flux to collapse and then build up in the opposite direction. It is not possible to measure this loss, which is the principle constituent of stray load loss in a motor running on ripple free DC. It is possible to perform an analysis which gives insight into the loss, however.

Liwschilz-Garik⁽¹⁰⁾ and Rudenburg⁽¹¹⁾ present methods of calculating (empirically) the increase in loss, due to eddy current effects in conductors due to cross slot leakage flux. The empirical equations yield different results, as will be shown in this section.

-Rudenburg Method-

(Revised to apply to multiconductors in the slot)

Figure 15 portrays the slot, the conductors and the value of flux density, calculated by Amperes law and assuming the iron is infinitely permeable.

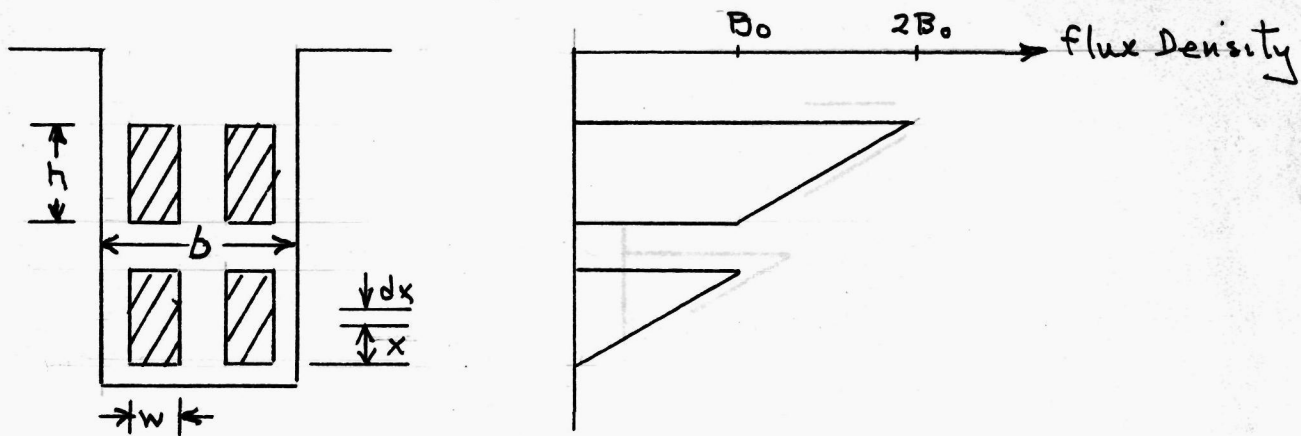


Figure 15. Slot Cross Leakage Flux Density

Rudenburg shows that flux density, B , and current density, J within the conductors are, assuming instantaneous current reversal;

For the Bottom Conductors

$$B = \frac{2}{\pi} B_0 \sum_{n=1}^{\infty} \pm \frac{1}{n} \epsilon^{-\frac{n^2 t}{T}} \sin \frac{n\pi x}{h} \quad (27)$$

$$J = 4 J_0 \sum_{n=1}^{\infty} \pm \epsilon^{-\frac{n^2 t}{h}} \cos \frac{n\pi x}{h} \quad (28)$$

For the Upper Conductors

$$B = \frac{4B_0}{\pi} \left[\epsilon^{-\frac{t}{T}} \sin \frac{\pi x}{h} + \frac{1}{3} \epsilon^{-\frac{9t}{T}} \sin \frac{3\pi x}{h} + \dots \right] \quad (29)$$

$$J = 8J_0 \left[\epsilon^{-\frac{t}{T}} \cos \frac{\pi x}{h} + \frac{1}{3} \epsilon^{-\frac{9t}{T}} \cos \frac{3\pi x}{h} + \dots \right] \quad (30)$$

where: n = harmonic number

$$T = \frac{\mu_o}{\pi^2 \rho} \frac{yw}{b} h^2 \quad (31)$$

w = conductor width, meters

y = number of conductors per layer

b = slot width, meters

h = conductor height, meters

ρ = resistivity, ohm-meter

x = distance from bottom of conductor

$$B_o = \mu_o \frac{2yI}{b} = \frac{2\mu_o}{b} \frac{I_a}{a} \quad (32)$$

$$\text{and: } J_o = \frac{I}{wh} \quad (33)$$

$$\text{if: } I = \text{current per conductor} = \frac{I_a}{ya}$$

I_a = armature current

a = number of parallel paths

The above equations are based on a current collapse from a current of $2I$ to zero, simulating a change from $+I$ to $-I$.

The loss produced by one current reversal can be determined from the initial energy, W , stored in the conductors and slot from consideration of the energy density. (Iron eddy current losses are neglected because the armature iron is laminated.)

$$\text{energy density} = \frac{B^2}{2\mu_o} \quad (34)$$

from which:

$$W = \frac{1}{2\mu_o} \int B^2 dv \quad (35)$$

where dv is the volume element, $\ell b dx$, with ℓ the length of the stack, and B defined based on Figure 15.

$$\begin{aligned}
W &= \frac{1}{2\mu_o} \int_0^h (B_o \frac{x}{h})^2 \ell b dx + \frac{1}{2\mu_o} \int_0^h (B_o + \frac{x}{h} B_o)^2 \ell b dx \\
&= \frac{B_o^2}{2\mu_o} \ell b \int_0^h (1 + \frac{2x}{h} + \frac{2x^2}{h^2}) dx \\
&= \frac{4 B_o^2 \ell b h}{3\mu_o} = \frac{16}{3} \mu_o \frac{\ell h}{b} \left(\frac{I_a}{a} \right)^2 \frac{\text{joules}}{\text{slot}}
\end{aligned} \tag{36}$$

For ripple free DC, the frequency of current reversal will be

$$f = \left(\frac{N}{60} \right) \left(\frac{P}{2} \right) \tag{37}$$

and total joule losses, W_t , is (since W is lost twice each cycle)

$$W_t = 2 f W = \frac{32}{3} \mu_o \frac{\ell h}{b} \left(\frac{I_a}{a} \right)^2 f \quad \text{watts/slot} \tag{38}$$

The "DC ohmic resistance" loss, W_{DC} in 2 y conductors (2 layers of conductors) is: (where k is half the coil length/slot length)

$$W_{DC} = \frac{\rho \ell k}{wh} \left(\frac{I_a}{ay} \right)^2 (2y) k \text{ watts/slot} \tag{39}$$

Of course, the "DC skin effect" due to non-uniform current distribution results in an actual joule loss greater than this value, but insight into the effect can be gained by finding the ratio:

$$\frac{W_t}{W_{DC}} = \frac{16}{3} \frac{\mu_o}{k} \left(\frac{w}{b} \right) \frac{h^2 y}{\rho} f = \frac{16}{3} \frac{\pi f}{k} T \tag{40}$$

where T is the fundamental time constant, equation (31).

Applying the foregoing to the RED motor (Appendix B), for which:

$w = 1.88 \times 10^{-3}$ meter	81 commutator bars
$y = 3$	
$b = 7.63 \times 10^{-3}$ meter	$\ell = 0.096$ meter
$h = 7.9 \times 10^{-3}$ meter	$k = 5.8$
$\rho = 1.67 \times 10^{-8}$ ohm-cm	
$a = 2$ parallel paths	

$$I = \frac{I_a}{2 \times 3} = \frac{I_a}{6}$$

$$T = \frac{\mu_o}{\pi \rho} \left(\frac{yw}{b} \right) h^2 = 0.35 \text{ ms} \quad (41)$$

The motor was tested over the speed range (See Figure 9) 930-2000 rpm, for a current reversal frequency range of 31-67 Hz, or periods of 15-32 milliseconds. Thus, the fundamental time constant, $T = 0.352 \text{ ms}$ is short, compared with the 15-32 ms time to the next commutation of that particular conductor, and the transient slot flux and eddy currents will have decayed prior to the next current reversal.

The validity of the assumption of instantaneous commutation can now be examined.

For 81 commutator bars, the time, t_c , for a bar to pass under a brush and accomplish current reversal will be, at the slower speed;

$$t_c = \left(\frac{1}{81} \text{ rev.} \right) \left(\frac{60}{930} \frac{\text{sec}}{\text{rev}} \right) = 0.8 \text{ ms}$$

and at the higher speed;

$$t_c = 0.37 \text{ ms}$$

These times are on the same order of magnitude as the fundamental time constant. Therefore, the eddy currents will decay within the commutation period and their magnetic fields will follow the reversing current. Thus, the energy will be dissipated in both conductors and in brush-commutator contact resistance⁽¹¹⁾.

For the RED motor, from Figures 9 and 10:

$$I = 200, \quad N = 960, \quad f = 32 \text{ Hz}, \quad P_o = 6640 \text{ watts}$$

$$\frac{W_t}{W_{DC}} = \frac{16}{3} \frac{\pi^2 T f}{k} = \frac{0.018}{5.8} f = 0.099$$

$$I = 100, \quad N = 1940, \quad f = 65 \text{ Hz}, \quad P_o = 3320 \text{ watts}$$

$$\frac{W_t}{W_{DC}} = 0.202$$

The measured DC resistance was 0.0189 ohms. For a 200 amp load;

$$W_{DC} = (200)^2 \times .0189 = 756 \text{ watts}$$

and
$$W_t = (0.099) \times W_{DC} = 75 \text{ watts}$$

which is
$$\frac{75}{6640} \times 100 = 1.13\% \text{ of } P_o.$$

For the 100 ampload

$$W_t = \frac{756}{4} \times 0.202 = 38.2$$

and this is 1.15% of P_o .

Since this loss is the major component of the stray load losses, commonly taken as 1% of P_o for ripple free DC current input, the theory presented here agrees reasonably well with the 1% figure arrived at through elimination of known losses to segregate the overall stray load losses.

When the motor is supplied from a Chopper source, under the assumptions previously made, the effect of the harmonic currents, I_1, I_2, I_3 , etc. of frequency f_1, f_2, f_3 , etc. can be superimposed upon the current of the commutation frequency, using equation (40) to obtain;

$$W_t = \frac{16}{3} \frac{\pi^2}{k} T \left\{ p \frac{N}{120} + f_1 \left(\frac{I_1}{I_{DC}} \right)^2 + f_2 \left(\frac{I_2}{I_{DC}} \right)^2 + f_2 \left(\frac{I_2}{I_{DC}} \right)^2 + \right. \\ \left. + \dots f_n \left(\frac{I_n}{I_{DC}} \right)^2 \right\} I_{DC}^2 R_{DC} \quad (41)$$

This equation neglects the retarding effect on flux build up due to eddy currents in the iron.

Equation (41) was used to calculate W_t for the average current and the additional W_t due to the various harmonic currents for four conditions, i.e. approximately 100 and 200 amperes average and at Chopper frequencies of 100 and 400 Hz. Results are tabulated in TABLE II.

The same calculations were performed for the BLUE motor, yielding a time constant, T , of 0.014 ms (1/25 of the constant for the RED motor) resulting in a negligible ratio W_t/W_{DC} . The reason for the extremely short time constant

TABLE II (RED MOTOR, $T_o/T = 0.45$)- Calculated Loss Due To Slot Cross Leakage Flux, W_t -

(Rudenburg Method)

A. - Condition: $T = 0.01$, $f = 100$, $I_m = 103$, $N = 1770$ rev/mm, $P_o = 2327$ watts

<u>I</u>	<u>f</u>	<u>W_t</u>
104	DC	38
29.6	100	8.1
4.3	200	.34
5.9	300	.97
2.8	400	.3
3.2	500	.5
1.9	600	.2
		<u>48.4</u>

due to chopper harmonics:

$$\% \text{ increase} = \frac{48.4 - 38}{38} \times 100 = 27\%$$

B. - Condition: $T = 0.01$, $f = 100$, $I_m = 201$, $N = 645$ rev/m, $P_o = 5562$ watts

201	DC	52.2
36.4	100	8.0
6.5	200	.5
6.6	300	.8
3.1	400	.2
3.4	500	.4
2.3	600	.2
1.7	700	.1
		<u>62.5</u>

% increase = 20%

C. - Condition: $T = 0.0025$, $f = 400$, $I_m = 98$, $N = 1380$ rev/m, $P_o = 3393$ watts

98	DC	26.5
11.9	400	5.9
.91	800	.1
2.4	1200	.7
.4	1600	--
1.5	2000	.5
		<u>34</u>

% increase = 27%

D. - Condition: $T = 0.0025$, $f = 400$, $I_m = 208$, $N = 632$ rev/m, $P_o = 5659$

208	DC	54.7
13.9	400	1.8
1.7	800	.1
2.4	1200	.2
1.3	1600	.1
1.1	2000	.1
		<u>5.7</u>

% increase = 4%

for the BLUE motor is that the coils are wound with 4-#15 wires paralleled. Each #15 is only 1.447 mm in height, whereas for the RED motor, the conductor height is 7.9 mm, a ratio of 5.5, and the loss effect is proportional to the square of the height.

-Liwschitz-Garik Method-

This method consists of the use of empirical equations for finding the skin effect losses in the conductors due to cross slot leakage flux, commencing with the "depth of penetration" equation:

$$\xi = 0.316 h \sqrt{\frac{wy f}{b \rho}} \quad (42)$$

where: w = conductor width, inches
 y = # of conductors per layer
 b = slot width, inches
 ρ = resistivity of conductor, micro ohm - inches = 0.825

$$f = \frac{N p}{120}, \quad N = \text{rev/m} \quad p = \# \text{ of poles}$$

Find:

$$\sigma = \frac{b_b + (y - 1) \Gamma_c}{\Gamma \left(\frac{D_c}{D} \right) \xi^2} \quad (43)$$

where b_b = brush width, inches
 Γ_c = commutator pitch, inches
 Γ = pole pitch, inches
 D_c = commutator diameter, inches
 D = armature diameter, inches

Find:

$$F = \frac{0.116}{.13 + \sigma} \quad (44)$$

Let: K_2 = skin effect loss as a % of DC copper loss at rated current

λ = core length / 1/2 mean turn length

m = # of layers of conductors in the slot

then:
$$K_2 = \left(\frac{4}{3\pi} m^2 \xi^2 \lambda F \right) 100 \quad (45)$$

K_2 was calculated for the motors with the following results:

RED MOTOR

$$K_2 = 6.7\%$$

$$I_{dc}^2 R_{dc} \text{ loss} = 756 \text{ watts}$$

Skin effect loss = 51 watts

BLUE MOTOR

$$K_2 = 0.39\%$$

$$I_{dc}^2 R_{dc} = 440 \text{ watts}$$

Skin effect loss \approx 2 watts

The value of 51 watts for the RED motor, as calculated here corresponds to W_t calculated for DC current, 200 amperes, conditions B and D, TABLE II, which were calculated by Rudenburgs procedure (modified by this investigator) yielding 52 watts for 201 amperes, 55 watts for 208 amperes.

-Observations and Conclusions-

- i) at light loads, the "stray load" loss, with the chopper increased about 27% over the calculated DC value,
- ii) for the 100 Hz, 200 ampere condition the loss increase was calculated at 20%, whereas for 400 Hz, 200 amperes it was only 4%. The variation is attributable to the fact that the fundamental harmonic current for the 400 Hz condition is only 7% of I_m , whereas for the 100 Hz drive it is 18%.
- iii) since the skin effect is proportional to the square of the height of the conductors, insulated strands built up to necessary conductor cross section are highly recommended for use.

D. In Pole Face Iron Due to Slot Effect

Eddy current losses occur in the pole face by virtue of the variation of the air gap flux density due to slot openings. This loss cannot be measured. However, an empirical procedure for estimating the loss has been developed⁽¹⁰⁾, and the results reproduced here. (This loss phenomena is independent of current variation within the conductors - due only to permeability variations in the air gap.)

In order to determine the magnitude of the flux density ripple, B_o , the ratio of the airgap length corrected for slot openings, etc. is found (the Carter Coefficient, k_c):

$$k_c = \frac{g + (\text{slot width}/5)}{g + (\text{slot width}/5)(1 - \text{slot width}/\text{slot pitch})} \quad (46)$$

where: g = gap length.

$$B_o = k_c \beta B_g \quad (47)$$

B_g is average flux density in the air gap, β is a function of b_g/g and can be determined from Figure 16. (b_g is slot width at the air gap.)

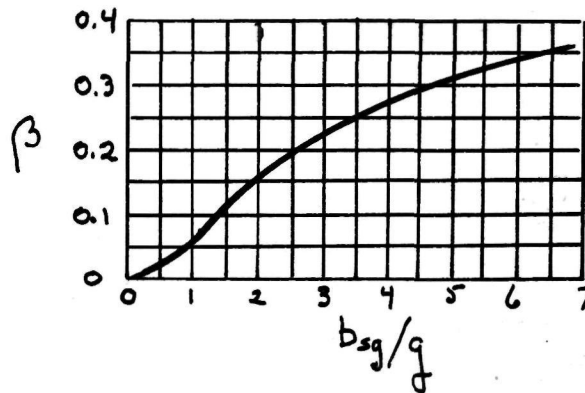


Figure 16. The quantity β as a function of b_{sg}/g

B, the flux density can be determined from

$$E = \frac{Z \phi_p N}{60a} \text{ or } V \frac{T_o}{T} \approx \frac{Z B A_p N}{60a} \quad (48)$$

neglecting armature/field circuit resistance.

The pole face loss is then estimated from

$$\text{Loss} = (p)(A_p) k_s \left(\frac{QN}{1000} \right)^{1.5} \left(\frac{B_o t}{1000} \right)^2 \text{ watts} \quad (49)$$

where: P = # of poles

A_p = area of pole face, inches²

Q = # of slots

N = rev/min

B_o = peak flux density ripple, lines/inch²

t = lamination thickness, inches, or if solid, pole face, it is slot pitch

$k_s = 24 \times 10^{-4}$ for solid steel

$= 6 \times 10^{-4}$ for 0.06" sheet steel

$= 5 \times 10^{-4}$ for 0.04 Dynamo steel

For the RED motor, with 26 gauge (0.018 inches) laminated poles, the loss, calculated using equation (45), 960 rev/m, yields a loss of 0.27 watts, which is negligible.

However, if the poles were not laminated, for the same conditions, the loss would be 593 watts.

-Observations and Conclusion-

This is an insignificant loss if the pole faces are laminated, but would be a major loss if solid poles are utilized!

E. In the Magnetic Circuit Due to Harmonics Resulting From Chopper Action

The apparent resistance increase with frequency⁽⁷⁾ described in APPENDIX D is a measure of skin effect in the conductors, with frequency. There are insufficient ampere turns available in the measurement technique for a series motor to force the harmonic flux throughout the magnetic circuit; thus this loss is not accounted for in the change in apparent resistance detailed earlier.

An attempt to estimate the losses associated with both eddy currents and hysteresis will be presented in Section 8. It is not possible to estimate these losses separately because of lack of data, as separate losses, is not available for the steel used.

F. In Steel Banding Wire Used to Secure the Armature Winding.

This loss is highly dependent upon longitudinal location of the banding, the resistivity of the wire used and the amount of wire used. The loss can be eliminated by using a non-metallic high tensile strength, high modulus of elasticity material, such as Dupont Kevlar, an Aramid which has a high modulus of elasticity (low stretch), very good tensile strength and stability, even at temperatures in excess of 280°C and is, or course, non-conducting.

II 3. Losses In The Equalizer Connection:

In a lap wound (parallel) machine, with p poles, $p/2$ voltage polygons exist. (A voltage polygon is obtained if the phases, representing the amplitude of the emf's of the winding elements, are shifted with respect to each other by an angle corresponding to a slot pitch and arranged in succession in the same order in which they follow one another.) Since it is a parallel winding, the points on the voltage polygon, when the $p/2$ polygons are placed are above the other should coincide. If the pole system is not symmetrical, or if armature bearings are eccentric, the voltages at the points where they should coincide do not in fact coincide. Since some of the points are connected by brushes of the same polarity, circulating currents will flow through the brushes and sparking at the commutator, and some loss, results. The same problem arises if the armature windings are not symmetrical.

Since each two parallel paths make one voltage polygon, the number of winding elements (commutator bars) must, for symmetry, be an integer, i.e.

$$\frac{\# \text{ of bars}}{a/2} = \text{integer} \quad (50)$$

and,
$$\frac{\# \text{ of slots}}{a/2} = \text{integer} \quad (51)$$

Those two conditions must be met for a lap winding for $p \geq 4$. For the simple wave (series) winding, no symmetry requirements (or equalizer winding are required).

The equalizer winding improves commutation but does introduce an un-measurable joule loss in the winding. The BLUE motor does have an equalizer winding. For it,

$$\begin{aligned}\# \text{ of bars} &= 64 \\ \# \text{ of slots} &= 32 \\ a &= 4\end{aligned}$$

Thus, the conditions for winding symmetry are met. However, (refer to Figure B-5, page B-8) the pole system is not symmetrical and thus the equalizer winding is necessary and undoubtedly contributes to joule loss in the motor. The RED motor winding is wave wound (Simplex) and thus does not require an equalizer winding. However, since it has 81 bars, 27 slots it would require an equalizer if it were duplex, or triplex wound ($a > 2$). If the duplex or triplex wave winding is utilized, it must not only satisfy the criteria of equations (50) and (51) but must also fulfill the additional criteria of:

$$\frac{p}{a} = \text{integer} \quad (52)$$

if an equalizer winding is not to be required.

II, 4. Losses in Commutated Coils:

As the commutator segments pass under the brushes, and the direction of current in the coils connected to the segments short circuited by the brush reverses, joule losses occur in the coils. These losses are an unavoidable aspect of DC machines and are minimized if the brushes are on magnetic neutral. If the brushes are not on magnetic neutral, the losses are considerably larger because the short circuited coils have a rotational emf induced in them due to the DC component of flux and a transformer emf induced due to the time varying flux if harmonic currents are exciting the field.

The magnitude of the loss depends on:

- a. the number of turns/coil, and the conductor resistance,
- b. the number of coils shorted (commutator segments shorted by the brush),
- c. the number and position of the brushes,
- d. whether lap or wave wound,

- e. the flux present (excitation current),
- f. the speed of the motor,
- g. the frequency of the harmonic currents.

Refer to Figures B-1 and B-4, APPENDIX B.

The wave wound RED motor brushes span 3 commutator segments; there are 2 pairs of brushes, thus resulting in 6 turns short circuited.

The lap wound BLUE motor, with skewed commutator, has 4 segments shorted by each brush. For the 2 turns/coil, 3 coils shorted and 4 brushes, there are a total of 24 turns shorted.

Since these motors rely on brush shift to achieve satisfactory commutation and location of proper brush shift is not an exact science, it is highly probable that the brushes will not be on magnetic neutral.

To investigate the effects of brush shift, as well as those of speed, average current and frequency effects on this type of loss, several tests were conducted, using the 0-12 Nm torque transducer and 5 Hp drive motor (APPENDIX A). The motor under test was driven over its full speed range, with the field excited at various levels of current, both ripple free DC and Chopper controlled. Since there was no current in the armature, the brushes on 0° (mechanical neutral) corresponds to magnetic neutral. Previously measured brush and bearing friction and windage loss were subtracted from calculated losses to drive the motor under test. That is:

$$P_c = \omega T - P_{rot} \quad (53)$$

where P_c = commutating loss
 ω, T = speed, torque
 P_{rot} = mechanical rotating loss

Figures 17 and 18 depict P_c as a function of speed, series field current and brush position for the BLUE motor, from ripple free DC supply. Figures 19 and 20 show the same information for the RED motor.

For the brushes on magnetic neutral, the losses for the RED motor increase nearly linearly with speed, (for constant current) (Figure 19) whereas theoretically (since $emf \propto \text{speed}$, $P_c \propto (emf)^2$) they should increase by the

BLUE MOTOR

Brushes on Neutral
Armature Open Circuited
Series Field from DC supply
Loss in Commutated Coils

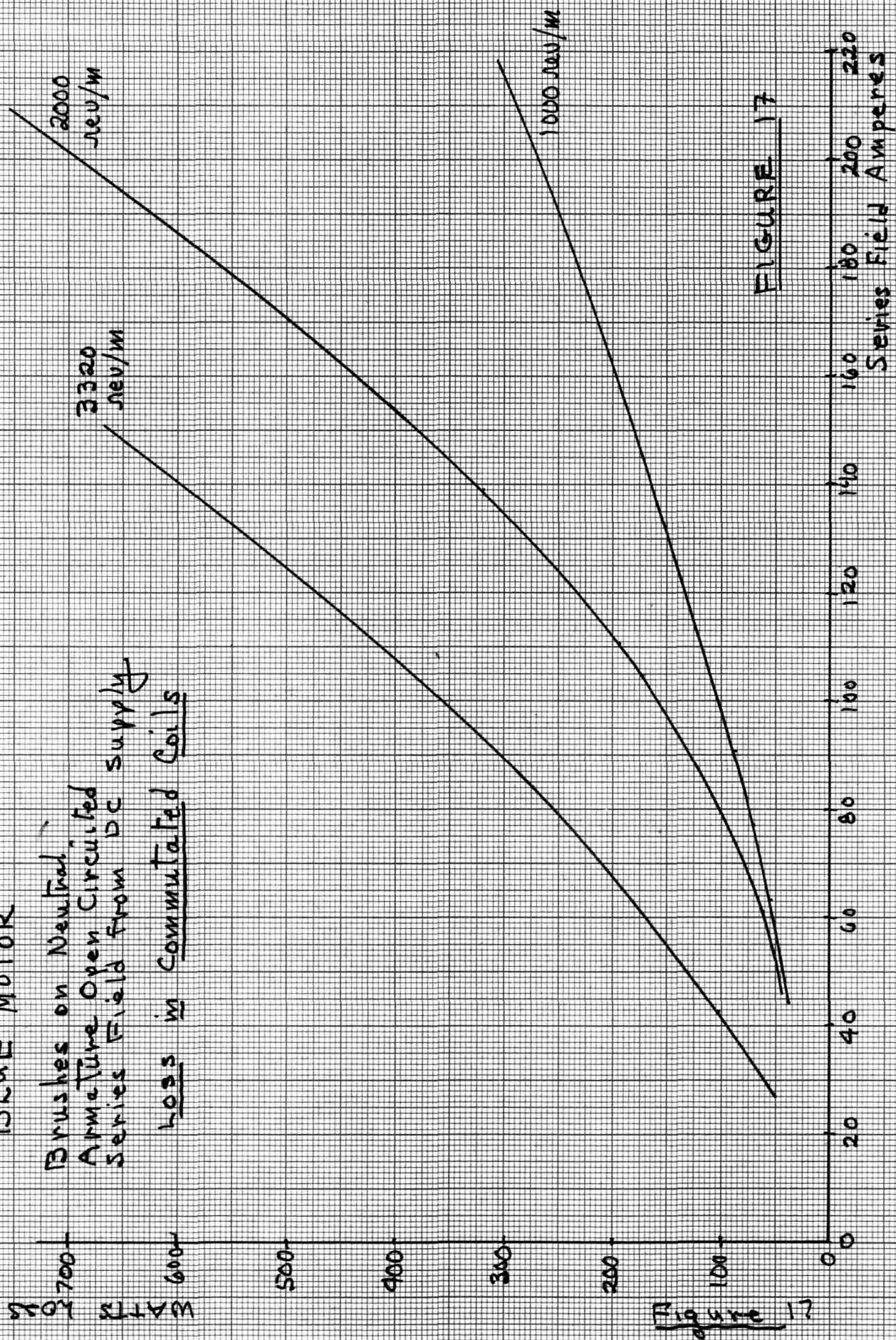


FIGURE 17

Figure 17

BLUE MOTOR

Armature on open circuit
Series field current from DC Gen

Loss in Commutated Coils

WATTS

1400

1200

1000

800

600

400

200

0

0

400

800

1200

1600

2000

2400

2800

3200

3600

rev/w

103 amperes I_f
Brushes Shifted
45° elec.

100 amperes I_f
Brushes on Neutral

FIGURE 18

Figure 18

RED MOTOR

Armature on Open Circuit

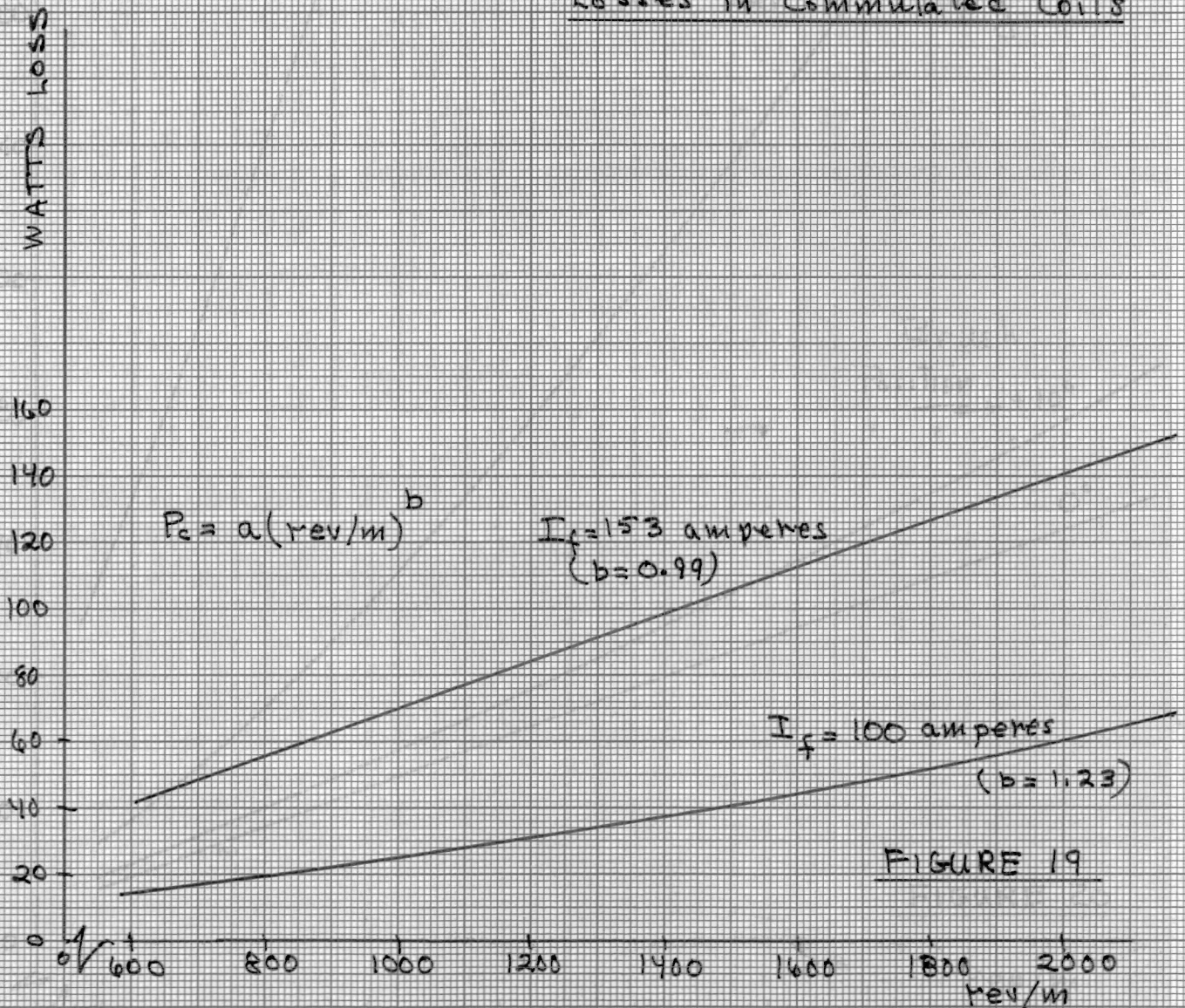
 I_f , Series Field Current from DCGen
 Brushes on Neutral (0°)
Losses in Commutated Coils

FIGURE 19

46 1512

 K&E
 10 X 10 TO THE CENTIMETER 18 X 25 CM.
 KEUFFEL & ESSER CO. MADE IN U.S.A.

Page Intentionally Left Blank

square of speed. For the BLUE motor, the increase with field current is linear at 1000 rpm, but approaches a second order variation at higher speeds. This leads to the belief that the contact resistance between brush and commutator varies with speed and current density. (The motors have different brush material, so the variation is different between the two motors.)

The variation, at constant speed, with field current is less than the theoretical squared value because of saturation of the magnetic circuit.

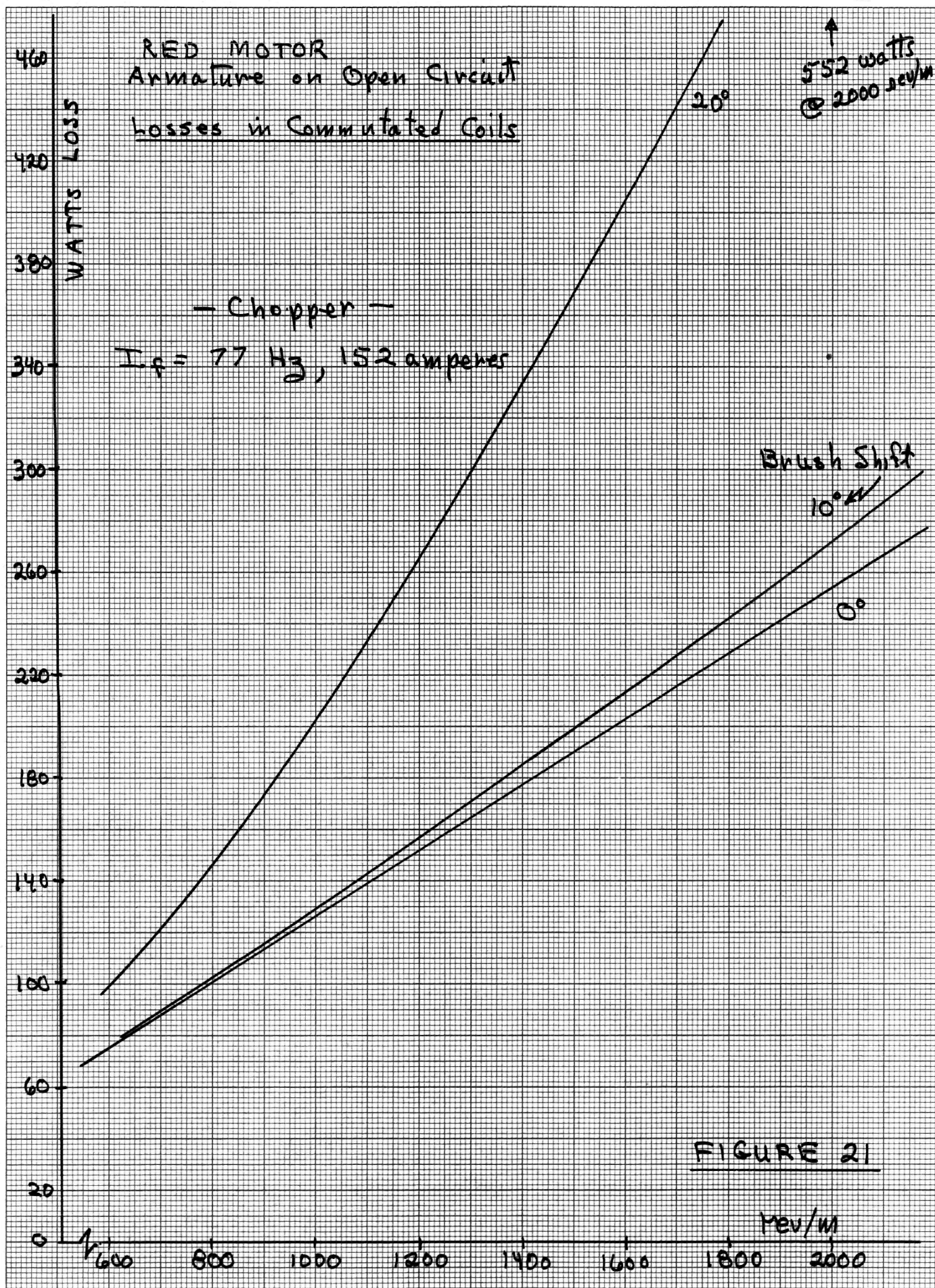
Figures 18 and 20 show the effects of improper brush location. For the RED motor, at 155 amperes, 1400 rev/m, a 10° electrical shift increase the losses by 17% over the 0° loss, whereas a 20° shift increased the losses by 113%. For the BLUE motor, a 45° electrical shift increased the loss at 2400 rev/m, 100 amperes, by 225%.

Figure 21 is similar to Figure 20, except it is for the brush shift effect when the motor is Chopper controlled at a frequency of 77 Hz. Comparison of these two figures indicates about a 75% increase in P_c due to the 77 Hz harmonic currents.

Figure 22 demonstrates a direct comparison between P_c from DC and from 77 Hz operation, with the brushes on magnetic neutral.

For the RED motor, on DC, at 155 amperes, 42 volts, 1250 rev/m, the total losses were observed to be 1318 watts. From Figure 20, at 1225 rev/m, $P_c = 90$ watts. This is 7% of the total loss. Under Chopper Control, at 77 Hz, under the same current/speed condition, total losses are 3207 watts, with $P_c = 156$, which is about 5% of the total loss.

Figure 23 depicts the variation of P_c as a function of speed and Chopper frequency for two levels of field current for the BLUE motor. As can be seen, P_c increases, for the same field current, with an increase in Chopper frequency. It appears that, for a given speed and current (average), P_c increases proportional to approximately the 0.5 power, rather than linearly as it theoretically should if the harmonic current magnitudes were equal. However, as shown in APPENDIX C, the relative harmonic magnitudes decrease with increasing frequency; thus P_c does not increase directly with frequency.



RED MOTOR

Armature on Open Circuit

Losses in Commutated Coils $I_f = 153$ amperesBrushes on 0° (magnetic neutral)

$$P = a(\text{rev/m})^b$$

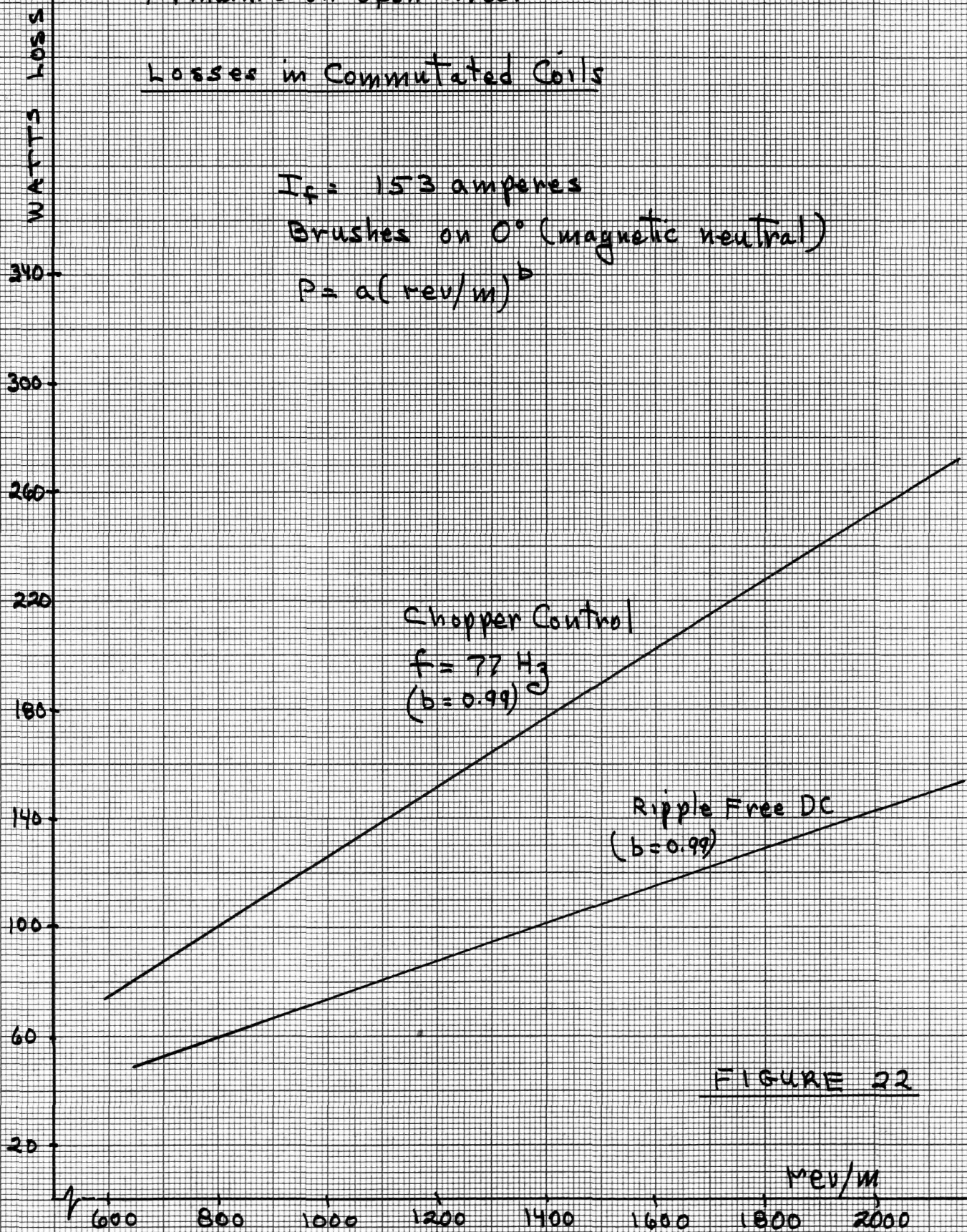


FIGURE 22

BLUE MOTOR

Armature on Open Circuit

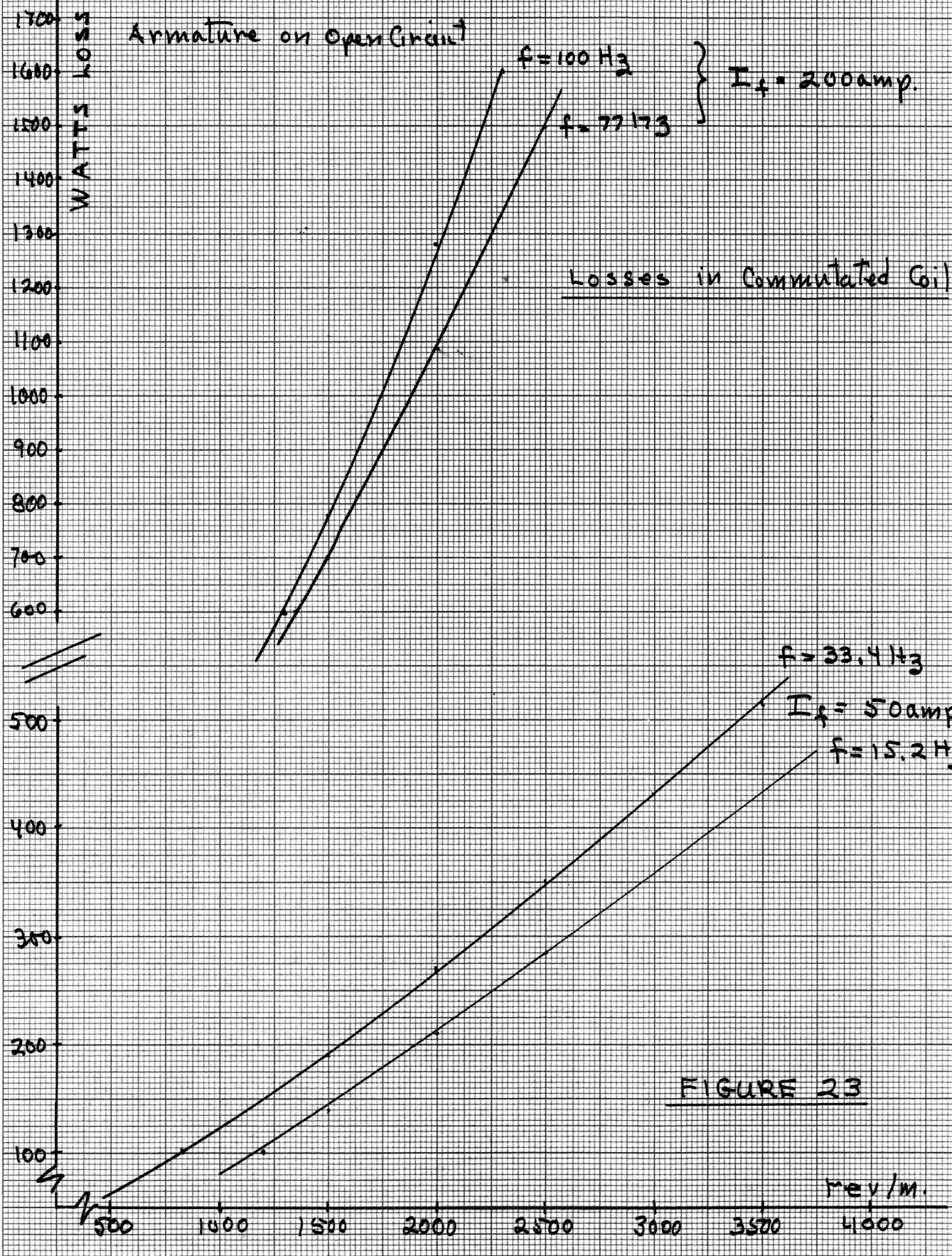


FIGURE 23

- Observations and Conclusions -

The loss in the commutated coil can be a substantial portion of the total losses in the motor, if the brushes are improperly located and if the Chopper repetition frequency is relatively high. The loss magnitude is very sensitive to brush position--if such position is off by more than 10 - 15 electrical degrees. In an Electric Vehicle, without interpoles, operation in reverse will result in brushes off magnetic zero by an angle of 60 - 90° and may cause overheating due to excessive losses.

This loss can be reduced by decreasing the number of turns shorted during the commutating process. This is accomplished by using a wave winding and/or increasing the length of the commutator which permits narrower brushes while retaining the same brush cross sectional area.

II, 5. Loss Due to Brush Resistance

Some brush resistance is essential for the commutating process. The basic equation of commutation is:

$$\frac{I_a}{a} \geq \frac{\text{Reactance Voltage} - \text{Commutating emf}}{R} \quad (54)$$

where: Reactance voltage = rotational emf in the coil due to armature cross magnetizing flux plus the induced emf due to self and mutual inductance and changing current

Commutating emf = rotational emf due to interpole flux or flux resulting from brush shift

R = contact resistance between commutator segment and brush plus internal brush resistance

By establishing the commutating emf to the proper value, minimum R can be utilized, i.e. brush material yielding minimum contact drop and internal brush resistance (low resistivity).

One of the motors tested was known to have electrographitic brushes. The motors had measured voltage drops of 0.5 and 0.53 volts, indicating that they were both probably equipped with electrographitic brushes.

Electrographitic brushes are composed of amorphous carbon material subjected to high temperature to obtain a more graphitic structure. Also available are metal-graphite brushes, made from natural graphite and finely

divided metal powders (copper, silver, etc.) Both materials yield low (below 0.22) coefficients of friction. However the metal graphite brush, with silver can yield an internal resistivity two orders of magnitude lower than that of the electrographitic brush and is recommended for applications such as these motors, i.e. relatively high current, low voltage, with minimum losses.

For the BLUE motor, at rated output (200 amperes) the brush loss amounts to 106 watts. This can not be reduced below some minimum value, but any reduction does improve efficiency and reduces heating at the commutator surface.

II, 6. Losses Due to the Free Wheeling Diodes (FWD)

The controller used in this investigation had two FWDs, one paralleling the armature only and the other paralleling the armature and the two series connected series fields. In tests made in the running mode, the former diode carried no measureable current. The tests were made on the Red motor, with brushes at -28° at frequencies of 100, 200, and 400 Hz.

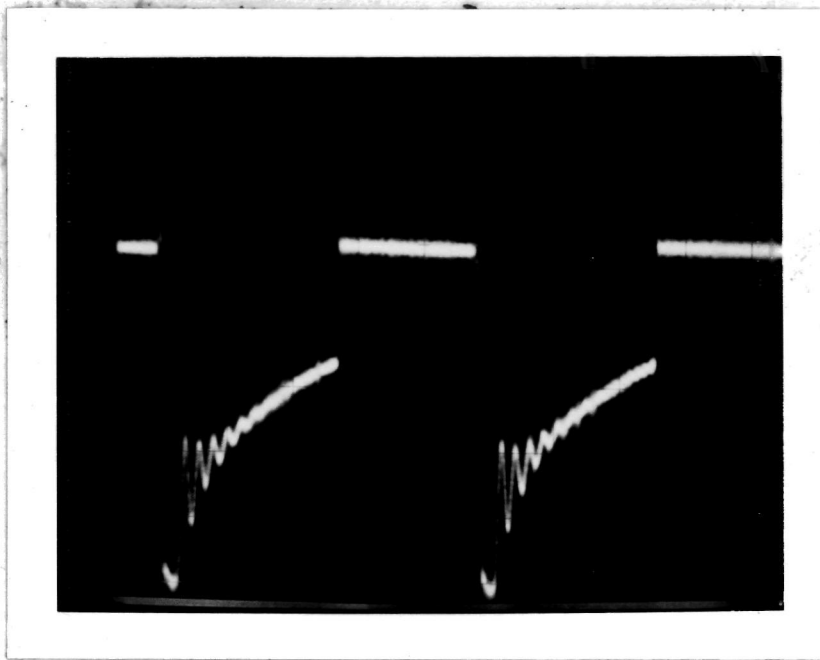
Observed results for the latter diode are tabulated in TABLE III.

TABLE III

$\frac{T_o}{T}$	freq- uency	I_{motor} Ave	I_{diode} Ave	I_{diode} peak	I_{diode} min	$\frac{\Delta i}{I_p - I_{\text{min}}}$	$\frac{I_d}{I_m}$	RPM
0.43	100	193	86.5	265	91	173.5	0.449	800
0.48	200	189	85.5	259	118	141	0.452	800
0.48	400	199	93.1	221	129.5	91.5	0.467	800
0.43	400	109	55.8	123.5	70.6	53	0.514	1500

Power dissipated in the FWD was measured as 74 watts, at 86.5 amperes, average, yielding an average voltage drop, across the diode, of 0.86 volts.

In each of the above runs, a pronounced 1100 Hz oscillation was evident. Figure 23 is typical of the diode currents observed.



Diode Current

2 ms/cm.

50 amperes/cm

Condition:

100 Hz

$$\frac{T_o}{T} = 0.43$$

Figure 24 FWD Current

The only use of the armature-only FWD is in the event power plugging is to be used for braking or in the event the car started rolling backward when connected for forward operation.

II, 7 Losses Due to Shaft, Bearing Housing Current From Shaft Induced Emf.

An emf can be induced in the motor shaft because of an unsymmetrical distribution of flux between the poles, which results in a net flux encircling the shaft and/or capacitive coupling between windings and the magnetic core in conjunction with current harmonics.

Large machines, with pedestal type bearings usually have one pedestal insulated from the machine base to preclude the damaging effects to the bearing surface that result if such currents exist. Small machines generally do not experience this problem. However, in the course of this investigation it was felt that it would be desirable to quantitatively examine the magnitude of the parameters to determine if a significant loss was present due to the phenomena.

The BLUE motor, with non-symmetrical pole geometry (see Figure B-5, page B-8) was the motor tested. This motor has a laminated magnetic frame clamped between aluminum end bells. The bearing at the end opposite the commutator was replaced by a thinner, smaller diameter bearing surrounded by an insulating material, thereby "opening" the closed conducting path formed by armature, shaft, bearings and frame (housing). An electrical connection was then made between the frame and shaft (via a slip ring) across the insulated spaces between bearing and housing. A Kelvin Bridge measurement indicated 0.760 ohms resistance existing between the two points. (The contact resistance between laminations probably accounts for this relatively high value of ohmic resistance).

The motor, with armature circuit open, was then driven over the speed range from 500 to 1650 rev/m. with no field excitation. The DC voltage measured (with a high input impedance electronic digital voltmeter) ranged from 1.0 mv to 2.3 mv. A true rms voltmeter indicated from 215 mv at 500 rev/m up to 650 mv at 1650 rev/m. Background noise, i.e. at zero speed, was measured at 0.05 and 7.5 mv, respectively.

At 1650 rev/m., with ripple free DC current applied to the series field (over the range 52 amperes up to 187 amperes, the DC volts fluctuated from 1-5 mv, the true rms voltage from 700 to 820 mv.

The test was then repeated using a 100 Hz repetition rate chopper current for field excitation. No apparent difference in induced voltage magnitude using chopper current rather than ripple free DC voltage was noted.

- Observations and Conclusions -

Even in a motor with unsymmetric pole structure, this type of loss is negligible and should not be of concern from an efficiency stand point.

III Iron Hysteresis Losses

8, In the Magnetic Structure Due to Chopper Harmonics

The series field current contains harmonics due to Chopper control. The harmonics do provide excitation resulting in harmonic flux which does result in core loss (hysteresis and eddy current). This loss cannot be calculated with any degree of accuracy but overall magnitude can be estimated.

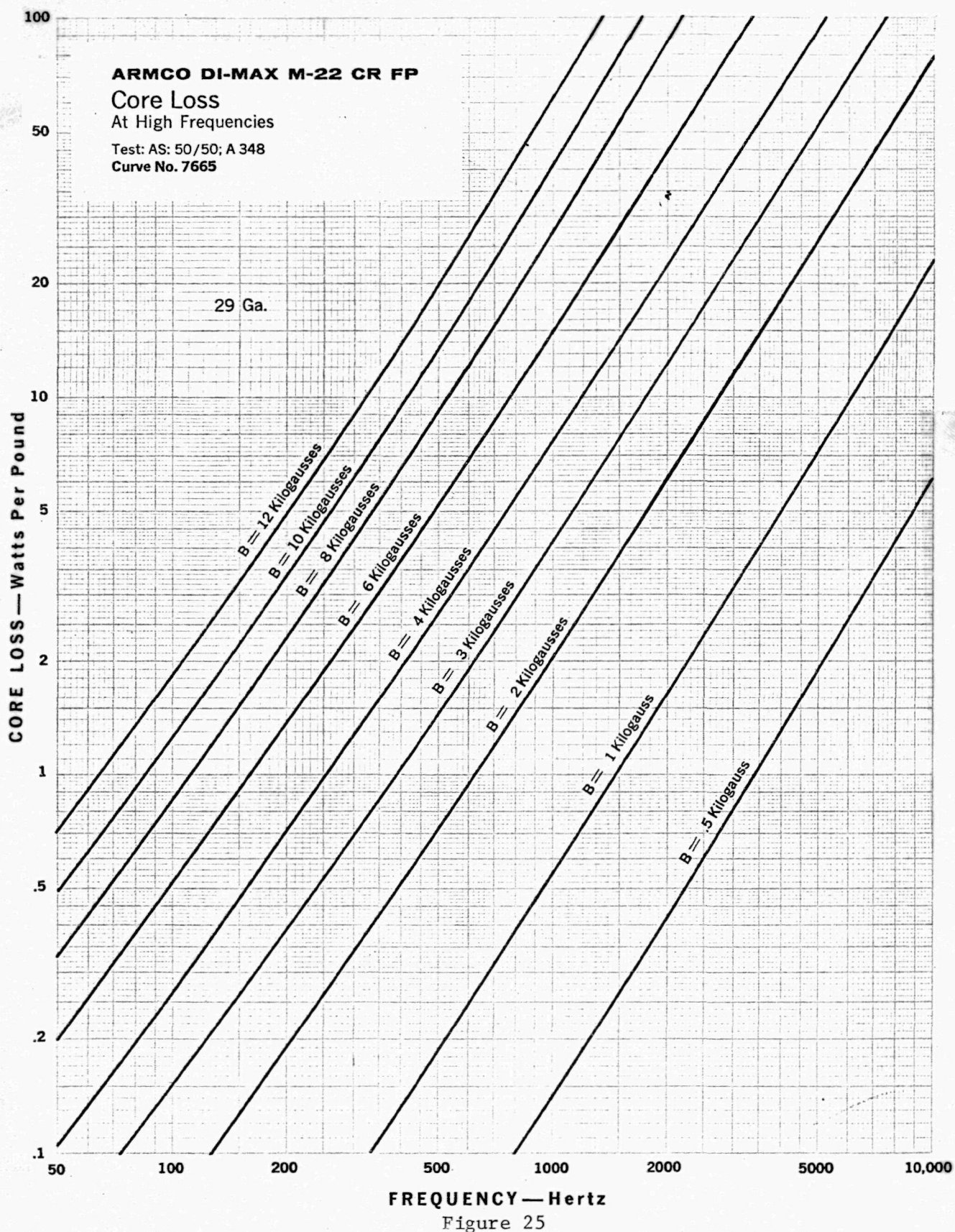
Refer to Figures C-8,9, APPENDIX C. This data shows that the fundamental harmonic is the predominate harmonic and can be used for estimating the harmonic current core loss.

Figure 25 is reproduced from the Armco Nonoriented Electrical Steel Manual and presents Core Loss data as a function of flux density and frequency for 29 gauge, M-22 steel, which is a little thinner than is normally used for motors, but it can be used for estimating purposes.

The iron in the magnetic path of the Blue motor is estimated to weigh 115 lbs. Flux density is estimated (average) at $1.0 \text{ Weber/meter}^2$ (10 Kilogauss) at 100 amperes average current. From Figure C-9, at 100 Hz chopper repetition rate, the fundamental harmonic is approximately 40 amperes rms, yielding a resulting flux density of 0.4 Kilogauss.

As seen from Figure 25, this represents an insignificant loss total. Again, from Figure C-9, as frequency is increased, the magnitude of the fundamental harmonic currents decrease with increasing frequency. For example, the 400 Hz fundamnet is approximately 1/3 of that of 100 Hz. It should be noted that the BLUE motor has a laminated frame.

If the machine has a solid frame, as does the RED motor, the hysteresis (and eddy current) losses could be substantial. Figure 26a depicts the flux lines in the RED motor, with solid frame and Figure 26a is a plot of the same motor, except eddy currents are not allowed to exist (ideal laminated frame). These plots^(10,11,12) were obtained using a finite element analysis.



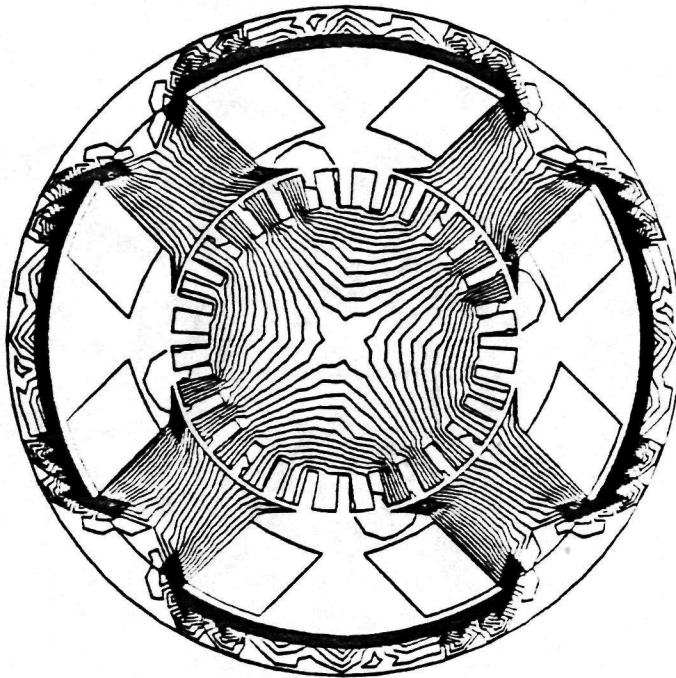


Figure 26a **Solid Frame**

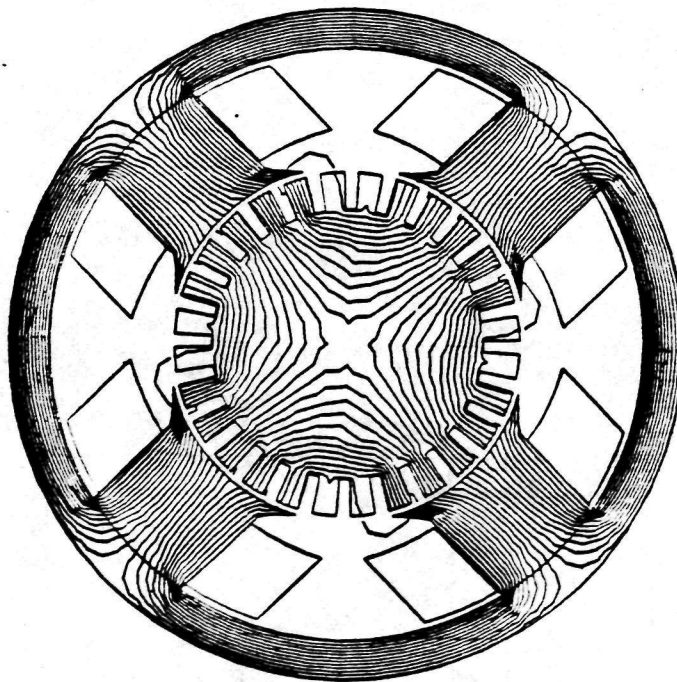


Figure 26b **Laminated Frame**

9, In the Pole Face Due to Variation of Flux Due to Slot Openings

Based on the estimates made in 8, above, it can be concluded that this loss is negligible also, if laminated poles are used.

-Observation and Conclusion-

In a machine with high grade, relatively thin laminations, for armature, poles, and frame these are negligible losses (8,9). However, they will be significant in a solid frame.

IV Mechanical Losses

10, 11 Bearing and Brush Friction and Windage

These losses include brush friction, bearing friction and windage. Total mechanical losses can be obtained by measuring the power necessary to drive the armature with zero excitation on the machine, then raising the brushes and again measuring the power as speed is varied. The latter yields the bearing friction and windage; the difference between the two power requirements yields brush friction.

Bearing friction and windage cannot realistically be separated by measurement, although empirical equations for these quantities are available. For example, the power required for bearing friction, P_T , is empirically given as:

$$P_T = K(\text{rev/m})^{5/3} \quad (55)$$

where K is a constant dependent on bearing dimension and loading.

Windage power, P_ω , is theoretically:

$$P_\omega = \pi C_d \rho R^4 \omega^3 \ell \quad (56)$$

where:

R = radius

ℓ = length

ρ = air density

ω = speed

C_d = skin coefficient

and:

$$\frac{1}{\sqrt{C_d}} = 2.04 + 1.768 \ln (R_e \sqrt{C_d})$$

where R_e = Reynolds number.

This equation represents turbulent flow conditions. The difficulty in applying this is determination of R_e for the complex geometry of armature, with slots, poles and gaps. The only usefulness of the equation is in noting the variation of P_ω with R , ω . It should be recalled that for a given speed, power rating of a motor is proportional to $R^2 \omega \ell$. Thus to attempt to decrease P_ω by decreasing R or ω would be counter productive. The only reasonable design steps to be taken are to reduce surface irregularities on the armature (slots, end connections) as much as possible and to use highest quality bearings.

Calculation of power loss to overcome brush friction, P_b , is suggested in IEEE Std #113⁽¹⁾ as

$$P_b = K v A \quad (57)$$

where $K = 0.004$ for carbon, graphite and electrographitic brushes

$= 0.0025$ for metal graphite brushes

v = surface velocity, meters/min.

A = brush area, square centimeters

Calculated values are:

<u>BLUE MOTOR:</u>	$A = (8)(5.04) = 40.32 \text{ cm}^2$
(2000 rev/m)	$v = (.327)(2000) = 654 \text{ meter/min.}$
	$P_b = (0.004)(40.32)(654) = 105 \text{ watts}$
<u>RED MOTOR:</u>	$A = (8)(4.16) = 32.28 \text{ cm}^2$
	$v = (.400)(2000) = 800 \text{ meter/sec}$
	$P_b = (.004)(32.28)(800) = 103.3$

Figures 27 and 28 depict the results of measurements taken on the RED and BLUE motors. The bearing friction loss, P_r , and the windage loss, P_ω are plotted as $(P_r + P_\omega)$ and also total rotating losses, P_r are shown as functions of speed. The difference between these two is the brush friction loss, P_b . As can be seen, the brush friction power loss is linear with speed. However, at 2000 rev/m, measured values are

BLUE motor, $P_b = 180$ watts

RED motor, $P_b = 440$ watts

It can be concluded that the IEEE formula does not give accurate results, at least for these motors.

The measured brush pressure on the RED motor brushes was found to be 7 psi, vs. 3.8 psi on the BLUE motor (usually brush pressure is approximately 4 psi). This may have been an attempt to secure low contact voltage drop across the brush-commutator surface for the RED motor. However, it appears unproductive in that $V_b = 0.050$ for the RED motor vs. 0.053 volts for the BLUE motor. At 200 amperes, this is a reduction of only 0.6 watts.

In order to verify the effect of brush pressure contributing to the higher rotating losses of the RED motor, calculations were made to determine the coefficient of friction for each, using brush area, commutator radius and brush pressure.

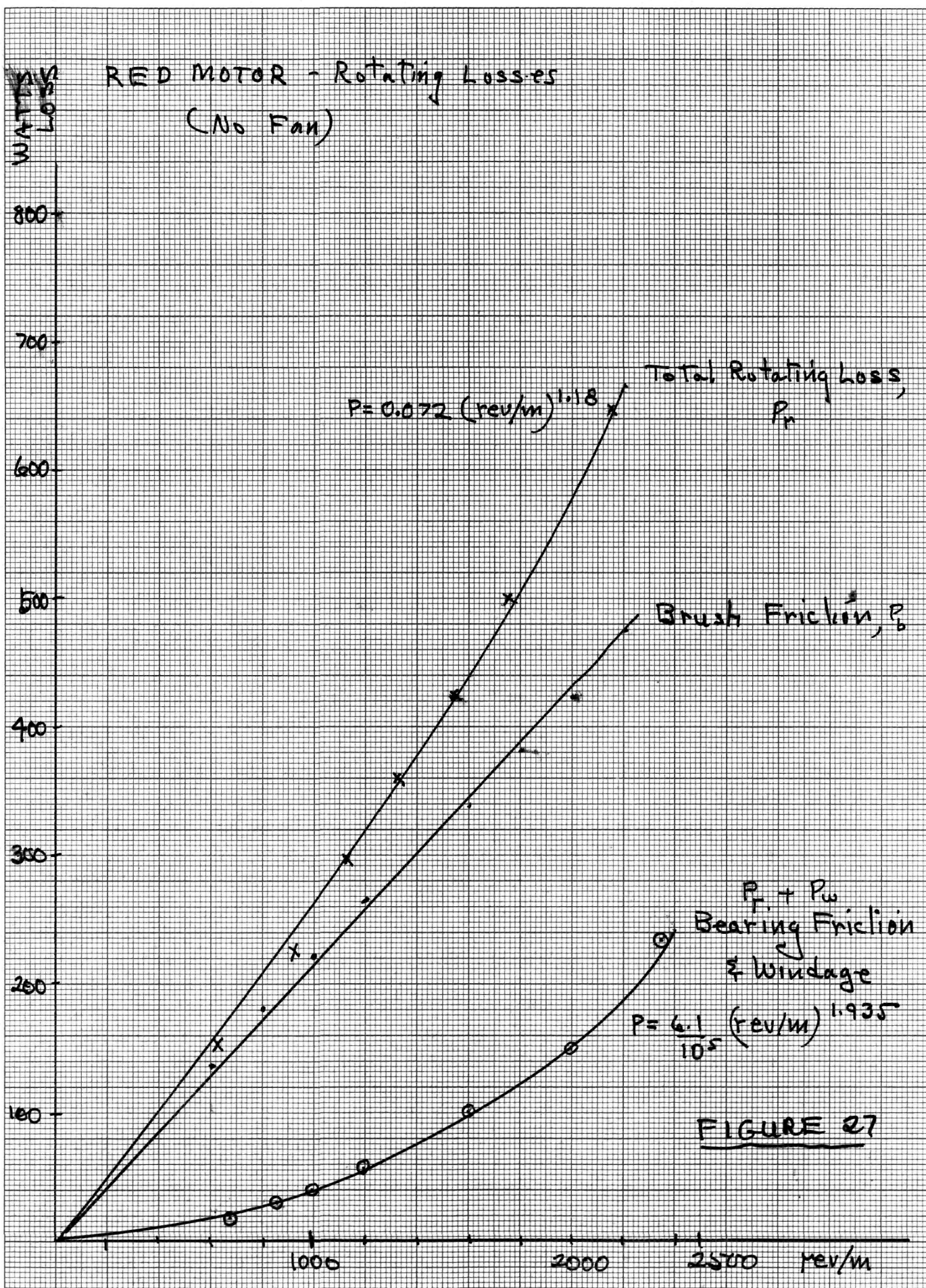
The coefficients obtained were

BLUE Motor $\mu = 0.19$

RED Motor $\mu = 0.22$

Low friction electrographitic brushes are so classified, generally, if $\mu < 0.22$; thus it appears that the added rotational losses of the RED motor are due to high brush pressure.

Using the power curve routine (APPENDIX E) the following empirical relationships were obtained:



BLUE MOTOR - ROTATING LOSSES

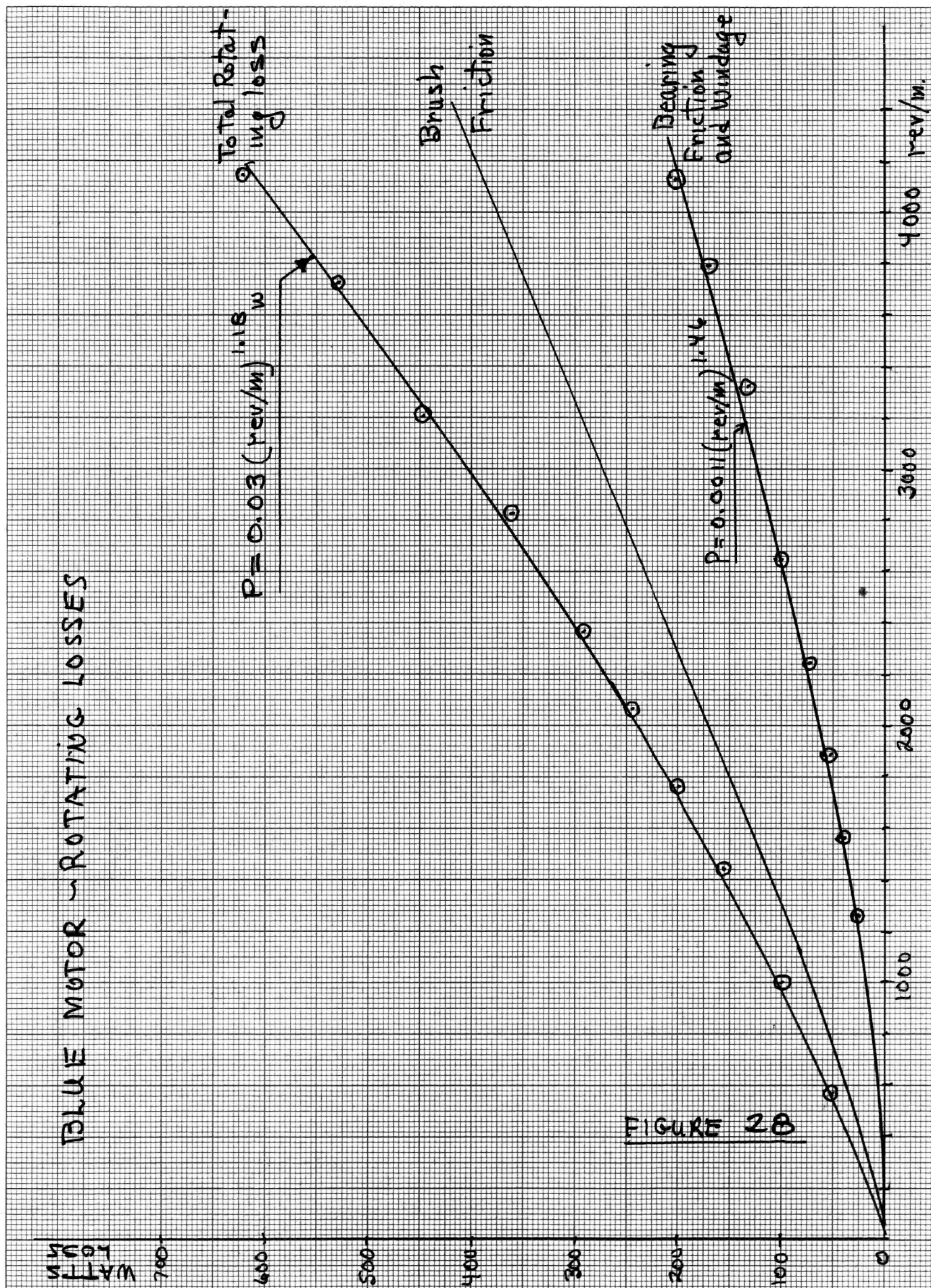


FIGURE 2B

BLUE Motor

$$(P_r + P_\omega) = (0.0011)(\text{rev/m})^{1.46}$$

$$P_{\text{rot}} = (P_r + P_\omega) + P_b = (0.03)(\text{rev/m})^{1.18}$$

RED Motor

$$(P_r + P_\omega) = \left(\frac{6.2}{10^5} \right) (\text{rev/m})^{1.935}$$

$$P_{\text{rot}} = (P_r + P_\omega) + P_b = 0.074 (\text{rev/m})^{1.18}$$

It is interesting to note that total mechanical rotating losses vary to the same power for both motors.

To evaluate the % loss mechanical losses comprise, at maximum load, i.e. 200 amperes on ripple free DC:

BLUE Motor (1635 rev/m, $P_r = 202$)

$$\frac{P_r}{I^2 R} = 0.167; \quad \frac{P_r}{P_{\text{out}}} = 0.03$$

RED Motor (965 rev/m, $P_r = 280$)

$$\frac{P_r}{I^2 R} = 0.198 \quad \frac{P_r}{P_{\text{out}}} = 0.042$$

At lighter loads, i.e. 100 amperes

BLUE Motor (2260 rev/m, $P_r = 290$)

$$\frac{P_r}{I^2 R} = 0.96 ;$$

$$\frac{P_r}{P_{out}} = 0.094$$

RED Motor (1940 rev/m, $P_r = 570$)

$$\frac{P_r}{I^2 R} = 1.6$$

$$\frac{P_r}{P_o} = 0.17$$

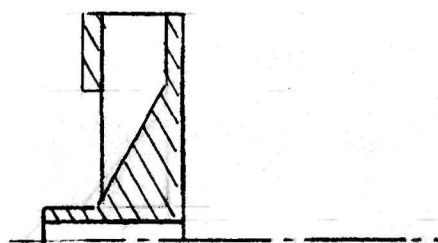
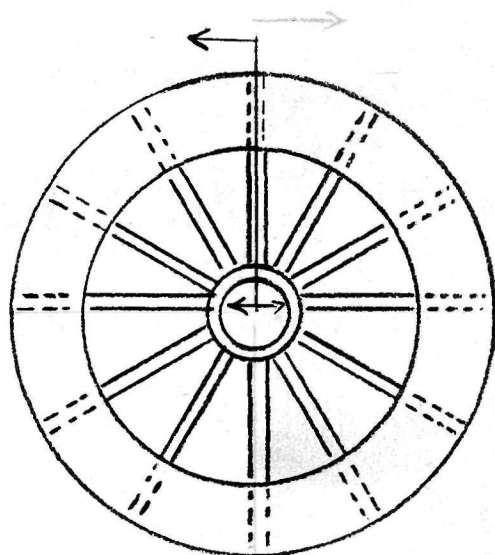
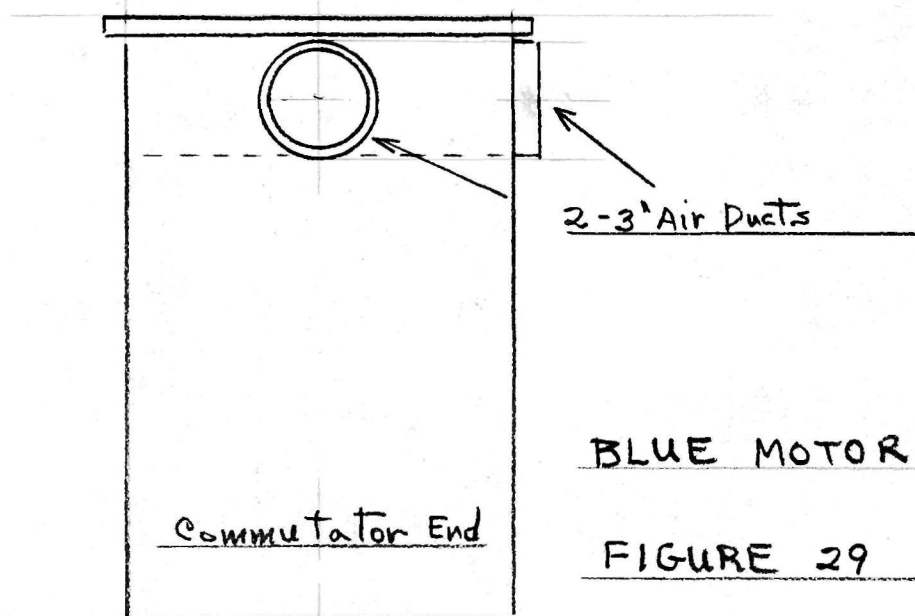
This indicates that total rotating losses play a very important role in motor efficiency at lighter loads, where EVs cruise! Attempts to secure low brush voltage drop by large brush pressure should be carefully evaluated against increased friction losses resulting.

IV, 12. Ventilation Losses:

The BLUE motor requires external ventilation, ("of not less than 250 cfm air flow"). It has two three inch ports for entrance and egress of cooling air. These openings are in the end opposite the commutator end and are spaced 90° apart, as shown in Figure 29. At the commutator end, the four brush rigging access openings are provided with a metal cover which prevents air from being discharged through the openings. Therefore it appears the manufactured intended air to enter one port; discharge out the other.

However, examinations of the two ports and their location with respect to the non symmetrical pole spacing (see Figure B-5, APPENDIX B, page B-8) indicates that one port is directly over an opening of only 0.75 in.², the other over an opening of 8.6 in.² (the word opening referring to interpolar area, and providing a passage down to the opposite end, where the commutator is located.) In addition, the two ports are connected by, in effect, paralleled 3 inch diameter flow areas (area between the end of the armature and the end bell of the housing). This appears to be a very poor ventilation arrangement in that if the commutator access panels are in place and one port is for entrance air, the other for egress air, little or no ventilating air will flow over the armature, across the commutator and return. Instead, it will divide through the paralleled 3 inch diameter flow areas. Thus it seems only proper to duct external air into the two 3 inch diameter parts and let it flow to the opposite end, across the armature, thru the interpole area and egress through the brush/commutator access openings, with cover removed.

IEEE 113⁽¹⁾ provides the following formula for calculation of power necessary to provide ventilation as follows:



RED MOTOR

FIGURE 30

$$P = \frac{0.117 Qp}{\eta} \quad \text{watts} \quad (58)$$

where: Q = volumetric flow, cubic feet/min. (cfm)

p = pressure, in inches of water

η = blower efficiency.

In order to determine p as a function of Q an air blower, driven by a shunt wound DC motor was ducted to an air manifold. The motor speed was varied and air velocity through a known cross sectional area duct was measured. Also, motor speed, input amperes and armature voltage were measured. The motor shunt field was maintained constant. The first run was made with the manifold exhausting to the atmosphere. Input power minus the loss across the brushes, the joule loss in the armature, and frictional losses and the volumetric air flow (calculated from the air velocity and duct cross sectional area) were used in equation (58) to obtain the ratio p/η for the blower, duct and manifold. The procedure was repeated for the second run, during which the manifold was further ducted into the air entrance ports on the motor and exhausted to the atmosphere through the brush access openings.

Armature resistance was determined by Kelvin Bridge measurements. The brush drop was assumed to be 2 volts and the mechanical friction (and motor windage loss) was estimated to be 5% of rated motor output (1.5 Hp) at rated speed (3600 rev/m.) and, proportional to speed.

The values of p/η as a function of flow, Q , for the two runs were plotted and the difference between the values yielded the value of p/η for the motor pressure and blower efficiency, yielding:

$$\left(\frac{p}{\eta}\right) \cong (0.04)Q \quad (59)$$

from which the power requirement for ventilation, for the BLUE motor is calculated as (from equations (58) and (59):

$$P = (0.117) (0.04) Q^2 \text{ watts} \quad (60)$$

yielding $P=292.5$ watts at 250 cfm flow, for the BLUE motor and the blower used. (Estimated blower efficiency, 70%). For a 70% efficient blower, the pressure drop across the BLUE, motor is, from equation (59), 7 inches of water (0.25 psia), at 250 cfm.

The RED motor had an integral die cast aluminum axial flow air pump as shown in Figure 30. This fan was located on the shaft end opposite the commutator. It sucks air in over the commutator thru 0.025 square meters (39 in.^2) of louvred openings. The air is pulled to the opposite end and discharged thru the same cross sectional area of vents covered by 1/4 inch mesh screen. The fan was damaged as it was removed for the friction and windage test and thus could not be tested for actual loss. Since the axial vanes are "non swirled", and the fan casting is not polished, i.e. with a rough surface, the fan efficiency is estimated to be in the 50-55% range.

A formula⁽¹⁹⁾ used for calculating theiretical pressure drop across electrical machines is:

$$P = \left(\frac{Q}{4030 K A} \right)^{1/2} \text{ inches of water} \quad (61)$$

where: A = flow cross sectional area, ft.^2

K = contraction coefficient

$$0.5 < K < 0.9$$

The BLUE motor has a flow cross sectional area of 0.13 ft.^2 , taking $K=0.5$ yields:

$$P = 0.91 \text{ inches of water}$$

compared with the measured valve across the manifold and inlet ducting of 7.0 inches of water. The additional drop must be due to friction (flexible hose of 3 ft. length to each duct) in the ducting. Using $p=0.91$ yields 38 watts loss with a 70% efficient blower.

For the RED motor, flow cross sectional area was measured as 0.13 ft.^2 . Using, again, $K=0.5$ in equation (59) yields 0.88 inches of water pressure drop which calculates out as a 49 watt loss using the estimated 50% efficient integral fan.

Another approach to the analysis of power required is to apply Bernoulli's principle to a fan, yielding

$$P = \frac{Q \rho V^2}{\eta} = \frac{\rho Q^3}{\eta A^2} \text{ watts}$$

where: ρ = density of air in $\text{Kg/m}^3 = 1.202 \text{ Kg/meter}^3$

V = air velocity in meters/sec

A = cross sectional area, meters^2

Q = cubic meters/sec

η = fan efficiency

For the motors, above:

$$A = 0.13 \text{ ft}^2 (0.3048)^2 = 0.0121 \text{ m}^2$$

$$Q = \frac{250 \text{ cfm}}{60} (0.0283) = 0.118 \text{ m}^3/\text{sec}$$

$$P = \frac{(1.202) (0.118)^3}{\eta (0.0121)^2} = \frac{13.5}{\eta} \text{ watts}$$

It should be noted that these equations are based solely on the change of kinetic energy of the air mass and do not take into account friction of the passage way. They are useful for estimating purposes.

- Observations and Conclusions -

Based on the 20 HP size motors, the expected approximately 50 watt loss - through the motor - represents about 0.33% of the output power. However, if an external source for blower air is required, extreme care must be exercised in manifold and duct design. Consideration of use of ram air ducted to the motor should be made.

-SUMMARY ON LOSSES-

Exact prediction of the magnitude of motor losses is a very difficult task. It is even more complex and difficult if the motor is chopper controlled. However, based on the analysis in this chapter, several important techniques and procedures can be formulated based on the following:

1. Efficiency of a motor is sharply reduced when it is chopper controlled. The higher the chopper frequency, the less the reduction in efficiency.
2. The decrease in efficiency is more pronounced at lower values of average current.
3. Chopper control introduces additional losses not accounted for from consideration of harmonic currents and apparent resistance as measured.
4. Eddy current losses in the armature due to tooth saturation and the main flux can be significant. For example, for the RED motor, at 2000 rev/m. this loss was calculated as 52% of the rated I^2R value.

This loss can be mitigated by:

- i) reducing conductor height
 - ii) using deeper slots
 - iii) using more iron (less flux density) in the motor
5. Eddy current losses in the armature due to cross slot leakage flux may be significant. This loss is one of the major components of "stray load" loss. Current harmonics due to chopper control increased this loss about 25% over the loss that exists without the harmonic currents.

This loss can be mitigated and greatly reduced if fine stranded conductors are used, since the loss is proportional to the square of the height of the conductor. Also, increasing the chopper frequency decreases this loss, since harmonic current magnitudes decrease with increasing frequency.

- 6) Losses in the pole face iron due to slot effect are negligible if the poles are laminated, but a major loss if the poles are solid iron.
- 7) Non-conducting banding (such as Kevlar) should be used to secure the armature winding end turns, to eliminating banding losses due to harmonic fluxes.
- 8) Equalizer connection losses are non-existent in a wave wound machine and are minimized in a lap winding if:

$$\frac{\text{\# of commutator bars}}{\text{parallel paths}/2} = \text{integer}$$

$$\text{and } \frac{\text{\# of slots}}{\text{parallel paths}/2} = \text{integer}$$

- 9) Losses in the coils undergoing commutation can be substantial if the brushes are located very far (10-15 degrees) off magnetic neutral and increase with chopper frequency. The loss can be reduced by decreasing the number of turns shorted during the commutating process - using a wave winding or by using longer, less wide brushes (increasing commutator length).

Interpoles will eliminate the need for brush shift and are strongly recommended.

- 10) Brush loss can be minimized by utilizing metal graphite brushes with silver if good commutation exists. Again, interpoles are strongly recommended.

- 11) With a FWD diode having 0.86 volt drop, 75 watts diode loss was measured at full load current. It is important to select a low voltage drop diode for this application.
- 12) Losses due to shaft, bearing, housing currents due to shaft induced emf are negligible.
- 13) Hysteresis losses in the magnetic structure due to chopper harmonics are negligible with laminated magnetic circuit. It is recommended that a laminated frame also be utilized (see Figure 26).
- 14) Attempts to secure low brush voltage drop by large brush pressure should be evaluated against increasing brush friction loss.
- 15) For an internally fan ventilated motor of the size for EV, the fan loss is on the order of 0.33% of the output power rating. This type of ventilation is recommended to avoid duct losses. For an externally ventilated motor, the ducting and manifold should be carefully designed to minimize losses. Consideration of the useage of ram air for cooling should also be given in lieu of blower produced ventilation.

- CHAPTER 4 -

TORQUE/AMPERE OBSERVATIONS

Stalled rotor torque tests were conducted on both motors; runs being made at 120° intervals. Tests were conducted using ripple free DC and with the chopper control operating at a frequency of 67 Hz.

Figure 31 portrays the typical variation with stalled rotor position which was observed.

Figure 32 shows the increased torque per ampere observed when the motors were chopper controlled. Figure 33 shows the same variation, in the form of the torque constant as a function of average current.

The increase is due to the harmonic current components creating torque due to the "universal" (AC/DC) properties of a series motor.

An analysis of these effects, as well as the change in torque/ampere due to brush shift was made. This analysis is included in this chapter, following the figures.

Stalled Rotor Tests
Generator DC
120° Intervals

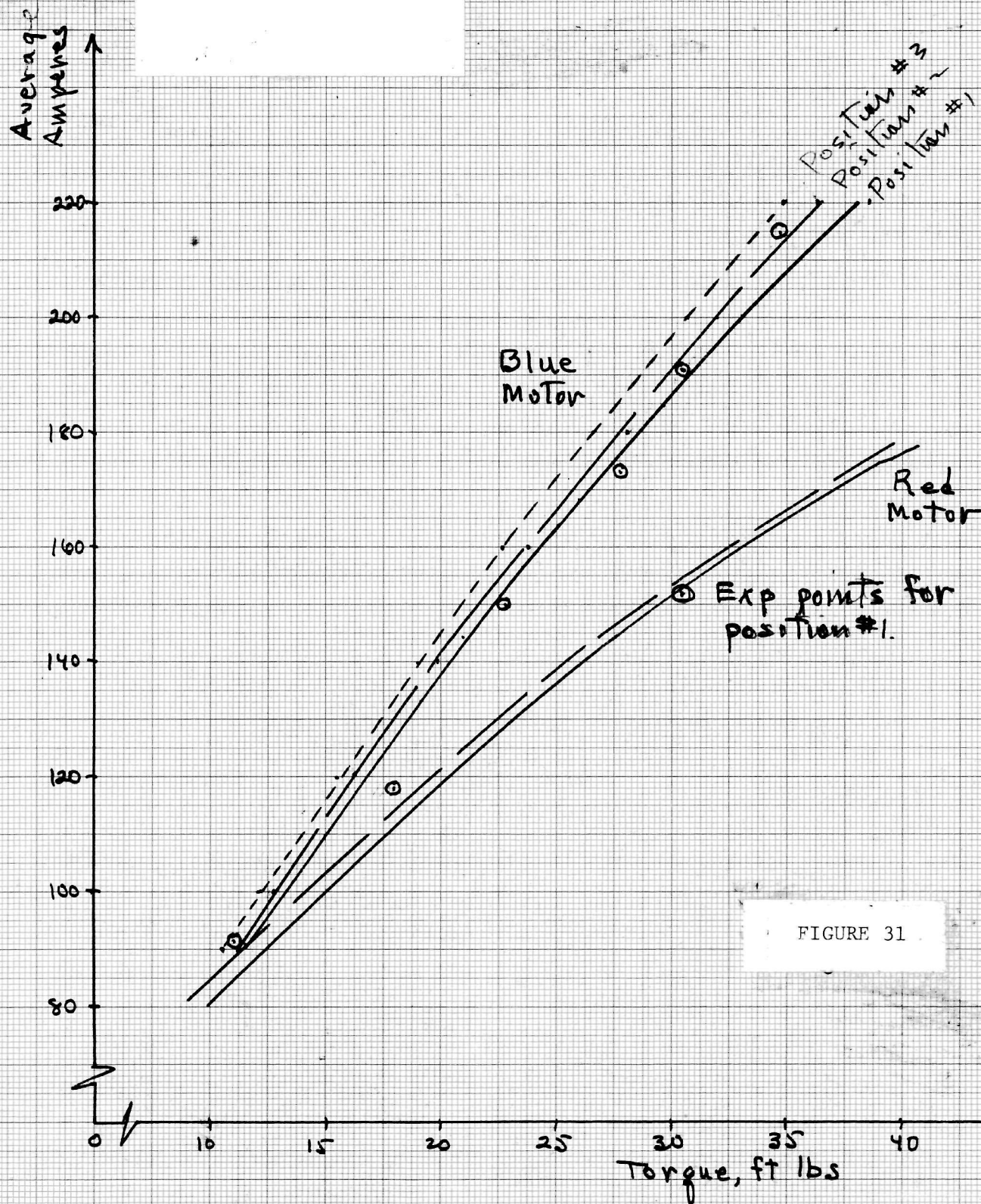


FIGURE 31

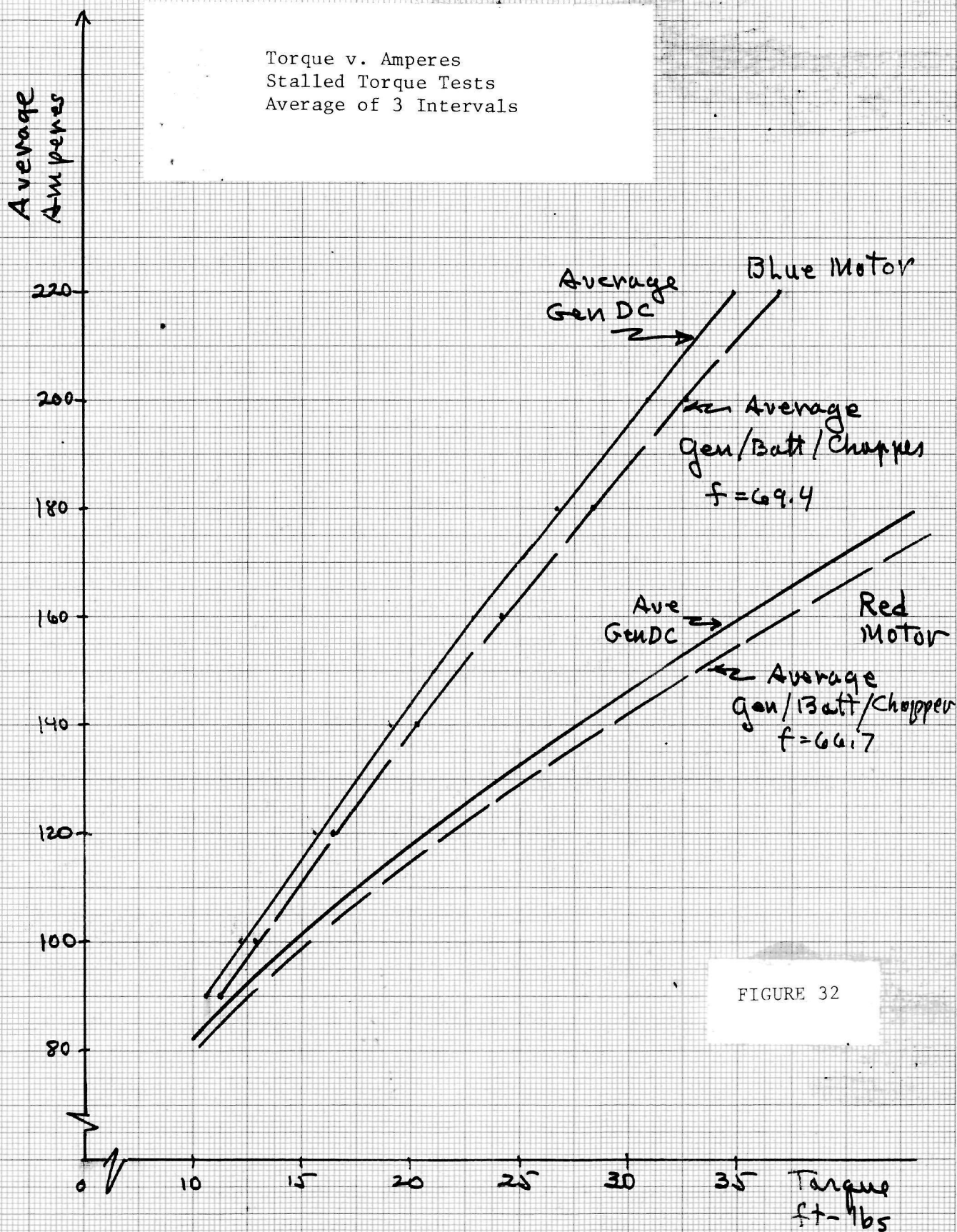


FIGURE 32

K_T v. I, -Stalled Torque Tests
Average of 3 Intervals

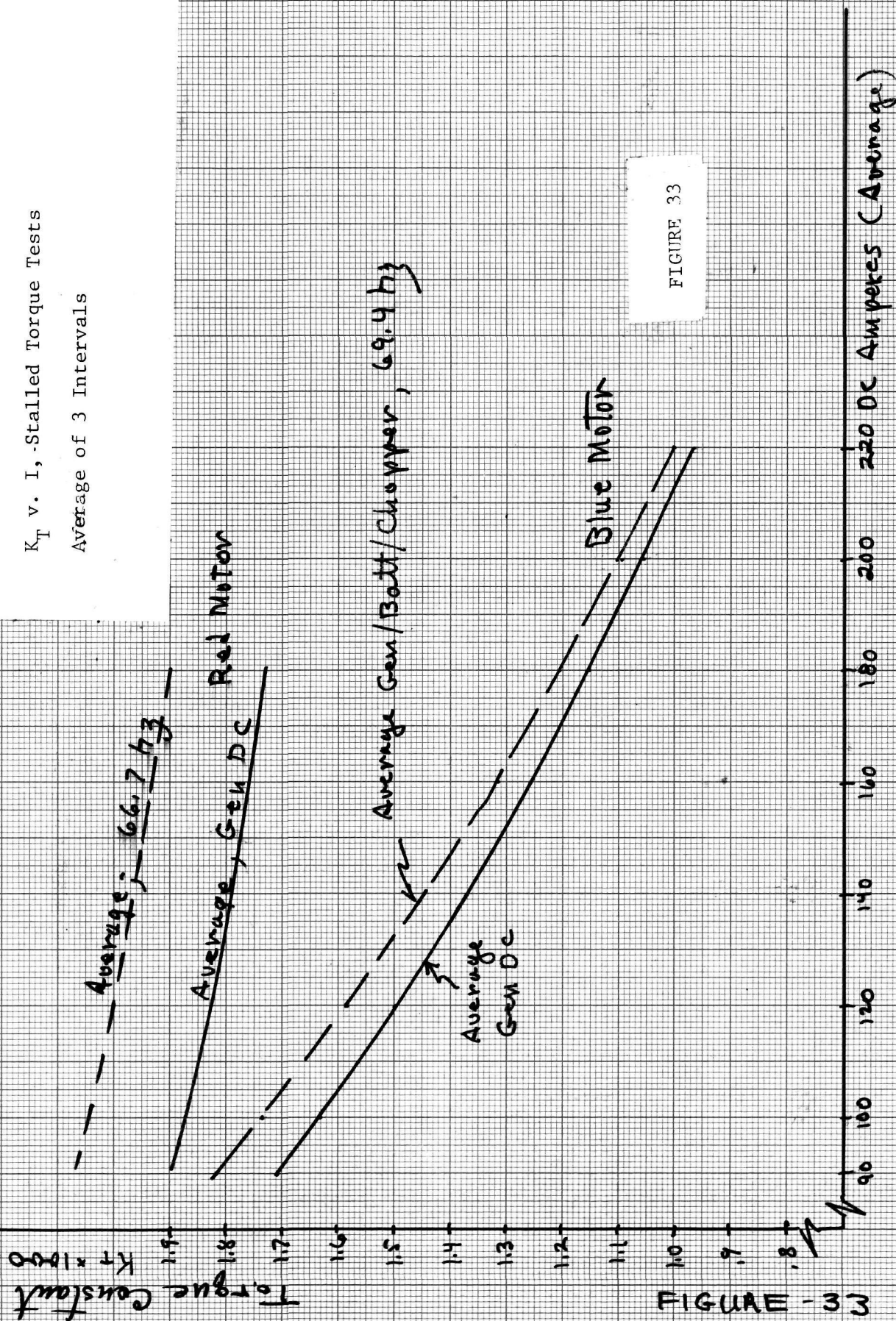


FIGURE 33

FIGURE - 33

TORQUE/AMPERE ANOMALIES AND THE NEED FOR INTERPOLES IN CHOPPER CONTROLLED DC SERIES TRACTION MOTORS

Howard B. Hamilton, SM

Elias Strangas, M

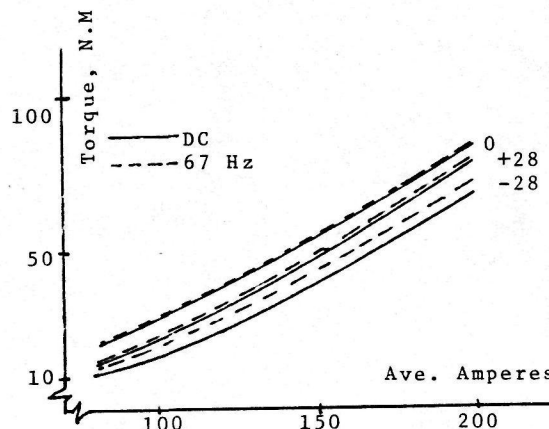
University of Pittsburgh
Pittsburgh, PA 15261

Abstract - Interest in battery powered electric vehicles has prompted Department of Energy sponsored investigations into the performance and efficiency of chopper controlled dc series motors in the 20-25 HP size range. During the course of the investigation the torque per ampere characteristics of the motors exhibited unexpected anomalies while being tested. This paper is an effort to explain the anomalies, which are due to the fact that the brushes of the motors are shifted off mechanical neutral in order to achieve proper commutation. (The motors were designed without interpoles). Although specific losses encountered are not the subject of this paper, some generalized results are presented in an attempt to make a strong case for the need for interpoles in machines of this size to be used in electric vehicles utilizing chopper control of the average applied voltage.

INTRODUCTION

During testing of series motors, of approximately 20 HP size, for use in electric vehicles, an increase in torque per ampere when powered through a chopper controlled source over that obtained when powered from a "pure" generator source was observed. This was observed in motors with laminated frame and in motors with solid frame. The motors did not have interpoles. Consequently, the brushes were shifted against rotation to obtain satisfactory commutation. Initially, it was thought that the observed results (blocked rotor), shown in Figure 1, were the result of instrumentation errors, but the results were repeatable and also observed by another investigator.

"Chopper control" is essentially pulse width and/or pulse rate modulation of a constant voltage source to control the average voltage applied to a motor. The motor armature and field are paralleled with a free wheeling diode which tends to exert a smoothing effect on the current which circulates in the motor circuit but it does still contain harmonics. If torque per average ampere is calculated, it is to be expected that some additional torque would be present due to the harmonic currents which are not measured by an average reading ammeter. This additional torque is due to the "universal motor" capability of a series wound motor to develop torque when powered from either ac or dc sources. The small additional torque (herein after referred to as due to conduction current) due to the universal motor effect is shown for the condition of zero degree brush shift in Figure 1. However, considerably greater harmonic



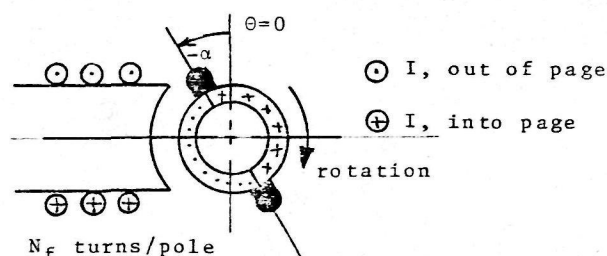
Torque vs. Amperes, Pure DC and Chopper Controlled
FIGURE 1

effect is present with the brushes shifted against (-) rotation or with the direction of rotation (+). The variation between (+) and (-) shift is as expected because of the magnetizing or demagnetizing effect of armature reaction for the pure dc situation, depending upon the direction of shift relative to rotational direction.

This paper presents the results of an analytical examination of the various torque producing mechanisms and an attempt to evaluate order of magnitude quantities. Production of dc torque and the effect of brush shift is examined and compared with experimental results, followed by an examination of the "repulsion" torques developed by the harmonic currents.

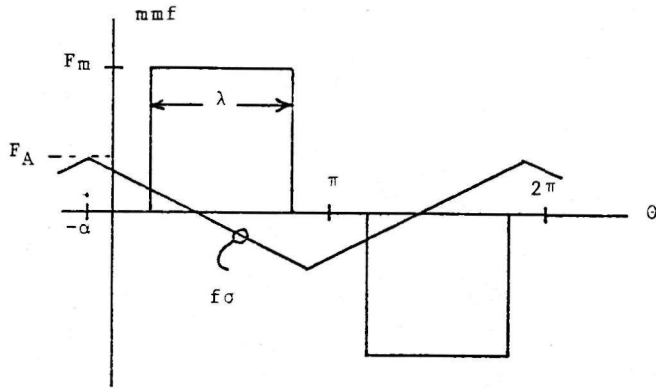
THE DC TORQUE

Figure 2 depicts the armature current/field polarity relationships in a dc motor with brushes shifted in a direction opposite to the direction of rotation of the armature.



DC Motor Polarities
FIGURE 2

A developed view of the relationship between armature and field mmf is shown in Figure 3.



Armature and Field MMF's
FIGURE 3

$$F_m = I_f N_f, \quad \frac{\pi-\lambda}{2} < \theta < \frac{\pi+\lambda}{2} \quad (1)$$

$$f_a = \left(F_A - \frac{2F_A \alpha}{\pi} \right) - \frac{2F_A \theta}{\pi}, \quad 0 < \theta < \pi - \alpha \quad (2)$$

$$f_a = \left(-3F_A + \frac{2F_A \alpha}{\pi} \right) + \frac{2F_A \theta}{\pi}, \quad \pi - \alpha < \theta < \pi \quad (3)$$

$$F_A = \frac{ZI_a}{2pa} \quad (3)$$

The field mmf is assumed to be rectangular, the permeability of the iron assumed to be much greater than that of air and the brush shift less than $(\pi-\lambda)/2$.

The net air gap mmf is the sum of the field and armature mmfs. Air gap flux density can be calculated from:

$$B_g = \frac{\mu_o F}{g} = \frac{\mu_o}{g} (F_m + f_a) \quad (4)$$

$$\text{and, for } \alpha=0, \quad \phi_o = \int_0^\pi B_g \ell r \left(\frac{2}{p} \right) d\theta \quad (5)$$

$$\phi_o = 2N_f I_f \frac{\mu_o \ell r \lambda}{pg} \quad (6)$$

ϕ_o is the total flux per pole with no brush shift. The dc torque developed is given by:

$$T_o = \frac{Zp}{2\pi a} \phi_o I_a \quad (7)$$

If finite brush shift exists, evaluating equation (5), using equations (1), (2) and (4) yields:

$$\phi_{-\alpha} = \phi_o \left(1 - \frac{ZI_a \alpha}{\pi p a N_f I_f} \right) \quad (8)$$

Since torque developed is proportional to the product of flux per pole and armature current,

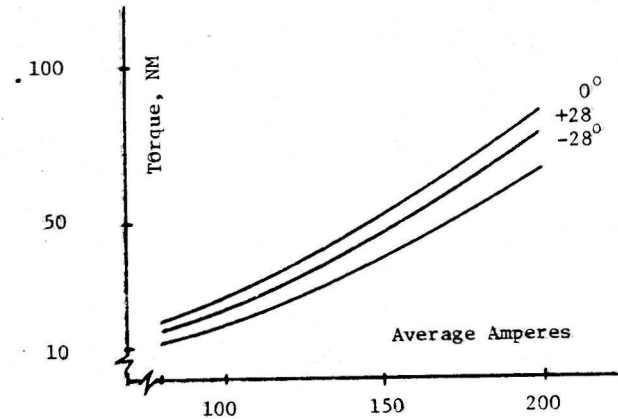
$$T_{-\alpha} = T_o \left(1 - \frac{ZI_a \alpha}{\pi p a N_f I_f} \right) = T_o (1-K_1) \quad (9)$$

The term in () represents the demagnetizing effect of armature mmf on the main field mmf. If the brushes were shifted in the direction of rotation, armature mmf would assist in magnetization and the minus sign would become positive.

There is also a reduction in torque, T_o , due to the "loss of active inductors" because of brush shift. The inductors in the region $(0-\alpha)$ and $\pi-(\pi-\alpha)$ are no longer contributing forward torque, but indeed develop backward torque because the current in these regions is opposite to the direction of current for forward torque. Theoretically, T_o would be reduced by the factor:

$$K_2 = \left(1 - \frac{2\alpha}{\pi} \right), \text{ or } 1-K_2 = \frac{2\alpha}{\pi} \quad (10)$$

To test the validity of these idealized relationships blocked rotor tests were run on a 4 pole, 200 ampere, 20 HP, wave wound series motor, without interpoles, using pure dc current and for brush shifts of 0, +28, and -28 degrees. The torque/ampere characteristics obtained are plotted in Figure 4.



Effect of Brush Shift, Ripple Free Current
FIGURE 4

As expected, the magnetizing effect of armature reaction with brushes shifted +28 results in larger torque/ampere than for -28 shift. However the loss of active inductor effect is present in both situations and there is a net loss of torque when the brushes are shifted.

In order to correlate the results of Figure 4, the effects expressed in equations (9) and (10) are combined to yield:

$$\frac{T_{-\alpha}}{T_{+\alpha}} = \frac{T_o (1-K_1)(1-K_2)}{T_o (1+K_1)(1-K_2)} \quad (11)$$

which can be solved, yielding:

$$K_1 = \frac{T_{+\alpha} - T_{-\alpha}}{T_{+\alpha} + T_{-\alpha}} \quad (12)$$

and:

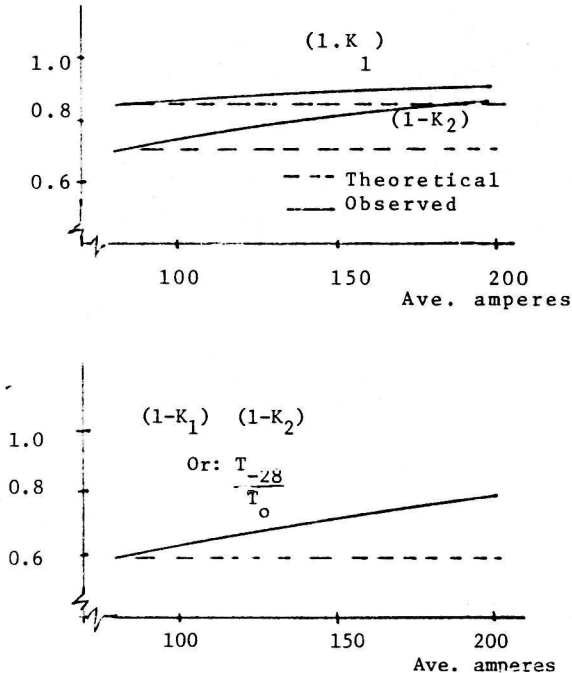
$$K_2 = 1 - \frac{T_{+\alpha} + T_{-\alpha}}{2T_o} \quad (13)$$

For the particular machine parameters, and at a brush shift of 28 degrees, the theoretical values of the constants were calculated as:

$$(1-K_1) = 0.842; (1-K_2) = 0.69 \quad (14)$$

The actual values of $(1-K_1)$ and $(1-K_2)$, from the data used to plot Figure 4 are plotted and compared with the theoretical values in Figure 5.

As shown, the theoretical values are approximately the same as the observed values at low saturation levels (30% of rated current) but are considerably in error at saturation, i.e. predicting only about 72% of the torque actually developed.



Theoretical and Observed Brush Shift Effects
FIGURE 5

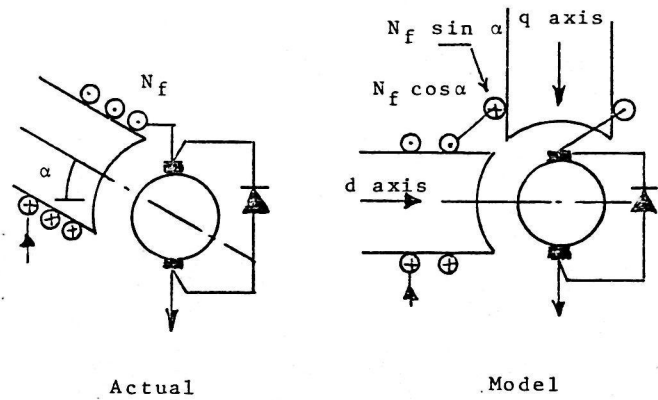
As will be shown, the technique for dealing with torques developed due to ac harmonic currents (resulting from the chopper effect) incorporates the effect of brush shift in a different fashion; therefore, the effects described in equations (9) and (10) are applicable to the calculation of net torque developed due to average, or dc values of current, only, (with brush shift).

THE AC TORQUES

There are two types of "repulsion motor" effects, or torques. Each results from interaction between field mmf (and flux density) and current flow in the armature resulting from voltage induced by transformer action from ac flux in the field circuit. The necessary condition for the transformer type induced emf is brush shift off of the neutral axis. There is also a torque produced, in the direction of rotation, by the ac current in the armature by virtue of direct conduction, or "universal" motor effect.

The brush shift situation can be modeled by considering that the field mmf acts along the d and q axis of the armature, as shown in Figure 6.

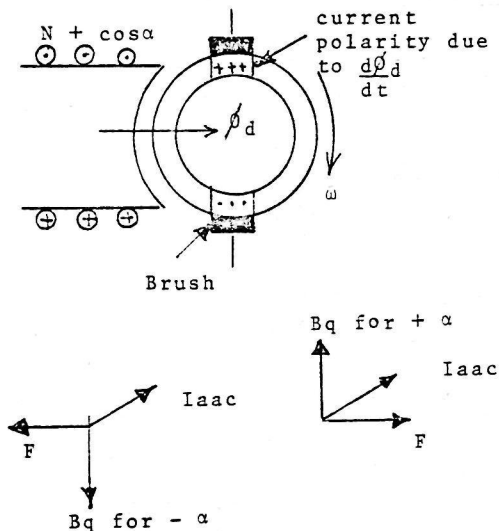
In these analysis, it will be assumed that only ac current flows. Torques developed can then be superimposed on the torques produced by the dc current.



BRUSH SHIFT MODELING

FIGURE 6

Using the model of Figure 6, note that the brushes bridge commutator segments and form a 'current sheet' as a result of a group of coils paralleled and a voltage induced by the time varying direct axis flux. Referring to Figure 7, and applying the $F = (I \times B)d\ell$ relationship, it can be seen that the torque developed as a result of the interaction of short circuited coil current and quadrature axis flux density is opposite to the direction of rotation if brush shift is (-) and with the direction of rotation if the shift is (+).



Repulsion Torque due to Shorted Coils

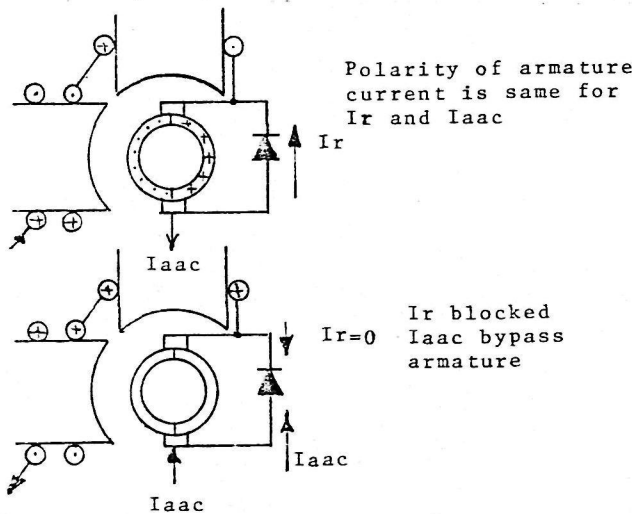
FIGURE 7

The coils shown are the coils undergoing commutation. In effect, the direction of brush shift determines the direction of B_q , whereas the direction of B_d (which determines current polarity) is independent of direction of brush shift.

An analysis was made to determine the order of magnitude of the torque developed by treating the paralleled, short circuited coils as a single coil and assuming that the brush spanned three commutator segments simultaneously. Since the resistance and inductance of 2, 3 or more paralleled coils is quite low, the resistance of the carbon brushes and their contact resistance become the dominate impedance in

the shorted coils, causing the current to be nearly in phase with the induced voltage which is in quadrature with the field current and the flux density, B . Thus, even though a relative heavy current may flow in the shorted coils, the quadrature relationship prevents development of significant torque. Estimated values of contact resistance, based on brush current density, were used to calculate values of negative torque of less than 1% of the dc torque developed. Since this is insignificant, the rather lengthy derivation for the torque so developed is omitted. The magnitude is proportional to the number of commutator segments bridged by the brushes and is thus controllable in the design stage by selection of the number of commutator bars and the aspect ratio of the brush collector system. In addition to the backward torque developed, there are joule losses associated with the current circulating in the parallel coils.

Another "repulsion" type torque results from current flowing in the armature as a result of voltage induced by the time varying quadrature axis flux via mutual coupling which exists. This current flows out of the brushes, through the free wheeling diode and returns to the armature via the other brush, if the brush shift is negative, as shown in Figure 8. If the brush shift were positive, the quadrature axis pole would be in a reversed position from that shown in Figure 8 and the repulsion current would have opposite polarity, if it could flow (which it cannot do because of the blocking effect of the diode). With negative brush shift and repulsion current flow, the current reacts with the direct axis flux to produce forward torque. In addition there is a torque due to interaction of armature current flowing by direct conduction and the direct axis flux density. This is the "universal" motor torque. Refer to Figure 8.



Repulsion and Conduction Current Flow
FIGURE 8

Because of the diode, the armature current (by conduction) by-passes the armature on the other 1/2 of the cycle and no current flow from induced voltage is possible because of blocking action of the diode.

The voltage induced in the armature circuit by the quadrature axis time varying flux is:

$$E = j\omega I_{fac} M(\alpha) \quad (15)$$

and the current that flows through the armature and diode is, (assuming 0.5 volts forward drop through the diode):

$$I_r = \frac{[M(\alpha)\omega I_{fac} - 0.5]}{\sqrt{(R_a + R_b)^2 + (\omega L_a)^2}} \angle 90 - \tan^{-1} \frac{\omega L_a}{R_a + R_b} \quad (16)$$

Again, even though brush resistance is variable, it is in series with the entire armature resistance and may be the dominate impedance in the circuit. R and L must be corrected to their values at the specific frequency of the harmonic current whose effect is being evaluated. The total armature current, Figure 8, is the sum $(I_{aac} + I_r)/a$. This current interacts with the direct axis flux density resulting from I_{fac} . Now,

$$B_d = (I_{fac} \frac{N_f \cos \alpha}{g}) \mu_0 \quad (17)$$

B_d and the armature currents are sinusoidal. B_d and I_{aac} are in time phase and I_r is at an angle $(90 - \theta)$, where:

$$\theta = \tan^{-1} \frac{\omega L_a}{R_b + R_a} \quad (18)$$

The average torque developed, for a machine with p poles and half cycle conduction is:

$$T = \frac{1}{2\pi} \int_0^\pi \left(\frac{\ell r Z}{a} \right) \sqrt{2} B_d \cos \omega t [\sqrt{2} I_{aac} \cos \omega t + \sqrt{2} I_r \cos (\omega t + 90 - \theta)] d(\omega t) \quad (19)$$

$$T = \frac{\ell r Z B_d}{2a} (I_{aac} + I_r \sin \theta) \quad (20)$$

Using the value of B_d , equation (17), in equation (20) yields:

$$T = \frac{I_{fac}}{2} \cos \alpha \left(\frac{\mu_0 N_f \ell r Z}{ag} \right) (I_{aac} + I_r \sin \theta) \quad (21)$$

Referring to equations (6) and (7),

$$\phi_o = \frac{2N_f I_f \mu_0 \ell r \lambda}{pg} = \frac{T_o}{I_a} \left(\frac{2\pi a}{Zp} \right) \quad (6), (7)$$

from which,

$$\frac{\mu_0 N_f \ell r Z}{ag} = \frac{\pi}{\lambda} \left(\frac{T_o}{I_a I_f} \right) \quad (22)$$

Using this in equation (21) yields:

$$T = \frac{\pi}{2\lambda} (I_{aac} + I_r \sin \theta) I_{fac} \left(\frac{T_o}{I_a I_f} \right) \cos \alpha \quad (23)$$

T_o is the dc torque which would be developed by specific "dc" currents I_a , I_f with the brushes on neutral. I_r is calculated from a test for $M(\alpha)$ and the use of equation (16).

Tests have shown that locating the brushes on arbitrary angles, δ , injecting a current, I , at harmonic velocity, ω , into the series field and measuring the open circuit voltage, E , induced between the brushes, yields the following relationship:

$$M(\delta) = \frac{E}{\omega I} \quad (24)$$

If the measurement is made at a specific ω and δ , the value of $M(\alpha)$, in equation (16) is:

$$M(\alpha) = \frac{M(\delta)}{\sin \delta} \sin \alpha \quad (25)$$

The motor described earlier was tested at three positions of brush shift and the relationship of equation (25) verified and the value:

$$\frac{M(\delta)}{\sin \delta} = 1.53 \text{ mH}$$

was calculated.

If $M(\alpha)$ from equation (25) is used to calculate the repulsion current, equation (16), and is inserted in equation (23) the product of I_r and $\cos \alpha$ yields a $\sin 2\alpha$ relationship indicating that repulsion torque developed is proportional to the sine of the twice the angle of brush shift and in the direction of rotation.

For the motor tested, saturated armature inductance was measured as 0.20mH and armature resistance was measured as 0.06 ohms, at 400 Hz. The current density of the alternating current across the commutator to carbon brush is very low; thus, substantial brush resistance exists. Tests on this motor, using copper blocks for measuring armature resistance as well as measuring through the carbon brushes, for various levels of DC saturation superposed indicates approximately 0.5 ohms resistance to AC current at 400 Hz.

Inserting the appropriate machine constants yields the following data; for 400 Hz., $\lambda = 2.22$ From equation (16)

$$I_r = \frac{3.85 I_{fac} \sin \alpha - 0.5}{0.56}$$

From equation (18)

$$\theta = \tan^{-1} \frac{\omega L_a}{R_a + R_b} = 42 \text{ degrees.}$$

From Figure 4,

$$\frac{T_o}{I_a I_f} = \frac{47.6}{140^2} = \frac{2.43}{10^3}$$

For $I_{fac} = I_{aac}$

$$T = \frac{1.73}{1000} I_{aac}^2 \cos \alpha + \frac{3.99}{1000} I_{aac}^2 \sin 2\alpha - \frac{1.04}{1000} I_{aac} \cos \alpha$$

For $\alpha = 28^\circ$, $I_{aac} = 15$ amperes, 400Hz

$$\begin{aligned} T &= 0.34 && \text{due to conduction current} \\ &= 0.73 && \text{due to repulsion current} \\ \hline &1.07 \text{ NM} && \text{total due to 400 Hz harmonic} \end{aligned}$$

which is 2% of the DC torque, and in general agreement with experimental results obtained.

SUMMARY AND CONCLUSIONS

Series motors of the size used in battery powered, chopper controlled electric vehicles (around 20 HP) are typically built without interpoles, thus dependent upon substantial brush shift to achieve proper commutation. As pointed out in this paper, this results in a degradation of torque per average

dc ampere of from 40% at light loads down to 20% at rated current loads. When the motor is chopper controlled, harmonic currents flow. If the brushes are shifted there are two types of repulsion current flowing; one (the smaller) yielding a backward torque and the other a forward torque. Both torques are functions of the sine of twice the angle of brush shift. Although the magnitude of torque produced is relatively small, the currents in the coils shorted by the brushes and the current circulating externally, through the free wheeling diode, may result in appreciable joule loss. A rather commonly used rule of thumb states that for electric automobiles, a decrease of 1% in efficiency, or the addition of 50 lbs of weight will reduce vehicle range one mile. In a typical 20 HP motor, with 12 lb total of series fields, interpoles could be added for an additional weight increase of 8, or less.

In tests previously conducted by these investigators to determine "rotating core" loss, i.e. joule heat loss in armature conductors shorted by the brushes during commutation if the brushes were not located at the proper angle for commutation, it was noted that these losses increased approximately 120% for a 10 degree and 270% for a 20 degree position off magnetic neutral, under load. Also, note that electric vehicles are occasionally operated in reverse. If a 30 degree brush shift against rotation is proper for the commutation process, opposite rotation operation places it 60 degrees off magnetic neutral, with the potential for extremely high losses, armature heating and excessive battery depletion. The percentages given above for the 10 and 20 degree brush position errors represents more than a 1% increase in loss of efficiency. Compared with the added weight of interpoles, the net trade off of gain in range points up the desirability of interpoles for motors to be used in electric vehicles.

The authors hope that an enlightening discussion of the observed torque anomalies and the need for interpoles in series motors for electric vehicles has been presented.

ACKNOWLEDGEMENT

This work was supported by NASA-Lewis Research Center and Department of Energy under Grant #NSG-3163. We wish to thank Mr. E. F. McBrien, NASA-Lewis Research Center, for his able assistance and guidance in this on-going project.

GLOSSARY AND SYMBOLS

(All are in the MKS System)

a	number of armature parallel paths, = 2 for wave, = p for lap wound winding
B	flux density. B_d , B_q are direct and quadrature axis. B_g is air gap flux density.
dℓ	incremental length of an inductor
E	an open circuit armature voltage, rms
F	force
f_a	armature mmf
F_A	peak value of armature mmf

F_g	air gap mmf, net	r	radius of the armature
F_m	single field pole mmf	R_a	armature resistance
g	air gap length	R_b	brush resistance
I_a	average or dc value of armature current	T_o	Torque, for I_a , I_f , no brush shift
I_{aac}	rms value of harmonic current of frequency f flowing in armature by conduction	$T_{-\alpha}$	Torque, for I_a , I_f , brush shift, $-\alpha$
I_f	average or dc value of field current in each pole field winding	Z	Total armature inductors
I_{fac}	rms value of harmonic field current of frequency f flowing in each pole field winding	α	Brush shift
I_r	rms value of repulsion current in the armature	δ	specific angle, in radians at which $M(\delta)$ is measured
ℓ	stack length	θ	angle commencing on the q axis of the machine and measured in the direction of rotation
L_a	armature self inductance	λ	effective pole span, in radians
$M(\alpha), M(\delta)$	field/armature mutual inductance with brushes shifted α, δ radians	μ_0	permeability of air, $4\pi/10^7$
N_f	field turns per pole	ϕ_0	total flux/pole, at $\alpha = 0$
p	number of poles	$\phi_{-\alpha}$	total flux/pole at brush shift, $-\alpha$ radians, against rotation
		ω	electrical angular velocity, $2\pi f$

-CHAPTER 5-

MODELS

In Chapter 2, two motors were analyzed for performance and efficiency, using the conventional series motor equivalent circuit, or model. Saturation and variations in rotating losses with speed were included. The analysis was based on ripple-free DC supply for the motor. Observed (experimental) values of torque power and efficiency were lower than calculated values, using the equivalent circuit. Observed speed was higher than calculated.

With chopper control, the measured torque per ampere is higher than that obtained from ripple-free DC. Figure 11 shows how chopper control affects the speed characteristic. The conclusion that can be drawn is that the "conventional" series motor model does not yield accurate predictions of performance and efficiency if the motor is chopper controlled.

Ewing⁽²¹⁾ proposed a "modified" conventional motor model with lumped parameters, as shown in Figure 34. R_A and $L_A + L_C$ are the lumped circuit resistance and inductance (armature plus field quantities). R_C is a fictitious resistance used to account for core losses resulting from the harmonic currents associated with operation of a motor from rectified alternating current.

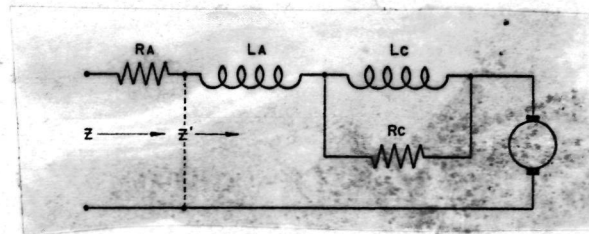


Figure 34. The Ewing Model.

This circuit appears to yield excellent results (for frequencies up to 360 Hz) in accounting for losses. However, in this investigation, over a much

wider frequency range, it was not possible to correlate the change in apparent resistance and inductance (as described in APPENDIX D) observed with the relationships presented by Ewing.

Franklin's⁽⁵⁾ model also does not yield accurate results, even though he does include saturation effects. He reports calculated errors of up to 15% in current values and 20% in calculated torque. This model, like most others, is based on a lumped impedance model and contains many assumptions which do not permit accurate results.

Dubey and Shepherd⁽²³⁾ and Yanase⁽²⁴⁾ also have proposed models for chopper controlled series motors. These approaches utilize the non-linear saturation curve as a three-segment curve approximated by straight lines.

In an attempt to develop a more representative model, a time-dependent finite element model was formulated. This development, culminating in a doctoral dissertation, is presented in SECTION II of this report. It is applicable to both DC and synchronous AC machines. Chapter 5 relates specifically to an analysis of the RED motor.

The results from the simulation are compared with test results in TABLE IV. It is felt that the discrepancies between actual test data and results from the computer simulation can be attributed to the lack of knowledge of many of the material parameters. The torque and current calculations depend not only on the coarseness of the grid used, but were also found to be very sensitive to the resistivity and permeability values chosen for the frame of the motor. Battery characteristics were not included in the simulation.

Two papers dealing with the computer simulation of the chopper controlled motor have been prepared.^{(13), (22)} Reference (22) is being submitted for presentation and is included in this chapter.

It is the opinion of this investigator that a lumped impedance motor model cannot yield accurate results - especially in efficiency calculations and the

TABLE IV

TEST				SIMULATION					
T (ms)	T _{on} /T	RPM (min)	I _{ave} A	ΔI/I _{ave}	M _{sh} (N m)	M _{gap} (N m)	I _{ave} A	ΔI/I _{ave}	M _{gap} (N m)
10	0.45	647	201.3	0.86	82.34	84.66	222.4	0.91	103.2
10	0.45	1102	104	1.18	28.93	31.43	115.2	1.205	40.6
5	0.45	725	174.8	0.63	67.37	69.69	195.6	0.69	88.6
5	0.45	1120	120.4	0.66	29.51	32.02	127.3	0.704	42.8
5	0.45	1820	63.5	1.10	9.67	12.43	68.6	1.23	18.03

T: period of chopper

 T_{on} : time on I_{ave} : average value of current ΔI : ripple current peak to peak M_{sh} : shaft torque M_{gap} : Air gap torque

*Calculated as the shaft torque plus friction and windage.

perfection of a user-oriented finite element model is a desirable research task.

The simulation presented in SECTION II is an excellent starting point for such a model.

Because of the extreme complexity of the motor magnetic circuit, the various loss mechanisms, etc., it appears doubtful if any model or simulation can yield exact performance and efficiency data. It is felt that this data can be obtained only by actual testing to standardized procedures and instrumentation along the lines described in APPENDIX A. However, it should be noted that no U. S. standard addresses itself to the testing of chopper controlled motors. Such a standard should be prepared and adopted in order to evaluate motors against each other, based on test results.

A MODEL FOR THE CHOPPER CONTROLLED DC SERIES MOTOR

Elias G. Strangas, M

University of Pittsburgh
Pittsburgh, PA 15261

Howard B. Hamilton, F

Abstract - This paper presents a method of accounting for the varying inductance and apparent resistance in the prediction of the performance of a chopper controlled DC series motor. The finite element technique is utilized to solve the electromagnetic field, at a cross section of the machine, in the time domain, taking eddy current and saturation effects into account. The rotational voltage is calculated and the incremental inductances are introduced and used for the calculation of currents; the torque is then calculated based on the Maxwell Stress Tensor in the air gap.

INTRODUCTION

The current in a DC series motor operating from a constant voltage source through a chopper controller contains besides the DC component, a ripple current which can be analyzed into harmonics of relatively large order and significant magnitude. This variation of the motor current with time changes the saturation of the iron portions of the machine within each cycle. It also causes skin effect in the conductors and eddy currents in the solid iron parts of the machine and, in the case of very high frequencies, even in the laminated sections.

The problems resulting from these phenomena affect not only the design of the motor, but also the operating considerations as well. As it was recently observed^[1,2], the inductance and apparent resistance assigned to a chopper controlled motor cannot be singled valued. Instead, they vary greatly with the saturation level and the frequency, affecting the current waveform and the torque and must be taken into consideration in the design and operation of the controller.

In this paper the electromagnetic field inside the machine is solved in the time domain, taking saturation and eddy currents into consideration. Subsequently, "incremental inductances" are defined and computed, and the currents are obtained from these inductances. The torque is calculated from the numerical field solution using the Maxwell stress tensor.

THE TIME DEPENDENT FINITE ELEMENT METHOD

Assuming that the electromagnetic field at a cross section of the machine is two dimensional, the z component of the magnetic vector potential, A_z , can be obtained from the partial differential equations:^[3]

$$\nabla \left(\frac{1}{\mu} \nabla A_z \right) = J_z \quad (1)$$

$$\text{and } \nabla_x \left(\frac{1}{\mu} \nabla_x A_z \right) = -\sigma \left(\frac{\partial A_z}{\partial t} - \text{grad} \phi \right) \quad (2)$$

where J is the current density, μ the permeability, σ the conductivity and $\text{grad} \phi$, the gradient of the electrostatic field. Equation (1) is applied to domains with known current densities and equation (2) to the remaining of the cross section.

The solution of these equations requires the knowledge of the current density distribution in the conductors, the voltages due to charges and the initial field distribution at $t = 0$. For simplicity, the solution can start at $t = 0$, where there is no current in the machine and the field is zero everywhere in the cross section. $\text{Grad} \phi$ can be considered zero in all iron parts and in the air, and the current densities in the conductors can be obtained from the currents calculated on the basis of the incremental inductances.

The finite element formulation of equations (1) and (2) fields a system of first order differential equations^[4]:

$$G \cdot A + K \cdot \frac{dA}{dt} = f \quad (3)$$

which can be reduced to a system of linear equations using the Crank-Nicolson method:

$$\{K + (1-\theta)\Delta t \cdot G\} A^{n+1} = \Delta t \cdot f + (K - \theta \Delta t \cdot G) A^n \quad (4)$$

From the solution of equation (4), the distribution of the magnetic vector potential can be calculated over the entire cross section as a function of time. The voltage V_n induced in a conductor of length ℓ due to the change ΔA of its magnetic vector potential during the time interval Δt , can be calculated as:

$$V_n = \ell \frac{\Delta A}{\Delta t} \quad (5)$$

The voltage induced in the winding, V is then:

$$V = \sum_i \pm \ell \frac{dA_i}{dt} \quad (6)$$

where the sum extends over all the conductors in series and the individual conductor voltages are added or subtracted according to the connections of the conductors.

The rotational voltage, V_ω , induced in a conductor, length ℓ , moving with angular velocity, ω , in a field of radial flux density, B_r , can be calculated as:

$$V_\omega = B_r \omega r \ell \quad (7)$$

where r is the distance of the conductor from the axis of rotation.

When the distribution of the magnetic vector potential is known, B_r at angle ϕ can be obtained as:

$$B_r = -\frac{1}{r} \frac{\partial A}{\partial \phi} \quad (8)$$

The voltage induced in n inductors between two brushes can then be calculated as:

$$V_\omega = - \sum_{i=1}^n \left(\frac{\partial A}{\partial \phi} \right)_i \omega \ell \quad (9)$$

Assuming linear distribution of the inductors in armature winding:

$$V_\omega = -n\omega \ell \int_{\phi_1}^{\phi_n} \left(\frac{\partial A}{\partial \phi} \right) d\phi = n\omega \ell (A_n - A_1) \quad (10)$$

where ϕ_1 , ϕ_n are the angular position of the first and last inductors between the brushes, and A_1 , A_n are the values of the magnetic vector potential at those inductors.

For small changes of current around an operating point, V_ω can be written:

$$V_\omega = K I \quad (11)$$

where:

$$K = \frac{-n\omega l(A_n - A_1)}{I}$$

INCREMENTAL INDUCTANCES

At every operating point of a machine, an incremental inductance can be defined as:

$$L_{incr} = \lim_{\Delta t \rightarrow 0} \frac{V}{\frac{\Delta I}{\Delta t}} \quad (12)$$

where Δt is a time interval, ΔI is the corresponding change in current and V is the voltage induced in the winding due to this change of current.

This definition has a meaning in the case of a finite number of circuits where self and mutual inductances can be defined, i.e. in the absence of eddy currents. Otherwise incremental inductances can be defined for a time interval Δt in which the current changes by ΔI as:

$$L_{incr} = \frac{V}{\frac{\Delta I}{\Delta t}} = \frac{\sum \pm k \frac{\Delta A}{\Delta t}}{\frac{\Delta I}{\Delta t}} \quad (13)$$

In this case the value of L_{incr} not only depends on ΔI and the previous operating condition but also on the finite time interval Δt . Equation (13) can be used to calculate the incremental inductance for a certain time interval and current change by solving equation (4) for the new value of current, $I_0 + \Delta I$, and calculating the induced voltage.

The connections of the motor for which the method was applied are shown in Figure 1. When the chopper is "on", the external voltage, V_{ext} , is equal to the sum of the counter EMF, the inductance voltage and the voltage drop across the motor resistance and the brushes. That is:

$$V_{ext} = (L_{incr} + L_{ext} + L_{end}) \frac{\Delta I}{\Delta t} + R(I + \frac{\Delta I}{2}) + K(I + \frac{\Delta I}{2}) + V_{brush} \quad (14)$$

where L_{ext} is the external inductance (source, wires, etc.), L_{end} the inductance corresponding to the end turns of the winding and V_{brush} the voltage drop across the brushes.

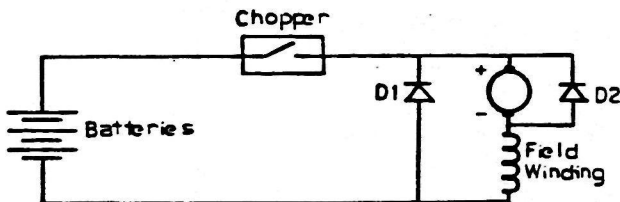


Figure 1. The external connections to a chopper controlled DC series motor.

From equations (13) and (14), the change of current, ΔI , can be predicted for a time interval Δt , using the following algorithm:

1. Starting from an initial distribution of A , and an initial current I_0 at $t = t_0$, assume a change of current ΔI_0 for the time interval Δt .

2. Solve the field for the new current, $I = I_0 + \Delta I$ at time $t + \Delta t$, using equations (1) and (2). Calculate the induced voltage, V , and the corresponding inductance, L_{incr} from equation (13).

3. Calculate a corrected current change, ΔI , from equation (14).

4. Repeat from Step 2 until the error in ΔI is less than a predetermined value. The convergence can be greatly improved if Aitkens extrapolation is used for the calculation of ΔI .

5. When convergence is achieved, calculate the torque (as detailed in the following section and move to the next time step, again commencing with Step 1.

TORQUE CALCULATION

When eddy currents are present, the torque cannot be calculated by taking the derivative with respect to the angle of the energy stored in the inductances, since the number of windings is not finite and forces act also on the eddy currents. To account for the latter effect, the Maxwell Stress Tensor⁽⁵⁾ is used to calculate the air gap torque.

dF_i , the component of force dF in the i th direction which is transmitted through a surface element, dS , whose component in the j th direction is dS_j is given as:

$$dF_i = \sum_j T_{ij} dS_j \quad (15)$$

where T_{ij} is an element in the Stress Tensor, T . When the surface lies in the air gap, T , for a two dimensional field takes the form:⁽⁵⁾

$$T = \frac{1}{\mu} \begin{bmatrix} \frac{1}{2} (B_x^2 - B_y^2) & B_x B_y \\ B_x B_y & \frac{1}{2} (B_x^2 - B_y^2) \end{bmatrix} \quad (16)$$

Torque, M , can be calculated by integrating the cross product of radius and incremental force vectors over a cylindrical surface in the middle of the air gap:

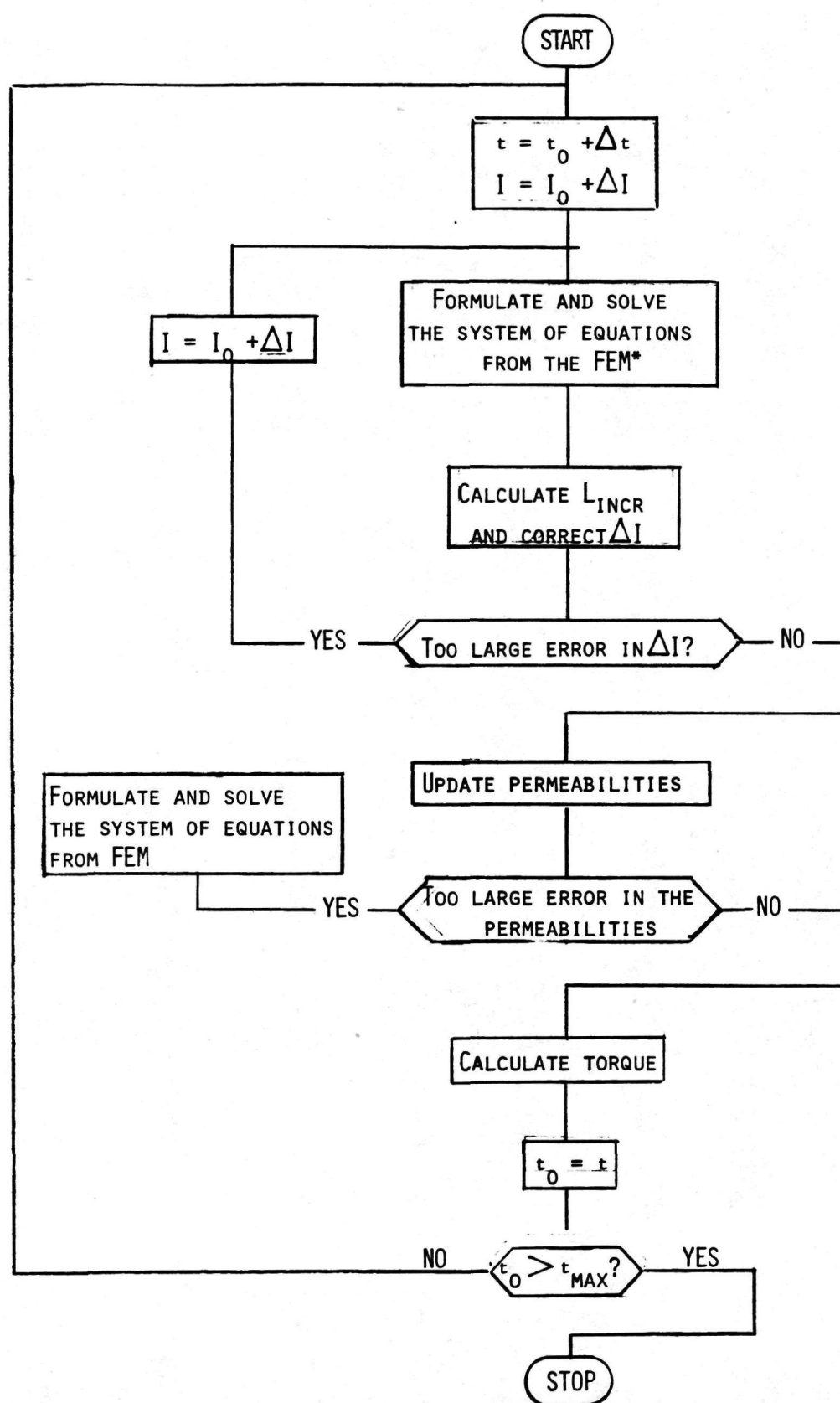
$$M = \int |\vec{r} \times d\vec{F}| = \int y dF_x - \int x dF_y \quad (17)$$

where x , y are components of \vec{r} .

APPROXIMATIONS AND ASSUMPTIONS

The technique described above was applied to a series motor designed for an electric vehicle drive usage. The motor was a wave wound, four pole machine with a solid frame and laminated poles. The chopper was a thyristor, whose control circuit permitted control from a minimum 'on' time of 0.8 msec. and up to a maximum period, or cycle of 2.5 msec. (400 Hz repetition frequency).

The motor armature had 27 slots, not integrally divisible by 4 poles, thus indicating modeling all 4 poles. Such an approach was considered unacceptable because of the large number of nodes needed, which would increase both the storage requirements and the solution time. Instead, it was preferred to solve the field for only one pole pitch, changing the number of slots in the model from 27 to 28, (7 per pole) and keeping the slot to tooth ratio the same as in the actual machine. In order to keep the armature magnetomotive force in the model the same as in the actual



* FEM, ABBR. FOR
FINITE ELEMENT METHOD

FIGURE 2: CURRENT AND TORQUE CALCULATION ALGORITHMS

machine, the current in the model armature conductors was the actual current multiplied by 27/28 and the calculated induced voltage was corrected by multiplying by the same number.

The end turn inductances were considered constant, independent of saturation and eddy currents, while the voltage drop at the brushes was assumed to be 2 Volts (constant).

THE SOLUTION METHOD

Figure 2 shows the algorithm used to calculate the current and the torque. The saturation level did not vary significantly between consecutive time steps, thus making it possible to use underrelaxation for the calculation of the permeabilities. From the field solution the value of the flux density, B , was calculated in every element and the permeability, μ_{new} was calculated from the B-H curve of the material. The actual value of permeability used was calculated from:

$$\mu = \alpha \mu_{\text{old}} + (1-\alpha) \mu_{\text{new}} \quad (18)$$

where:

$$0 \leq \alpha \leq 1$$

and:

μ_{old} is the μ from the previous iteration.

The system of equations⁽⁴⁾ derived from the finite element formulation were solved using the preconditioned conjugate gradient method.^(6,7) The reason an iterative technique was preferred is that indirect methods make good use of a "guess" solution which, in the problem examined here, is provided either by the solution at the previous time step, or by the solution at the previous iteration for the calculation of permeabilities. The conjugate gradient method corresponds well with the equations obtained from the finite element method,^(6,7) and the preconditioning improves the convergence rate, which is slow due to the ill-conditioning of the stiffness matrix. This ill-conditioning arises because of the interface between elements in iron and air, or copper, which have vastly different permeabilities.

Figure 3 shows the discretization of the one pole pitch of the machine. The value of the magnetic vector potential was assumed zero at the outer surface of the frame while the other two boundaries were negatively coupled (periodicity condition). The grid at the air gap was generated by the computer program in order to connect the grids of the rotor and the stator.

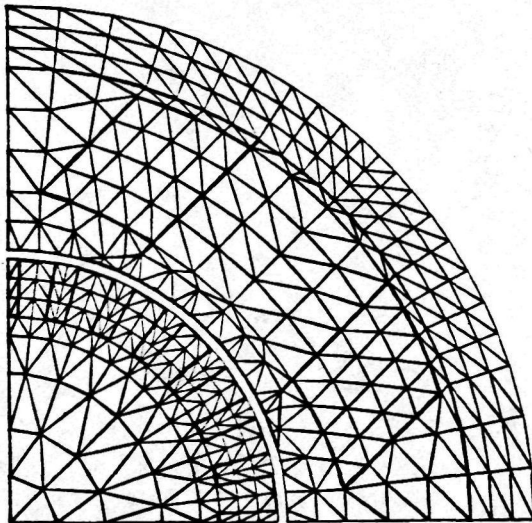


Figure 3. The grid for the electric vehicle motor.

RESULTS

The algorithm described above predicted both average and ripple currents of the motor with a maximum error of 12%. The specific yoke or frame material permeability relationship was not known and had to be assumed. Use of the exact values, and use of a more fine grid would reduce the error. Voltage, current and torque wave forms for the motor from $t = 0$ to steady state are presented in Figure 4.

Figure 5 is a computer plot of the flux in the machine cross section at a specific time.

Figure 6 is a flux map for a hypothetical machine with laminated frame of the same dimensions and winding as the actual machine.

SUMMARY

Space limitations preclude a detailed description of the mathematical derivations and techniques utilized and the results presented do not exhaust the capabilities of the technique of continuous modeling of the electromagnetic field. The method can be applied to the skin and eddy current effects in solid conductors, either by constructing a finer grid, or by solving separately a finer grid for one inductor, or one slot, every time the larger grid for the pole segment is solved.

Also, a flux map of the radial flux in the air gap can easily be obtained⁽³⁾. This map presenting flux density as a function of angular position on the rotor surface can be utilized to predict either commutating pole mmf required, or brush position angle for non-interpole machines.

An extension to the work performed in this investigation would be application of the method to separately excited shunt DC machines and to a study of the commutation process.

ACKNOWLEDGEMENT

This investigation was supported by NASA/Lewis Research Center and the Department of Energy under Grant #NSG-3163.

REFERENCES

- [1] Hamilton, H.B. and Strangas, E., "Series Motor Parameter Variations As A Function of Frequency and Saturations," IEEE Trans., PAS July/Aug. 1980, Vol. PAS-99, No. 4, p. 1567.
- [2] DeWolf, F.T., "Measurement of Inductance of DC Machines," IEEE Trans., PAS Sept./Oct. 1979, Vol. PAS-98, No. 5, p. 1636.
- [3] Strangas, E., "The Time Dependent Finite Element Modeling Of the Electromagnetic Field In Electrical Machines - Methods and Applications," Ph.D. Dissertation, University of Pittsburgh, 1980, pp. 12-14.
- [4] J.T. Oden and J.N. Reddy, "An Introduction to the Mathematical Theory of Finite Elements," (Book) Wiley Interscience, 1976.
- [5] W.K.H. Panosky, M. Phillips, "Classical Electricity and Magnetism," (Book) Addison-Wesley, 1972.
- [6] J.R. Whitman, editor: "The Mathematics of Finite Elements and Applications," "The Analysis and Application of Sparse Matrix Algorithms in the Finite Element Method," by D.J. Evans, Academic Press, 1973, pp. 427-447.
- [7] D.J. Evans, "The Use of Preconditioning in Iterative Methods for Solving Linear Equations with Symmetric Positive Definite Matrices," J. Inst. Math. Applics., 1967, No. 4, pp. 295-314.

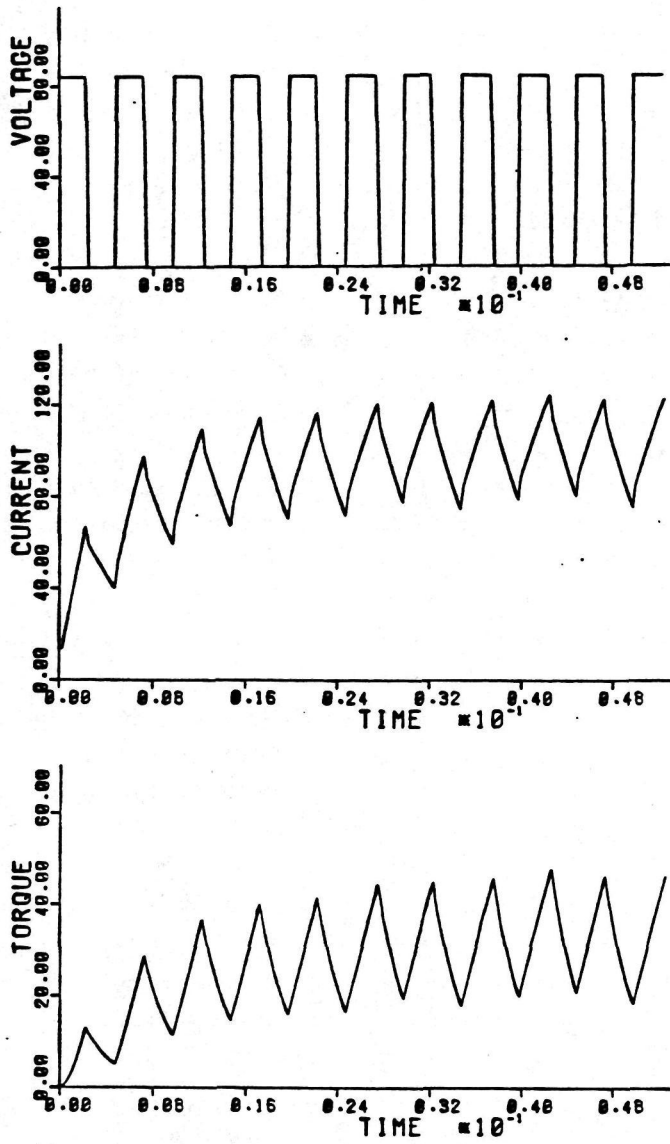


Figure 4. Waveforms from $t = 0$.

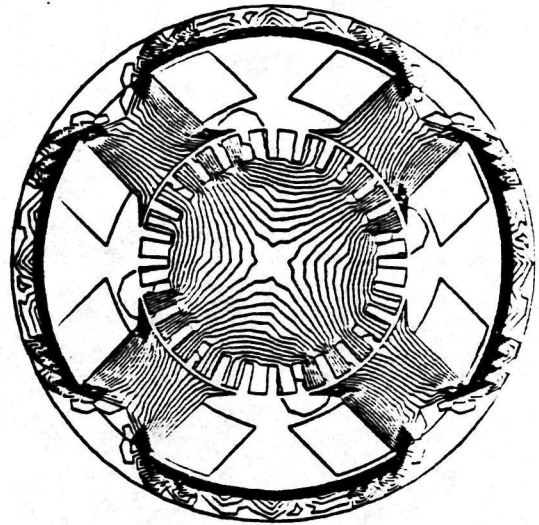


Figure 5. Solid Frame.

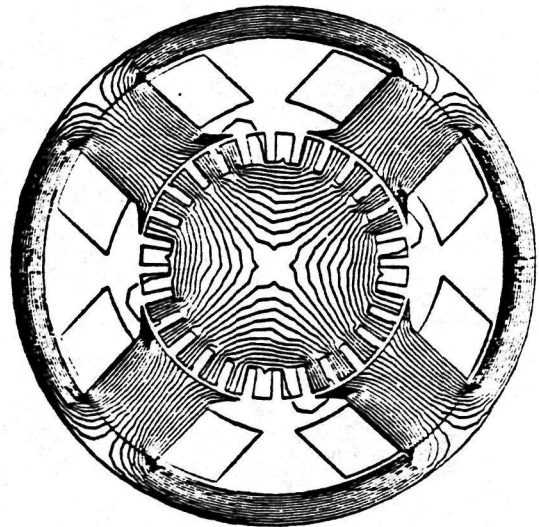


Figure 6. Laminated Frame.

REFERENCES

1. IEEE Standard #113 "IEEE Standard Test Code for Direct Current Machines," 1973 IEEE, Inc., 345 E. 47th Street, New York, NY 10017.
2. DeWolf, F.T., "Measurement of Inductance of DC Machines," IEEE Trans. PAS, Sept./Oct. 1979, Volume PAS-98, No. 5, pp. 1636-1644.
3. H.B. Hamilton, "An Investigation of Possible DC Power Sources for Testing Electric Vehicle Motors," submitted to NASA-Lewis/DOE under Grant #NSG 3163, 1978.
4. H.B. Hamilton, E.F. McBrien, E. Strangas, "A DC Power Source for Testing Battery Powered Electric Vehicle Motors," presented at the 1979 IEEE, IAS Society Meeting, Cleveland, OH, Oct. 1979.
5. P.W. Franklin, "Theory of the DC Motor Controlled By Power Pulses," Part I and II. Presented at the 5th Annual Meeting of IEEE, IAS Gp. Chicago, Ill., Oct. 1970.
6. Saunders, R.M., "Measurement of DC Machine Parameters," American Institute of Electrical Engineers, Vol. 70, 1951.
7. Hamilton, H.B. and Strangas, E., "Series Motor Parameter Variations As A Function of Frequency and Saturation," presented at the IEEE PES Winter Meeting, Feb. 1980. IEEE Trans. PAS, July/Aug. 1980, Vol. PAS-99, No. 4, pp. 1567-1575.
8. H.B. Hamilton, E.F. McBrien, E. Strangas, "Chopper Controlled DC Traction Motor Testing: Some Methods and Results," presented at the Monterrey, Mexico IEEE Meeting, September 1979 in Monterrey, Mexico.
9. "Direct Current Machinery," Book, Kloeffer, Brenneman, Kerchner. The MacMillan Co., New York, 1934, p. 79.
10. "Direct Current Machines," Book, Liwschit-Garik and Whipple. Van Nostrand Co., Princeton, NJ, 1961, pp. 176, 179.
11. "Transient Performance of Electrical Power Systems," Book, R. Rudenberg, McGraw-Hill, 1950, MIT Press, 1970, p. 117.
12. E. Strangas, "The Time Dependent Finite Element Modeling of the Electro-magnetic Field in Electrical Machines - Methods and Applications," Ph.D. Dissertation. University Microfilms, Ann Arbor Michigan, 1980.
13. E. Strangas, H.B. Hamilton, "Computer Modeling of Chopper Controlled DC Machines," presented at the International Conference on Electric Machines, Sept. 1980, Athens, Greece.
14. E. Strangas, H.B. Hamilton, "A Model for the Chopper Controlled DC Series Motor," submitted for the IEEE Summer Power Meeting, 1981.

15. NASA-Lewis Research Center, "STATE-OF-THE-ART ASSESSEMENT OF ELECTRIC AND HYBRID VEHICLES" MCP/M1011-01, uc-96 available from NTIS, U.S. Dept. of Commerce, 5285 Part Royal Road, Springfield VA 22161.
16. Snively, H.D. and Robinson, P.B., "Measurement and Calculation of DC Machine Armature Inductance" AIEE Transactions, 1950, Vol. 69, pp. 1228-1237.
17. Kusko, A., "Solid State Motor Drives" Book, MIT Press, Cambridge, MA, 1969.
18. Mazda, F.F., "Thyristor Control" Book, Chapter 5 and Appendix to Chap. 5, Newner-Butterworth, London, 1973.
19. A.R. Knowlton "Standard Handbook for Electrical Engineers", 8th Edition, Book McGraw-Hill Book Co., NY (7-120).
20. Thompson, M. A. and Waters, L. A., "The Design of DC Commutator Motors for High Performance Electric Vehicles" SAE Paper #740169.
21. Ewing, J. S., "Lumped Circuit Impedance Representation for DC Machines," IEEE PAS Transactions, Vol. PAS-80, No. 4, April, 1968.
22. Strangas, E. and Hamilton, H. B., "A Model For the Chopper Controlled DC Series Motor." To be submitted to IEEE for presentation at the 1981 SPM.
23. Dubey, G. K. and Shepherd. "Analysis of DC Series Motor Controlled by Power Pulses," Proc. IEEE, Vol. 122, 1975.
24. Yanase, A., "Starting Characteristics of Chopper Controlled DC Series Motor with Non-Linear Magnetization Curve," EE in Japan, Vol. 97, No. 1, 1977.

DETERMINATION OF EFFICIENCIES, LOSS MECHANISMS,
AND PERFORMANCE DEGRADATION FACTORS IN CHOPPER
CONTROLLED DC VEHICLE MOTORS

SECTION I, APPENDICES

"TEST PROGRAM RESULTS AND RECOMMENDATIONS"

Prepared for: NASA - Lewis Research Center and The Department of Energy

by: Electrical Engineering Department
University of Pittsburgh
Pittsburgh, PA 15139

Howard B. Hamilton, Principal Investigator
Elias Strangas, Research Assistant

FINAL REPORT

GRANT NSG #3163

DECEMBER 30, 1980

APPENDIX A

- THE TEST FACILITY -

Tests detailed in this report were conducted using generator and battery sources, dynamometers for loading the test motors and necessary instrumentation for obtaining desired parameters and results.

Figure A-1 is a schematic of the test circuit used throughout, except for the tests to determine R and L variations as a function of frequency and saturation (the circuit for those tests is shown in Figure A-2).

The test circuit provides for powering the motor under test from either a 625 amp, 0-125 volt generator or from an 84 volt battery pack or from paralleled generator and batteries and with the chopper in for control or with the chopper bypassed. The generator has 69000 μ F of capacitance across its terminals for surge voltage suppression. Two battery packs were utilized. They were 14-6 volt EV 106 'golf cart' batteries and 7 - 12 volt Exide RC-27 Heavy Duty batteries.

A complete series of tests were run on the generator and batteries in order to evaluate their characteristics and to explore the feasibility of using the generator only as a power source when the test motor is under chopper control. These tests were conducted at the request of NASA-Lewis and the test results were submitted, under this grant number in a report entitled, "AN INVESTIGATION OF POSSIBLE DC POWER SOURCES FOR TESTING ELECTRIC VEHICLE MOTORS"⁽³⁾. In addition, a paper entitled, "A DC POWER SOURCE FOR TESTING BATTERY POWERED ELECTRIC VEHICLE MOTORS"⁽⁴⁾ was written and presented at the IEEE 1979 Annual Industry Applications Meeting. A copy of that paper is included in this appendix. They present wave form and regulation data as well as recommendations for surge voltage control.

The dynamometer used for load tests was a General Electric TLC-2332, Model 26G236, S/N 2483254, with cradled bearings. Maximum torque capability

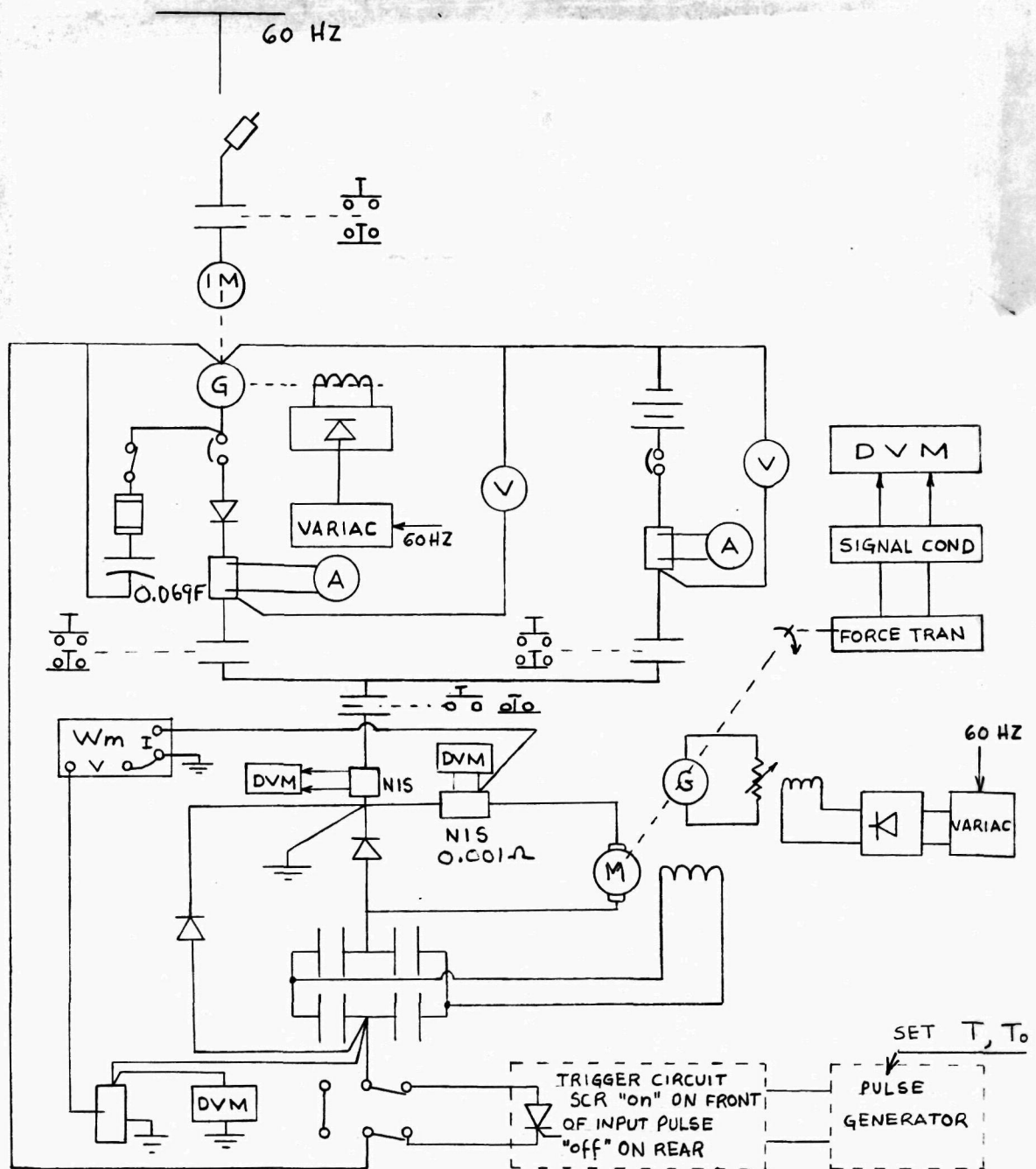


FIGURE A-1

is 114 n-m (84 ft-lbs) up to 2500 rpm, falling to 71 n-m at 4000 r/min. (29.8 Kw, or 40 hp) with maximum speed rating of 6000 r/min. Torque was measured using a BLH Load Cell Model T3P2B, S/N 38025, rated 100 lbs., which with the 1.3125 ft. arm resulted in a maximum torque measuring capability of 178 N.m (131 ft-lbs). Calibration tests indicated linearity down to 8 N.m, minimum. Speed was measured using a digital strobometer.

In order to obtain data such as friction, rotating core losses, etc. a 5 hp DC shunt motor driving through an Ametek CE-30-100, 00072-2 torque transducer was utilized. This unit was found to be linear over the range from 0.5 up to 12 N.m.

The chopper used was a Cableform Model 4013-2, S/N 76073918 rated 600 amperes. The on-off time of the chopper was controlled by inserting a 5 volt square wave pulse into the chopper control module as shown in Figure A-2. The thyristor in the chopper unit conducts only during the time the 5 volt square wave pulse is present. Minimum on time is 0.8 milliseconds (time necessary to charge the commutating capacitors which force the thyristor shut off). A HP1217B CRO was used to monitor and measure the square wave repetition frequency and pulse width.

- OTHER INSTRUMENTATION -

Current measurements and CRO photos were made using noninductive shunts (NIS), T&M Research Products, Inc. Model K5000-10, 0.001 ohms, 6.5 MHz bandwidth, 275 amperes with voltage drop measured using a Fluke 2874 DVM (one ampere = one millivolt).

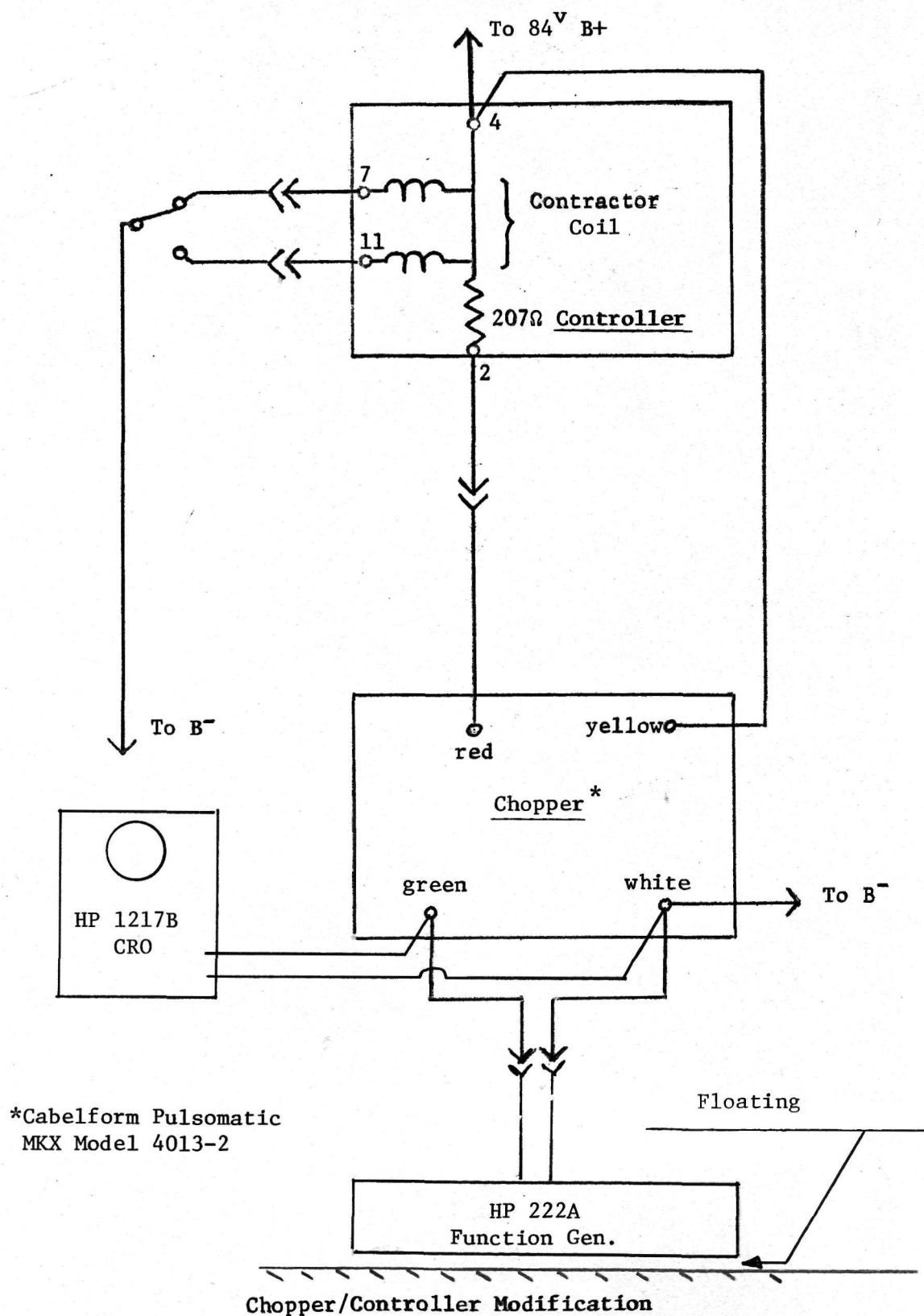


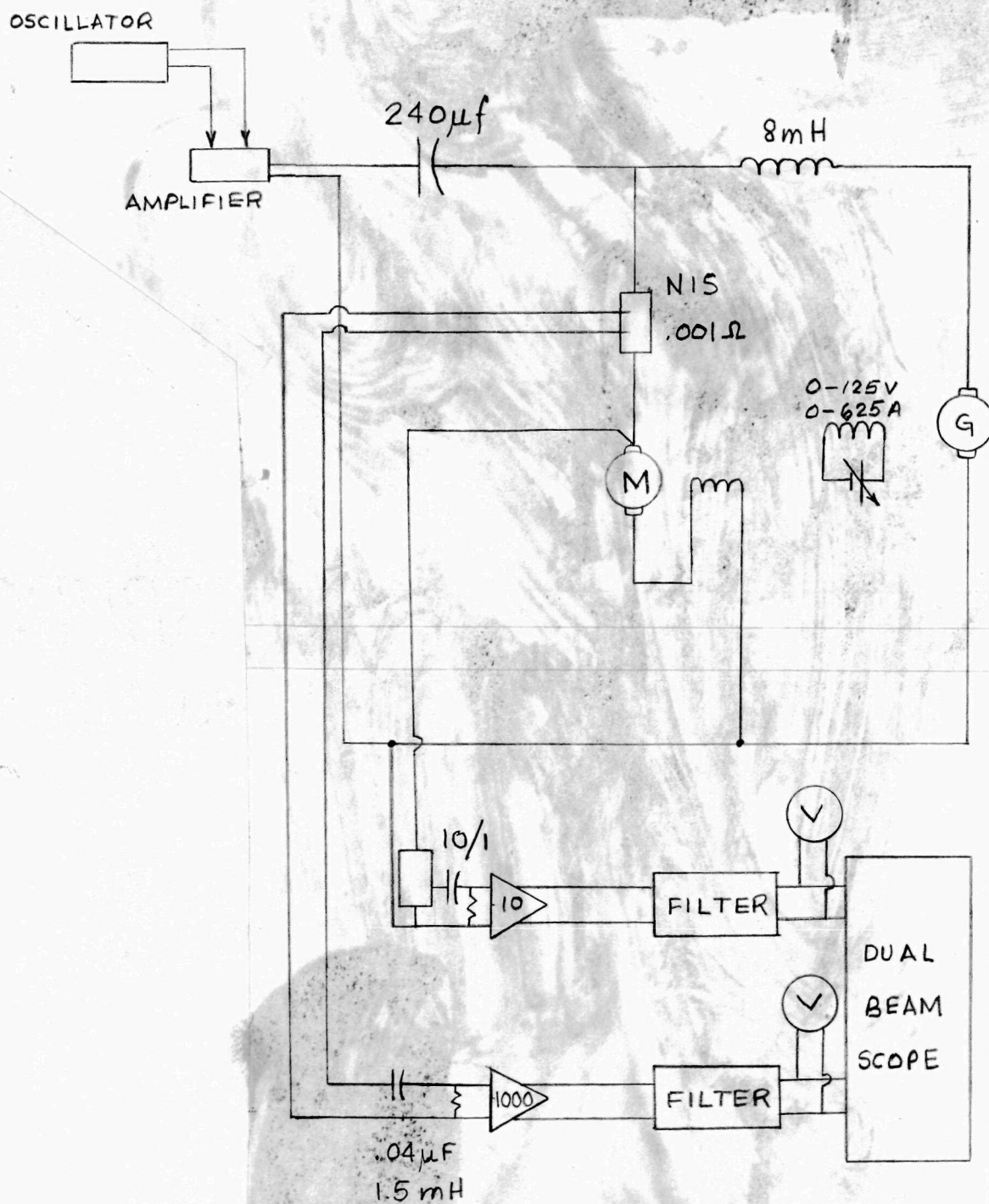
Figure A-2

Voltage measurements were made using DVMs with adjustable sample rate. (Fairchild 7100 A).

Power measurements were made using a Clark-Hess Model 255 electronic wattmeter, which was modified to accept the output from the NIS rather than utilizing the 5 ampere internal shunt. The internal shunt yielded 100 mv for 5 ampere input. The NIS yields 100 mv for 100 amperes. Thus a multiplying factor of 20 times watt reading is required.

Instruments and the circuit used in the tests to determine R & L parameters (see APPENDIX D) are shown in Figure A-3.

Harmonic spectrums were measured using a Tektronix 5L4N Spectrum Analyzer, a Storage Type CRO and Polaroid Camera.



OSCILLATOR: HP651B
 AMPLIFIER: ZONIC ZPA-1
 FILTERS: KRONE-HITE 3500
 VOLTMETERS: HP-400E
 AMPLIFIER: PRESTON 8300 XWB

FIGURE A-3

A DC POWER SOURCE FOR TESTING BATTERY POWERED ELECTRIC VEHICLE MOTORS

H. B. Hamilton, SM
University of Pittsburgh
Pittsburgh, PA

E. F. McBrien, M
NASA-LEWIS
Cleveland, OH

E. Strangas, Student Member
University of Pittsburgh
Pittsburgh, PA

ABSTRACT

Battery powered electric vehicles often control the average voltage applied to the motor by varying the duty cycle of "chopper" type controllers. These controllers usually use a thyristor as the modulation device and may vary pulse width, pulse rate or a combination of both.

In order to obtain meaningful test results, motors must be tested as a part of the source-chopper-motor system. However, electric vehicle batteries change their characteristics as a result of age, temperature, state of charge and prior use. Battery characteristics also vary with size, type and manufacturer. Batteries also have undesirable safety and maintenance requirements. Consequently a battery simulator to replace the actual battery bank appears desirable.

This paper details the results of an investigation into the factors that merit consideration when designing a rotating machine battery simulator. The size and number of units of surge over voltage protective capacitors as well as recommendations for protective fusing are discussed.

INTRODUCTION

Present methods of testing electric vehicle motors, controllers and combinations of them do not produce uniform and comparable results. The inability to obtain repeatable test data is largely due to motor, controller and power supply interactions. For instance, electric vehicle motors are often connected to the battery through a chopper type controller. The controller reduces the average value of voltage that is applied to the motor. However, the motor response is not the same as when the motor is connected directly to a battery or other ripple free source having the same average voltage value. Variations of performance also appear when choppers are supplied from power sources with different characteristics.

Because of the interactions it is presently necessary to test specific combinations of motors, controllers and power supplies. Unfortunately, electric vehicle batteries change their characteristics as a result of age, temperature, state of charge and prior use. Changes in size, type and manufacturing techniques also produce different characteristics.

The effective battery impedance is the parameter that produces the performance variations. Since the battery consists of a number of series connected cells, the total effective impedance is the sum of the effective impedances of the individual cells. Literature sources indicate that the internal impedance of typical lead acid batteries ranges from about 3×10^{-4} ohms per cell, to about 1.6×10^{-3} ohms per cell, depending upon battery design (i.e., anticipated duty, such as heavy starting duty, desire for maximum number of deep discharge cycles possible over the life of the battery, etc.), the battery manufacturer, and the state of charge of the battery.

For a 96 volt battery pack, the above range yields an ohmic variation, for the pack, of approximately 0.015 to 0.080 ohms. Since a typical motor, as used in electric vehicles has an armature circuit resistance in the vicinity of 0.020 ohms, the variation in battery resistance has an appreciable impact on the time constant of the power circuit. Since a chopper type controller causes repetitive transients, the time constant variation is especially important. Inductance and capacitance of the battery is generally negligible relative to the remainder of the power circuit.

IEEE Std. 113, Test Code For DC Machines, does not address this problem. Thus, a need exists for specifying not only the test procedures but also the nature of the test facility used for obtaining test data.

In the laboratory, batteries have several other undesirable features. Among them are the need to regularly check water levels, measure specific gravities, inspect and tighten terminal connections and be periodically recharged. Batteries also contain either sulfuric acid or caustic electrolytes. Batteries generate hydrogen when overcharged and comprise an electrical voltage source which cannot be easily turned off.

The variability of batteries and their maintenance and safety requirements have fostered a need for a laboratory power supply which can reasonably simulate a battery and yield repetitive results. There are several possible approaches. One method which reduces the variability consists of floating a battery across the output of a power supply. By making the output impedance of the power supply considerably higher than the battery impedance, the pulses of current will be drawn largely from the battery. The power supply serves to maintain the state of charge of the batteries. The power supply could be either a motor/generator set or a static type. In either case a resistor will usually be needed in series with the power supply to increase the power supply impedance.

Use of DC generator - AC motor set without batteries is another approach and yields a battery simulator which can be more easily tailored to meet specific source characteristics. The motor-generator set has thermal time constants of the same order of magnitude as the traction motors being tested and acts as a buffer between the controller and the utility power system. The nature of rotating DC machines is such that sudden removal of load from a machine in the generating mode results in high reactance voltages in the armature coils; possibly resulting in failure of insulation between commutator bars and initiation of bar-bar arcing or 'flashover'. Alternatively, the inductance of the generator armature causes switching transients. Each time the controller interrupts the armature current the energy stored in the inductance must be either dissipated in resistors, or stored in filter capacitors, or in an arc-over across commutator bars. Conventional load dropping using a contactor or circuit breaker involves relatively slow interruption and reduces the likelihood of arc-over or insulation failure. Thus a thyristor switching chopper re-

quires special considerations if the source is to be a rotating DC generator. The use of a conventional generator with paralleled energy absorbing capacitors is the approach taken in this investigation.

A practical battery simulator must cover the range of sizes and characteristics of presently used batteries and those contemplated in the foreseeable future. The present voltage range for electric vehicle motors is from 24 volts to 216 volts. The current range depends on the kind of controller in the vehicle. Unless current limiting is employed, stall currents over 1000 amps are possible. The continuous current rating of the supply needs to be at least equal to or greater than the continuous current rating of the motor. For the foreseeable future an average continuous current rating of 300 amps appears to be adequate. At 100 volts and 75% efficiency, 300 amps corresponds to about 30 HP.

BATTERY/CHOPPER CHARACTERISTICS

Tests were conducted using nominal 84 volt battery supplies. One such supply consisted of fourteen series connected 6 volt batteries designed for golf cart service; i.e., for a large number of relatively deep discharge cycles. The other bank consisted of seven series connected 12 volt batteries of the type known as "heavy duty" auto or truck batteries. Under both static loading, and dynamic loading, i.e., with chopper, the apparent resistance, defined as incremental change in voltage for incremental change in current, for the latter type was about 25% lower than for the former. The order of magnitude for the 84 volt bank was found to be approximately 0.05 ohms - 0.07 ohms.

It was recognized that a suitable DC generator, with added external resistance, could be utilized to yield the same apparent resistance if the generator could be protected against surge overvoltages and commutator flashover.

Figure 1 shows the battery current and terminal voltage across a chopper/series motor load under the condition of $T_o/T_{total} = 6.6/13.4$ milliseconds.

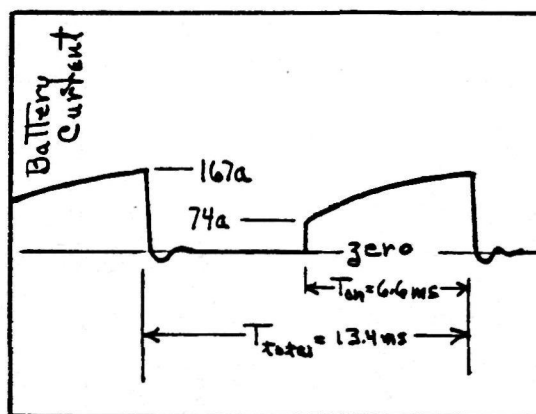
Average current was 69 amperes, average battery voltage was 80.7 volts. The motor load is paralleled with a free wheeling diode. When the chopper turns on, current immediately jumps to 74 amperes, increasing to 167 amperes at turn off. The bus voltage drops 5.5 volts initially with a 10.2 drop at maximum current condition, yielding an "apparent" resistance of 0.05 ohms.

The oscillation following thyristor cut off is a characteristic of the thyristor and its forced commutating circuit.

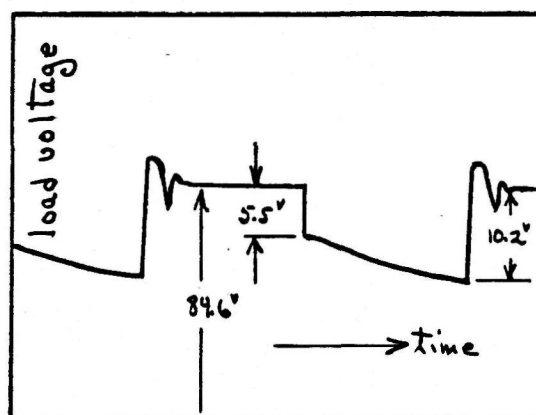
GENERATOR/BATTERY/CHOPPER CHARACTERISTICS

An available compound wound generator was used as the battery simulator. The generator rating was 625 amperes, 120 volts. The generator was operated at 84 volts (nominal battery pack rating) by shunt field excitation control. The series field was not connected. Armature circuit inductance, as furnished by the manufacturer, was 0.16 millihenry. A static load test on the generator and its associated contactor, circuit breaker and connecting leads yielded an observed total circuit resistance of 23.5 milliohms.

A series of tests were run with the generator and battery paralleled and supplying a motor load through a chopper. Figure 2 shows battery cur-



$$I_{\text{average}} = 69 \text{ amperes}$$

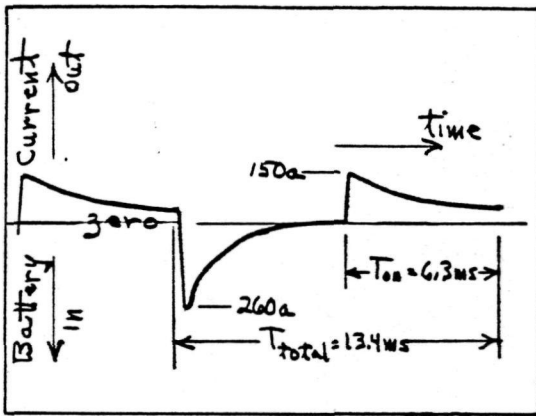
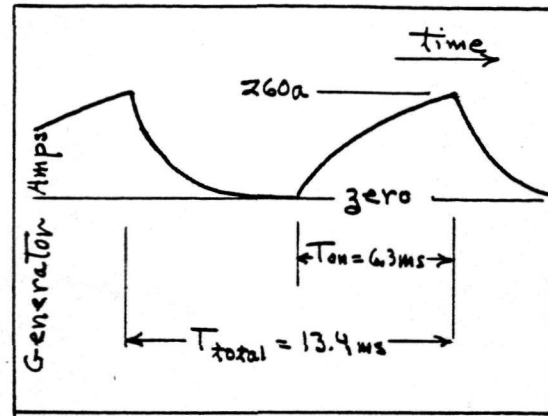
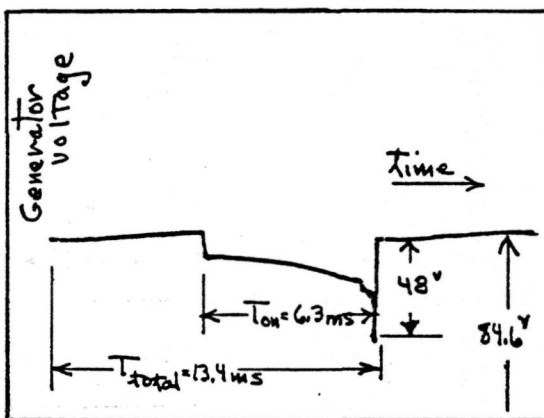
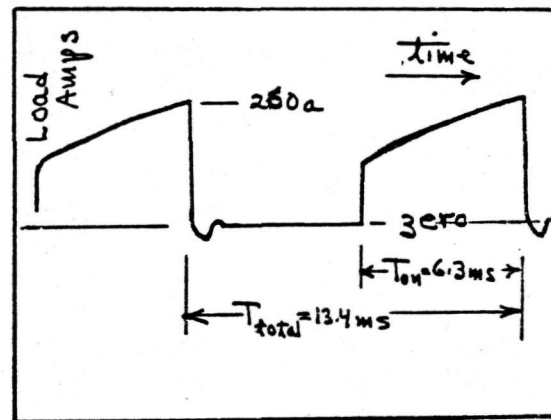


$$V_{\text{average}} = 80.7 \text{ volts}$$

V and I, Battery/Chopper/Motor Load
FIGURE 1

rent, generator current, load (or total) current and bus voltage for the same chopper condition, i.e., $T_o/T_{total} = 6.6/13.4$ as for the battery/chopper test of Figure 1. The battery used was the "golf cart" type battery. However, the "apparent" resistance of the supply has changed from 0.05 ohms down to 0.027 ohms, with the result that the peak current is 260 amperes (as compared to 167 amperes in Figure 1) and average current is 100 amperes (vs. 69 amperes before). Also present in the test with the generator in parallel with the batteries is a 48 volt spike at the instant of chopper cut off. The origin of this spike is believed to be in the generator coil undergoing commutation at the instant of the cut off. Cut off time is very rapid relative to generator commutation period and the trapped flux linkage sets up an oscillation at the natural frequency of the generator armature coil because of the coil inductance and inherent capacitance. The frequency

involved for DC generators lies in the $10^3 - 10^7$ hertz range. The battery supplies only 3+ amperes average current, although peak battery currents of +91.5 and -186 are observable. The generator supplies 94+ average amperes with a peak current of 232 amperes.

Battery Current, $I_{\text{average}} = 3$ amperesGenerator Current, $I_{\text{average}} = 94$ amperesGenerator Voltage, $V_{\text{average}} = 83.7$ voltsLoad Current, $I_{\text{average}} = 97$ amperes

Battery/Generator/Chopper with Motor Load

FIGURE 2

The same test was conducted using the heavy duty car/truck battery (lower internal resistance battery). The observed voltage spike was reduced to 39.5 volts and the battery supplied 11.5 amperes average current. Both of these changes are attributable to the difference in internal resistance of the two types of batteries.

Tests were also conducted with a shunt connected DC motor "floating" on the bus to observe if its equivalent capacitance (corresponding to stored inertial energy) would have any affect on the voltage transients. The equivalent capacitance was estimated as 8 F. However, the inherent armature circuit inductance of the floating motor made this method ineffective.

GENERATOR/CAPACITOR/CHOPPER CHARACTERISTICS

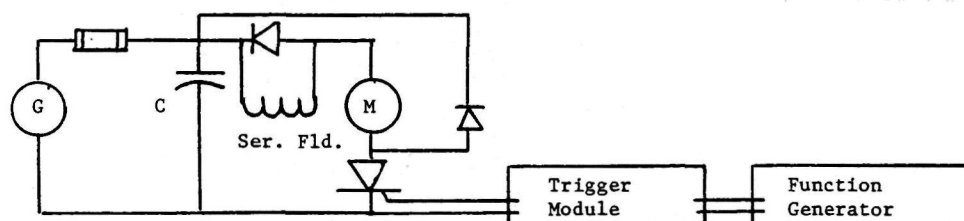
Tests with the generator and capacitor paralleled, Figure 3, established the feasibility of using a DC shunt generator as a source for a chopper controlled motor load if provision was provided for absorbing the magnetic energy stored in the generator inductance at the time of chopper (thyristor) cutoff. Either batteries or capacitors can accomplish this. Capacitors are preferred because of their smaller

size, reduced maintenance, reduced hazards, more uniform characteristics and lower costs.

In selecting the number of capacitor units to be used, and the capacitance of each unit the factors to be considered are the surge overvoltage resulting from armature circuit inductance interaction with the capacitor and the ripple current resulting from this interaction. In the interest of economy, electrolytic capacitors should be used and this type of capacitor does have a maximum ripple current rating.

At the instant of chopper cutoff, with negligible resistance in the circuit, the current in the generator armature circuit will be transferred, in its entirety, to the capacitor. In the previous tests, maximum load current (peak) encountered was 270 amperes. Assuming that this would be the peak capacitor current to be encountered and that the current oscillating between the generator and the capacitors required was determined. Electrolytic capacitors with a ripple current rating of 31 amperes rms and 150 VDC rating are available. The number of capacitor units required was thus determined to be:

$$\# \text{ Units} = 270 / \sqrt{2} (31) = 6$$



Generator/Capacitor/Chopper with Motor Load

FIGURE 3

When the chopper is "on", both capacitor bank and generator deliver current into the load. The voltage at the capacitor terminals is ΔV volts less than E_g , the generator open circuit voltage. ΔV is

composed of both generator resistance drop and an inductance voltage drop since the current may be still increasing with time. The amount of inductive drop is a function of the ratio of T_o/T_{total} for a complete cycle, since the motor counter emf is related to this ratio. Since this ratio can vary over wide ranges, it is not felt useful to attempt to quantify ΔV . Rather, previous tests had indicated that with capacitors of approximately 8000 μF in parallel, ΔV was 12 volts, or less.

The relationship between surge overvoltage, ΔV , the generator lumped inductance, L , the capacitance in parallel with the generator, and the current $I(0)$ at chopper cut off are related by the following theoretical relationship:

$$V_{\text{surge max}} = \sqrt{I(0)^2 \frac{L}{C} + \Delta V^2}$$

This formula is derived based on lumped L , no resistance in the circuit, an initial current of $I(0)$ and an initial capacitance charge voltage, $V_c(0) = E_g - \Delta V$. In the investigation described in this paper, it was desired to limit V surge to 20% of 84 volts, or 16 volts, well below the 125 volt rating of the generator. With $I(0) = 270$ amperes, $L = 0.16$ millihenry, $\Delta V = 12$ volts, C was calculated as 84,375 μF . The capacitor units alluded to above are available in 13,500 μF sizes. Six such units, when paralleled, comprise 81,000 μF . Because of availability, 4 of the 13,500 μF units were paralleled with 2 - 7500 μF units, making up a 6 unit bank of 69000 μF . Each capacitor unit was 3 inches in diameter and 8 5/8 inches in length. Therefore all six units occupy about the same physical space as one of the batteries. The cost of one capacitor unit is less than the cost of one battery. In the formula, this capacity would permit a theoretical 18 volt surge, rather than the arbitrary 16 volt surge.

Tests were conducted on the generator paralleled with 69000 μF for various values of average load current from 10.5 to 190 amperes average. Figure 4 depicts the bus voltage for values of

T_o/T_{total} of 1.4/12.4, 4/12, 6/12.4 and 7.4/12.4, corresponding to average currents of 13, 50, 122 and 190 amperes. As can be seen ΔV was 14 volts (for 190 amperes average) or less, and maximum surge overvoltages were less than 6 volts. The peak spike voltage observed was 36 volts.

Figure 5 is a CRO photo of capacitor current when the average current was 40.5 amperes. Under this condition, the capacitor current jumped to 45

amperes when the chopper went on. Load current at that instant was 58 amperes. When the maximum peak load current of 216 amperes was reached, the capacitor was supplying about 150 amperes, and the generator the remainder, 66 amperes. When the chopper when off, capacitor current reversed, i.e., came into the capacitor with a 160 ampere spike, then dropped to about 66 amperes and decaying as the capacitor became charged, prior to the next turn-on.

Tests were run with external resistance added on the load side of the capacitor-generator terminals. Figure 6 shows current and voltage wave forms for the condition of 0.05 added. The maximum voltage drop, ΔV is observed as 19 volts. The current jumps to about 75 amperes on turn on and reaches a peak of 180 amperes at turn off, as compared to 74 and 167 for the battery supply tests shown in Figure 1.

SUMMARY AND CONCLUSIONS

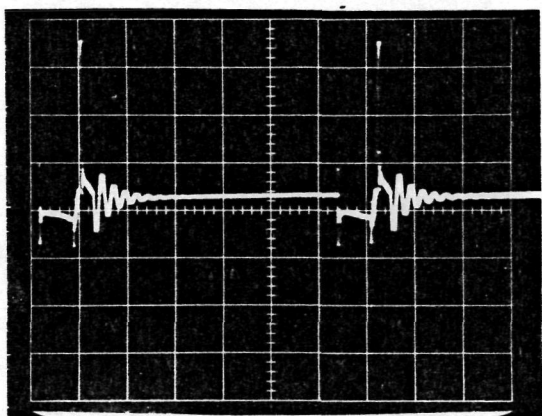
The tests described in this paper have demonstrated that it is feasible to use a DC generator, paralleled by a capacitor bank, as a source for testing chopper controlled motor loads. The wave forms of current and voltage are similar to those obtained using a battery as a source. External resistance can be added to obtain a desired voltage regulation, or "apparent" resistance of the source supply.

RECOMMENDATIONS

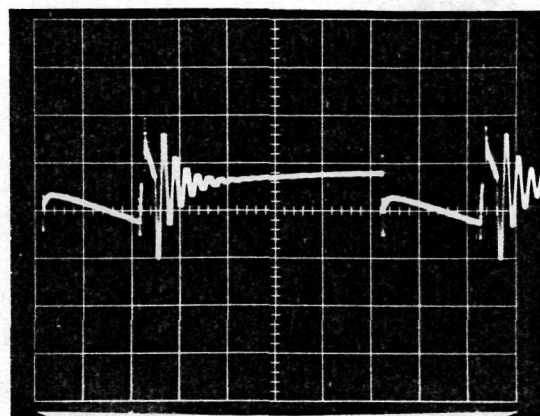
In order to secure uniformity in test results on electric vehicle motors to be powered from batteries with a chopper control of average voltage, it is recommended that a working group, or task force be appointed by the IEEE DC Machinery Subcommittee of the Rotating Machinery Committee to establish guidelines for rotating machine source systems to be used to test such motors.

A possible recommended source configuration could be that the continuous current rating of the DC generator be at least three times the maximum average current rating of the motor to be tested, that external R and L be added to the generator/capacitor to bring the source total to the same values as those of the battery to be simulated, and that the paralleled capacitance be of such a size as to minimize surge overvoltages. Since the latter specification is extremely general and difficult to quantify, a more acceptable recommendation may well be, for example, 100,000 μF or some other acceptable fixed value.

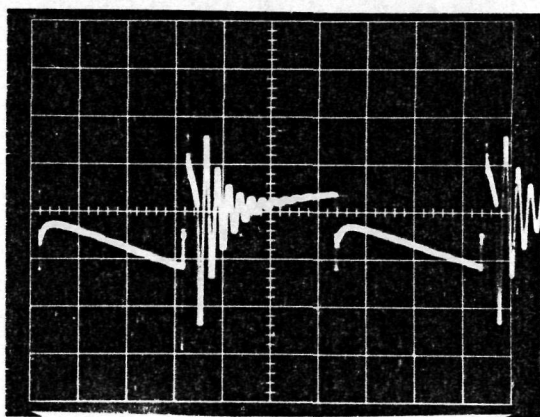
A further recommendation is to fuse the generator between the generator terminals and the capacitance bank, to provide short circuit protection for the generator in the event of a capacitor unit



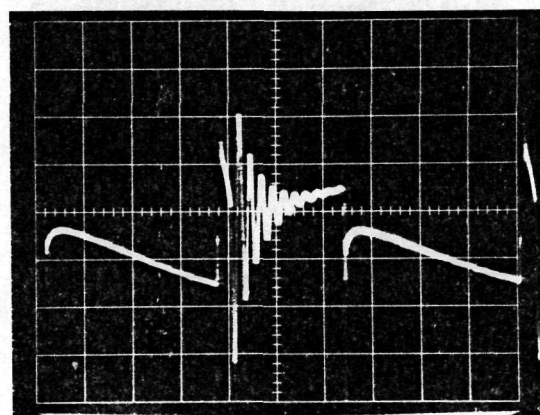
$I_{\text{average}} = 13 \text{ Amperes}$



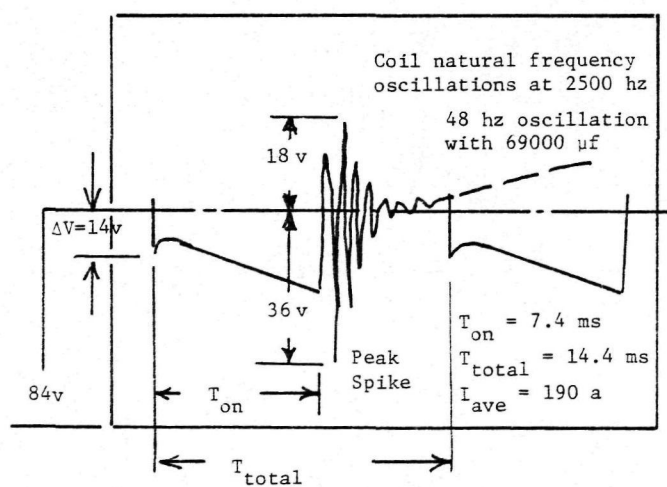
$I_{\text{average}} = 50 \text{ Amperes}$



$I_{\text{average}} = 122 \text{ Amperes}$

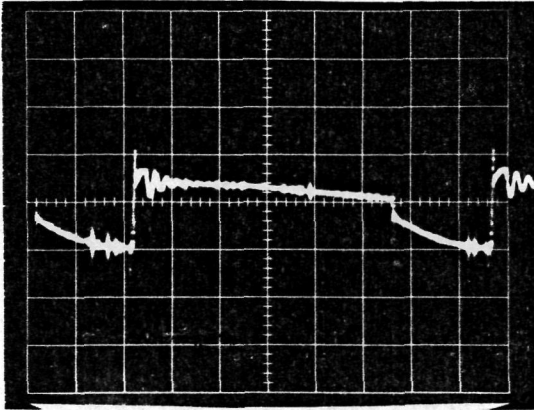


$I_{\text{average}} = 190 \text{ Amperes}$



Load Bus Voltage for Various Currents
(69000 μF of Capacitance in Parallel with Generator)

FIGURE 4



$I_{\text{capacitor}}$ 150 amp/Div, 2 ms/Div

Capacitor Current for $I_{\text{average}} = 40.5$ Amperes

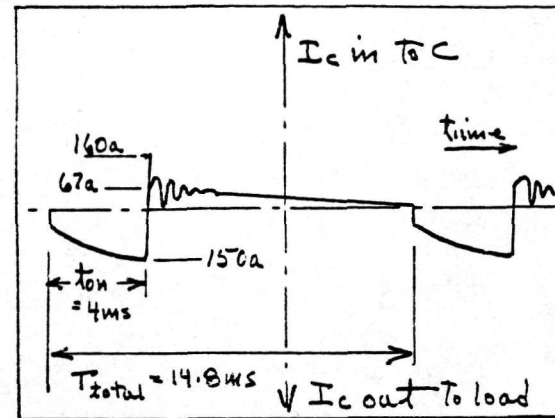
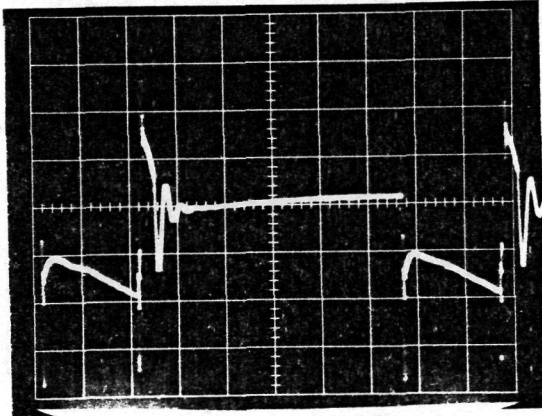
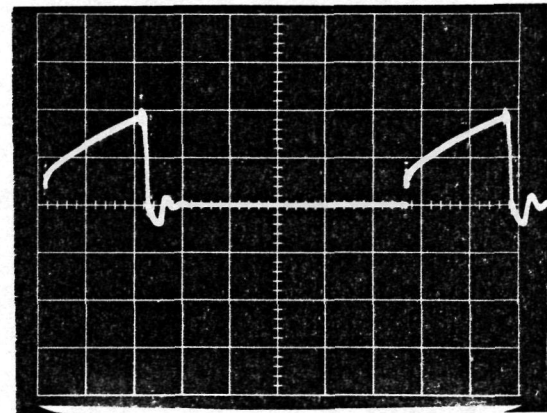


FIGURE 5



I_{Load} - 100 amp/Div, 1 ms/Div, $I_{\text{avg}} = 40.5$ amp



V_G - 10 volts/Div

Current and Voltage, with 0.05 ohms External Resistance

FIGURE 6

failure. The source system should be shut down in the event of a capacitor failure or an internal fault within the generator. Such a fuse, located as recommended, would accomplish this protection.

The recommended fuse should be of the type used for semiconductor applications, known as "fast acting", i.e., no time delay. In a circuit involving a 200 ampere average current, a 200 ampere fuse could be used. Such a fuse size typically will pass 400 amperes for 1000 seconds but will clear a 1000 ampere fault in 0.025 seconds. In the 130 volt version, this fuse adds less than 0.5 milliohms to the circuit.

The generator should also be protected by a voltage sensitive device (comparator) which will shut down the system, if the voltage spikes exceed a predetermined value, based on the operating voltage and voltage rating of the generator.

ACKNOWLEDGEMENT

This work was supported by NASA and the Department of Energy under Grant #NSG - 3163.

APPENDIX B

DESIGN DETAILS OF MOTORS TESTED

(From Manufacturer or Physically Measured)

RED MOTOR

Open ventilation with internal fan (fan removed for tests)

(150 CFM @ 2000 rpm)

Speed 1800-2500 r/min

Rated Current: Armature 175 amperes

Voltage: 144 Maximum

Wave Wound (2 parallel paths), No interpoles

4 pole, 27 slots, 6 conductors/slot, 81 commutator bars, $Z = 54$ conductors

Field Winding: 20 turns/pole, Series (No shunt)

Frame Material: Wrought iron

Pole and Armature: Laminated, M-27 electric sheet steel

0.46 mm (0.018 inches, 26 gauge)

Armature Radius: 92.075 mm (3.625 in.)

Air Gap: 3.23 mm (0.127 in.)

Stack Length: 96 mm (3.78 in.)

Pole face arc span: 63.59 mechanical degrees, 1.109 rad

Pole face area: 0.0101 m^2 (15.726 in.²)

Brushes: 8 electrographic (#417 stackpole or #201c Kirkwood)

Force: 1800-2200 grams (3.96 - 4.84 lbs)

Area: (each 13x32 mm) 416 mm^2 (0.645 in.²) each

Commutator: 400 mm (15.748 in) circumference.

Each segment 3.9 mm (0.15 in) width

0.8 mm (0.03 in.) separation.

— represents 3 conductors

Note: 3 coils shorted per pair
of brushes
2 pairs of brushes
∴ 6 coils shorted

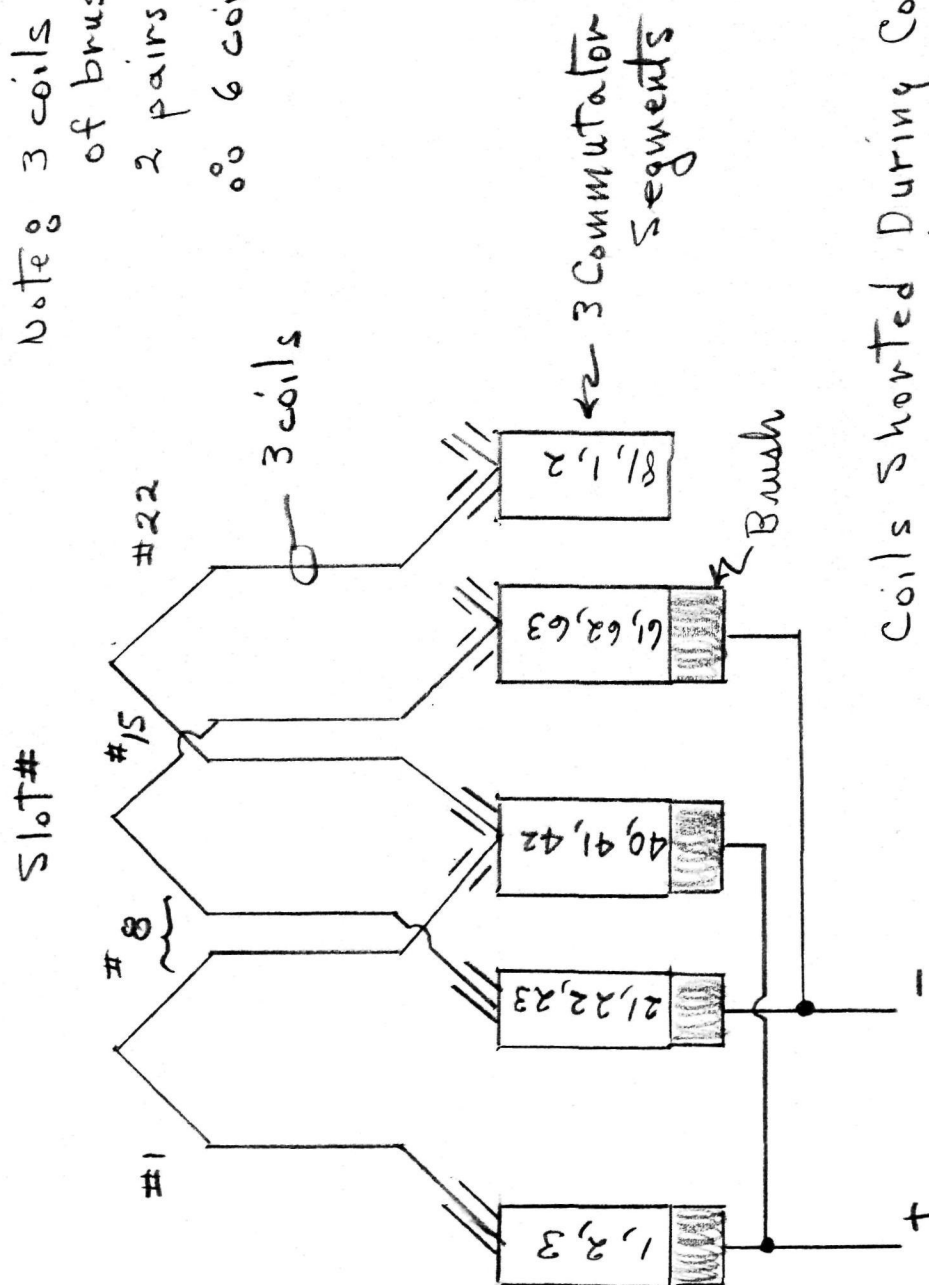
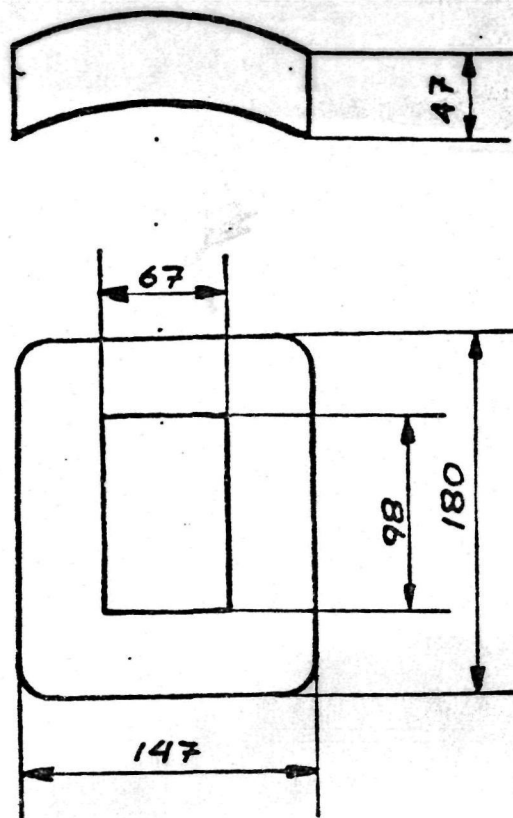
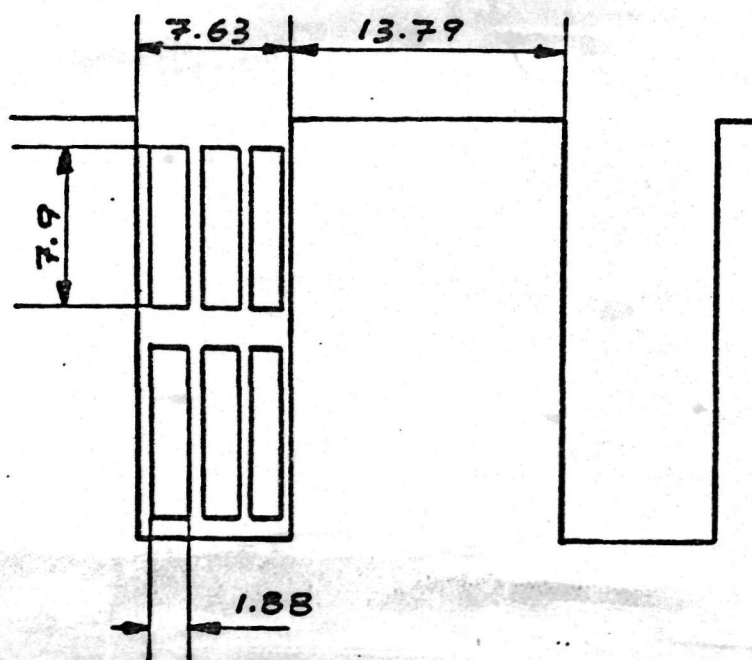


FIGURE B-1

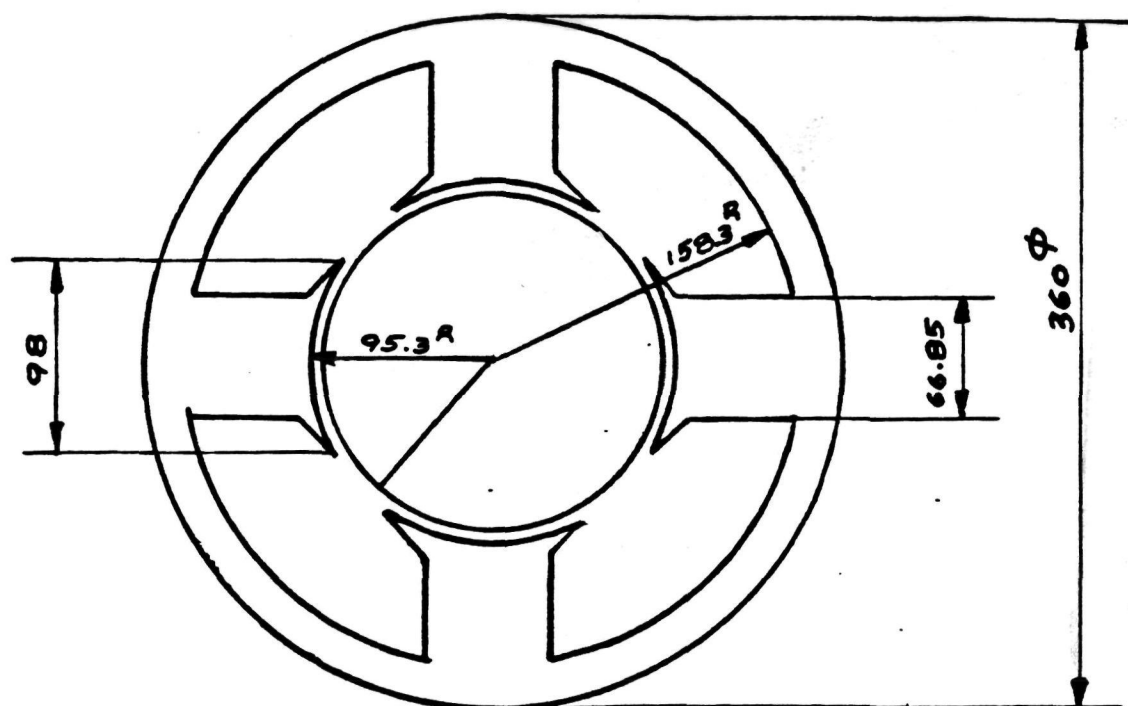
Coils Shorted During Commutation
Red Motor (Wave Wound)



Dimensions of the field winding (in millimeters)



Dimensions of slot and armature conductors (in millimeters)



Dimensions of rotor and stator (in millimeters)

FIGURE B-3 RED MOTOR

Each brush spans 3 commutator segments (3 coils). Total of 6 coils shorted during commutation. See Figure B-1.

Figures B-2 and B-3 depict frame, field winding and slot dimensions.

Armature Resistance (DC) 0.0189 ohms

Field Resistance (DC) 0.0165 ohms

(All Fields in Series)

BLUE MOTOR

External Ventilation, 250 CFM external blower required.

Speed: 4000 rpm, 20 hp (maximum)

Rated Current: 208 amperes

Voltage: 84 volts

Lap Wound (4 parallel paths). No interpoles. Equalizer Winding Present.

4 pole, 32 slots, 4 conductors/slot, 2 turns/coil (4 - #15)

64 Commutator Bars, $Z = 256$

Field Winding: 24 turns/pole, Series (No Shunt). (1 = #4, square)

Frame Material: Integral with poles

Pole and Armature: Laminated, 24 gauge Electrical Sheet

0.635 mm (0.025 in.)

Armature radius: 75.8 mm (2.984 in.)

Air gap: 1.59 mm (0.0625 in.)

Stack Length: 92.1 mm (3.625 in.)

Pole face arc span: 53 mechanical degrees, 0.925 rad

Pole face area: 0.0066 m^2 (10.22 in.²)

Brushes: 8

Force: 1365 grams, (3 lbs.)

Area: (each 15.9 x 31.75 mm) 504 mm^2 (0.7813 in.²)

Commutator: 326.67 mm (12.86 in.) circumference. Each segment

3.97 mm (0.156 in) width, 1.016 mm (0.04 in) separation.

Commutator is skewed 2.17 degrees, hence, each brush bridges 4 commutator segments (3 coils). Total of 12 coils shorted during commutation. See Figure B-4.

Figures B-5 and B-6 depict frame and slot dimensions.

Armature Resistance:	(DC); 0.011 ohms
Field Resistance:	(DC); 0.008 ohms
Armature Inductance	0.16 mH (Saturated)
Armature Inertia	1.4 lb-ft ²

- 2 paralleled conductors
- 3 coils/brush
- 4 brushes
- 12 coils (24 turns) shorted

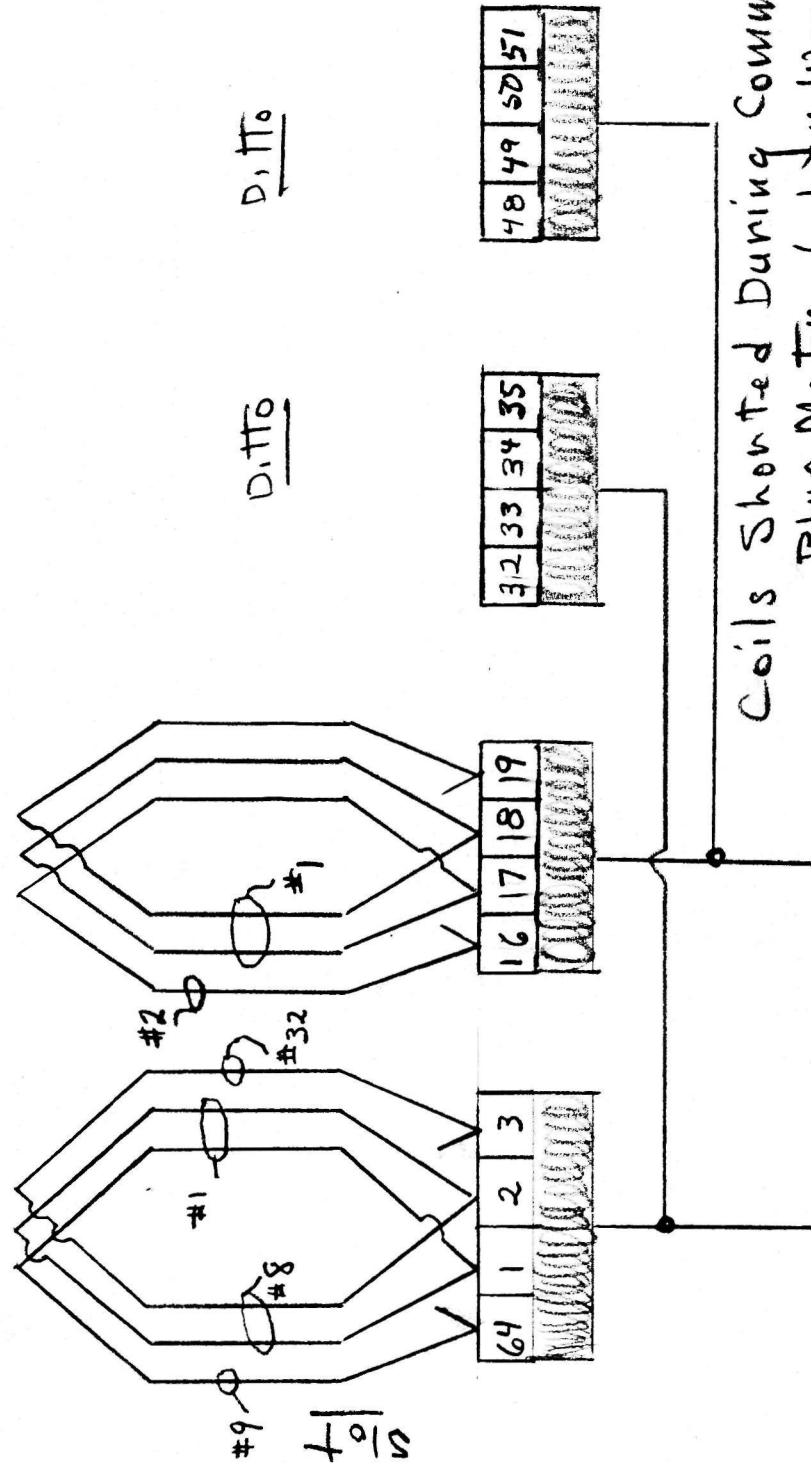
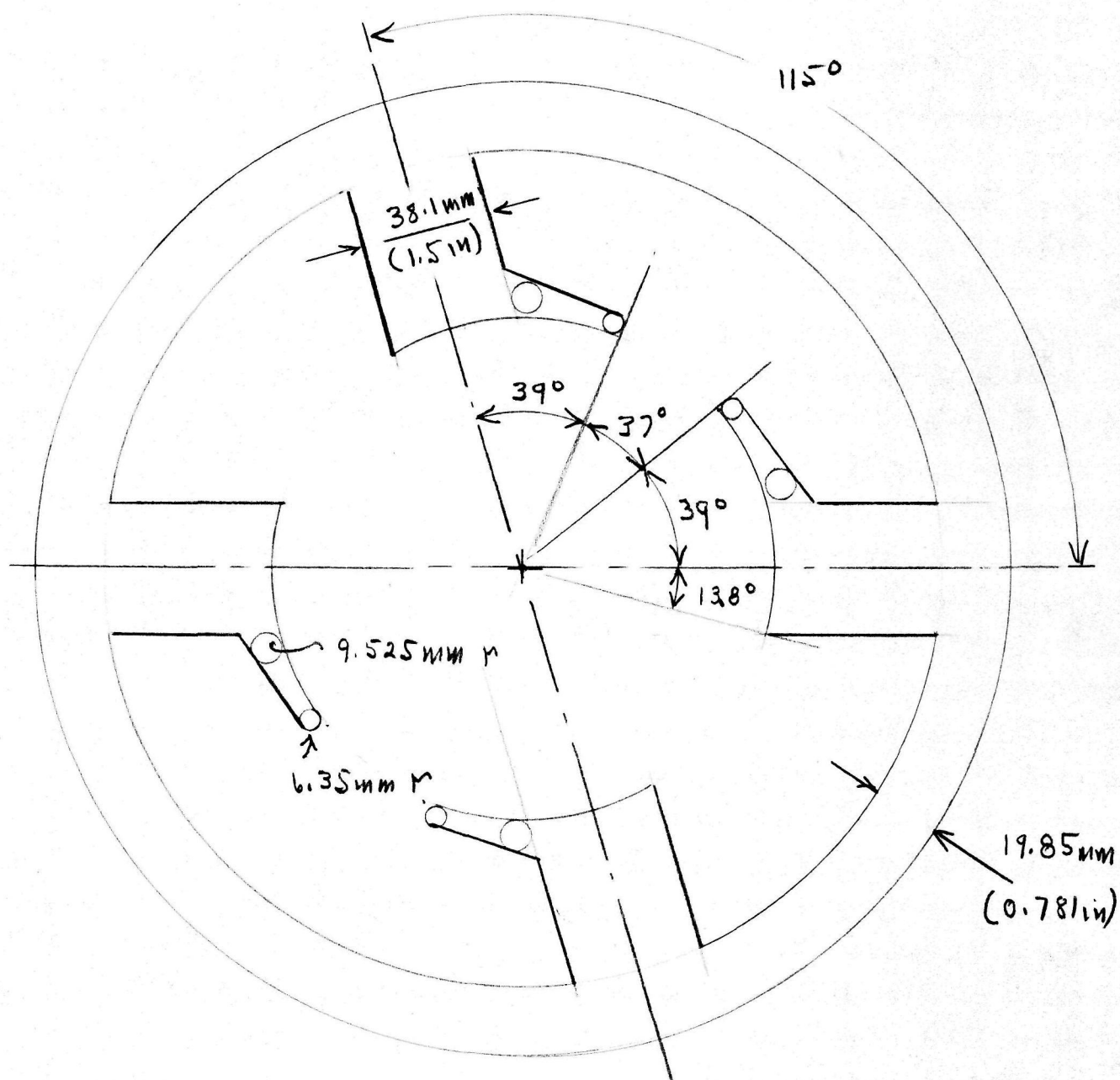
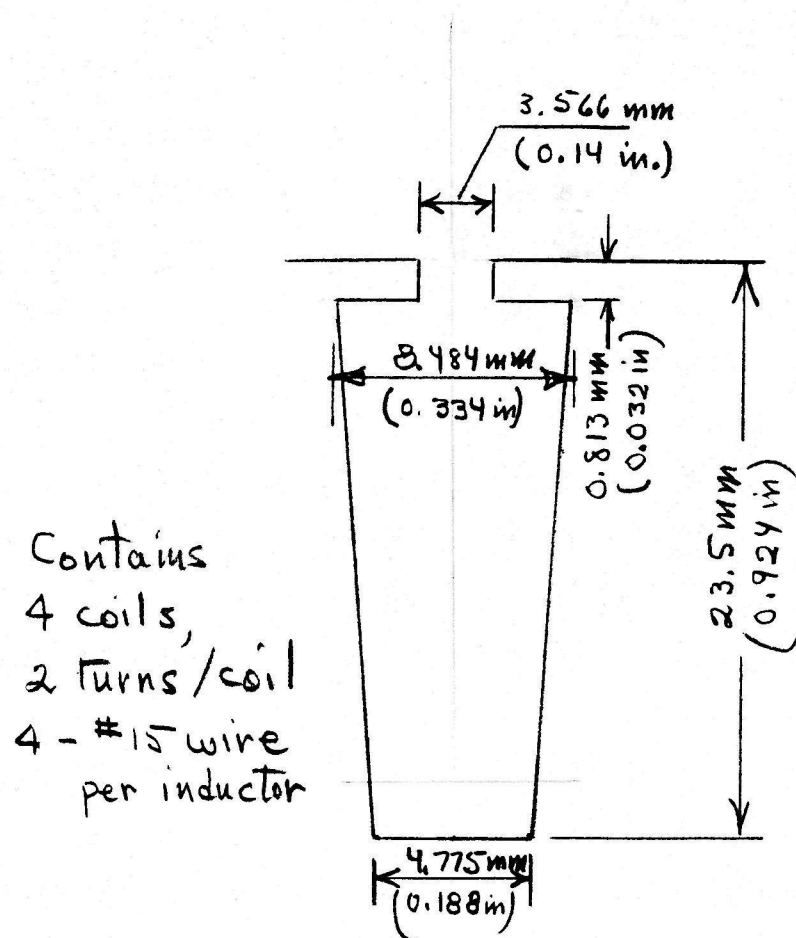


FIGURE B-4



Frame Dimensions - Blue Motor

FIGURE B-5



Slot Detail, Blue Motor

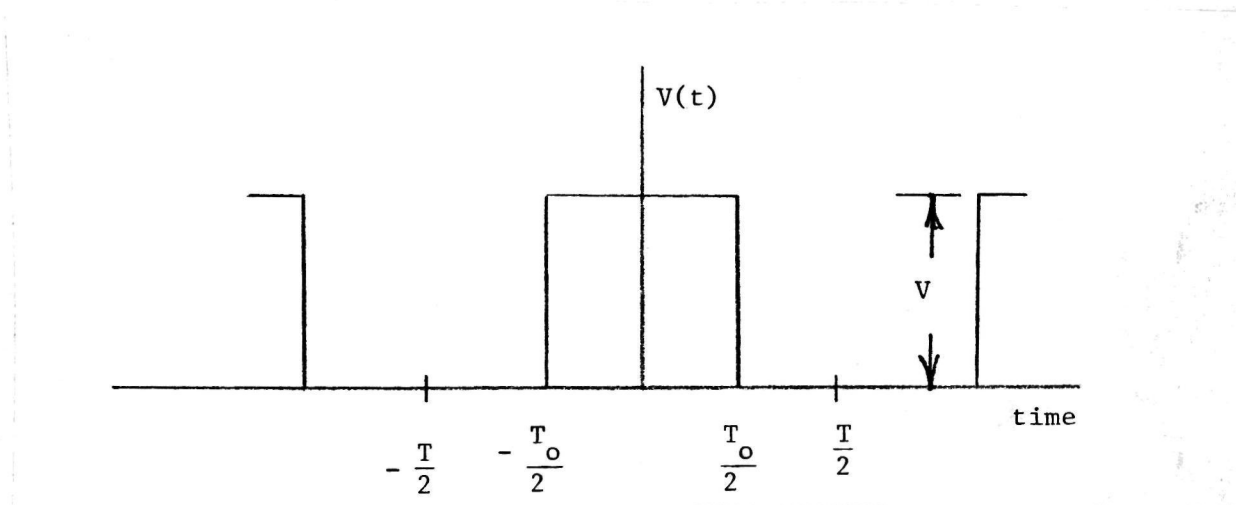
FIGURE B-6

WAVE FORMS AND THEIR HARMONIC CONTENT- Introduction -

A chopper controlled DC source impresses a step voltage on the armature and field (if a series motor) at regular intervals, determined by the frequency at which the chopper is operating. Neglecting voltage drop in the supply circuit, the voltage wave has a constant value, V , equal to the source voltage during the 'on' time, T_o and is zero during the remainder of the period, T where:

$$T = 1/f \quad (C-1)$$

and f is the chopper repetition frequency. Such a wave is shown in Figure 1.

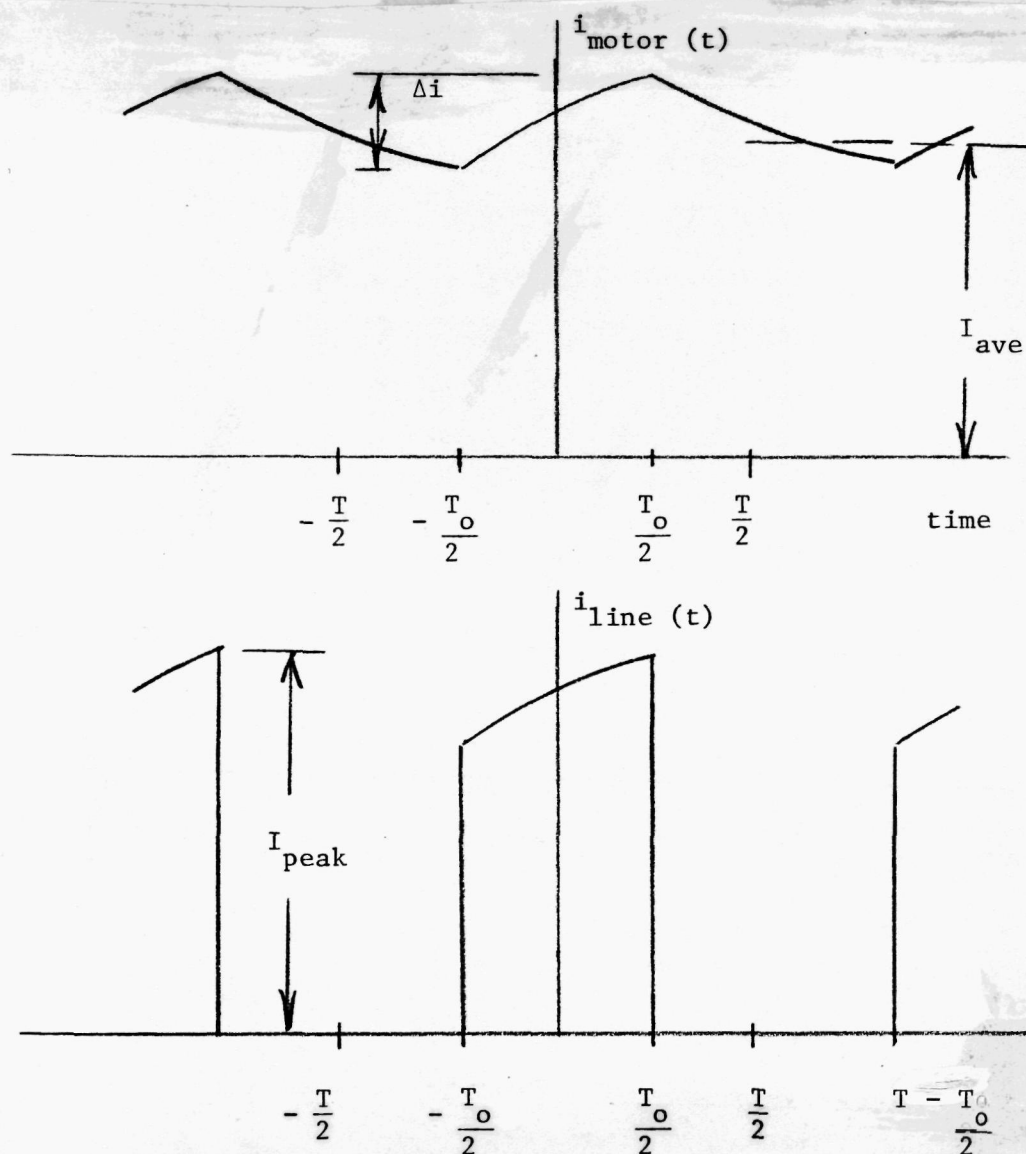


Chopper Controlled Motor Voltage
Figure C-1

$v(t)$ can be expressed as a Fourier Series by:

$$v(t) = \frac{V T_o}{T} + \frac{2V T_o}{T} \sum \left(\frac{\sin n\pi T_o/T}{n\pi T_o/T} \right) \cos \frac{2\pi n t}{T} \quad (C-2)$$

The current wave forms resulting are as shown in Figure C-2 (For continuous conduction).



Motor and Line (Source) Current
Figure C-2

The motor current flowing from $T_0 / T - \frac{T_0}{2}$ circulates through the Free Wheeling Diode (FWD) which is connected back biased and in parallel with the armature and series field.

Franklin⁽⁵⁾ presents the Fourier Series for the motor current as shown. The coefficients are extremely complex and are functions of T , T_o and V as well as circuit resistance and inductance, and the voltage constant (volts/ampere, radians/sec).

Since the inductance, resistance, and voltage constant are all functions of frequency and saturation of the magnetic circuit,⁽⁷⁾ Franklin's Fourier Series does not appear to be neither widely nor can it be feasibly used. However, with the use of simplifying assumptions it is possible to obtain an approximate solution for the currents and obtain insight into what may be expected in the way of harmonic content. The assumptions are:

- 1) constant inductance, L
- 2) the armature-field time constant (L/R) is long relative to the on time, T_o , i.e., di/dt is constant. (This was found not to be a reasonable assumption on the motor tested in this investigation, as shown later in this appendix.)

With these assumptions, the exponential variations become linear and the Fourier Series for the current become:

for line current:

$$i(t) = I_o + \sum \left(\frac{\Delta i}{T_o} \frac{T}{n^2 \pi^2} \sin \frac{n\pi T_o}{T} - \frac{\Delta i}{n\pi} \cos \frac{n\pi T_o}{T} \right) \sin \frac{n2\pi t}{T} + \frac{2I_o}{n\pi} \left(\sin \frac{n\pi T_o}{T} \right) \cos n \frac{2\pi t}{T} \quad (C-3)$$

for motor current:

$$i(t) = I_o + \frac{\Delta i T}{(T - T_o)\pi} \sum \frac{1}{n^2} \left(\frac{\sin n\pi T_o/T}{n\pi T_o/T} \right) \sin \frac{n2\pi t}{T} \quad (C-4)$$

It should be noted that an expression for Δi can be derived as follows:

$$\frac{di}{dt} = \frac{\Delta i}{\Delta t} = \frac{\Delta i}{T_o} = \left(V - \frac{VT_o}{T} \right) \frac{1}{L}$$

or,

$$\Delta i = \frac{V}{L} \left(1 - \frac{T_o}{T} \right) \left(\frac{T}{T} \right) T_o = \frac{V}{Lf} \left(1 - \frac{T_o}{T} \right) \frac{T_o}{T} \quad (C-5)$$

In order to examine the validity of using the "linearized" equations presented above and to check Franklin's rigorous equation, tests were conducted to obtain the harmonic content under various chopper-motor operating conditions.

The motor used for the tests was the RED motor, rated 200 amperes with all field windings in series. Harmonic content was measured with a Tektronix Model 5L4N Spectrum Analyzer, calibrated to read harmonics 1 through 11, in rms values. The CRO display was photographed and values scaled from the photos.

The test objectives were:

- 1) to determine harmonic magnitudes for loss and efficiency calculations,
- 2) to check for correlation with derived Fourier Series, for both currents and voltage.

To determine, for currents, the variation with respect to saturation, frequency and brush shift of:

- 3) the percent ripple
- 4) the ratio of peak to average current, I_p/I_{ave}
- 5) the ratio of current excursion to average current, $\Delta i/I_{ave}$
- 6) the ratio of root mean square to average current, I_{rms}/I_{ave}
- 7) the harmonic amplitudes
- 8) to determine the error introduced in calculating motor current excursion, Δi , during the duty cycle under continuous conduction situations using the formula that neglects circuit resistance and assumes constant circuit inductance.

RESULTSFor Voltage:

Figures C-3, -4a,, -4b, -5a and -5b present the wave forms and spectra for $T = 0.01$ seconds (100 Hz), 0.005 (200 Hz) and 0.0025 (400 Hz) for conditions of motor current of ≈ 100 amperes and 200 amperes, line currents of ≈ 65 amperes and 108 amperes. (Exact values are shown on the captions.) Open circuit voltage was 80 volts; $T_o/T = 0.5$. Table C-1 tabulates scaled values of the harmonics for the various frequencies and loads.

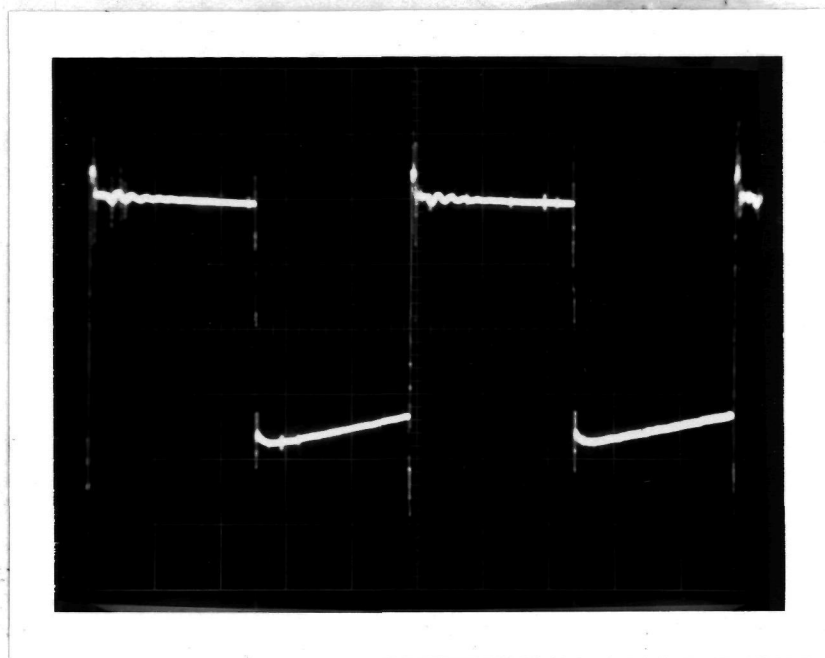
TABLE C-1

- Voltage Harmonics, RMS Values -

-Observed-

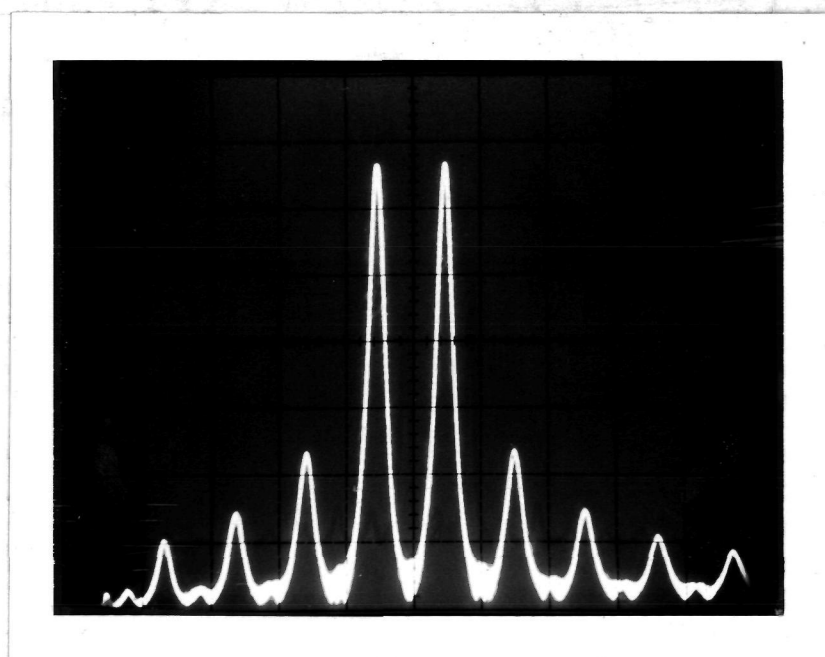
Harmonic Number

<u>FREQ</u>	<u>I_m</u>	<u>1</u>	<u>2</u>	<u>3</u>	<u>4</u>	<u>5</u>	<u>6</u>	<u>7</u>	<u>8</u>	<u>9</u>	<u>10</u>	<u>11</u>
100	198	31.4	---	10.8	1.6	6.4	1.1	4.4	1.1	3.4	---	---
200	107	32.7	3.3	11.5	2.9	7.3	3.2	5.5	3.1	4.0	2.7	3.6
200	199	31.1	---	10.9	---	6.9	1.6	4.9	1.4	4.4	1.1	4.1
400	110	32.6	4.3	12	3.9	7.6	3.2	5.5	1.9	3.9	.8	2.7
400	199	31.1	1.6	11.5	2.2	7.4	2.7	6	2.5	4.5	2.3	3.8



19.2 volts/div

2 msec/div

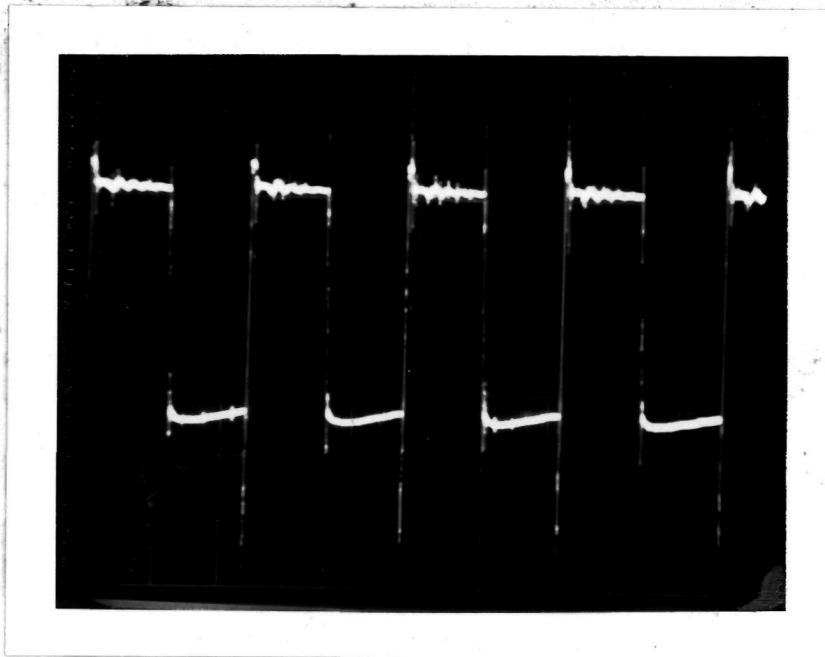


200 Hz/div

4.8 volts/div
(rms)

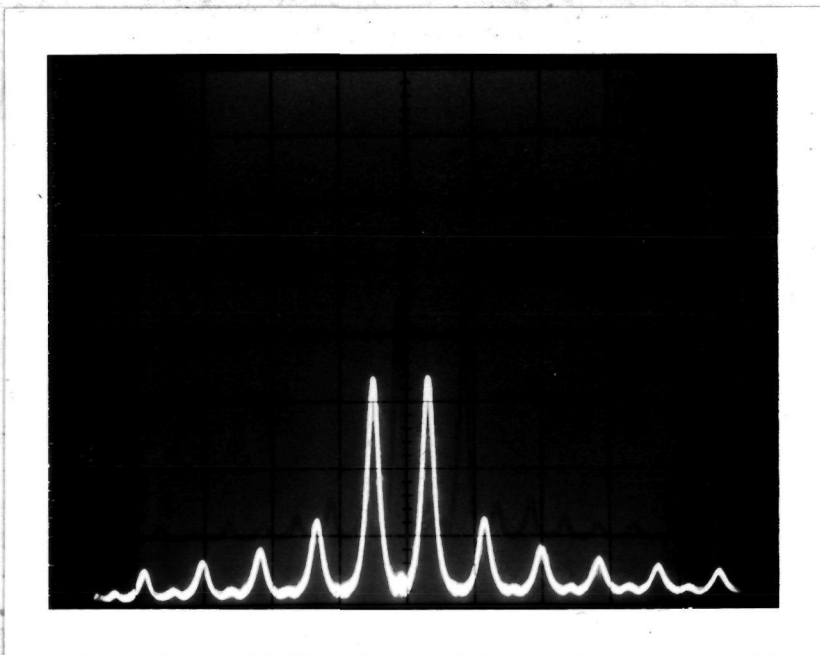
100 Hz, $T_o/T = 0.5$; $I_{\text{motor}} = 198$; $I_{\text{line}} = 111.6$

FIGURE C-3



19.2 volts/div

2 msec/div

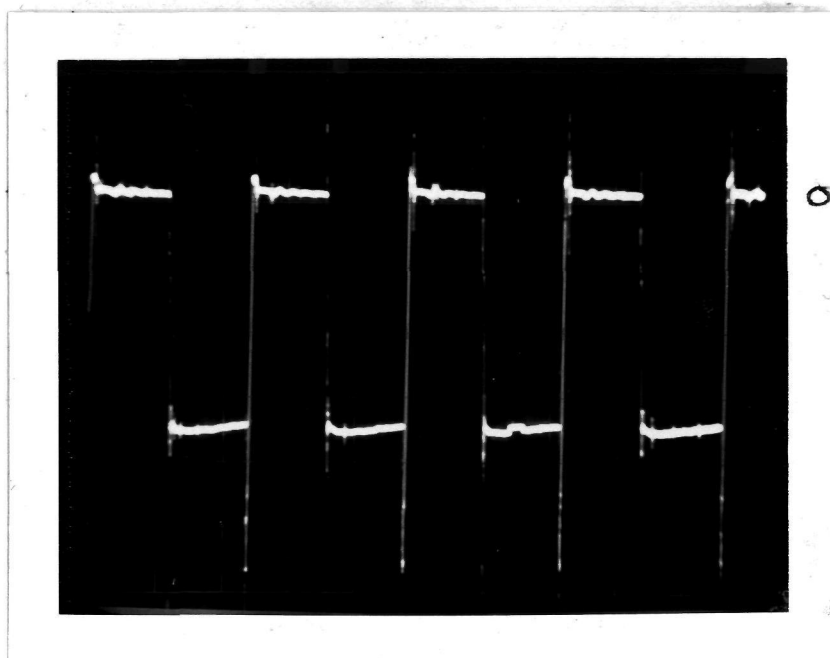


400 Hz/div

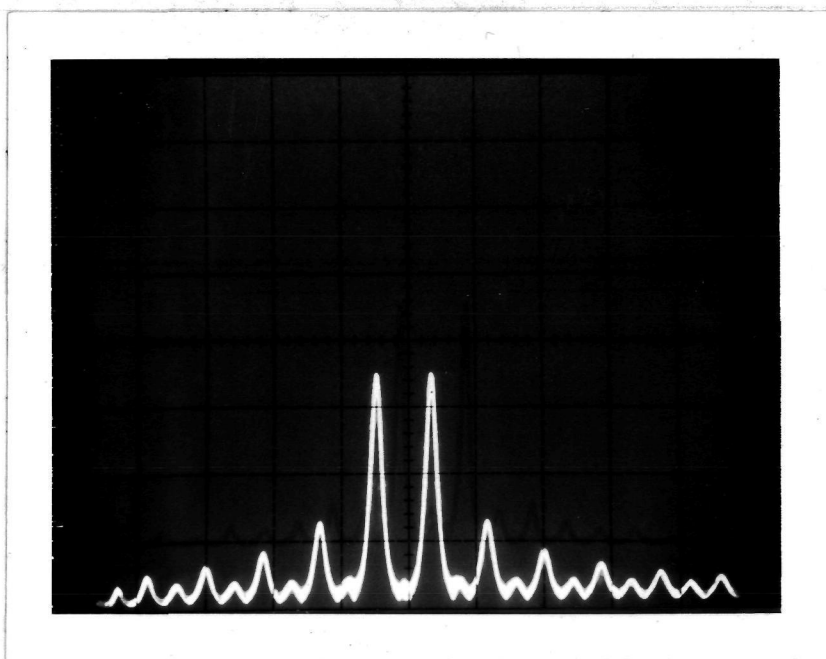
9.6 volts/div
(rms)

200 Hz, $T_o/T = 0.5$; $I_{\text{motor}} = 199$; $I_{\text{line}} = 108.5$

FIGURE C-4a



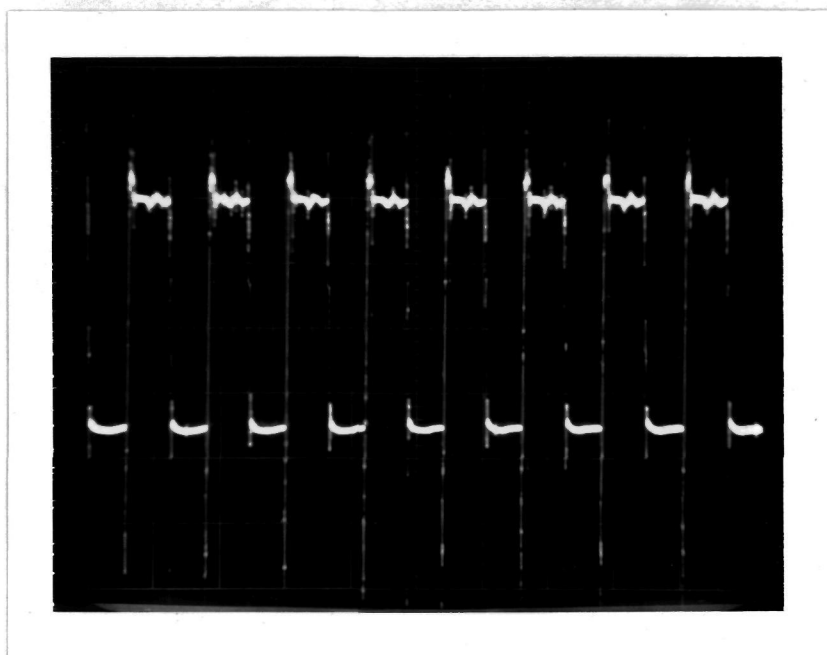
19.2 volts/div
2 msec/div



400 Hz/div
9.6 volts/div
(rms)

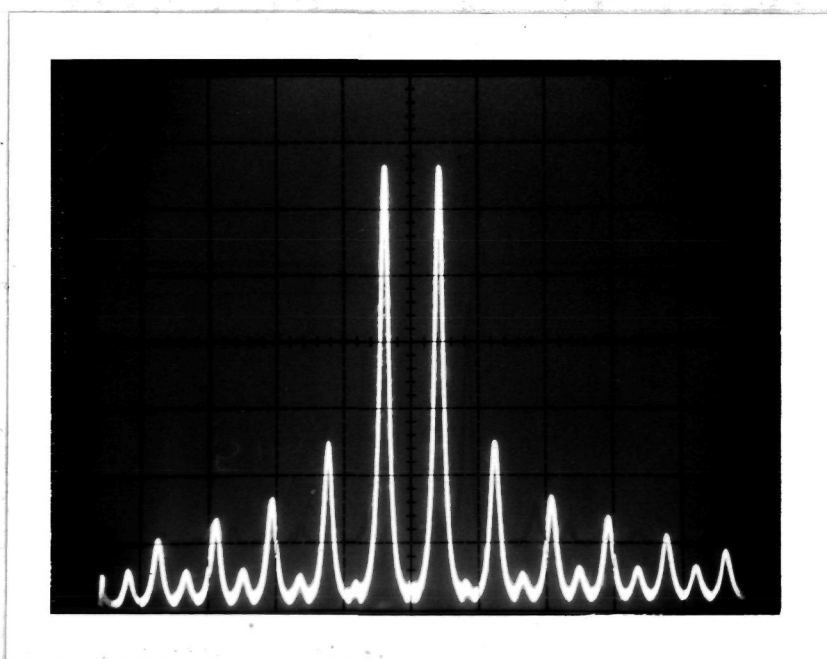
200 Hz, $T_o/T = 0.5$; $I_{\text{motor}} = 107$; $I_{\text{line}} = 64.3$

FIGURE C-4b



19.2 volts/div

2 ms/div

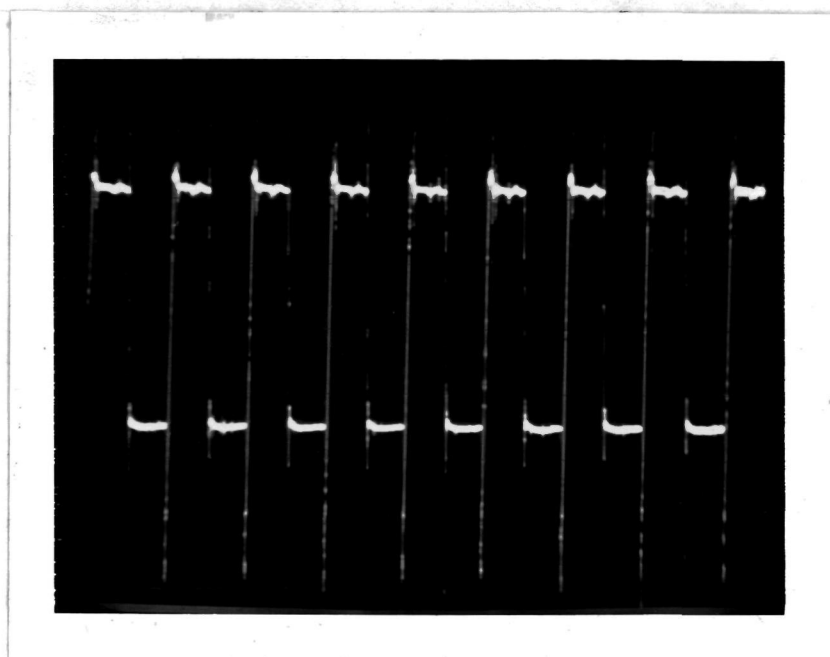


1 KHz/div

4.8 volts/div
(rms)

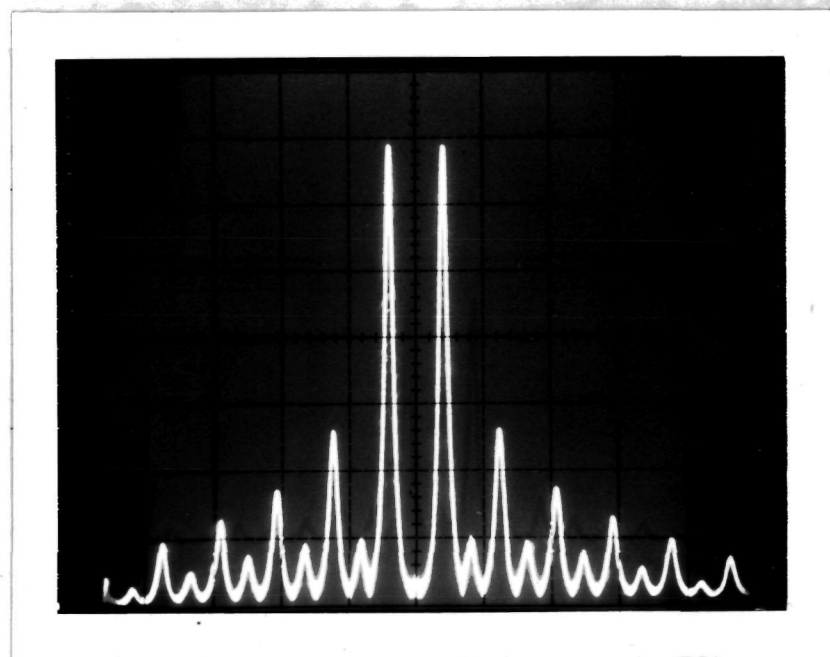
400 Hz, $T_o/T = 0.5$; I motor = 199; I line = 105

FIGURE C-5a



19.2 volt/div

2 ms/div



1 KHz/div

4.8 volts/div
(rms)

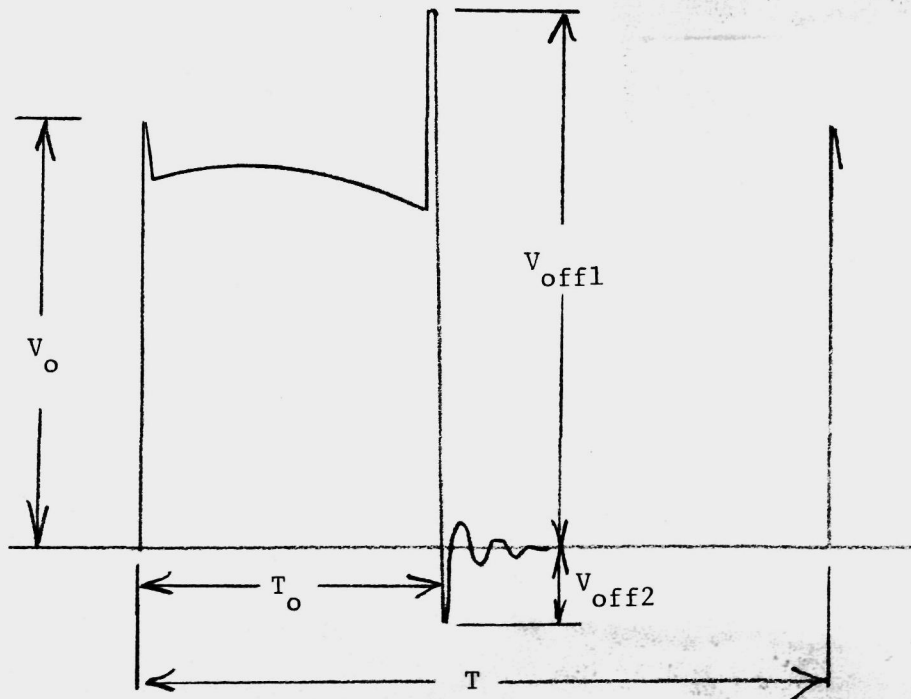
400 Hz; $T/T_o = 0.5$; $I_{\text{motor}} = 110$; $I_{\text{line}} = 64$

FIGURE C-5b

Although theoretically no even harmonics are generated, they are in fact present. This is explained by the fact that the voltage is a) not a constant during "on time" (due to resistance drop), b) is not zero during "off time", (due to FWD drop) and c) surges and oscillations are present. Scaling errors are also present.

The rms value of the alternating components of, for example, the test at 400 Hz, $I_m = 110$, is 36.9 volts. The average voltage (based on 80 volts open circuit) was 40 volts. The net rms voltage is $\sqrt{40^2 + 36.9^2} = 54$ volts.

The zero voltage level is at the top of the photos. (For instrumentation reasons, voltage-increase is in the down direction.) A typical voltage wave form is reproduced in Figure C-6 (inverted, with + upward).



Typical Voltage Waveform
FIGURE C-6

High frequency surge oscillations occur on turn on and on turn off due to distributed capacitance interacting with circuit inductance. Typical values of some of the voltage surges V_o , V_{off1} , V_{off2} observed are shown in Table C-2.

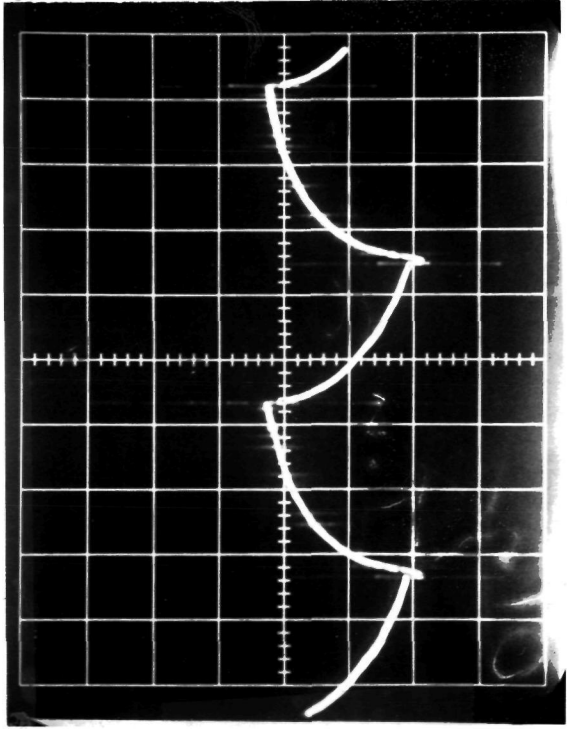
TABLE C-2
- Voltage Surges -

<u>FREQ</u>	<u>I_m</u>	<u>V_o</u>	<u>V_{off1}</u>	<u>V_{off2}</u>
100	198	77	90	15
200	107	77	107	23.5
200	199	73	107	30
400	110	80	113	15
400	199	80	113	28

The observations that can be made here are that the peak surges (up to 1.41 p.u. at turn off, 400 hz) are independent of current level but do increase with frequency, approximately to the 0.24 power.

FOR CURRENTS:

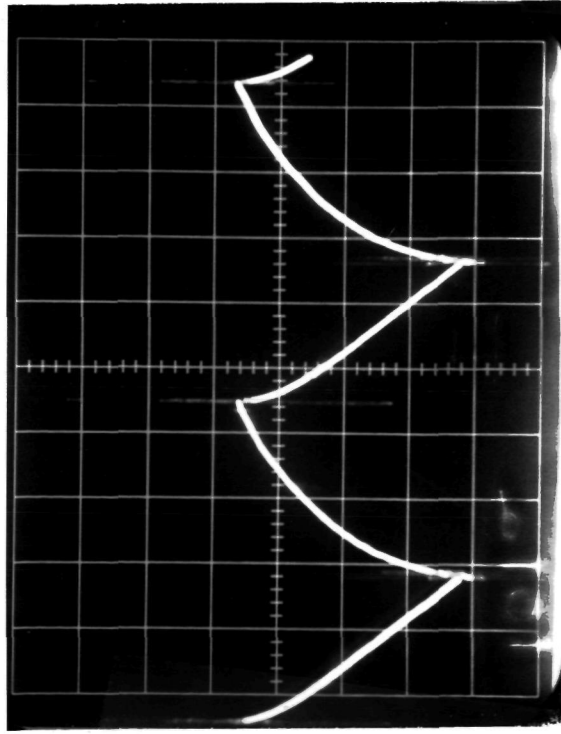
The CRO photos shown in Figure C-7 are typical of the current wave forms observed. As average motor current increases, or as frequency increases, the wave forms change rather dramatically. Current excursion, Δi , decreases



I motor = 62 amperes

I line = 42 amperes

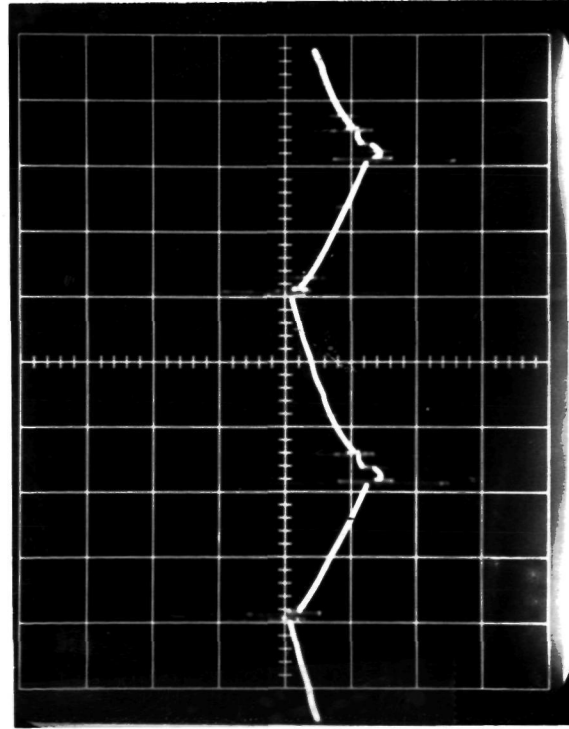
$f = 100 \text{ Hz}$, 50 a/div, 2 ms/div, $T_o/T = 0.45$



I motor = 201 amperes

I line = 105 amperes

$f = 100 \text{ Hz}$, 50 a/div, 2 ms/div, $T_o/T = 0.45$



I motor = 208 amperes

I line = 102 amperes

$f = 400 \text{ Hz}$, 50 a/div, 0.5 ms/div, $T_o/T = 0.45$

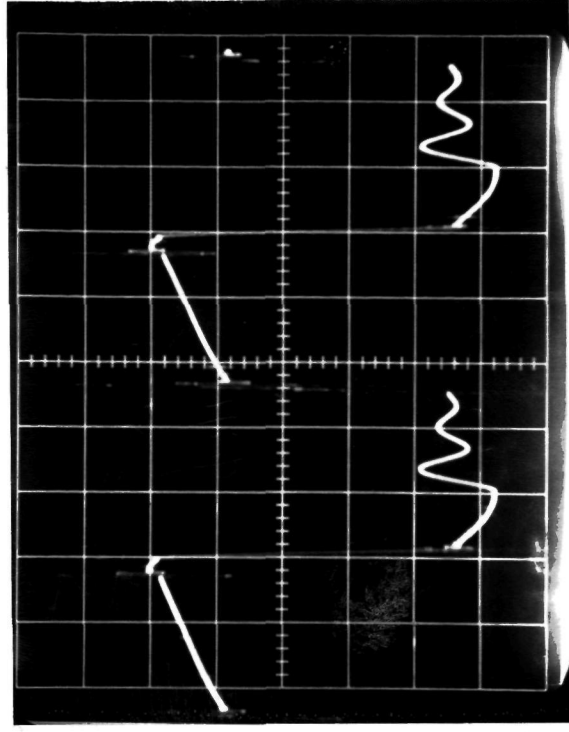


FIGURE C-7

sharply as frequency is increased from 100 to 400 Hz (as expected and discussed later in this section). Also, the excursions tend to become more 'linear' as both frequency and average current are increased (due to decreasing inductance with increasing current level). However, based on measured values of inductance and apparent resistance as a function of frequency and saturation on this motor, L/R of the motor was found to be:

$$\frac{L}{R} \propto \frac{I^{0.15}}{f^{0.94}} \approx \frac{0.24}{f^{0.94}} \quad (C-6)$$

The tests, for photos shown, were conducted with $T_o/T = 0.45$. Since $T = f^{-1}$

$$T_o = \frac{0.45}{f}$$

and:

$$\frac{T_o}{L/R} = \frac{0.45}{f} \frac{f^{0.94}}{0.24} \approx 1.9 \quad (C-7)$$

from which it can be seen that 'on' time is nearly 2 time constants in duration and approximately independent of frequency, which indicates the assumption made in deriving the linear relationships is not a valid assumption and considerable error will result if used. Also, it contradicts the increasing Δi linearity with increasing frequency.

The observed fact that current increase and decay becomes more linear with increase in saturation and frequency is apparently due to eddy current effects which retard the change of flux in the iron surrounding the conductors.

Tests were conducted over the frequency range of 67 to 400 Hz, at brush positions from mechanical neutral to 28 degrees against rotation (magnetic neutral). Data obtained from the photos taken (wave form and spectrum analyzer) is the basis for the results plotted in the following figures.

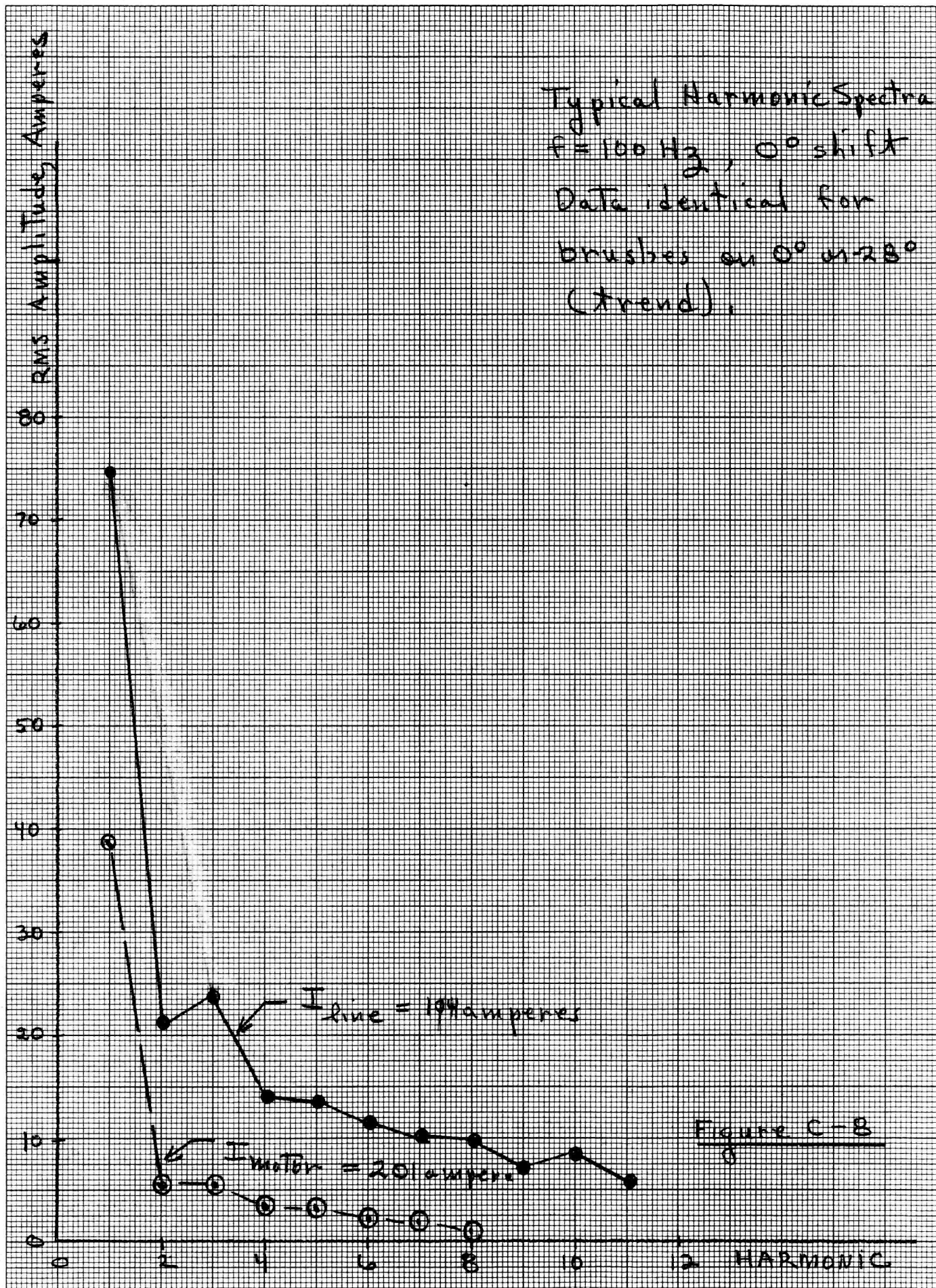
Figure C-8 shows a typical harmonic spectra for motor and line current. These spectra are for 100 Hz, with the brushes on 0 and on -28 degrees. Brush shift has no effect on harmonic magnitude distribution. The average motor current was 200 amperes, the average line current, 104 amperes. Figure C-9 is a plot of the fundamental harmonic magnitude of motor and line currents as a function of frequency, average current and brush shift. As can be seen, the fundamental component of line current is nearly independent of frequency, but highly dependant on average value; whereas the fundamental component of motor current is nearly independent of average current level but highly frequency dependent, (very nearly inversely proportional to frequency).

The ratio of root mean square to average value of current was calculated. For all frequencies, the ratio, for line current, varied from 1.25 to 1.3. The variation, for motor currents, $100 < I_m < 210$ was as shown in Table C-3.

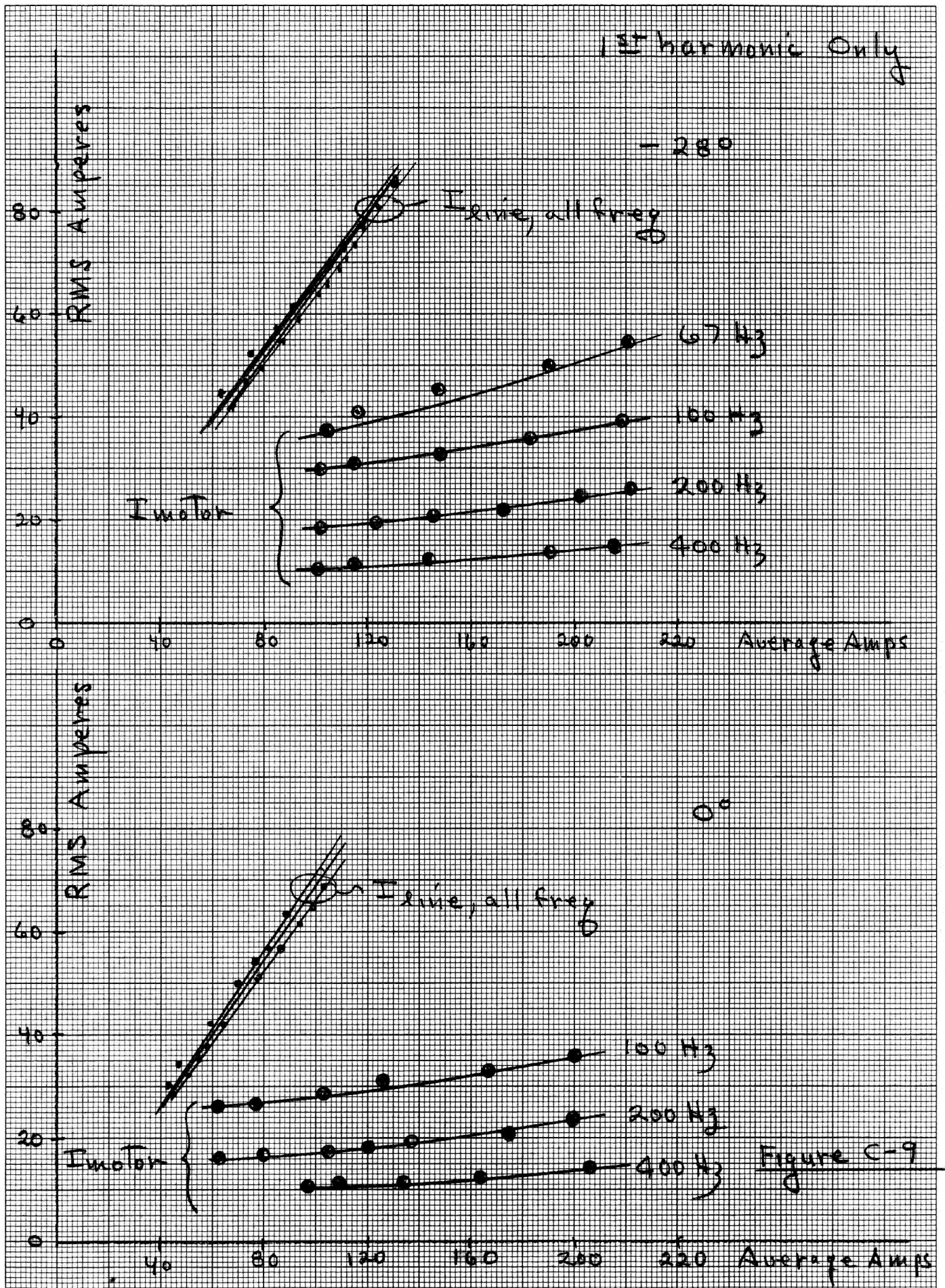
TABLE C-3

<u>Frequency</u>	<u>I_{rms}/I_a (motor)</u>
67	1.03 - 1.07
100	1.02 - 1.05
200	1.01 - 1.02
400	1.002 - 1.008

46 1512

K&E 10 X 10 TO THE CENTIMETER 18 X 25 CM.
KEUFFEL & ESSER CO. MADE IN U.S.A.

46 1512

K&E 10 X 10 TO THE CENTIMETER 18 X 25 CM.
KEUFFEL & ESSER CO. MADE IN U.S.A.

The percentage of ripple current, calculated as:

$$\% \text{ Ripple} = \sqrt{\frac{\sum I_i^2}{I_{\text{ave}}^2}} \quad (\text{C-8})$$

is shown in Figure C-10 for various frequencies and average amperes. As can be seen, motor current ripple is nearly inversely proportional to frequency (lower Δi) whereas line current ripple is not so heavily frequency dependent. Motor current % ripple decreases considerably (by about 33%) as average current increased from 30-100% of rating. The percent ripple current is independent of brush shift. Figure C-11 depicts the variation of the ratio of peak to average motor current; Figure C-12 shows the ratio of current excursion, (Δi) during a duty cycle, to average line and motor current. These ratios are nearly inversely proportional to frequency. These latter ratios were found to be brush position sensitive, running 20-30% higher for the situation with the brushes shifted -28 degrees, (because L decreases about 20% with a -28° brush shift).

Observed values of Δi as T_o/T is varied from 0.1 to 0.6 are plotted in Figure C-13. The values are for $T = 0.010$ seconds, (100 Hz), speed at 1000 rpm, voltage at 86 volts. The variation in average motor current is also shown.

Equation (C-5), with $L = 0.91$ mH (value for 100 amperes, 100 Hz, which occurs at $T_o/T = 0.3$) and $V = 86$ was used to calculate Δi for various T_o/T . This theoretical, linearized variation is also shown on Figure C-13. Considerable error is present. For example, at $T_o/T = 0.3$ the calculated value of $\Delta i = 198$ amperes is 1.42 times the observed experimental value of 140 amperes.

According to equation (C-5) the value of Δi at $T_o/T = 0.6$ should be the same as the value at 0.4. The actual value at 0.6 is 1.14 times greater than the value at 0.4. This is no doubt due to the heavy level of saturation, (230 amperes) (lower inductance) than at $T_o/T = 0.4$ (140 amperes).

$$\% \text{ Ripple} = \frac{\sum I_n^2}{I_{ave}^2}$$

(Note: % ripple is independent
of brush shift angle)

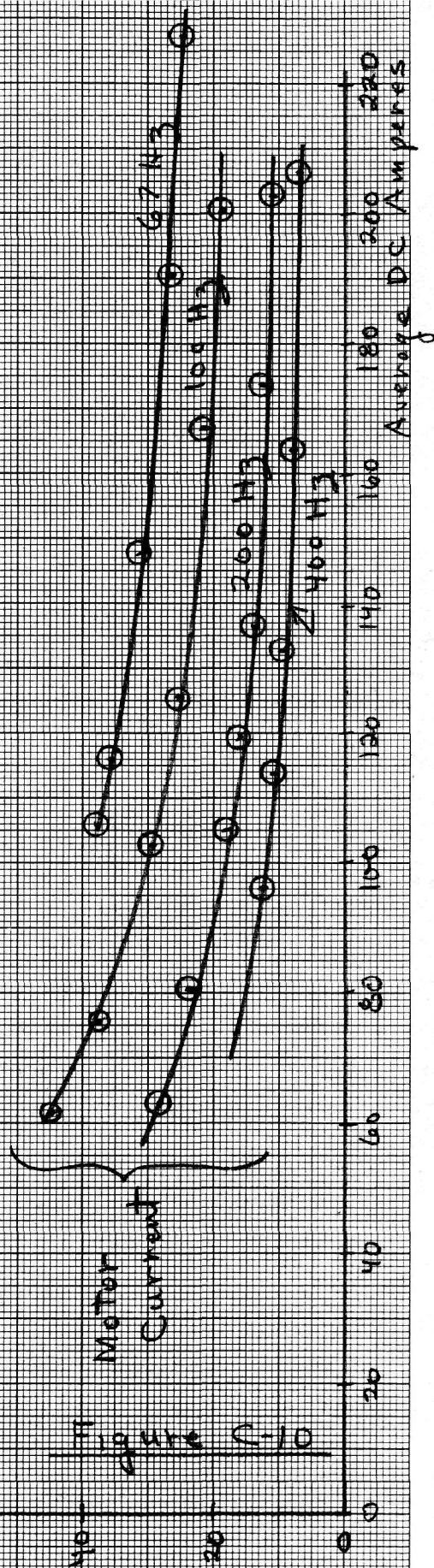
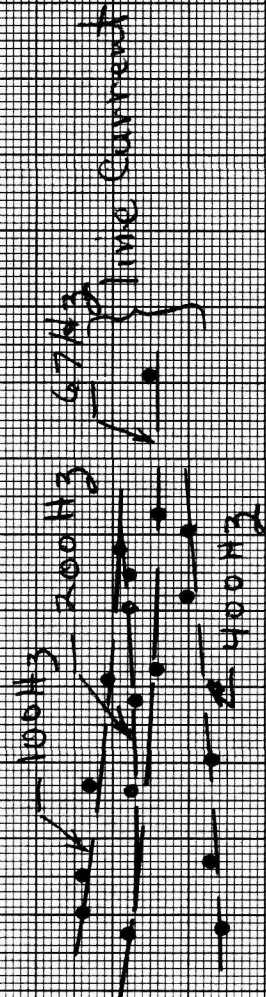


Figure C-10

$I_{peak}/I_{average}$ as a function
of $I_{average}$. Data shown for
 0° brush shift, $T_o/T = 0.45$
 -28° brush shift yields
values $\approx 20\%$ higher

$I_{peak}/I_{average}$

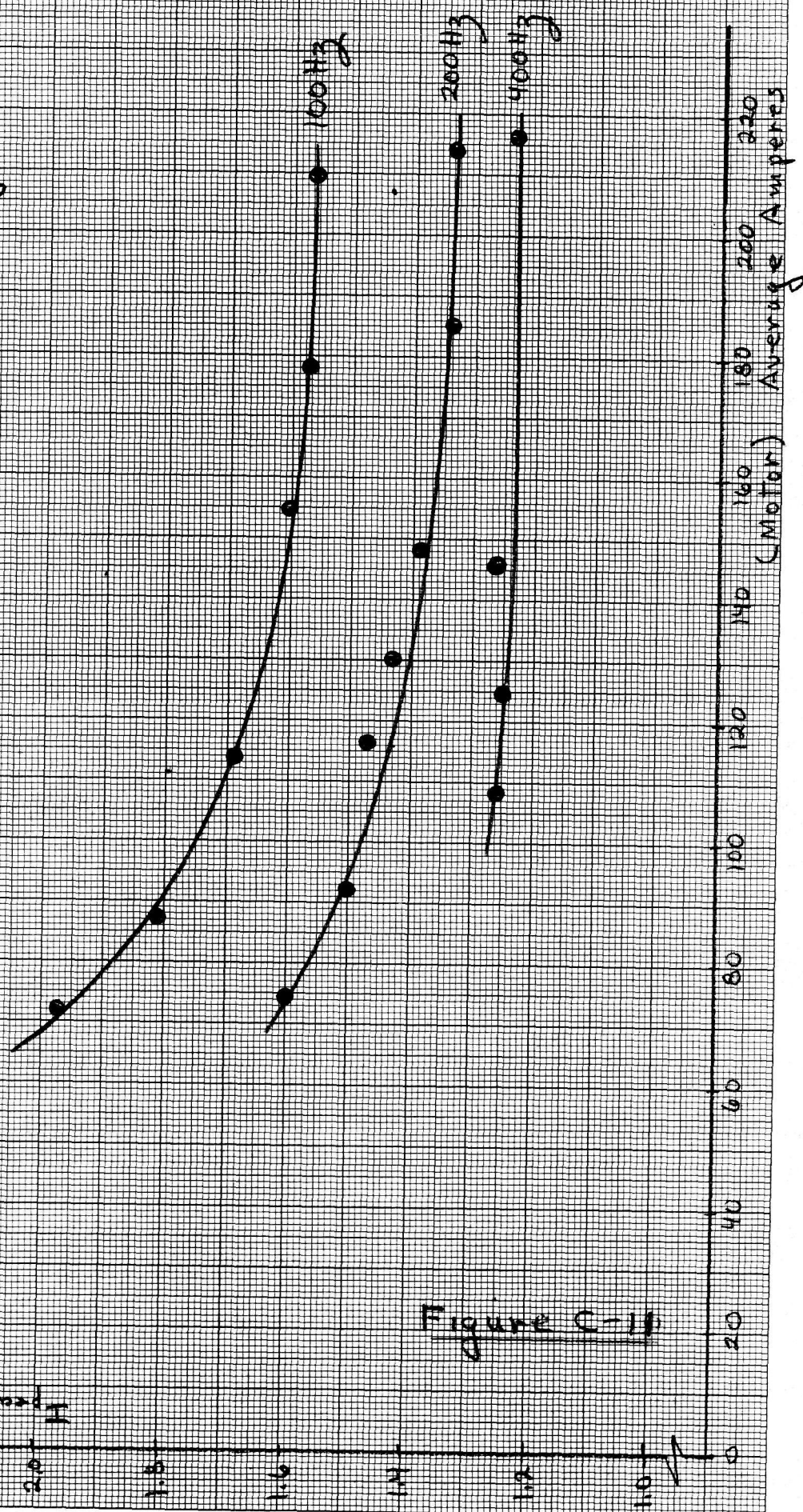


Figure C-11

Variation of $\Delta i / I_{\text{average}}$
as a function of frequency,
brush shift & saturation.

$$T_0/T = 0.45$$

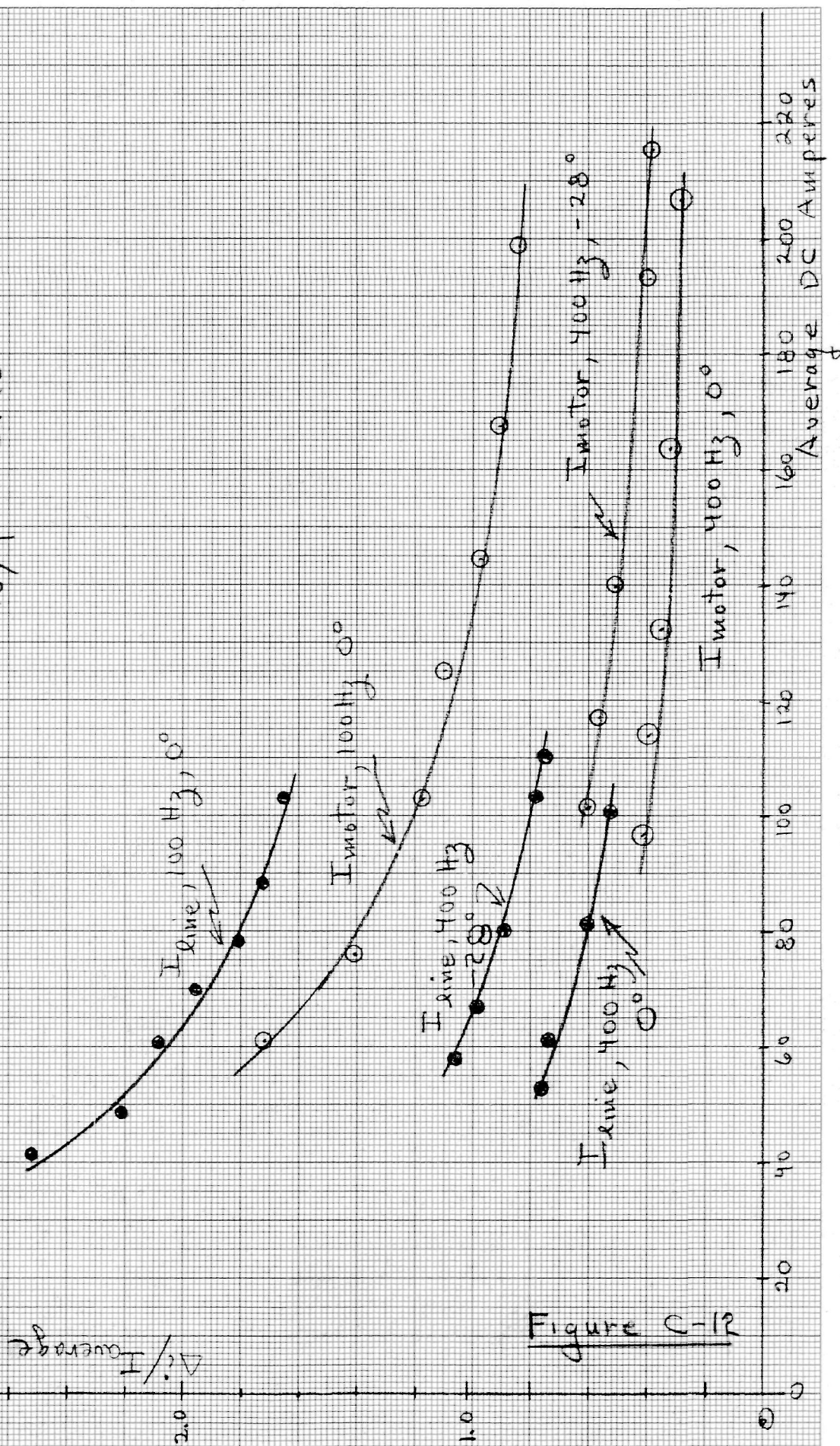
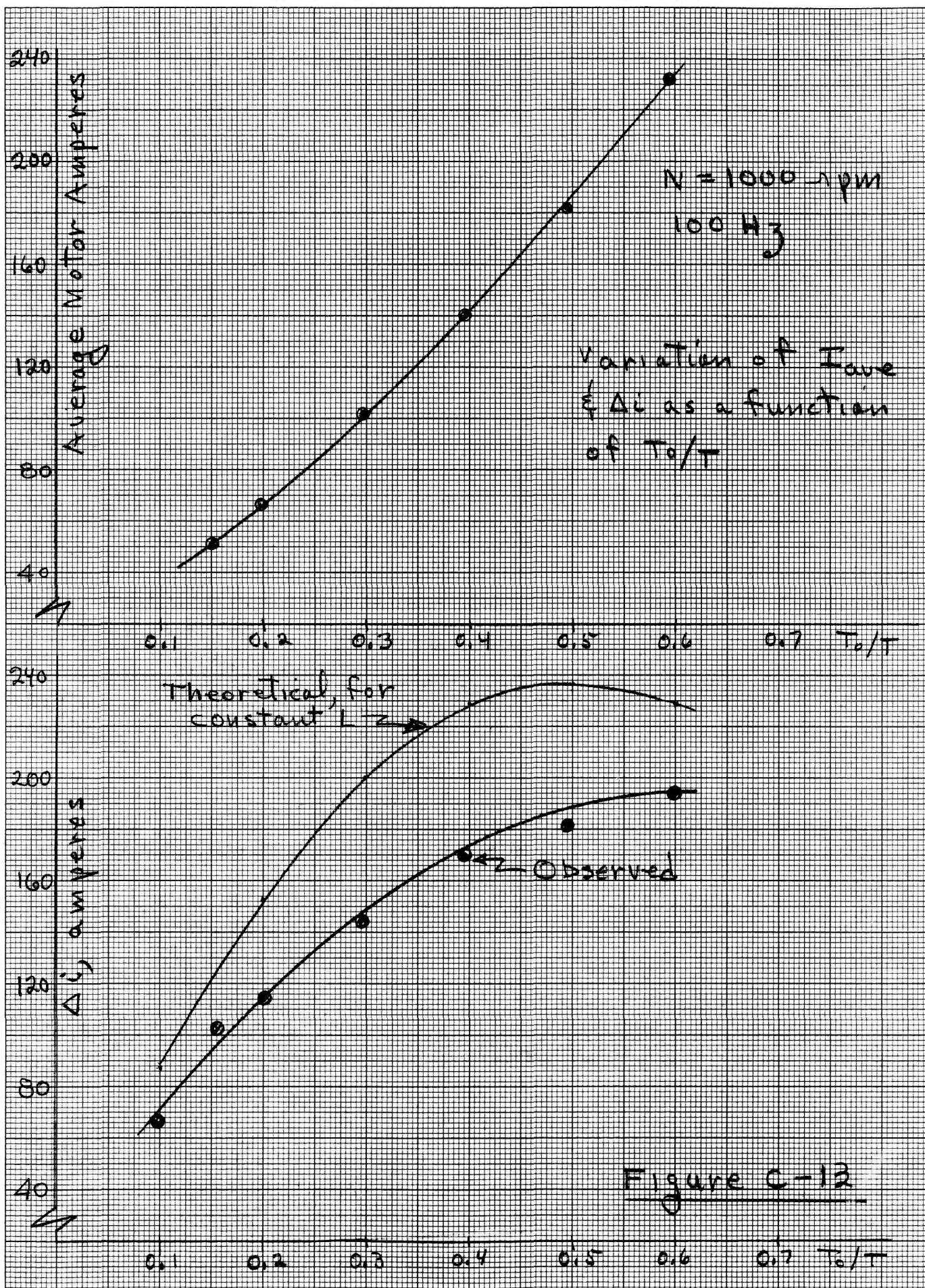


Figure C-12



Typical measured harmonic values, for 100, 200 and 400 Hz, $T_o/T = 0.45$ and saturated and relatively unsaturated conditions are presented in Table C-4. The significance of the values in (), beneath the observed values of motor current harmonics is explained later in this section.

Attempts were made to try to correlate calculated values of the Fourier Series representations with observed current wave forms.

Referring to equations (C-4, -5), pertaining to the linearized representation of motor current, it can be seen that the motor current harmonics are proportional to the current excursion, Δi , and inversely proportional to n^3 , where n is the order of the harmonic. Since Δi is inversely proportional to the chopper frequency, the harmonic magnitude is also.

Table C-5 is a tabulation of observed and calculated (from the observed Δi , using equation C-4) rms values of the fundamental harmonic of motor current. Harmonic values calculated using the value of Δi from equation (C-5) were greatly in error.

Higher harmonic values are not listed because they are grossly in error. For example, at 100 Hz, 201 amperes, a second harmonic current of 6.5 amperes rms was observed. The value calculated from the linear version was 1.9 amperes.

TABLE C-5
Fundamental Harmonic, Motor Current

Frequency	Ave. I_m	Obs. Δi	-1st Harmonic -		% error
			Observed Value	Calculated Value	
100	201	173	36.5	49.6	36 %
100	104	123	29.6	36	21.6%
200	204	125	22.7	35.7	57.3%
200	106	77	18	22	22 %
400	208	57	13.9	16.3	17 %
400	98	41	11.9	11.7	2 %

TABLE C-4
OBSERVED MOTOR AND LINE CURRENT HARMONICS (RMS Amperes)
(TYPICAL)

-Harmonic-

HZ	AVE. LINE	AMPS MOTOR	ΔI	1	2	3	4	5	6	7	8	9	10	11
100	104	201	173.5	75	21.6	23.9	14.1	14.8	11.8	10.2	10.5	8.2	9.1	5.7
				36.4 (13.5)	6.5 (7)	6.6 (4.9)	3.1 (3.9)	3.4 (2.9)	2.3 (2.7)	1.7 (2.2)	- (1.7)	- (1.5)	- (1.5)	- (1.5)
100	61	104	123	43	13	13	8.2	8.2	6	5.7	5.7	4.6	4.7	3.6
				29.6 (4.2)	4.3 (2.1)	5.9 (1.4)	2.8 (1.4)	3.2 (.83)	1.9 (.7)	- (.8)	- (.83)	- (.79)	- (.71)	- (.61)
200	102	204	125	61.2	11.8	25	8	15.5	5.7	10.2	3.4	-	-	-
				22.7 (11.9)	2.1 (6)	3.6 (4.2)	1.1 (3.1)	1.7 (2.8)	1.3 (2.4)	1 (2.1)	1 (1.8)	- (1.5)	- (1.3)	- (1.2)
500	59	106	77	38.6	7	13.6	4.6	8.3	3.4	4.8	1.6	-	-	-
				18.2 (2.9)	.7 (1.6)	3.1 (1.3)	.6 (.9)	1.7 (.6)	- (.47)	1.0 (.38)	-	-	-	-
400	101	208	57	71.6	9.6	25.5	2.7	11.8	5.7	13.4	-	7.73	2.7	7.3
				13.9 (13.1)	1.7 (6.3)	2.4 (4.5)	1.3 (3.3)	1.1 (2.5)	.9 (1.9)	- (1.5)	- (1.3)	- (1.1)	- (.93)	- (.82)
500	54	98	41	33.5	7.4	10.5	5.7	4.6	4.6	3.4	3	3	1.9	4.6
				11.9 (.95)	.91 (.12)	2.4 (.06)	.4 (.1)	1.5 (.15)	.7 (.17)	-	-	-	-	-

NOTE: $T_o/T = 0.45$ Throughout, RED MOTOR

It can be generalized that the linearized current Fourier Series is useful only in yielding insight into the variational trend of harmonic component magnitudes with the variation of f , L and T_o/T , but calculated values are higher than actual values.

Finally, an attempt was made to correlate harmonic magnitudes calculated using Franklin's formulae, with observed results. Franklin's equations do take into account the variation of voltage constant with saturation but are based on a constant value of L and R . Use of the DC resistance of 0.0254 ohms and the value of L , at 100 Hz, saturated, of 0.91 mH were chosen as representative values which should yield maximum value of harmonics.

The calculated results are shown, for motor current, in (), immediately below the observed values in Table C-4. As can be seen, the calculated values are grossly in error and predict only a fraction of the magnitude of harmonic observed - especially for the lower harmonics. The magnitude of lower harmonics may have some error due to error in magnitude measurement.

The error is much greater than that resulting from calculations using the linearized version of motor current!

The inescapable conclusion of these tests is that accurate analytical prediction of harmonic current magnitude is not possible with either representation and that accurate values can be obtained only by actual measurement.

Instrumentation Requirements

Average values of current and voltage can be measured using noninductive shunts (NIS) and variable sample rate digital voltmeter (DVM). The NIS shunt used in this test program was a T&M Research Products Model K5000-10, 0.001 ohm, 275 amps continuous with a 6.5 MHz bandwidth.

The report "AN INVESTIGATION OF POSSIBLE DC POWER SOURCES FOR TESTING ELECTRIC VEHICLE MOTORS" submitted to NASA-Lewis/DOE, in 1978, under this grant,

discusses in its (Appendix 4) test results comparing voltage drop wave forms and average values of the response from the noninductive shunt, a "conventional" off the shelf instrument shunt and a conventional shunt modified to attempt to cancel the field established by the shunt itself. The modification was not noticeably effective. A difference of about 2% was noted in the average readings of the conventional and NIS and as much as 2 to 1 difference in observed magnitude of high frequency oscillations after thyristor cut off. If accuracy of wave forms and current values is required, it is essential to use non-inductive shunts.

Power measurements also require consideration due to the complex wave forms of voltage and current.

The necessity for a wattmeter with a wide bandwidth response is portrayed graphically in Figure C-14, which shows the ratio of power indicated by the Clark-Hess electronic wattmeter (with 0.6% fs accuracy over the frequency range DC to 30 kHz) and the product of motor current and voltage as read by the average reading DVMs. Errors shown range from 4% at 400 Hz, with reduced current excursion, Δi , to 33% at 100 Hz (increased Δi).

A theoretical insight into wattmeter bandwidth can be obtained by multiplying equations (C-2) and (C-3) to obtain the product of instantaneous, linearized, voltage and line current which yields instantaneous power. When this is integrated over a complete period, true power is obtained as

$$P_{\text{true}} = V I_o \frac{T_o}{T} + \sum_{n=1}^{\infty} 2 V I_o \left(\frac{T_o}{T} \right)^2 \left(\sin \frac{n\pi T_o/T}{n\pi T_o/T} \right)^2 \quad (\text{C-9})$$

whereas actual power, P_{act} measured is, with a wattmeter with bandwidth to the k^{th} harmonic, the same except the summation is from $n = 1$ to $n = k$.

P_w ~ Power read by wide band electronic wattmeter, Clark-Hess Mod 255

V_{ave} ~ average voltage across motor

I_{ave} ~ average motor current

Condition $\frac{T_o}{T} = 0.45$

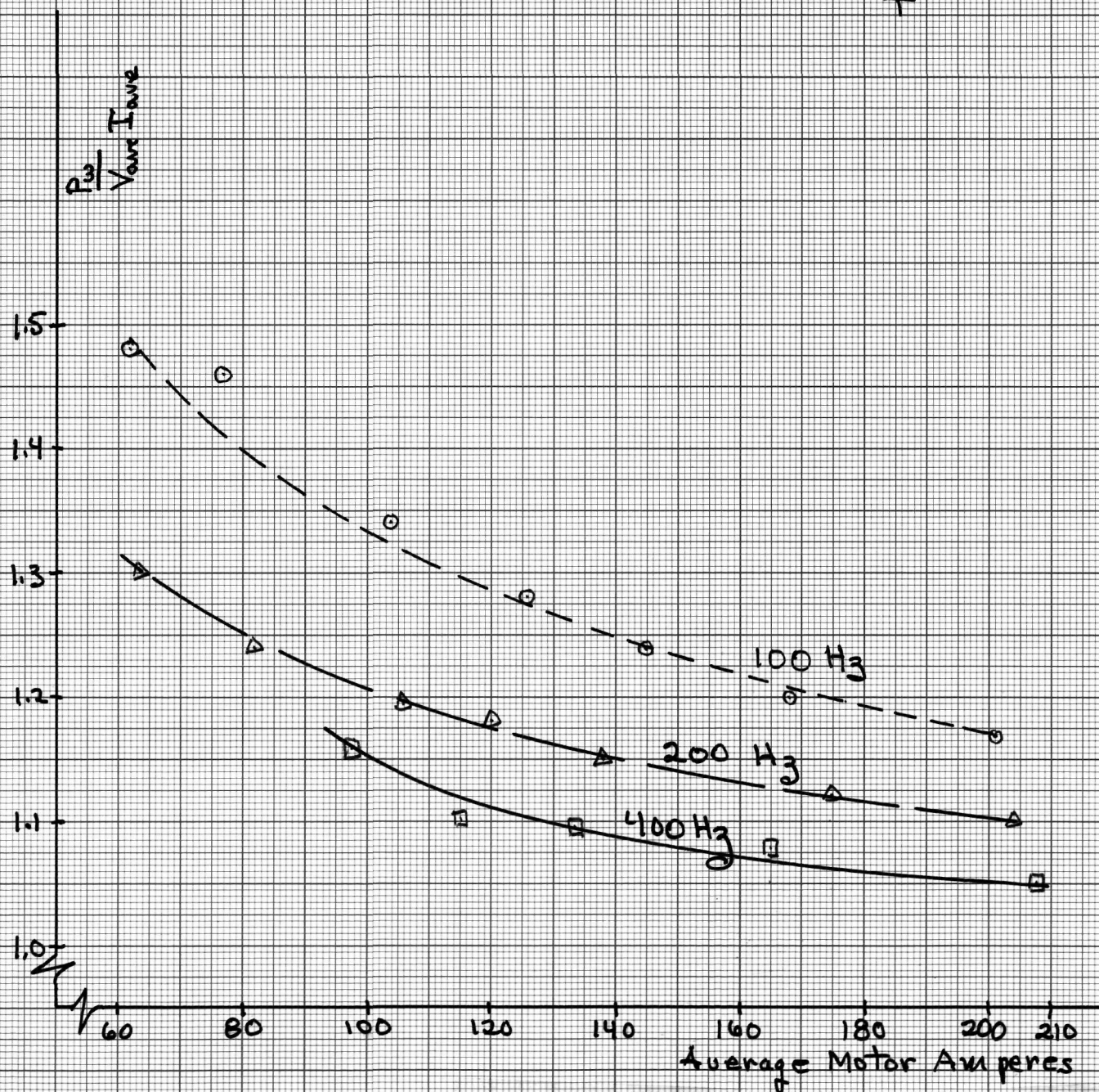


Figure C-14

The percentage error is:

$$\% \text{ error} = \frac{P_{\text{true}} - P_{\text{act}}}{P_{\text{true}}} 100 \quad (\text{C-10})$$

The error for values of $T_o/T = 0.5, 0.25$ and 0.10 for values of harmonic up to 10 are plotted in Figure C-15. Theoretically, using the linearized relationships, error is independent of frequency and load current; however, in reality, as seen by the results in Figure C-14, which is observed error as a function of motor current, the actual error is both average current and frequency dependent.

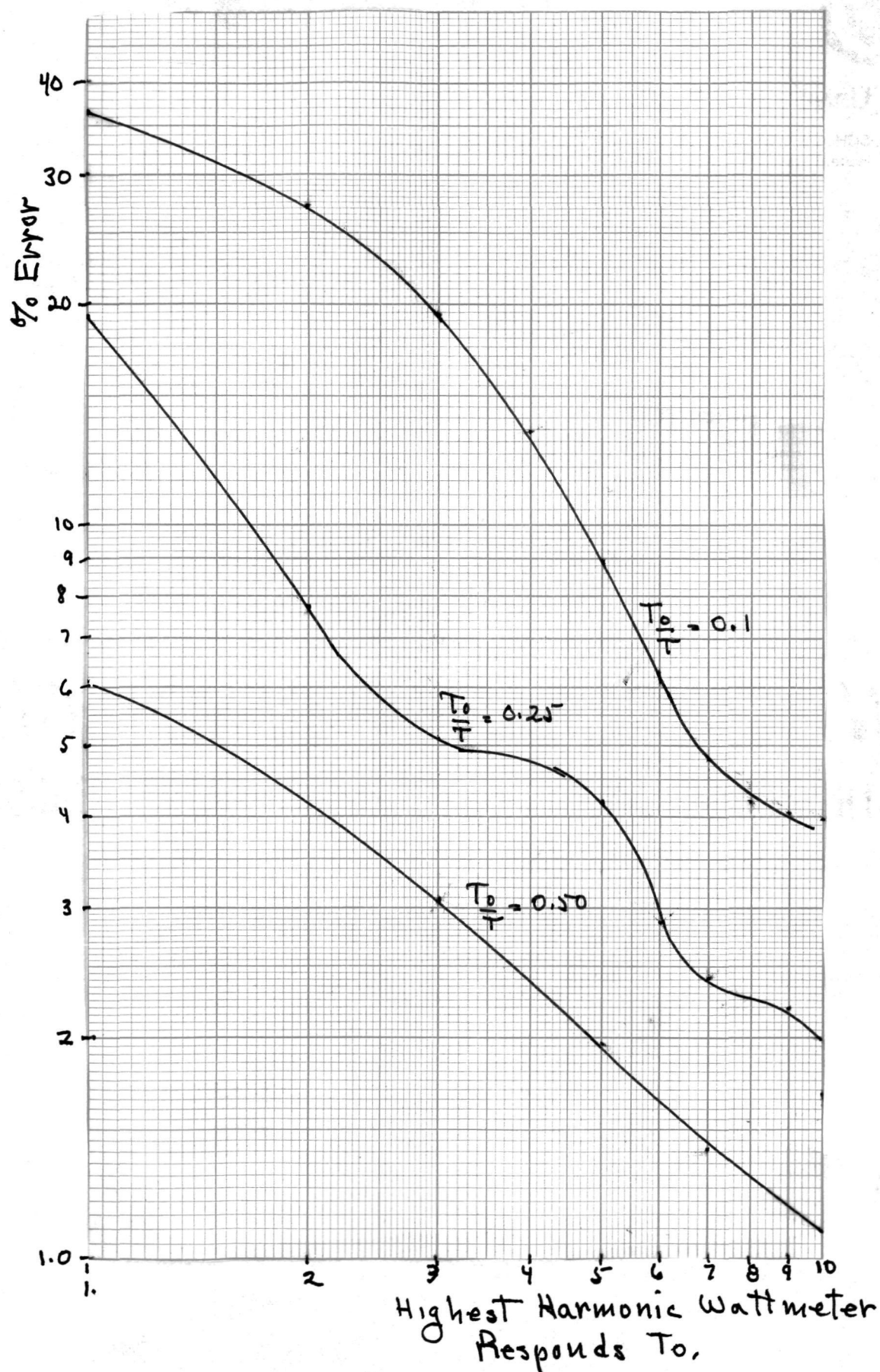


FIGURE C-15

APPENDIX D

MEASUREMENT OF RESISTANCE AND INDUCTANCE

(AS A FUNCTION OF FREQUENCY AND SATURATION)

A knowledge of the inductance of the DC series motor is essential if a meaningful model of the machine, for dynamic studies, is to be configured and it is a necessary parameter in the application if a specific chopper type controller is to be made with a particular motor.

IEEE Standard #113⁽¹⁾ briefly notes procedures for measuring inductance, although the standard is primarily addressed to the shunt connected machine. The technique for measuring armature inductance involves a 60 Hz supply, with series field out of the circuit. Frequency variations and saturation are not addressed. Saunders⁽⁶⁾ proposed a test scheme involving a DC source, through a choke, paralleled with an AC source with blocking capacitor as a scheme to determine, in effect, incremental inductance as a function of DC saturation.

DeWolf⁽²⁾ used this scheme for determining armature inductance. He found that the armature circuit inductance of the series wound motor varied widely with frequency and degree of saturation. Prior to publication of Mr. DeWolf's results, this investigator was also concerned with the problem of inductance and apparent resistance changes with frequency and degree of saturation, particularly in the series field type motor without commutating poles and thus with a necessary brush shift yielding coupling between armature and series field at saturation levels other than those for which the brush shift was set.

As Mr. DeWolf states, "... it is concluded that both DC and variable frequency AC power supplies... are required to obtain meaningful measurements of armature circuit inductance of series wound machines."

Accordingly, experimental work was undertaken to investigate the techniques and problems involved in series field parameter determination.

The first step was selection of an AC power supply and a rather formidable problem manifested itself. In essence, what appeared to be a harmonic free source displayed relative large harmonics in the voltage that appeared across the brushes of the blocked rotor and series field and series wound motor.

Initially, variable frequency single phase generators were explored for suitability as an AC source. Visual observation of the open circuit voltage indicated a relatively harmonic free voltage. Actually, the 3rd and 9th harmonics were measured as 3% and 1% respectively of the fundamental, yielding distortion in the range of 0.05% where:

$$\% \text{ Distortion} = \left(\frac{\sqrt{\sum (\text{RMS})^2} - \text{RMS}_{\text{fundamental}}}{\text{RMS}_{\text{fundamental}}} \right) \times 100$$

The generator was then connected across the armature and field of the RED motor through a 200 μF capacitor bank. Because the capacitor impedance decreases with increasing frequency and the choke (inductance) in series with the DC source (and shunting the motor under test) increases with increasing frequency, harmonic currents are magnified in the test motor circuit.

To determine R, L at various frequencies and saturation levels, it is necessary to accurately measure voltage, current and the angle between them. The harmonic distortion resulting from the straightforward use of a rotating machine as an AC source was found to be intolerable and was discarded.

The scheme that was developed and from which meaningful data was obtained is described in the IEEE paper⁽⁷⁾ "SERIES MOTOR PARAMETER VARIATIONS AS A FUNCTION OF FREQUENCY AND SATURATION" which is a part of this Appendix.

A description of the measurement technique is not repeated here but some pertinent data obtained is repeated because of the larger scale possible.

The majority of the measurements were made with the carbon brushes replaced by radiused copper blocks in order to eliminate carbon-copper contact resistance effects; however, some test results using carbon brushes are presented and compared with copper block measurements.

As discussed in the attached paper, scaling errors and CRO trace width can introduce as much as 3.5% error in calculating inductance values and 10% error in the resistance determination.

-Inductance Variations-

Figure D-1 shows the variation in inductance measured, for the RED motor over the frequency range from 30 to 1500 Hz from the unsaturated to full saturation condition. Figure D-2 presents the variation of inductance of the RED motor as frequency is varied and current is held constant at values of 50, 100 and 175 amperes. Figure D-3 depicts the effect of brush shift and shows the division of inductance between the armature and field in the RED motor. As can be seen, brush shift does not affect the armature noticeably but does have a noticeable effect, over all. This result was obtained at 400 Hz, and the two field windings series connected. Figure D-4 is at 400 Hz but with the two field windings paralleled. The difference between measurements made with carbon brushes and copper blocks is shown for the RED motor, in Figure D-5.

Figure D-6 shows the variation in unsaturated inductance and also apparent resistance of the BLUE motor as the frequency is varied up to 1500 Hz. Figure D-7 presents data on variation of inductance of the BLUE motor as a function of frequency and saturation.

-Apparent Resistance Variations-

The apparent resistance, as seen by the current fundamental and harmonics changes with both frequency and saturation, since the variations are due to eddy current, skin and proximity effects.

Figure D-8 presents apparent resistance variation, for the RED motor with frequency and level of saturation changes, and Figure D-9 depicts the same type of information in a different fashion. The effect of brush shift and the division between series fields and armature for the RED motor at 400 Hz are shown in Figure D-10. As can be seen, since the vast majority of the apparent resistance is in the field windings, and fine stranded wires (rather than solid conductors) appear to hold promise of reducing the apparent resistance (and the harmonic current joule losses) appreciably. Figure D-11 presents the same type of information for the BLUE motor as is presented in Figure D-8 for the RED motor.

Although the actual values differ between the RED and BLUE motors, the variational form of the change in parameters is almost identical.

$-\omega L/R$ Variation-

A curve fit routine, applied to the experimental data obtained for both motors indicates that R and L , as functions of frequency and saturation, varied in an identical fashion, although the actual values for the two motors were different. (One had a solid frame, the other a laminated frame.) Total variation in L and R were⁽⁸⁾, for the RED motor:

$$L = 3.8 f^{-0.24} I^{-0.063} \text{ mH}$$

$$R = 0.0167 f^{0.7} I^{-0.07} \text{ ohms}$$

from which:

$$(2\pi f) \frac{L}{R} = \frac{\omega L}{R} = \frac{X}{R} \approx \text{constant}$$

-SUMMARY AND CONCLUSIONS-

(Extracted from the Attached Paper)

Inductance Variations:

The armature inductance is independent of brush position and armature-only excitation. It accounts for about 1/3 of the total armature circuit inductance.

The armature circuit, including the series field is about 30% less under saturated conditions than unsaturated, decreasing approximately as the -0.06 power of the DC current level. Also, it decreases proportional to the -0.24 power of frequency (over the frequency range tested, i.e. to 1500 Hz). The armature circuit inductance is dependent upon brush position, decreasing in proportion to the angle of the shift against rotation. For the motor tested, with the brushes located for proper commutation, it decreased by 15%.

It should be noted that in a constant inductance circuit, higher frequency current harmonics are suppressed in magnitude but in the motors tested, with decreasing inductance with increasing frequency, the suppression (or decreasing trend) is not as pronounced.

Resistance Variations

For the motor, with results detailed here, the DC resistance of the armature and fields was measured as 0.0189 and 0.0165 ohms respectively for a total of 0.0254 ohms. The ratio of armature to field DC resistance is 1.15. From Figure D-10, the 400 Hz AC resistance ratio is 0.15 for a change of $1.15/0.15 = 7.65$.

About 90% of the resistance to AC harmonic current is associated with the series field winding. This indicates that this loss could be decreased by using multiple insulated small wires in parallel rather than fewer heavy strands for the series field winding. Apparent resistance decreased about 15% with brush shift. The values observed under saturated conditions were 20-30%

less than the unsaturated values (depending upon frequency). For a given degree of saturation, the apparent resistance increased with the +0.7 power of frequency. For a specific frequency, the resistance decreased approximately as the -0.07 power of DC current level.

Carbon Brush vs Copper Block Valves:

- (1) The value of inductance measured using copper blocks was found to be about 6% less than values from measurements with carbon brushes.
- (2) Measurement of apparent resistance with carbon brushes in place yielded a value of approximately 75% greater than found using copper blocks.

Magnitude of Losses:

The combination of relatively high harmonic currents and the apparent resistance (reflecting hysteresis and eddy current skin and proximity effect losses) yields a loss component which should be included in any efficiency determination.

Motor/Chopper Interface Influence:

Since the chopper is sensitive to the amount of inductance in the circuit, care should be taken to use the saturated value of inductance, obtained at the maximum operating frequency, when evaluating the interface details.

On Measurement Techniques:

The circuit used in this test does yield accurate values of R and L. Because of the harmonic multiplier effects, special care must be used in the selection and application of the instrumentation used. Copper blocks should be substituted for the carbon brushes and the effective resistance function of the brushes added.

It was noted that, for the motors tested, the ratio of reactance to apparent resistance is nearly independent of frequency and level of saturation.

If proper test facilities for running tests over the complete frequency range are not available, a good estimate of the ratio R to L can be obtained by a single frequency test, (60 Hz). If saturated inductance is known, an estimate of the variation of apparent resistance can then be obtained.

Summary

The dependance of circuit parameters on frequency and saturation indicate the need for inclusion of these factors in a model of the motor from which performance is to be calculated.

X 30 Hz

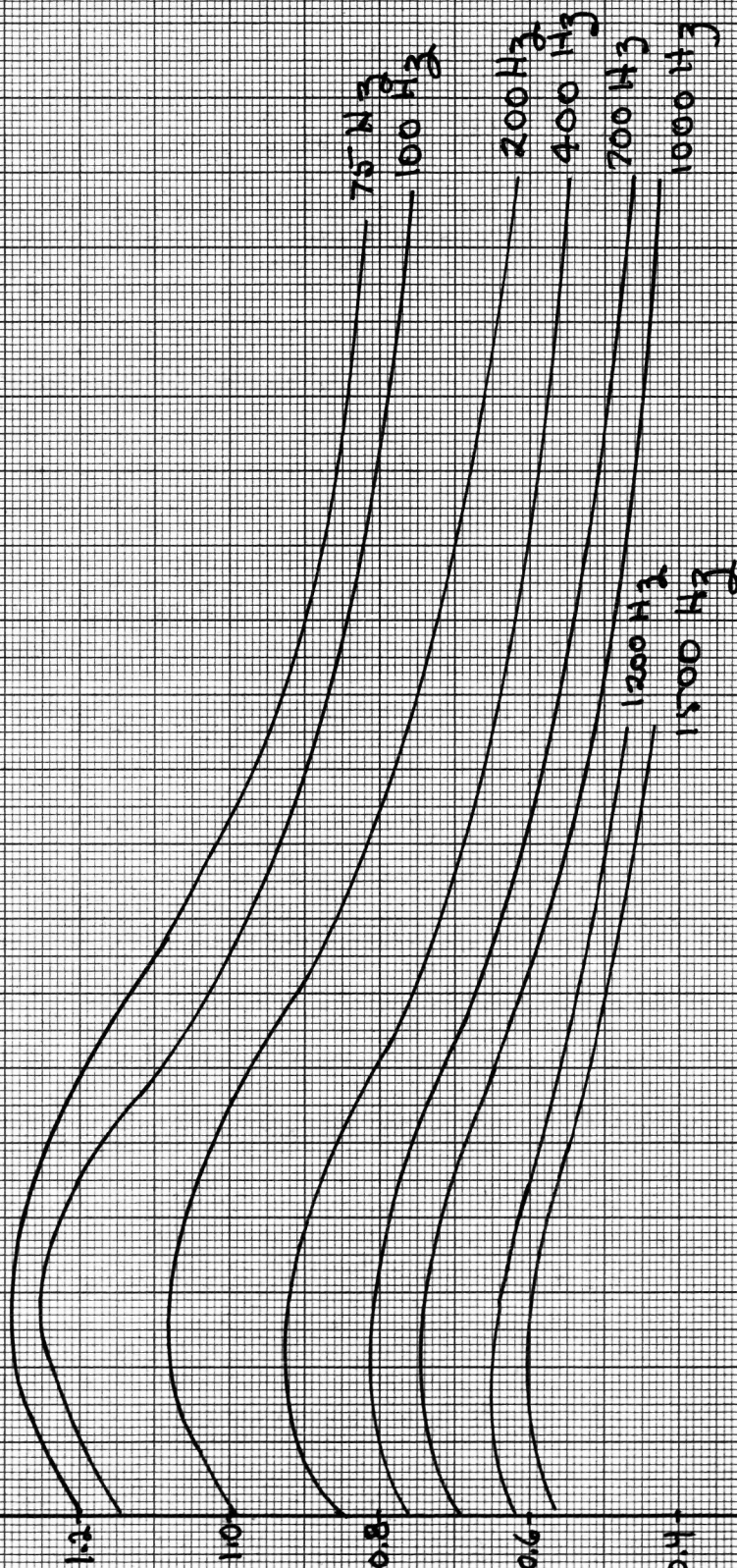
X 50 Hz

RED MOTOR - FIELDS IN SERIES
Copper Blocks, at 0°

L as a function of frequency & saturation

Inductance, mH

FIGURE D-1

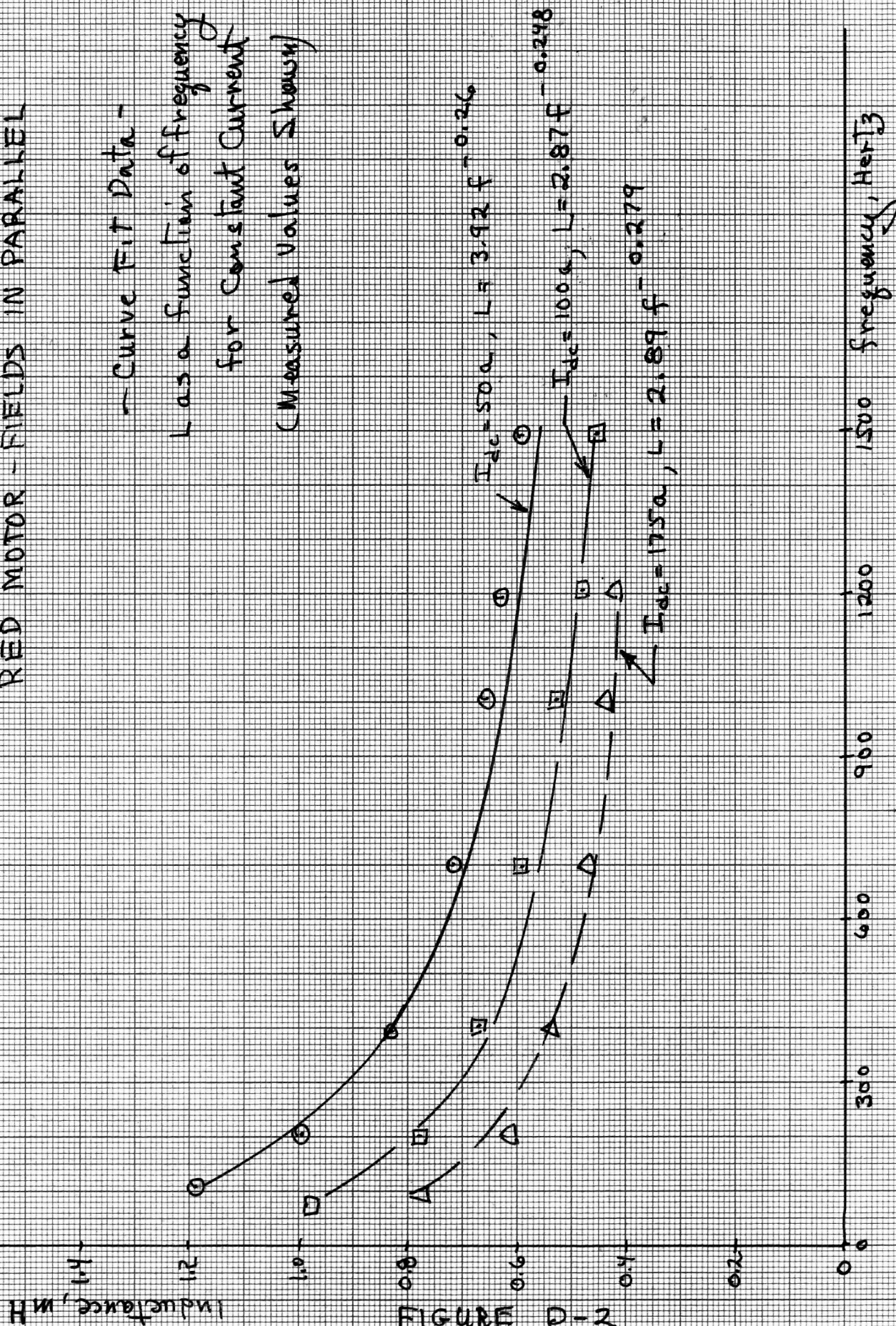


Saturation DC Amperes

RED MOTOR - FIELDS IN PARALLEL

- Curve Fit Data -

L as a function of frequency
for Constant Current
(Measured Values Shown)



RED MOTOR - FIELDS IN PARALLEL

(Cu Blocks)

400 Hz

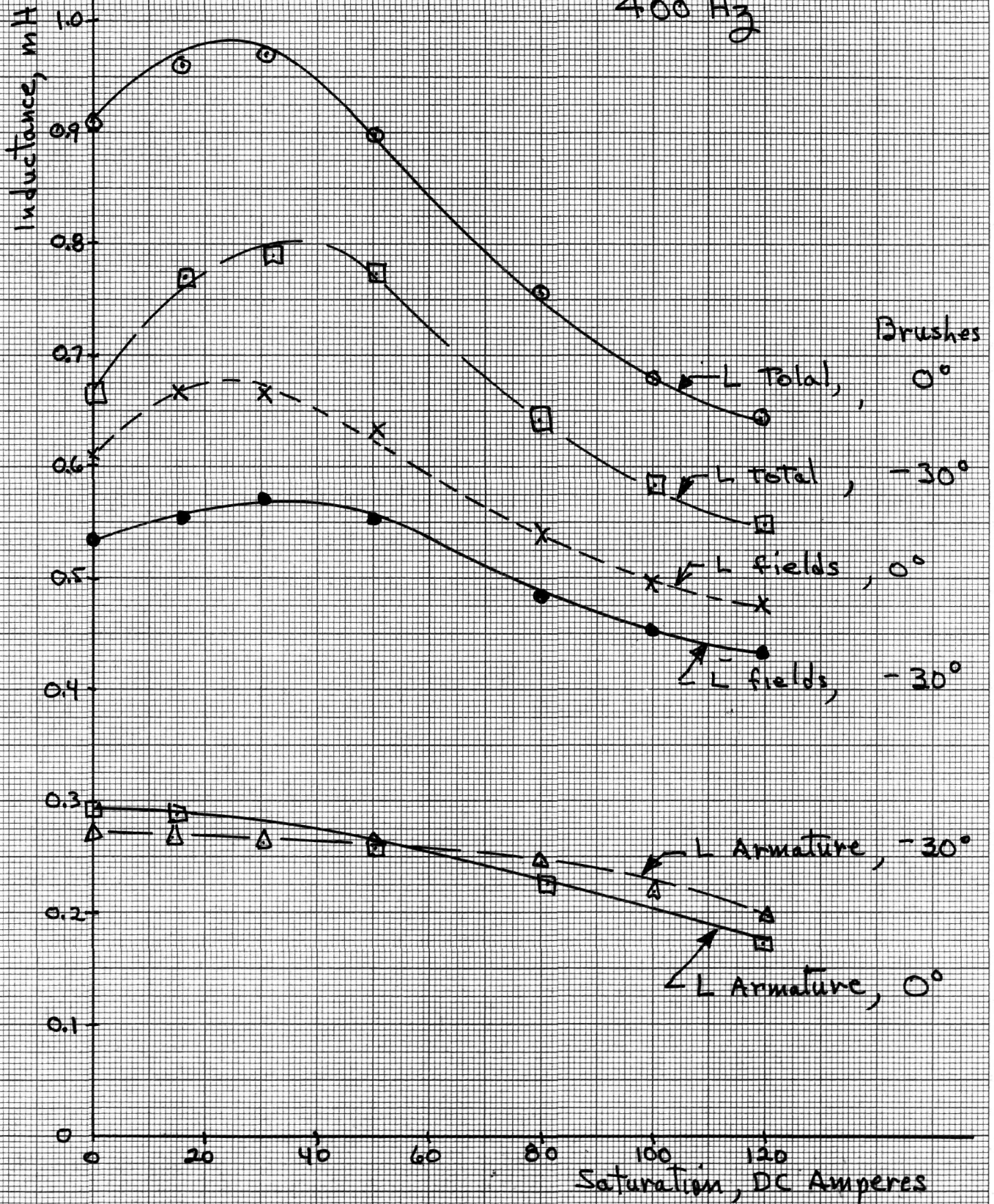


FIGURE D-3

RED MOTOR - FIELDS IN PARALLEL
(Cu Blocks, Brushes on 0°)

400 Hz

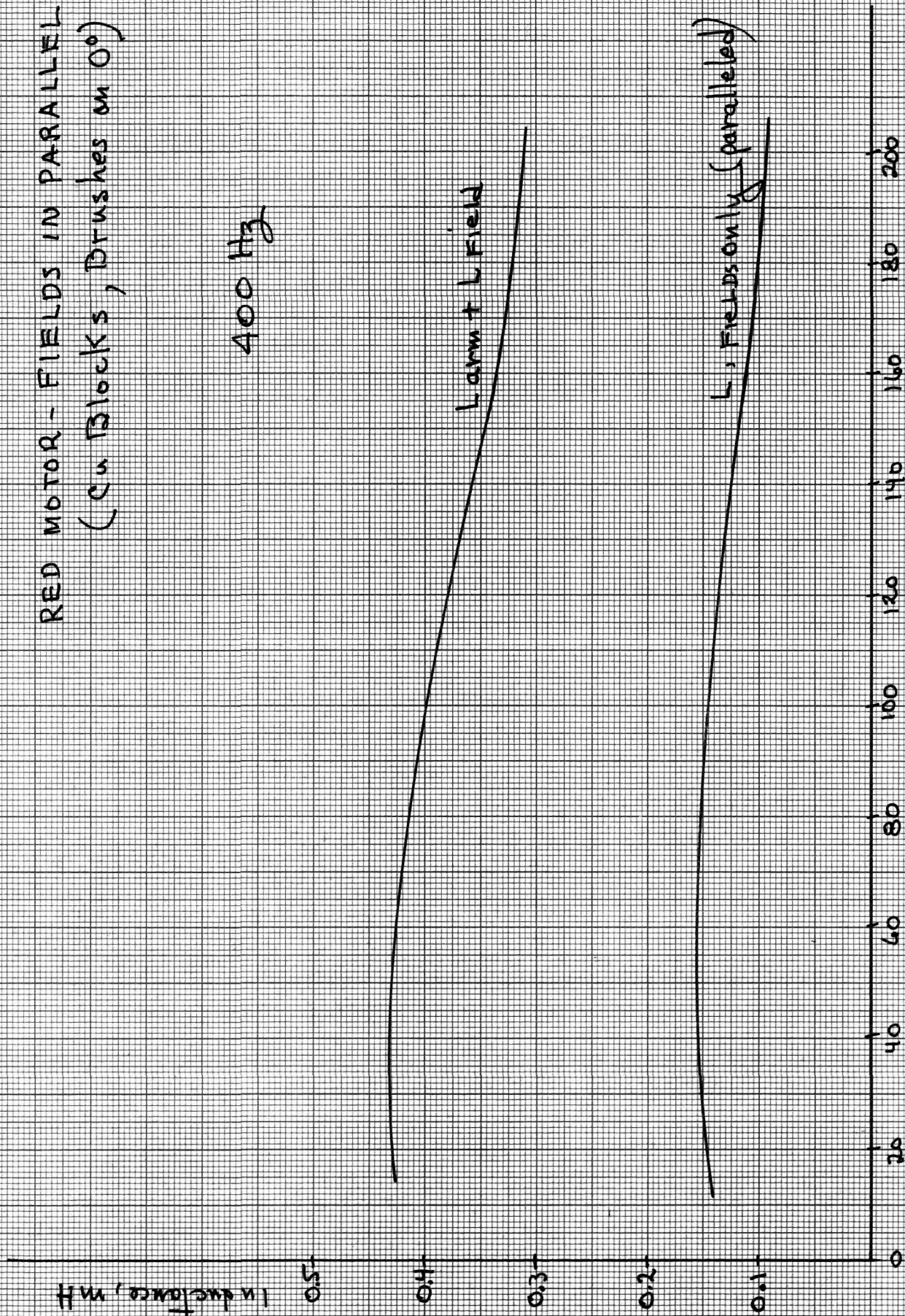
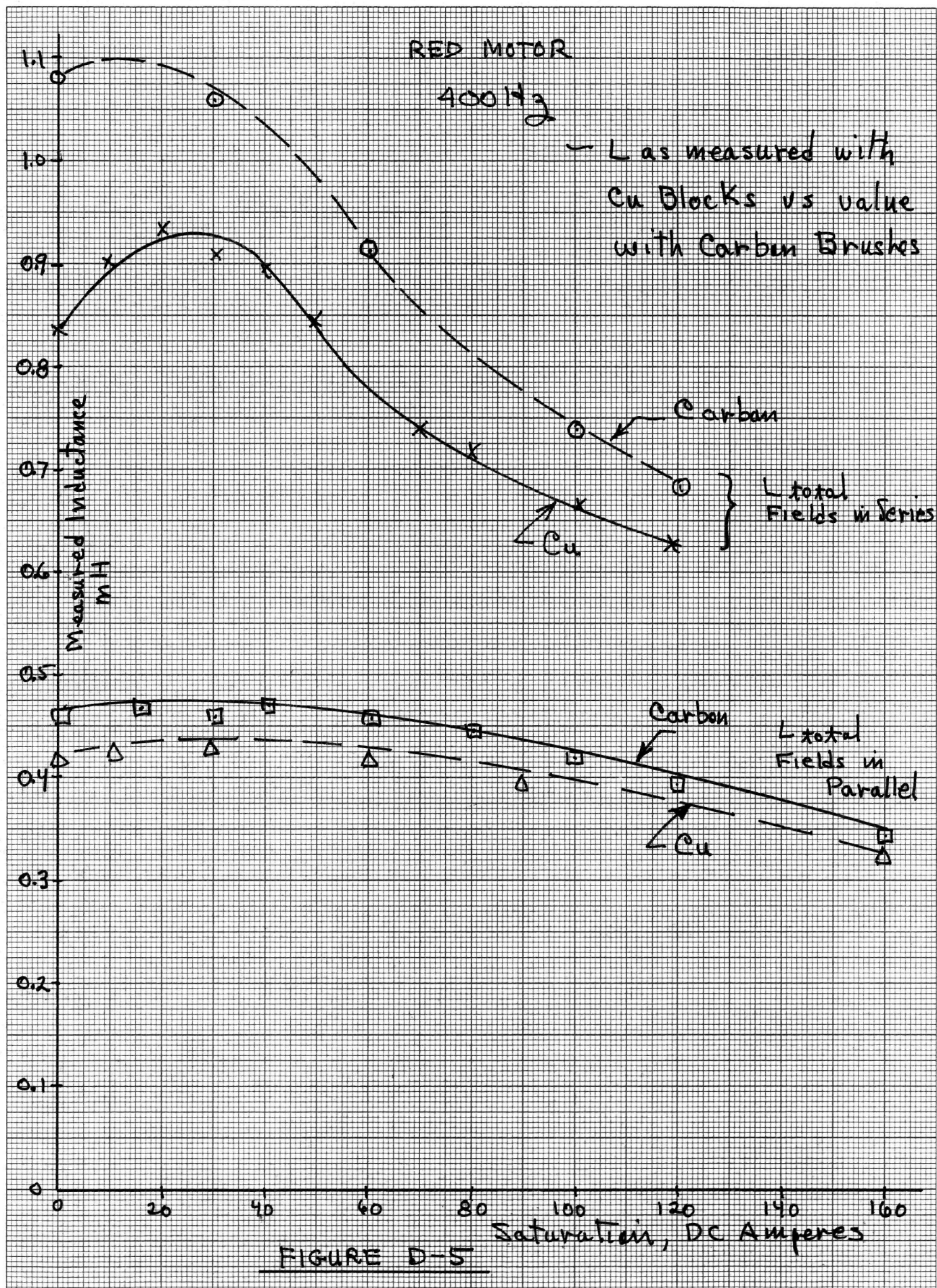
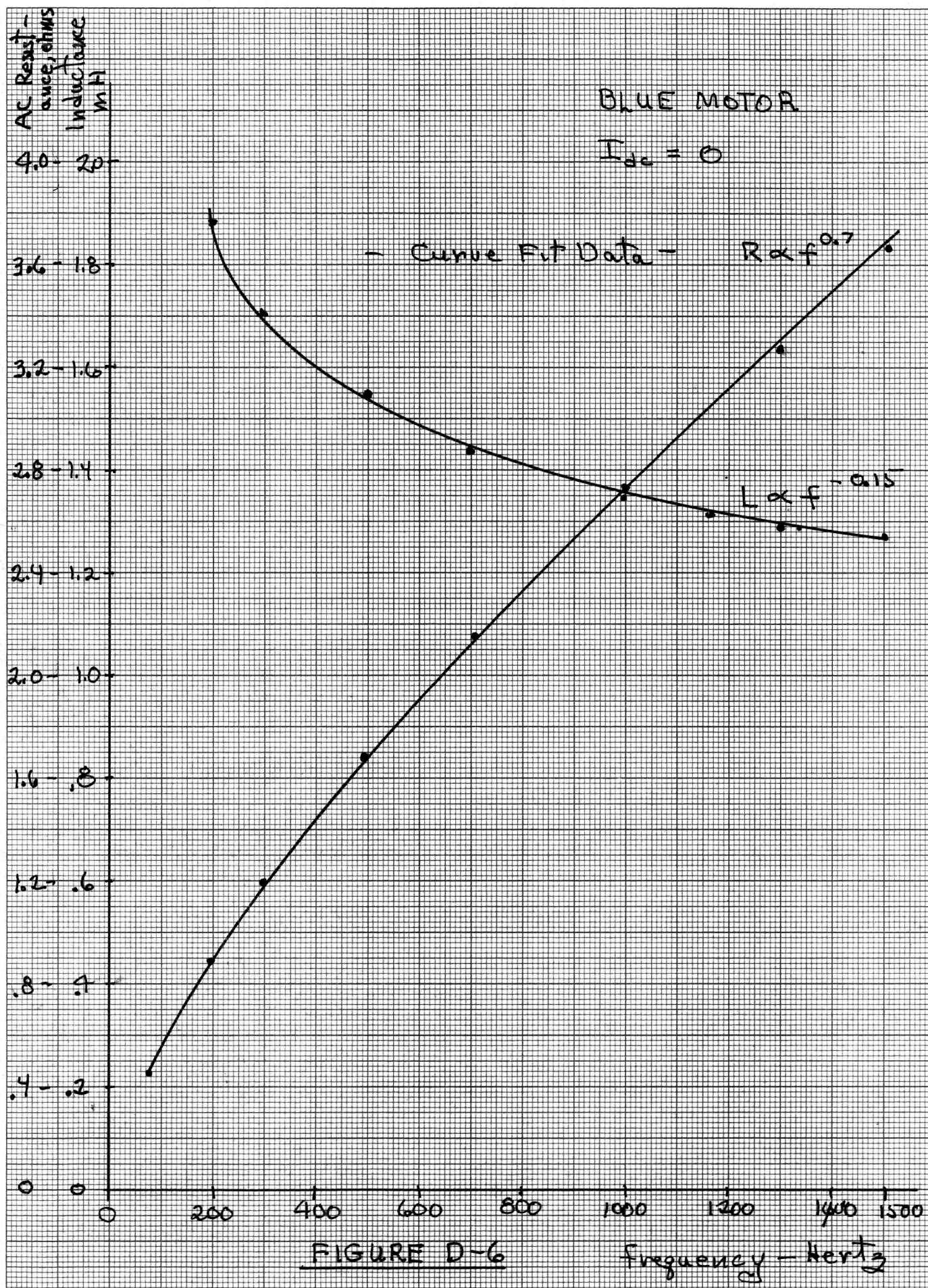


FIGURE D-4

Saturation, DC Amperes





BLUE MOTOR, FIELDS IN SERIES (Cu Blocks)

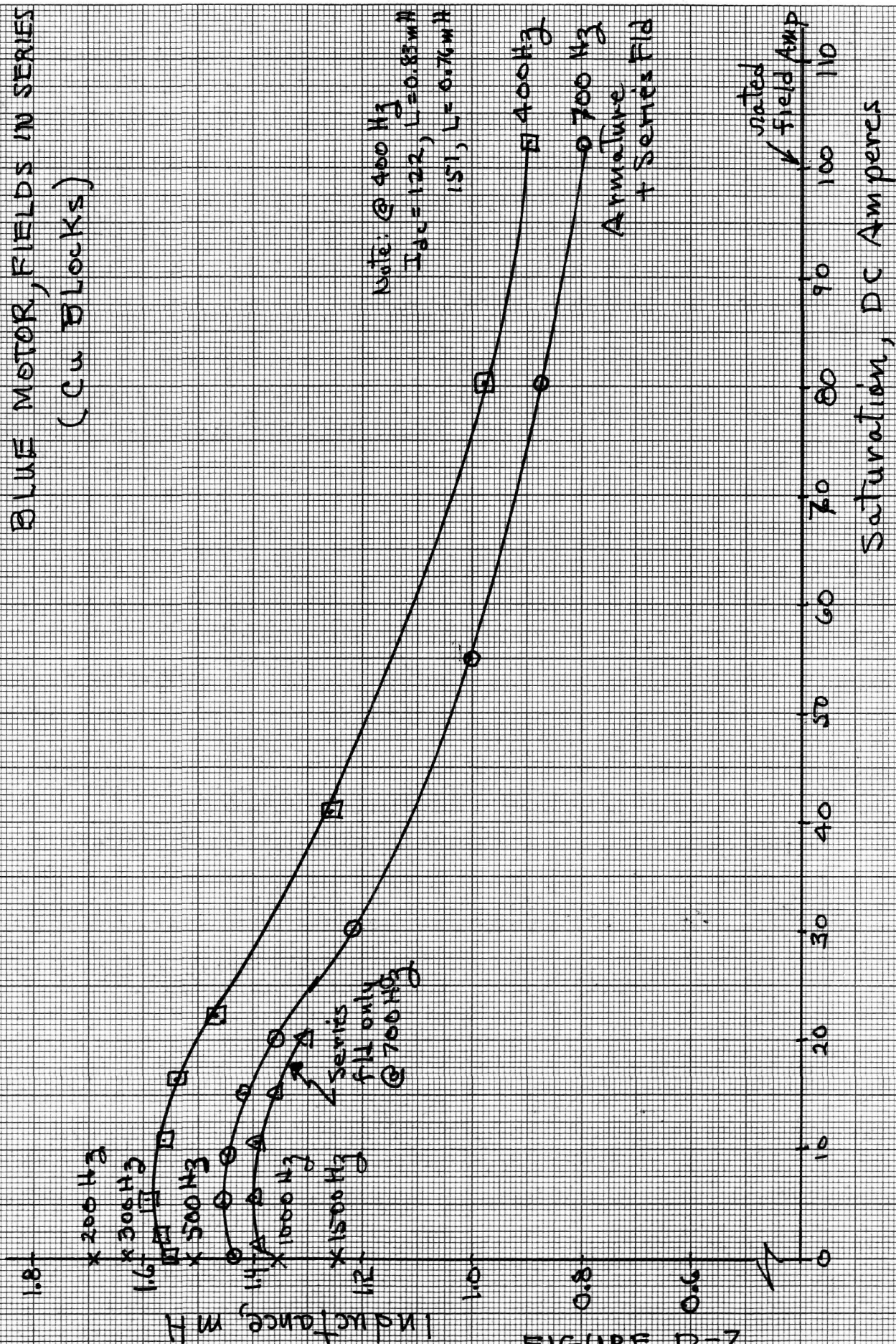


FIGURE D-7

D-15

RED MOTOR - FIELDS IN SERIES
Copper Blocks at 0°

Apparent Resistance As A Function
of Frequency & Saturation

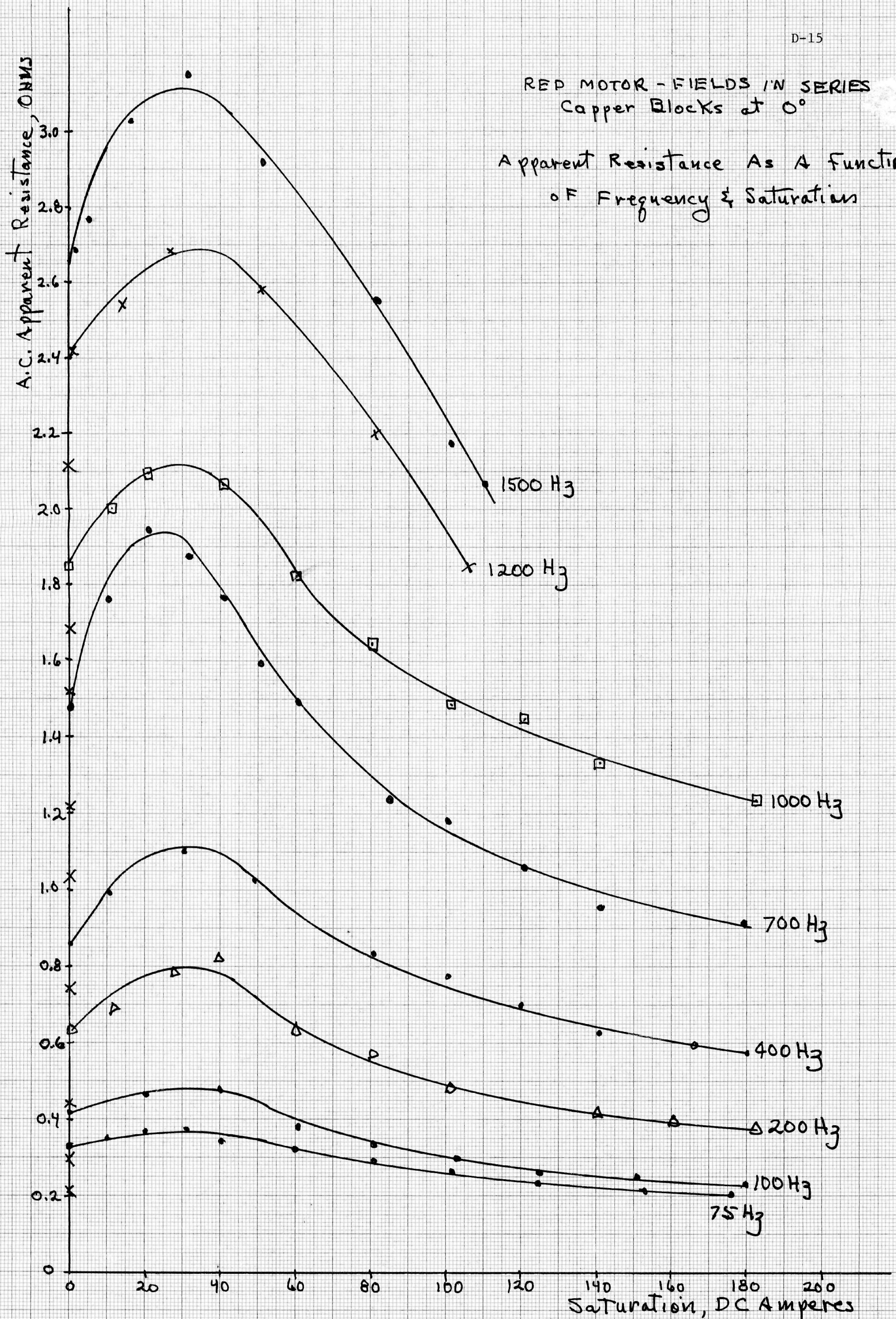


FIGURE D-8

46 1512

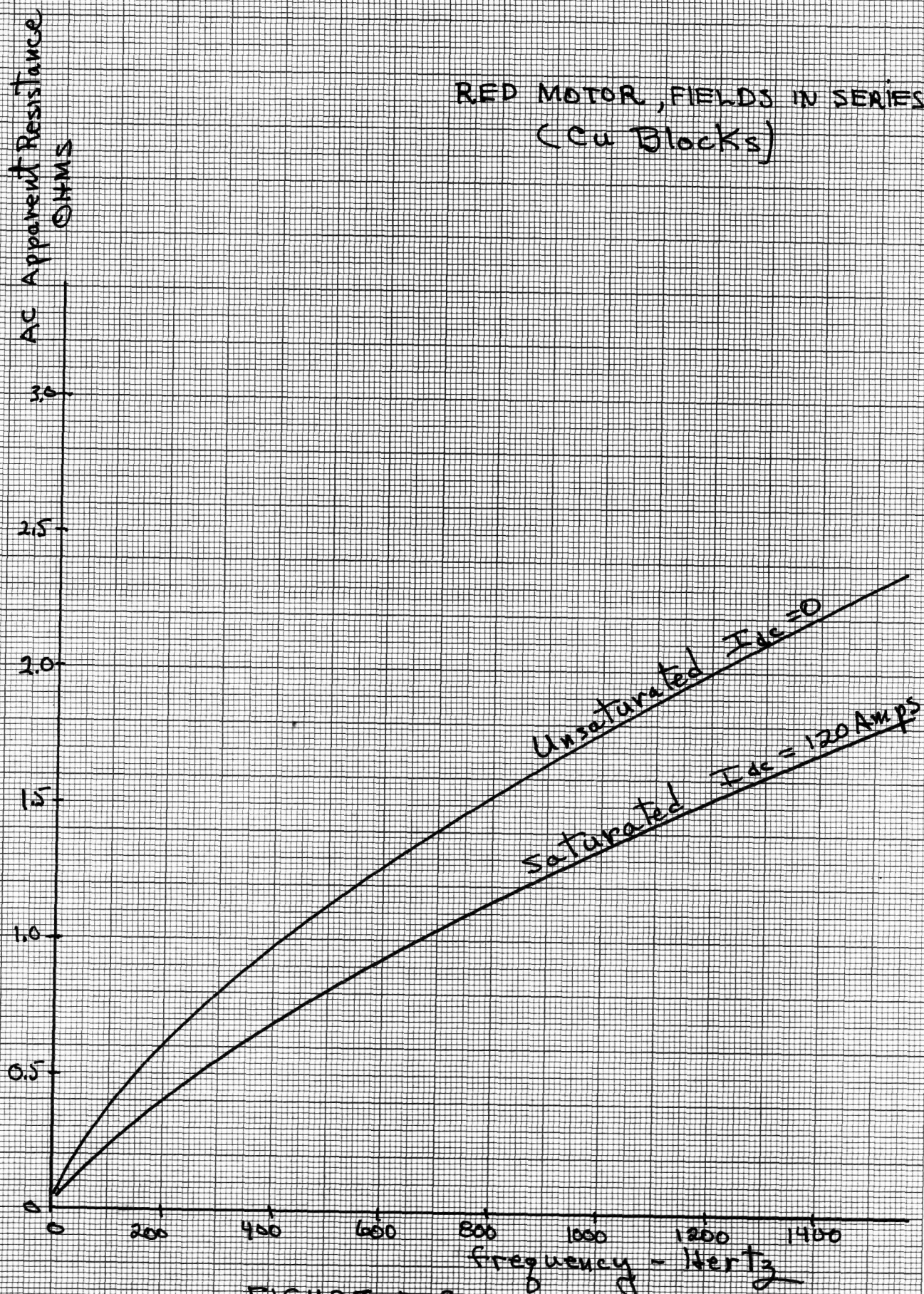
K&E 10 X 10 TO THE CENTIMETER 18 X 25 CM.
KEUFFEL & ESSER CO. MADE IN U.S.A.

FIGURE D-9

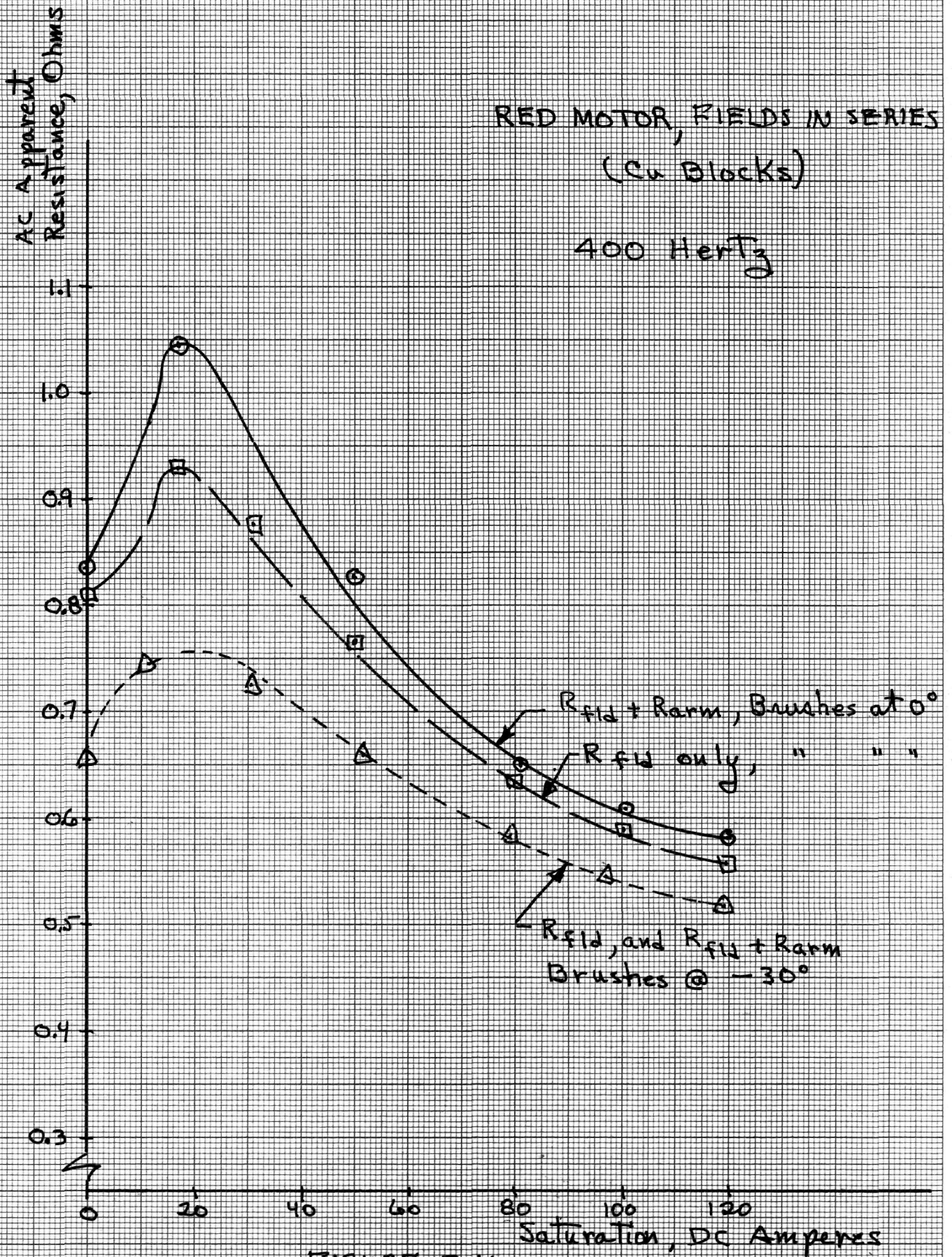
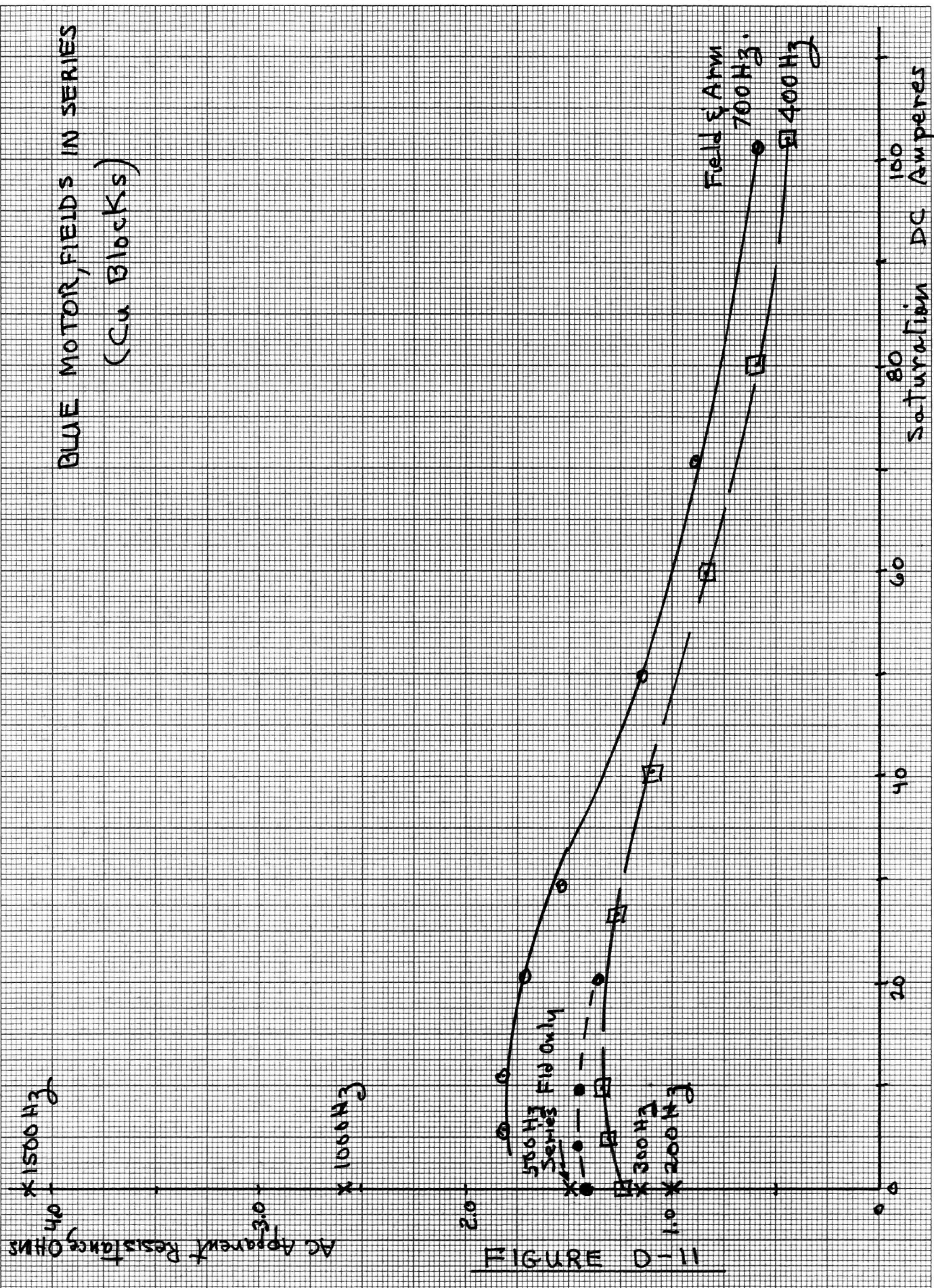


FIGURE D-10



SERIES MOTOR PARAMETER VARIATIONS AS A FUNCTION OF FREQUENCY AND SATURATION

H. B. Hamilton

Elias Strangas

Department of Electrical Engineering
University of Pittsburgh
Pittsburgh, PA 15261

Abstract - Knowledge of Dc series motor parameters as a function of frequency and degree of magnetic saturation are essential in applications where the motor is to be chopper controlled, such as in electric vehicles. Knowledge of the inductance is necessary for proper chopper selection; knowledge of all parameters is necessary in order to predict dynamic performance and efficiency. The latter is directly related to the range of a battery powered electric vehicle.

This paper presents measurement and instrumentation techniques and results obtained in testing of DC motors in the 84-96 volt, 20 HP size range.

Tests were run at frequencies from 30-1500 Hz and at levels of dc saturation from zero up to and including 115% of rated armature current. The incremental inductances and resistances were measured for these conditions. Apparent resistance values of over two orders of magnitude greater than the dc resistance were measured. The difference between the apparent and the DC resistances is due to skin and proximity effects in the conductors and hysteresis and eddy current losses in the iron. The associated losses are generally referred to as stray load losses. In typical chopper control applications these stray load losses can be an order of magnitude larger than the conventionally assumed 1% of output. The stray load loss may be larger than the dc joule losses and have a marked effect on the range to be expected from a battery powered electric vehicle.

INTRODUCTION

Knowledge of the inductance of the armature and field circuits of a DC machine is essential in order to permit dynamic performance calculations and to properly interface the machine with electronic controllers, such as variable pulse width, pulse rate choppers. Also, if the motor power supply has relatively high frequency components, a knowledge of the apparent resistance to harmonic currents, representing the core and eddy current losses (commonly classed as "stray load" losses) is necessary in order to predict motor efficiency. The latter is of extreme importance in evaluating motors to be used in battery powered electric vehicles.

IEEE Std #113 "IEEE Standard Test Code For Direct Current Machines" Section 5-5-4 specifies that the dc stray-load loss component can be taken as one percent of the output power or can be determined by subtracting all other losses from the total loss supplied to the machine. As will be shown in this paper, the former method is completely inadequate and the latter requires power measurements with an electronic watt meter with wide band width (to 20 KHz) response. Watt meters are available, but calibration facilities for such wattmeters under complex wave forms inputs are not widely available.

IEEE #113, Section 7.5 addresses the winding inductance measurement problem for the armature circuit and the shunt field. The series connected motor inductance measurement problem is not dealt with. In general, the armature circuit measurement is to be made with an alternating current and voltage, assuming negligible resistive component in the impedance of the winding or armature being measured. Application of this technique to the series machine yields inaccurate data, as will be shown in this paper, especially when frequency and saturation effects are present.

The literature ^{1,2} suggests the basic technique shown in Figure 1 as a method of determining the resistance and inductance of the armature circuit as a function of frequency and magnetic saturation level. Reducing this scheme to practice is not straight forward because of the harmonics problem and the need for selective instrumentation techniques.

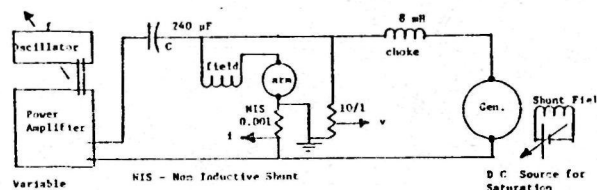


Figure 1 Basic Measurement Scheme

The loop which carries the ac component of current tends to multiply the effect of the presence of harmonics in the ac voltage supply because the circuit impedance is lower to the harmonics than to the fundamental frequency. It was found that even with a "distortionless" source, i.e. a high quality oscillator driving a high fidelity power amplifier, that the actual voltage and current values measured across the machine contained substantial harmonic components, and the impedance obtained from the measured RMS values was unacceptably in error! Since the impedance angle was measured from oscilloscope pictures, wave forms with harmonics also introduced an error in angle measurement.

The instrumentation techniques utilized to overcome those problems is detailed in the following section.

INSTRUMENTATION AND PROCEDURE

The basic power circuit of Figure 1 was utilized. The motor tested is rated (approximately) 20 HP, 84 volts and had a series field plus armature circuit inductance in the range around 1 mH. An 8 mH air choke was selected to retard AC current flow into the variable voltage (0-125 Vdc, 600 ampere shunt connected) generator armature. The capacitance chosen to block DC into the variable frequency source, was a bank of 240pF, total. The capacitance was sized to keep the voltage across the capacitance to relatively low values, especially at lower frequencies.

NIS is a non-inductive shunt, rated 0.001 ohms, 345 amperes continuous. The voltage divider is required because of input voltage limitations in the instrumentation amplifiers used. To reject the DC component of current and voltage in the signals, capacitor input filters, as shown in Figure 2 were utilized. Since the ratio of voltage to current and their phase angle is desired, the slight attenuation and phase shift introduced does not affect results if both signals are equally affected.

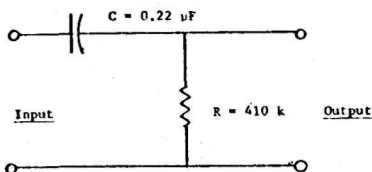


Figure 2 DC Rejection Filters

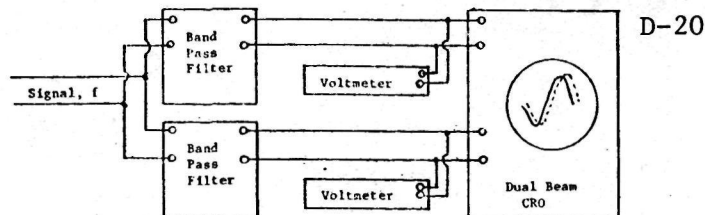
After filtering, the voltage and the current signals were amplified using Preston 8300 XWB Floating Differential amplifiers with gains of 10 (for the voltage signal) and 1000 (for the current signal), yielding amplifier outputs, in volts, proportional to the actual current and voltage levels.

In order to isolate the frequency desired for the measurement, Krone-Hite Model 3500 Band Pass Filters were placed between the Preston Amplifier outputs and the voltmeters and the oscillograph. These filters have dial settings for low and high frequency cutoff, f_L and f_H . Some attenuation and phase shift (lead through the low pass; lag through the high pass sections) does occur. From the attenuation characteristic, for these filters, if f/f_H and f_L/f are set at 0.4 for 0 db attenuation, i.e.,

$$f_H = 2.5 f; \quad f_L = 0.4 f$$

where f is the pass frequency, the phase shift through the low pass section is $+60^\circ$; the phase shift through the high pass section is -60° , yielding zero net phase shift and zero attenuation. Because of the error inherent in dial settings, the final adjustment of the dial settings is made by the calibration connection shown in Figure 3.

After filter setting adjustments were made, the common input signal was removed and the differential amplifiers with gain setting noted above were connected between the NIS and the voltage divider outputs and the filter inputs. The voltmeters used were wide frequency response, high accuracy, true RMS reading Hewlett-Packard Model 300E voltmeters.



(Adjust Filter cut off frequencies for zero phase shift, equal amplitude)

Figure 3, Band Pass Filter Adjustment

Tests for R and L were conducted using a 1.5 - 2 ampere ac current derived from the oscillator-amplifier source, at various frequencies from 30-1500 Hz and at various levels of dc current.

Readings of voltage and current and a photo of the CRO traces were taken. From the photo, the angle, ϕ , between voltage and current was determined. From the data; R and L can be calculated as:

$$R = \frac{V}{I} \cos \phi; \quad L = \frac{V}{2\pi f I} \sin \phi \quad (1)$$

To obtain the phase shift, ϕ , in radians from the scope photos, the ratio of the length from peak-peak to the length of the period times 2π was calculated. Inherent errors are introduced in making the length measurements. The magnitude of the errors can be visualized from:

$$\Delta R = \left(\frac{V}{I} \sin \phi \right) \Delta \phi \quad (2)$$

the % error, in determining R is:

$$\%R = \left(\frac{\Delta R}{R} \right) 100 = 100 \tan \phi (\Delta \phi) \quad (3)$$

where ΔR is the calculated error based on a measure angle error of $\Delta \phi$.

Similarly, % error in determining L is:

$$\%L = 100 \cot \phi (\Delta \phi). \quad (4)$$

Actual ϕ is in the range 55-65 degrees.

Assuming $\phi = 60^\circ$;

$$\%R = 173 \Delta \phi \quad \%L = 58 \Delta \phi \quad (5)$$

For a scope picture with a cycle length of 60 mm, and an error in measurement of 0.5 mm (trace width), about 10% error in the calculation of R and a 3.5% error in the calculation of L can be expected.

TEST RESULTS

The test results presented in this paper are from a 4 pole series motor with solid frame, without interpoles. The motor had two series fields (one for each pair of poles) with 20 turns/pole and was intended for use in a battery powered electric vehicle application.

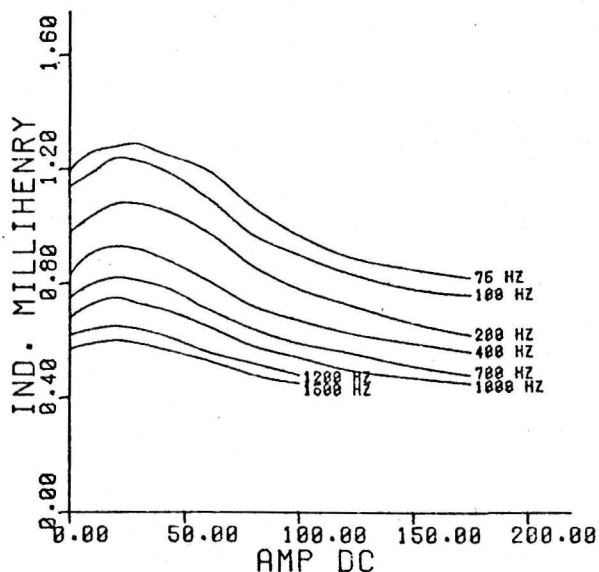
The armature is wave wound with a continuous rating of 175 amperes, 144 volts. Electrographic (low voltage drop) type brushes are used. The majority of the tests were conducted with the fields in series. Where noted, paralleled fields were used. Tests by others³ have shown that values obtained with stationary rotor show essentially no variation from those obtained under running conditions. These tests were conducted on blocked rotor. As protection

against overheating, dc current was limited to 200 amperes maximum. A couple of quickly taken data points at higher current demonstrated that a rather high level of saturation prevails at currents between 120 and 200 amperes when the fields are connected in series. The dc resistance of the armature and the two fields in series is 0.022 ohms. Because of lack of interpoles, the brush position for continuous operation at rated output was shifted against rotation 30 electrical degrees.

The carbon brushes were replaced with properly radiused copper blocks, the rotor blocked against rotation and data as described above was taken to determine the circuit inductance and apparent resistance as functions of frequency and magnetic saturation.

The current level of the AC current injected was 2 amperes or less; thus the inductance calculated is incremental inductance. Test Results will be presented, followed by a discussion of those results. Figures 4 and 5 present the variation of armature circuit (armature plus the two series fields connected in series) inductance and apparent resistance as functions of frequency and saturation (dc current).

After the frequency trends were established from these tests, tests were run at 400 Hz to isolate other phenomena.



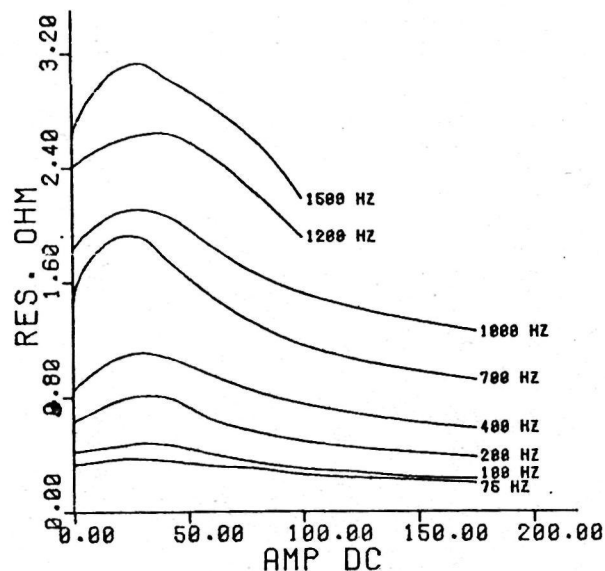
TOTAL L vs. I dc
Copper Blocks on 0 Degrees
Fields in Series

Figure 4

Figure 6 shows the variation of total circuit inductance and armature only inductance when the armature only is excited and when both armature and series field are excited.

Figure 7 shows the same data for the brushes on both 30° and on zero (neutral), as functions of magnetic saturation.

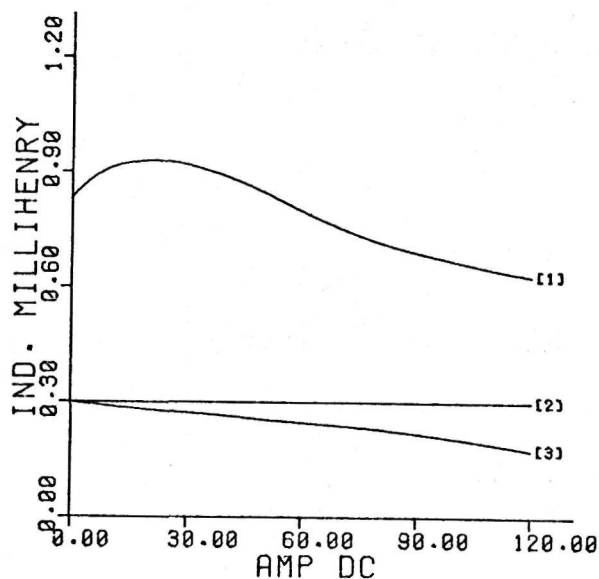
Figure 8 presents the variations of apparent resistance for the armature and series field, at 400 Hz as a function of saturation.



TOTAL R vs. I dc
Copper Blocks on 0 Degrees
Fields in Series

Figure 5

The variation of total inductance and the inductance of the series fields only, for the condition of paralleled series fields, at 400 Hz is shown in Figure 9. Figure 10 shows the variation of apparent resistance of the parallel connected series fields as a function of saturation at 400 Hz.



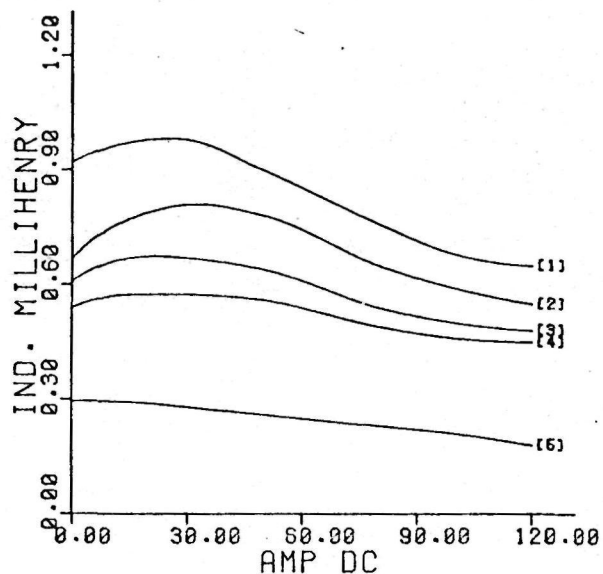
1 - Total L vs. I dc
2 - Armature L vs. I dc (armature excitations only)
3 - Armature L vs. I dc (Arm and Series Field Excitations)
Copper Blocks on 0 Degrees, 400 Hz.

Figure 6

In order to ascertain the effect of using regular carbon brushes, rather than copper blocks in making the measurements, tests duplicating some of

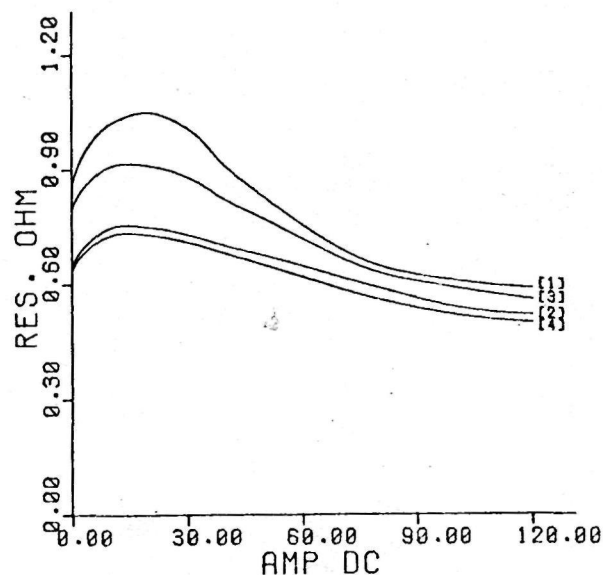
the previous tests, at 400 Hz, were conducted. The results for the two brush conditions are shown in Figures 11 and 12 for the inductance and apparent resistances.

Figures 13 and 14 show L and R of the armature only over the frequency range from 70 to 1500 Hz for the condition of 30 degree brush shift and zero amperes dc.



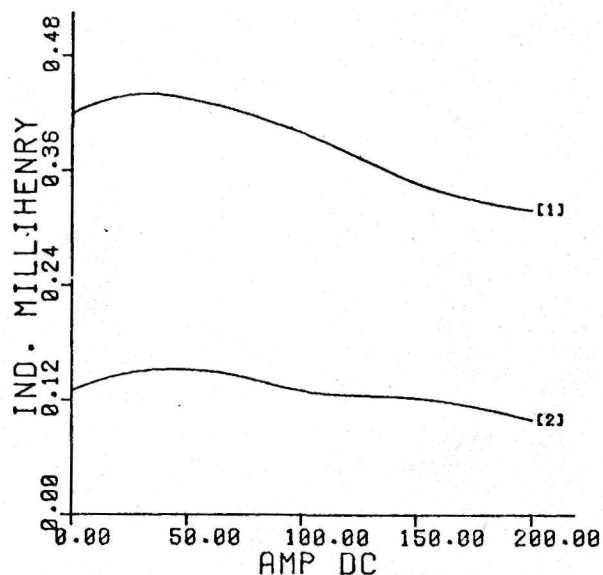
- 1 - Total L vs. I dc, 0 Degrees
- 2 - Total L vs. I dc, 30 Degrees
- 3 - Series Field L vs. I dc, 0 Degrees
- 4 - Series Field L vs. I dc, 30 Degrees
- 5 - Armature L vs. I dc, 0 and 30 Degrees
Copper Blocks, 400 Hz

Figure 7



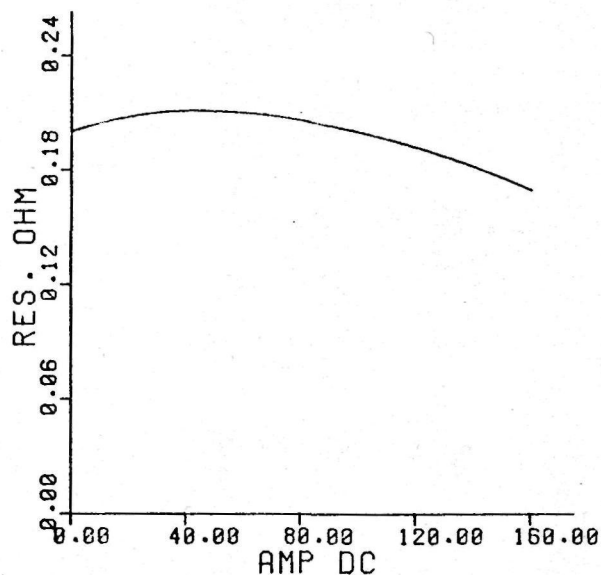
- 1 - Total R vs. I dc, 0 Degrees
- 2 - Series Field R vs. I dc, 0 Degrees
- 3 - Total R vs. I dc, 30 Degrees
- 4 - Series Field R vs. I dc, 30 Degrees
Copper Blocks, 400 Hz.

Figure 8



- 1 - Total L vs. I dc
- 2 - Series Field L vs. I dc
Series Fields Paralleled, 400 Hz
Copper Blocks on 0 Degrees

Figure 9



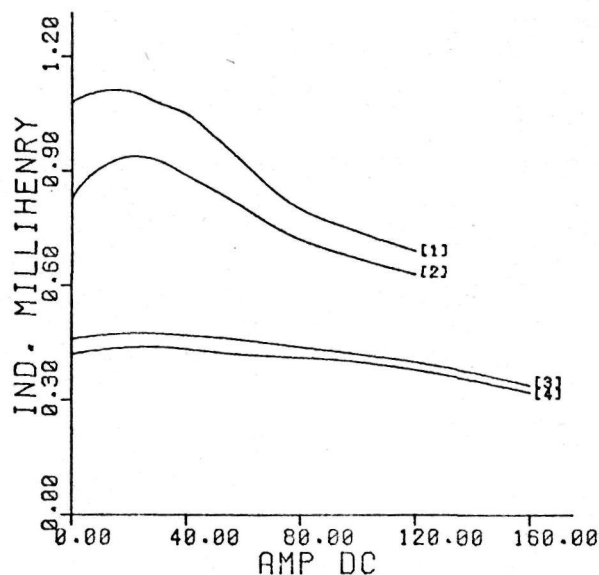
- Total R vs I dc
Series Fields Paralleled, 400 Hz.
Copper Blocks on 0 Degrees

Figure 10

DISCUSSION OF RESULTS OBTAINED

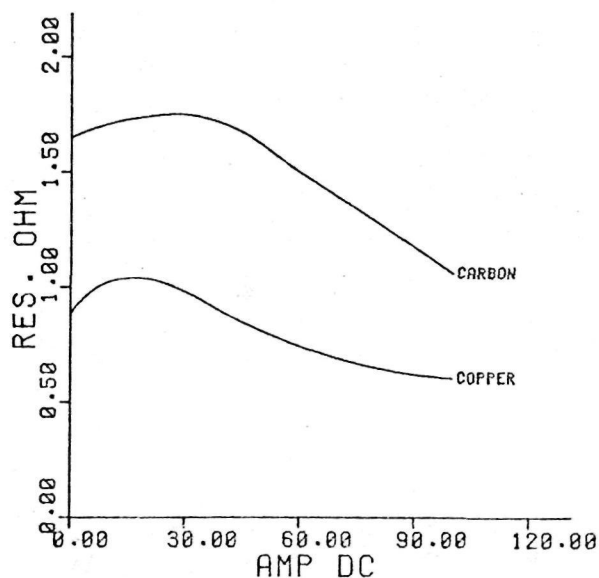
The B-H curve for a magnetic circuit commences with a modest slope, increases, then decreases in slope as saturation is reached. Since inductance is proportional to permeability and the slope of the B-H characteristic is permeability, the variation of L with respect to saturation current level, for a fixed frequency, as shown in Figures 4, 6, 7, 9, 11 and 15 is as expected. The data shown in Figure 6 is also in agreement with theory in that series field exci-

tation tends to saturate the armature because of the closed magnetic path whereas armature excitation only does not, i.e. from curve (2), Figure 6 armature L does not change with armature only excitation because the armature mmf acts largely through an air path in a machine without interpoles.



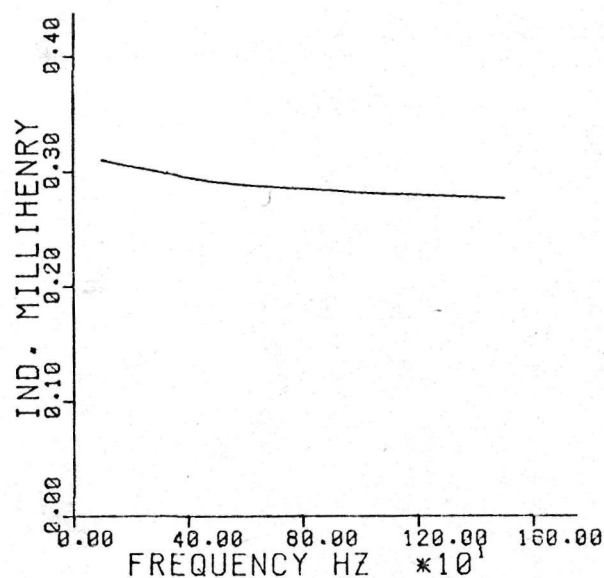
- 1 - Total L vs. I_{dc} , Carbon Brushes
 2 - Total L vs. I_{dc} , Copper Blocks
 3 - Series Field L vs. I_{dc} , Carbon Brushes
 4 - Series Field L vs. I_{dc} Copper Blocks
 Fields in Series
 Blocks or Brushes on 0 Degrees, 400 Hz
 Variation of L By Brush Type

Figure 11



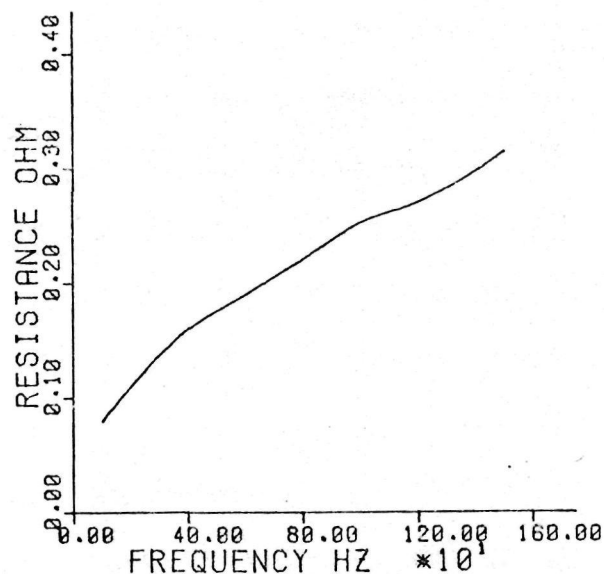
- Fields in Series
 Blocks or Brushes on 0 Degrees, 400 Hz
 Variation of R by Brush Type

Figure 12



Variation of Armature L With Frequency, $I_{dc} = 0$
 Copper Blocks on 0 Degrees

Figure 13

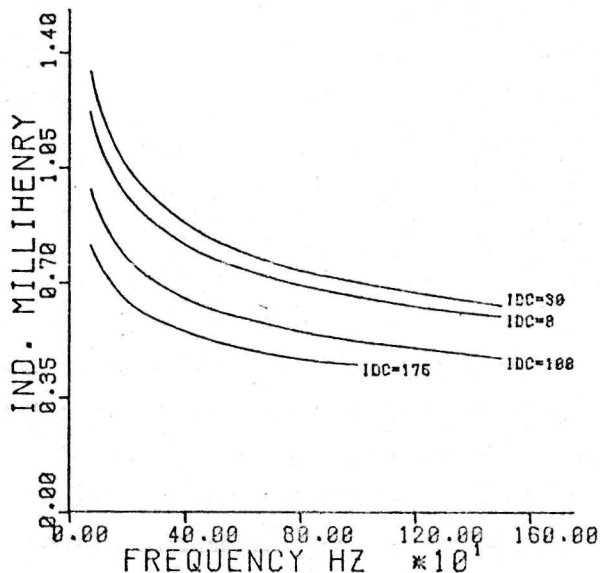


Variation of Armature R With Frequency, $I_{dc} = 0$
 Copper Blocks on 30 Degrees

Figure 14

Since the skin and proximity effect, yielding an apparent increase in resistance, is also related to permeability, the trend in resistance, as a function of saturation, as shown in Figure 5, is as to be expected. Hysteresis and eddy current losses increase with frequency, as does the resistance increase depicted in Figure 5.

Skin effect and eddy currents both increase with frequency. Eddy currents tend to establish a magnetic field in opposition to the field established by the conductor current, resulting in a decreasing net field, and flux linkages, with increase in frequency. Thus, it is to be expected that the inductance would decrease with frequency, for a given level of DC saturation as shown in Figures 4, and 15.



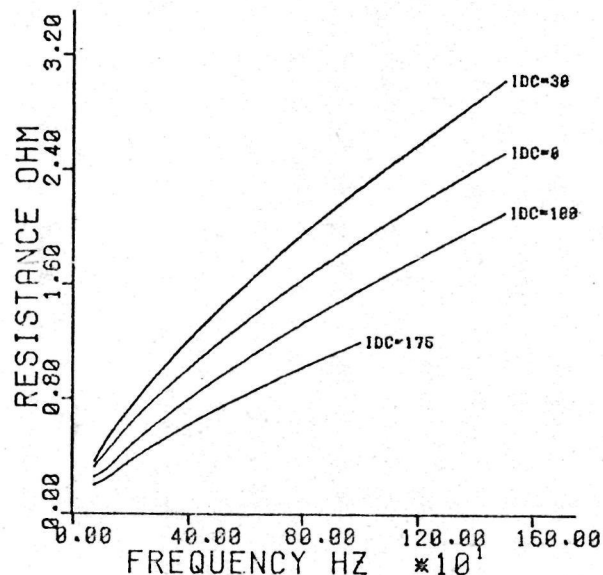
Variation of Total L With Frequency, Saturation Copper Blocks on 0 Degrees, Fields in Series

Figure 15

Curve (5) of Figure 7 verifies that armature inductance is independent of brush position and that in the particular motor tested about 75-80% of total armature circuit inductance is in the series fields. Theoretically, the net mmf is decreased, by brush shift α , (against direction of rotation) by α/π . In a constant permeability situation (saturated) the incremental inductance would be decreased by the same amount. For a 30 degree shift, the reduction theoretically would be by a factor of 1/6. As shown by curves (3) and (4), in Figure 7, the measured decrease in series field L is approximately this value.

Figure 8 can be used to determine the relative magnitude of the stray load losses in the magnetic structure of the field and the armature. Since, from Figure 7, the armature is completely unsaturated, the R of the armature would be predicted as being small (due to low flux density). This is borne out by the test results shown in Figure 8 which indicates that over 85% of the losses occur in the field structure. Thus, any efforts to minimize eddy current losses in the armature (by smaller strand conductors) would not be meaningful.

The test results shown in Figure 11 and 12 indicate the differences in values of L and R when measurements are made with carbon brushes, as collectors, as opposed to the use of copper blocks. The inductance measured with carbon is about 10% higher than with copper whereas the calculated values of R are about 75-100% greater. It is felt that the 10% difference in L is experimental error, whereas the large difference in R is attributable to the well known variation of brush to commutator contact resistance which is a function of current density. The ac current density used in these measurements is quite low (1% of rated). The conclusion here is that reasonably accurate values of L can be calculated from measurements taken using carbon brushes but that (at the low level of AC used) the apparent resistance measurements will be grossly in error. Brush resistance, or voltage drop, must be accounted for by



Variation of Total R With Frequency, Saturation Copper Blocks on 0 Degrees, Fields in Series

Figure 16

separate calculations based on total brush current level.

The various figures depict the variation of L and R with frequency and DC current, or saturation level and indicate that the variations are reasonably independent of each other. Power curve fit analysis yields, approximately:

$$L \propto f^{-0.24}, I^{-0.25}$$

$$R \propto f^{0.7}, I_{dc}^{-0.4}$$

The curve fit used above includes all data points greater than zero. However, if the data points in the region where the curves "hump" (corresponding to the rapidly changing permeability at low levels of saturation) are not included in the curve fit, the variations are considerably different and are believed by the authors to represent more realistic functional relationships and more accurate data to be used in performance analysis because the motor is more likely to be running at load currents greater than 25% of rated, i.e. greater than 40-50 amperes. For this condition, the variations with frequency and current are different, somewhat.

For total motor inductance (fields connected in series) and resistance, the variations found were:

$$L \propto f^{-0.24}, I^{-0.0627}$$

$$R \propto f^{0.7}, I^{-0.07}$$

These are values with the brushes on neutral. The values with 30° brush shift were found to be approximately 15% lower in absolute value but the dependence was noted to be the same.

Measurements made on the armature circuit only, Figures 7 and 8, indicate that armature resistance and inductance are independent of brush position and that their variations are:

$$L_a \propto f^{-0.05}, I^{-0.11}$$

$$R_a \propto f^{0.47}, I^{0.0}$$

Similar tests, not detailed here, on a 4 pole lap wound machine with laminated magnetic field structure but of approximately the same rating yielded almost identical variations in parameters as did the motor for which test results are presented here.

The data obtained in these tests will be used as parameters in development of a model for the motors. As an example, measurements taken indicate that:

$$\begin{aligned} L &= 0.68 \text{ mh at } I_{ac} = 100, f = 400 \text{ hz} \\ L_a &= 0.18 \text{ mh at } I_{dc} = 100, f = 400 \text{ hz} \\ R &= 1.19 \text{ ohms at } I_{ac} = 100, f = 700 \text{ hz} \\ R_a &= 0.217 \text{ ohms at } I_{ac} = 0, f = 800 \text{ hz} \end{aligned}$$

from which, for total inductance,

$$L = K_L f^{-0.24} I^{-0.0627}$$

Solving, using the data point given yields:

$$K_L = \frac{0.68}{(400^{-0.24})(100^{-0.0627})} = 3.8$$

Similar solutions, using data and variations presented above yield; for the motor

$$L = 3.8 f^{-0.24} I^{-0.063}$$

$$L_a = 0.58 f^{-0.05} I^{-0.11}$$

$$R = 0.0167 f^{0.7} I^{-0.07}$$

$$R_a = 0.0095 f^{0.47}$$

HARMONIC CONTENT AND AC LOSSES

Franklin⁴ presents two versions of the Fourier series for the current in a chopper controlled motor. The more rigorous "exponential time relation" is based on constant R, L whereas his "approximate (linear) time relation" is based on constant rate of change of current, i.e. time on/time off less than the time constant of the circuit involved. Because of the variation of apparent R and L and the fact that in the motor tested for data in this paper the apparent time constant is on the order of 0.5 milliseconds (saturated), neither relation will yield exact results. However, order of magnitude hysteresis and eddy current losses can be estimated, using the simplified linear relationship (continuous conduction assumed) for rms harmonic current, I_q :

$$I_q = \frac{\Delta i T}{\sqrt{2} 2\pi^2 q^2 T_o (1 - \frac{T_o}{T})} \sqrt{2(1 - \cos q(\frac{T_o}{T} 2\pi))} \quad (6)$$

A typical operating situation involves a duty cycle $T_o/T = 0.5$, at a frequency of 300 Hz with current excursions of 50 amperes at an average current of 120 amperes. The harmonic rms currents calculate approximately as: (From Figure 16)

$q = 1$	$I_q = 14.3$	$R = .58$
3	= 1.59	= 1.16
5	= .57	= 1.8

The ac power loss (hysteresis and eddy currents) would be:

$$P_{ac} = 14.3^2 (58) + 1.59^2 (1.16) + .57^2 (1.8) = 123W$$

If the motor were operating from an 84 volt source, this loss represents 1.25% of the input power and is in addition to the "stray load" losses usually associated with operation from "pure" dc. In this motor, the joule loss in the circuit, due to average current of 120 amperes is 330 watts.

SUMMARY AND CONCLUSIONS

Inductance Variations:

The armature inductance is independent of brush position and armature-only excitation. It accounts for about 1/3 of the total armature circuit inductance.

The armature circuit, including the series field is about 30% less under saturated conditions than unsaturated, decreasing approximately as the -0.06 power of the DC current level. Also, it decreases proportional to the -0.24 power of frequency (over the frequency range tested, i.e. to 1500 Hz). The armature circuit inductance is dependent upon brush position, decreasing in proportion to the angle of shift against rotation. For the motor tested, with the brushes located for proper commutation, it decreased by 15%.

It should be noted that in a constant inductance circuit, higher frequency current harmonics are suppressed in magnitude but in the motors tested, with decreasing inductance with increasing frequency, the opposite effect is the situation.

Resistance Variations

For the motor, with results detailed here, the DC resistance of the armature and fields was measured as 0.0189 and 0.0165 respectively for a total of 0.0254 ohms. The ratio of armature to field DC resistance is 1.15. From Figure 8, the 400 Hz AC resistance ratio is 0.15 for a change of 1.15/0.15 = 7.65.

About 90% of the resistance to ac harmonic current is associated with the series field winding. Apparent resistance decreased about 15% with brush shift. The values observed under saturated conditions were 20-30% less than the unsaturated values (depending upon frequency). For a given degree of saturation, the apparent resistance increased with the +0.7 power of frequency. For a specific frequency, the resistance decreased approximately as the -0.07 power of DC current level.

Carbon Brush vs Copper Block Valves:

- (1) The value of inductance measured using copper blocks was found to be about 6% less than values from measurements with carbon brushes.
- (2) Measurement of apparent resistance with carbon brushes in place yielded a value of approximately 75% greater than found using copper blocks.

Magnitude of Losses:

The combination of relatively high harmonic currents and the apparent resistance (reflecting hysteresis and eddy current skin and proximity effect losses yields a loss component which should be included in any efficiency determination.

Motor/Chopper Interface Influence:

Since the chopper is sensitive to the amount of inductance in the circuit, care should be taken to use the saturated value of inductance, obtained at the maximum operating frequency, when evaluating the interface details.

On Measurement Techniques:

The circuit used in this test does yield accurate values of R and L. Because of the harmonic multiplier effects, special care must be used in the selection and application of the instrumentation used. Copper blocks should be substituted for the carbon brushes and the effective resistance function of the brushes added.

Summary

The dependance of circuit parameters on frequency and saturation indicate the need for inclusion of these factors in a model of the motor from which performance is to be calculated.

Acknowledgement

This work was supported by NASA-Lewis Research Center and Dept. of Energy under Grant #NSG-3163.

References

1. Saunders, R. M., "Measurement of DC Machine Parameters," AIEE Transactions, 1951, Volume 70.
2. Snively, H. D. and Robinson, P. B., "Measurement and Calculation of DC Machine Armature Circuit Inductance," AIEE Transactions, 1950, Volume 69.
3. DeWolf, F. T. "Measurement of Inductance of DC Machines." Presented at the WPM, PES 1979 and pending publication.
4. Franklin, P. W. "Theory of the D. C. Motor Controlled By Power Pulses, Part I and Part II. IEEE Transactions, PAS Vol. PAS-91, Jan./Feb. 1972.

APPENDIX E - CURVE FITTING

Because of the repeatability problems generally experienced with DC Machine (hysteresis effects), and to assist in data plotting, curve fitting techniques were resorted to when the data yielded acceptable correlation. Two types of curve fit were utilized. They were:

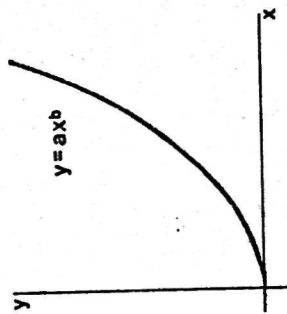
The Power Curve, $y = ax^b$

The Exponential Curve, $y = a e^{bx}$

The form of these curves, and the formulas for the calculation of the regression coefficients, a and b , from data points x_i and y_i are shown on page E-2, as is the calculation of the "coefficient of determination, r^2 ". Perfect correlation corresponds to an $r^2 = 1.0$.

The majority of the data taken yields r^2 values close to 1.0, yielding confidence that the calculated curve is indeed a "best fit". Calculations were made on an HP-97 calculator program. The program is exceptionally useful because once the curve coefficients have been determined, specified-easy-to-plot values of one variable can be entered and calculated values of the other variable are outputted; thus facilitating the handling of data.

Power Curve Fit

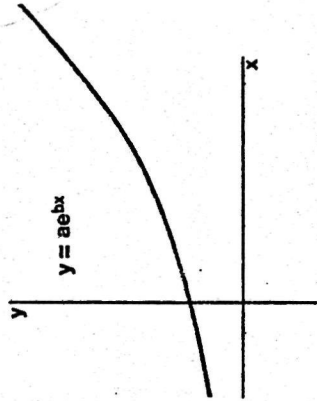


$$b = \frac{\sum (\ln x_i)(\ln y_i) - \frac{(\sum \ln x_i)(\sum \ln y_i)}{n}}{\sum (\ln x_i)^2 - \frac{(\sum \ln x_i)^2}{n}}$$

$$a = \exp \left[\frac{\sum \ln y_i}{n} - b \frac{\sum \ln x_i}{n} \right]$$

$$r^2 = \frac{\left[\sum (\ln x_i)(\ln y_i) - \frac{(\sum \ln x_i)(\sum \ln y_i)}{n} \right]^2}{\left[\sum (\ln x_i)^2 - \frac{(\sum \ln x_i)^2}{n} \right] \left[\sum (\ln y_i)^2 - \frac{(\sum \ln y_i)^2}{n} \right]}$$

Exponential Curve Fit



$$b = \frac{\sum x_i \ln y_i - \frac{1}{n} (\sum x_i)(\sum \ln y_i)}{\sum x_i^2 - \frac{1}{n} (\sum x_i)^2}$$

$$a = \exp \left[\frac{\sum \ln y_i}{n} - b \frac{\sum x_i}{n} \right]$$

$$r^2 = \frac{\left[\sum x_i \ln y_i - \frac{1}{n} \sum x_i \sum \ln y_i \right]^2}{\left[\sum x_i^2 - \frac{(\sum x_i)^2}{n} \right] \left[\sum (\ln y_i)^2 - \frac{(\sum \ln y_i)^2}{n} \right]}$$

APPENDIX F - EV MOTOR/CHOPPER APPLICATION CRITERIA

An excellent exposition on aspects of EV design and performance, including information on laboratory and field test, EV components, motors, etc is contained in "STATE-OF-THE-ART ASSESSMENT OF ELECTRIC AND HYBRID VEHICLES" prepared by NASA-Lewis Research Center (HCP/M 1011-01, uc-96).⁽¹⁵⁾

In this appendix a brief, cursory discussion will be presented in order to acquaint motor designers with the application aspects of motors for EV applications.

-MOTOR RATING-

A number of factors enter into the determination of the motor and control scheme for the drive train in electric vehicles. Basic decisions to be made are: (not necessarily in order).

- 1) Type of motor, i.e. series or shunt?
- 2) If shunt wound,
 - a) constant field excitation or chopper controlled variable?
 - b) How will armature voltage be controlled - by chopper or switched in finite, discrete steps?
 - c) transmission gear ratios?
 - d) is regeneration to be utilized?
- 3) tire size
- 4) system voltage
- 5) vehicle performance, based on frontal area and weight, to include the following:
 - a) maximum acceleration
 - b) maximum speed on a specified maximum grade for a minimum time period
 - c) cruise speed

- d) top speed
- e) regeneration, if utilized

Since these require varying speed/torque and speed/power combinations and result in an intermittent load on the motor, a standardized duty cycle must be resorted to in order to establish a rating, based on thermal considerations, for the motor. The speed requirements will fix the drive train gear ratio/motor speed-torque relationships.

Figures F-1 and F-2, from NASA-Lewis, depict duty cycles that have been used in studies of motor loading for specific EV designs. The Society of Automotive Engineers have established various driving cycle schedules which can be used as standardized requirements for evaluation purposes. Figure F-3 depicts the driving cycle for SAE J 227 B, C and D schedules.

The motor must be capable of supplying sufficient power to overcome the following load conditions.

1. Aerodynamic drag
2. Rolling resistance
3. Changing grade
4. Acceleration requirements
5. Provide for losses in the mechanical gearing and bearing friction
in the mechanical drive train

Figure F-4, F-5 graphically present the Horsepower required, as a function of velocity, in miles per hour for the first four conditions above.

Figure F-4 presents the aerodynamic drag for various values of the product of frontal area, A and dimensionless drag coefficient, C_d . NASA-Lewis suggests a typical EV will have a frontal area of 20 ft^2 and C_d of 0.3.

The data in Figure F-5 is for each 1000 lbs. of vehicle weight. Grade climbing data is based on the percent grade, i.e. the increase in elevation in

ROAD LOAD FOR IDEAL, 3600 POUND VEHICLE

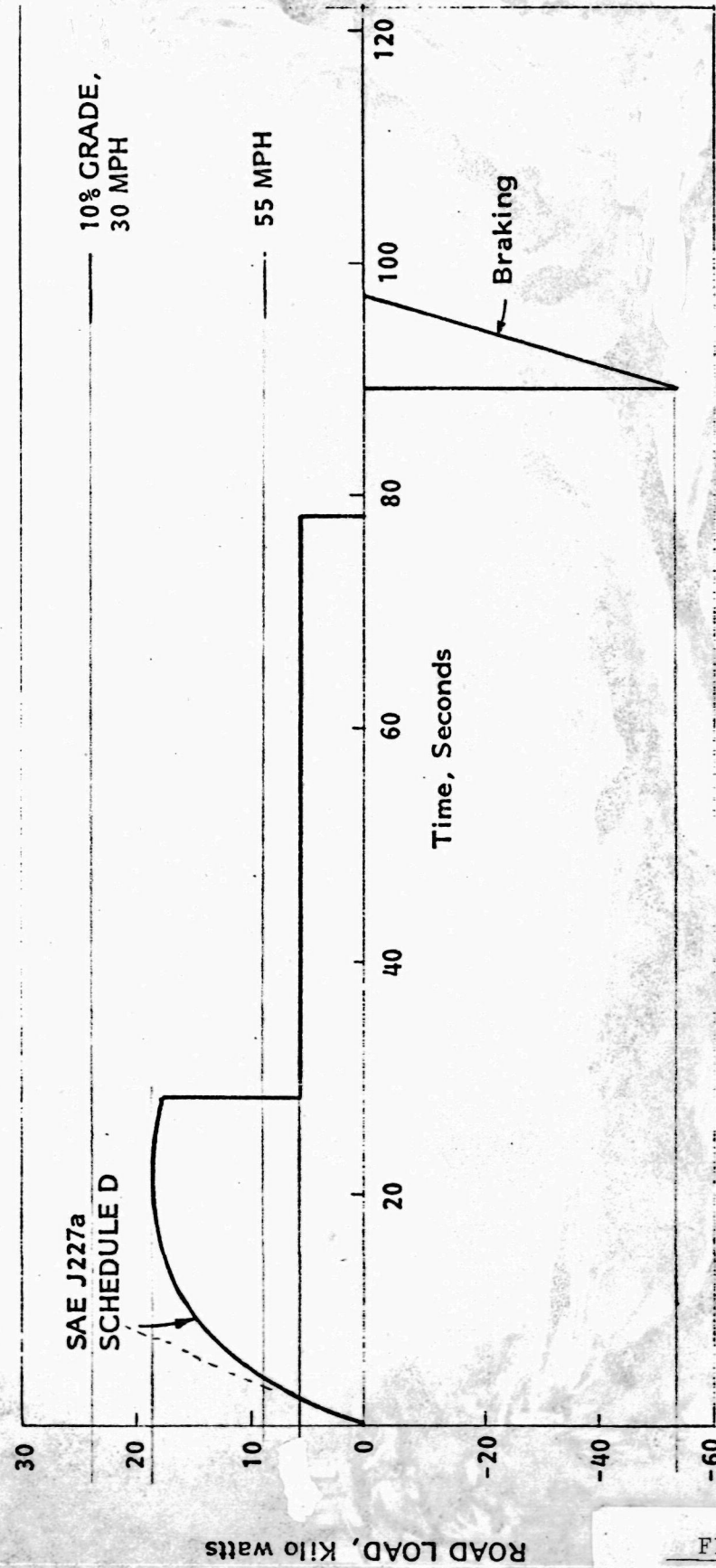


FIGURE F-1

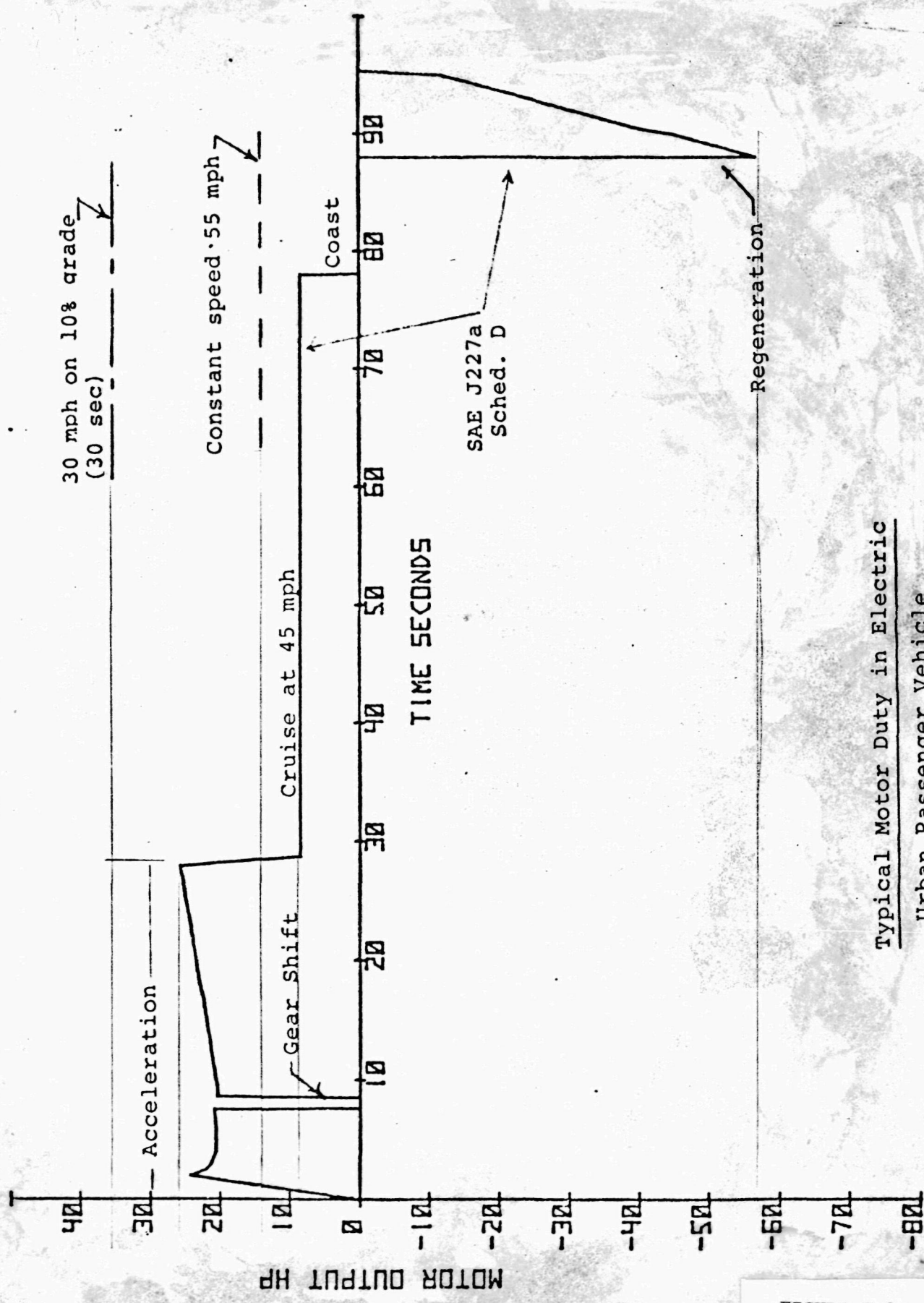
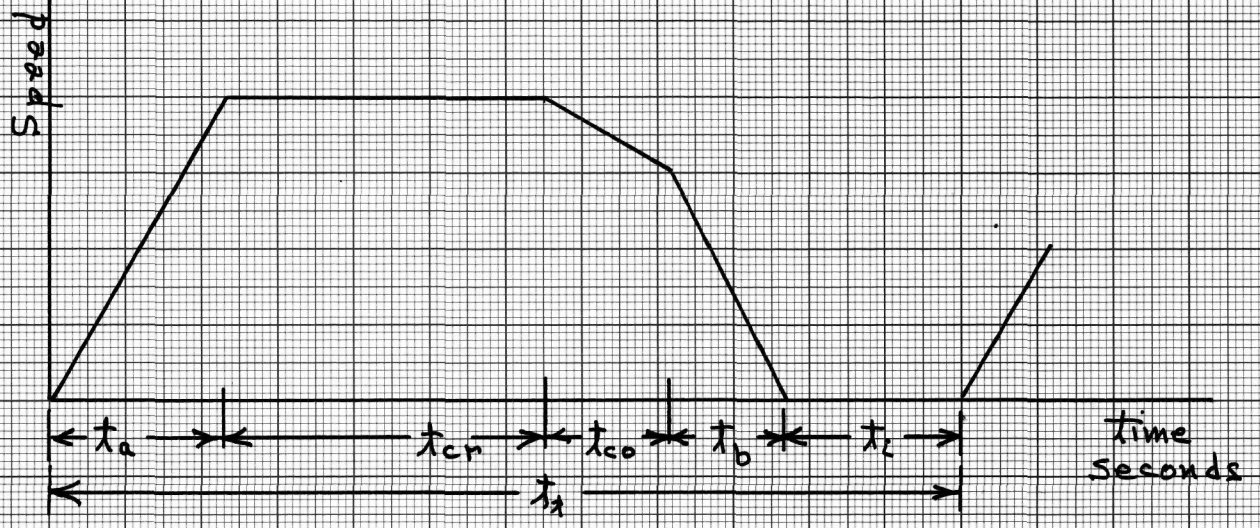


FIGURE F-2

Typical Motor Duty in Electric
Urban Passenger Vehicle

SAE EV DUTY CYCLE SCHEDULES



SAE SCHEDULES

	B	C	D
Maximum Speed Kt/hr, (MPH)	32 (26)	48 (30)	72 (45)
Accelerating Time, t_a , seconds	19	18	28
Cruise Time, t_{cn}	19	20	50
Coast Time, t_{co}	4	8	10
Brake Time, t_b	5	9	9
Idle Time, t_i	25	25	25
Total Time, t^*	72	80	122
Approx. Number of cycles/mile	4-5	3	1

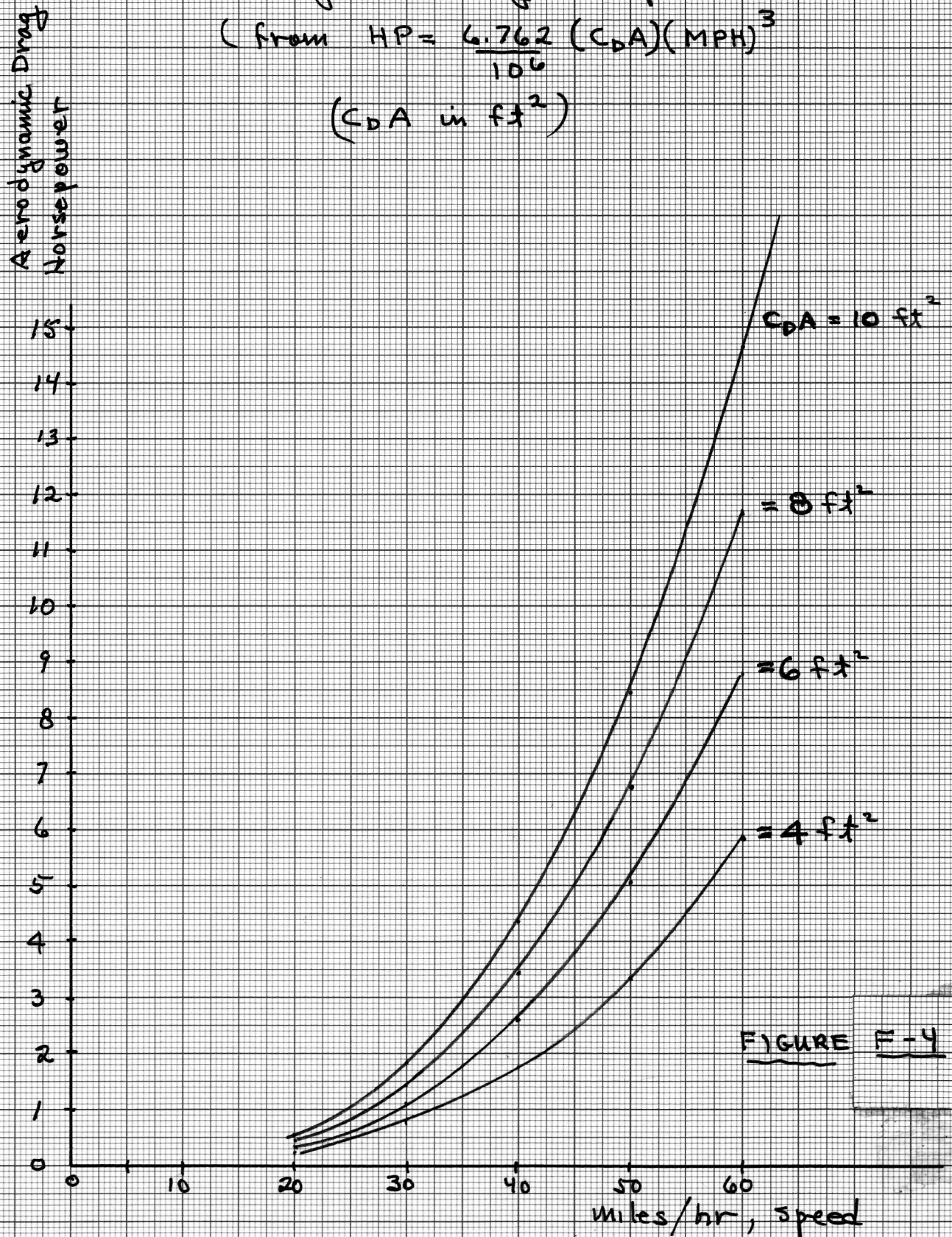
Note: B - fixed route urban driving, $a = 1.54 \text{ ft/sec}^2$
 C - variable route urban driving, $a = 2.44 \text{ ft/sec}^2$
 D - variable route suburban driving, $a = 2.34 \text{ ft/sec}^2$

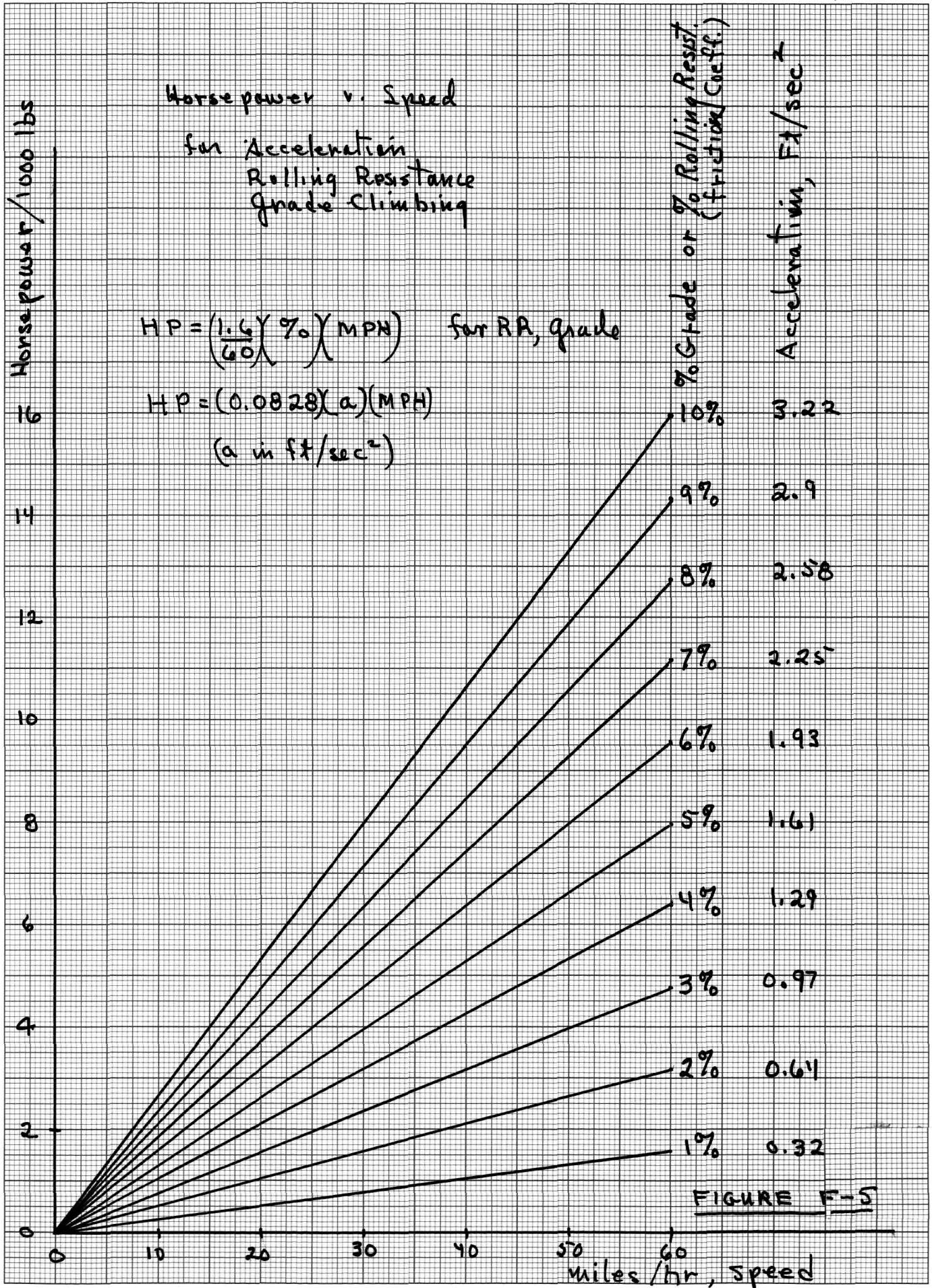
FIGURE F-3

46 1510

10 X 10 TO THE CENTIMETER 18 X 25 CM.
 KEUFFEL & ESSER CO. MADE IN U.S.A.

Aerodynamic Drag vs Speed
 (from $HP = \frac{6.762}{106} (C_D A) (MPH)^3$)
 ($C_D A$ in ft^2)





Conversion Factors

(Multiply the first column of the tables below to obtain units in horizontal row)

	$\frac{\text{Meter}}{\text{sec}}$	$\frac{\text{Km}}{\text{hr}}$	$\frac{\text{Miles}}{\text{hr}}$	$\frac{\text{Feet}}{\text{min.}}$	$\frac{\text{Feet}}{\text{sec}}$
$\frac{\text{Meter}}{\text{sec}}$	1.0	3.6	2.24	197	3.28
$\frac{\text{Km}}{\text{hr}}$	0.277	1.0	0.621	54.7	0.912
$\frac{\text{Miles}}{\text{hr}}$	0.447	1.61	1.0	88	1.46
$\frac{\text{Feet}}{\text{min.}}$	0.0051	0.018	0.011	1.0	0.0167
$\frac{\text{Feet}}{\text{sec}}$	0.305	1.097	0.682	60	1.0

	Horse Power	Kilowatts
Horse power	1.0	0.746
Kilowatts	1.341	1

	lbs.	Kgm
lbs	1	0.454
Kgm	2.20	1

FIGURE F-6

feet per hundred feet of horizontal travel. The percent rolling resistance (RR) is the coefficient of friction (tires to road surface) multiplied by 100, and is typically in the range $1.2 < RR < 1.7$ with conventional bias tires at the upper value and steel belted radial tires at the low end of the range. It is a function of speed, also. ⁽¹⁵⁾

Power requirements to accelerate are based on acceleration rates expressed in ft/sec^2 (see the note, under the SAE Schedules, Figure F-3.) Conversion factors are presented in Figure F-6.

EXAMPLE: For a 3000 lb. EV, with $C_d A = 0.6$ and

Rolling resistance = 1.2%

Determine the maximum power and the series wound motor size required for this vehicle to meet the SAE 227 C Schedule. The vehicle will be driven on 5 mile trips, 6 times/day, and must climb a 10% grade for 5 seconds during each cruise cycle. It should be capable of a top speed of 55 miles/hr.

Acceleration: to 30 MPH in 18 seconds

$$a = \frac{(30)(1.46)}{18} = 2.43 \text{ ft/sec}^2$$

$$\text{Max HP} = (0.0828)(a)(\text{MPH}) = 6.04 \text{ HP}$$

$$\text{Rolling resistance: Max HP} = \left(\frac{1.6}{60}\right) (\%) (\text{MPH}) = 0.96 \text{ HP}$$

$$\text{Aero Drag: Max HP} = \frac{1.1 \text{ HP}}{\text{Total Max HP} = \frac{8.1 \text{ HP}}{1000 \text{ lbs.}}}$$

$$\text{Cruising: RR + Aero drag} = 2.06 \text{ HP/1000 lbs.}$$

Coasting, Braking, Idle ~ no power

$$\text{Grade Climbing: RR and Drag} = 2.06 \text{ HP}$$

$$\text{Climb, from Figure F-5} = \frac{8.0 \text{ HP}}{10.06 \text{ HP}}$$

Assuming a 95% efficient mechanical drive train, the 3000 lb vehicle will have the following maximum power requirements:

accelerating:	25.58 HP
cruising:	6.51 HP
grade climbing:	31.77 HP

Figure F-7 is a plot of the motor power required during a Schedule c driving cycle. As can be seen, grade climbing is the most demanding of the various operations and the motor selected must be capable of delivering 31.77 HP on a short time overload basis.

To determine the continuous power rating of the motor, the Root Mean Square power (heating effect) must be determined.

Under Schedule C, there are 3 cycles per mile, and 15 cycles/hr for 5 mile trips. With the specification of 6 trips/day, analysis over a 1 hour time frame should be adequate.

$$\begin{aligned}
 P_{rms} &= \left(\frac{1}{T} \int_0^T P(t)^2 dt \right)^{\frac{1}{2}} & (F-1) \\
 &= \left[\frac{15}{3600} \left(\int_0^{18} \left(\frac{25.58}{18} t \right)^2 dt + (31.77)^2 \int_0^5 dt + \right. \right. \\
 &\quad \left. \left. + (6.51)^2 \int_0^{15} dt \right) \right]^{\frac{1}{2}} = 6.31 \text{ HP}
 \end{aligned}$$

It should be noted that the motor is not delivering power during coast or braking periods (42 seconds out of each 80 second cycle, which accounts for the low ratio of RMS power to peak power.

Motor Power Req'd SAE 227C
3000 lb EV, $C_d A = 0.6$, $RR = 1.2\%$

↑ 31.77 HP ↑ grade climb
(10%, 30MPH)

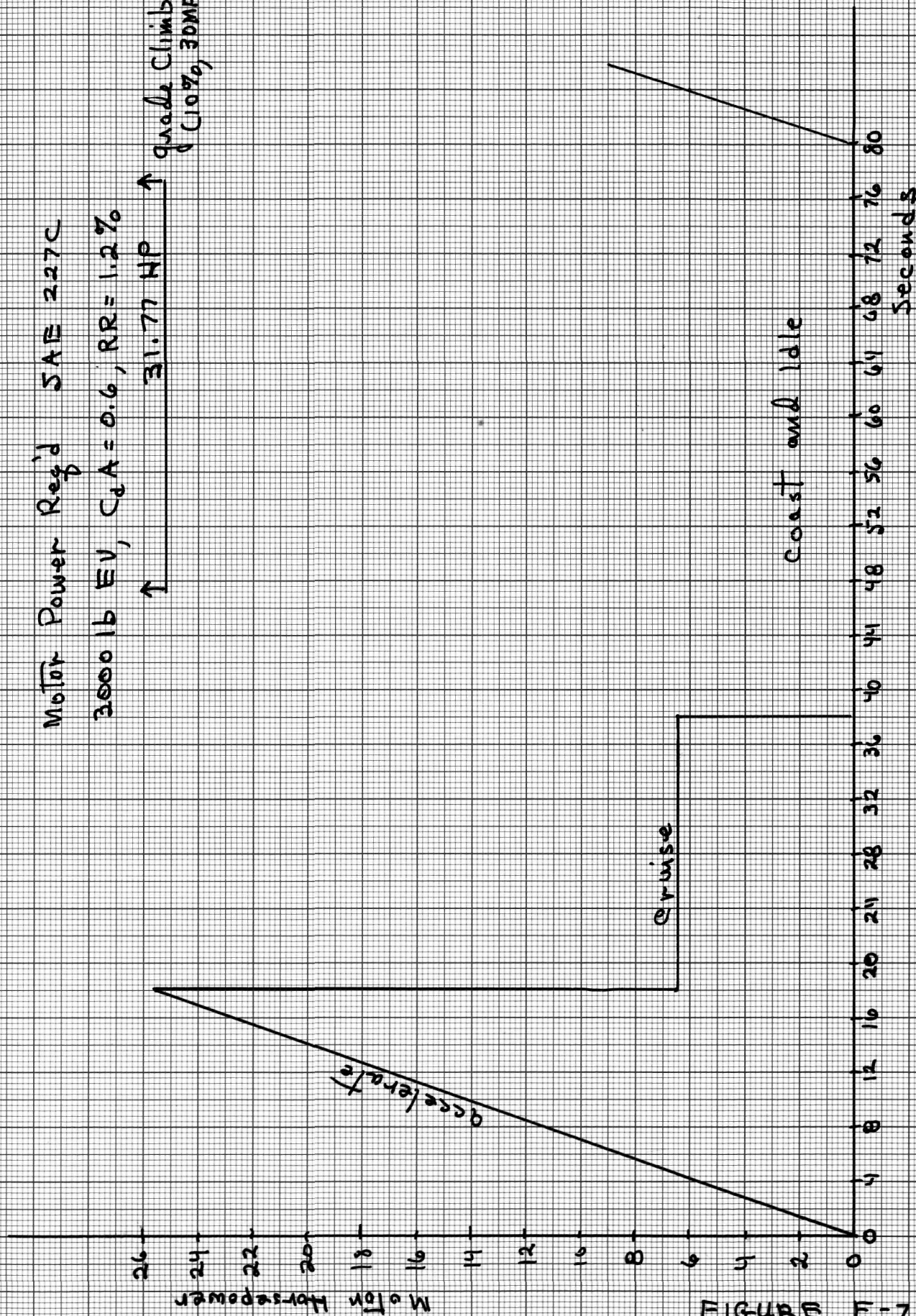


FIGURE F-7

To meet the requirement of a top speed of 55 MPH, the motor power required is:

$$RR = 1.76 \text{ HP/1000 lbs}$$

$$\text{Drag} = 7 \text{ HP/1000 lbs}$$

For 3000 lbs, 95% drive efficiency, the total power requirement would be 27.67 HP.

If the tire diameter is D feet, maximum velocity is v ft/sec, and a motor speed step down gear of ratio $G/1$ is between motor and axle, the motor speed, in radians/sec. is:

$$\omega_m = \frac{2G}{D} v \quad (F-2)$$

or, in terms of speed in rev/min, v in MPH,

$$N = (27.884) \left(\frac{G}{D}\right) (\text{MPH}) \quad (F-3)$$

A typical series motor characteristic is shown in Figure F-8. This is the open circuit saturation characteristic reduced to per unit and is thus a plot of torque/ armature ampere and cemf/angular velocity in per unit as a function of per unit field current. Applying a curve fit routine to the data yields

$$\left(\frac{T}{I_a}\right)_{pu} = \left(\frac{E}{\omega}\right)_{pu} = 0.95 I_f^{0.454} \quad (F-4)$$

The equations describing the series motor can then be formulated as (assuming $I_a = I_f$):

$$T_{pu} = 0.95 I^{1.454} \quad (F-5)$$

$$\omega_{pu} = \frac{V - IR}{0.95 I^{0.454}} \quad (F-6)$$

$$P_{pu} = (T_{pu})(\omega_{pu}) \quad (F-7)$$

where: V = per unit applied voltage = $\frac{T_o}{T}$ (Source voltage)

R = per unit armature and field resistance.

$K\phi(I_f) \propto I_f$
"Universal" Series Motor Curve

$1.4 \left(\frac{I}{I_a} \right)_{p.u.}$ and $\left(\frac{E}{\omega} \right)_{p.u.}$

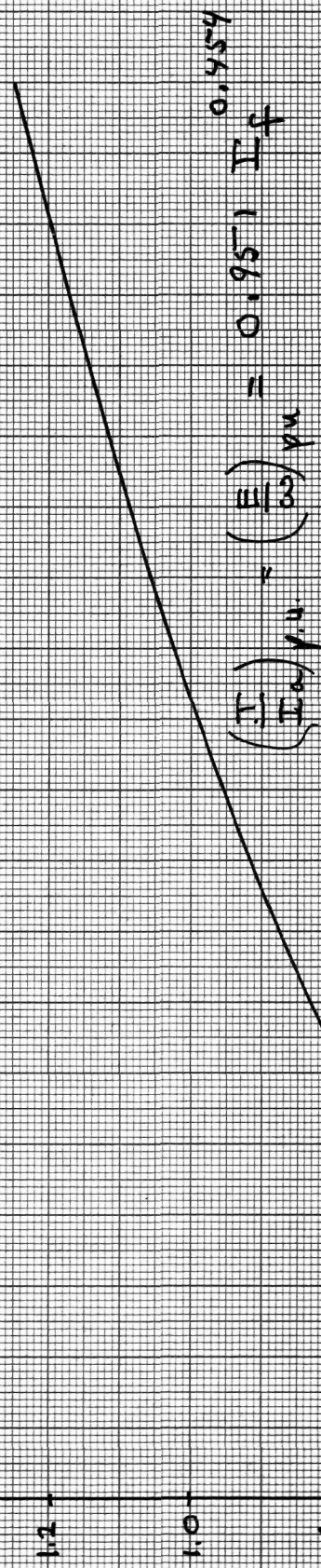


FIGURE F-8

Values of I from 0.2 to 3.0 per unit were chosen and T , ω and P were calculated for $V = 1.0, 0.8, 0.6$ etc. For the values calculated at a specific current value, the T vs ω curves and the P vs. ω curves, shown in Figures F-9 and F-10 were constructed (based on an assumed value of $R = 0.045$ per unit). Figure F-10 also has the per unit current loci drawn in.

The EV power requirements in the previous example can be used, with these "universal" motor characteristics to demonstrate how a motor rating can be determined and to illustrate the influence of a motor's ability to commute overloads on motor size required.

Using the power requirements from the example,

Accelerating 25.58 HP at 30 MPH

Cruise 6.51 HP at 30 MPH

Grade climbing 31.77 HP at 30 MPH

Top speed 27.67 HP at 55 MPH

Assume that top speed is chosen as 0.8 per unit. With $V = 1.0$ the per unit power is 1.45. If the efficiency is assumed to be 74.6%, the motor rating for the top speed requirement is:

$$P = \frac{27.67}{1.45} = 19.08 \sim 20 \text{ Kw}$$

From Figure F-10:

$$I = 1.5 \text{ pu} \quad N = 0.8 \text{ pu}$$

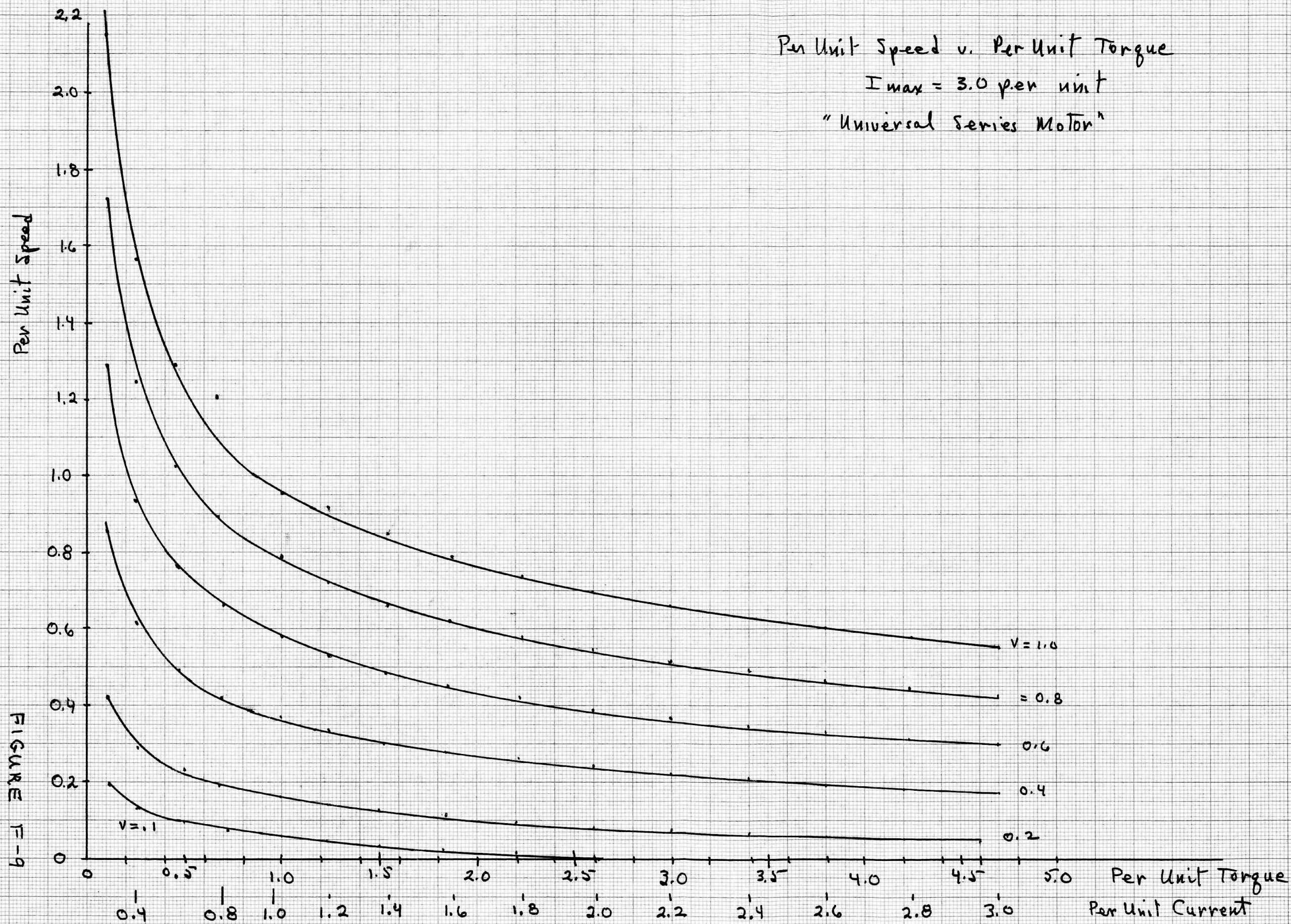
Grade climbing will require a per unit power of;

$$P = \frac{31.77}{20} = 1.59$$

at a speed of $\left(\frac{30}{55}\right) (0.8) = 0.44$

From Figure F-10, for this power and speed,

$$I = 2.5, V \sim 0.75$$



Per Unit Speed v. Per Unit Power
as a function of Per Unit I_a
Universal Series Motor

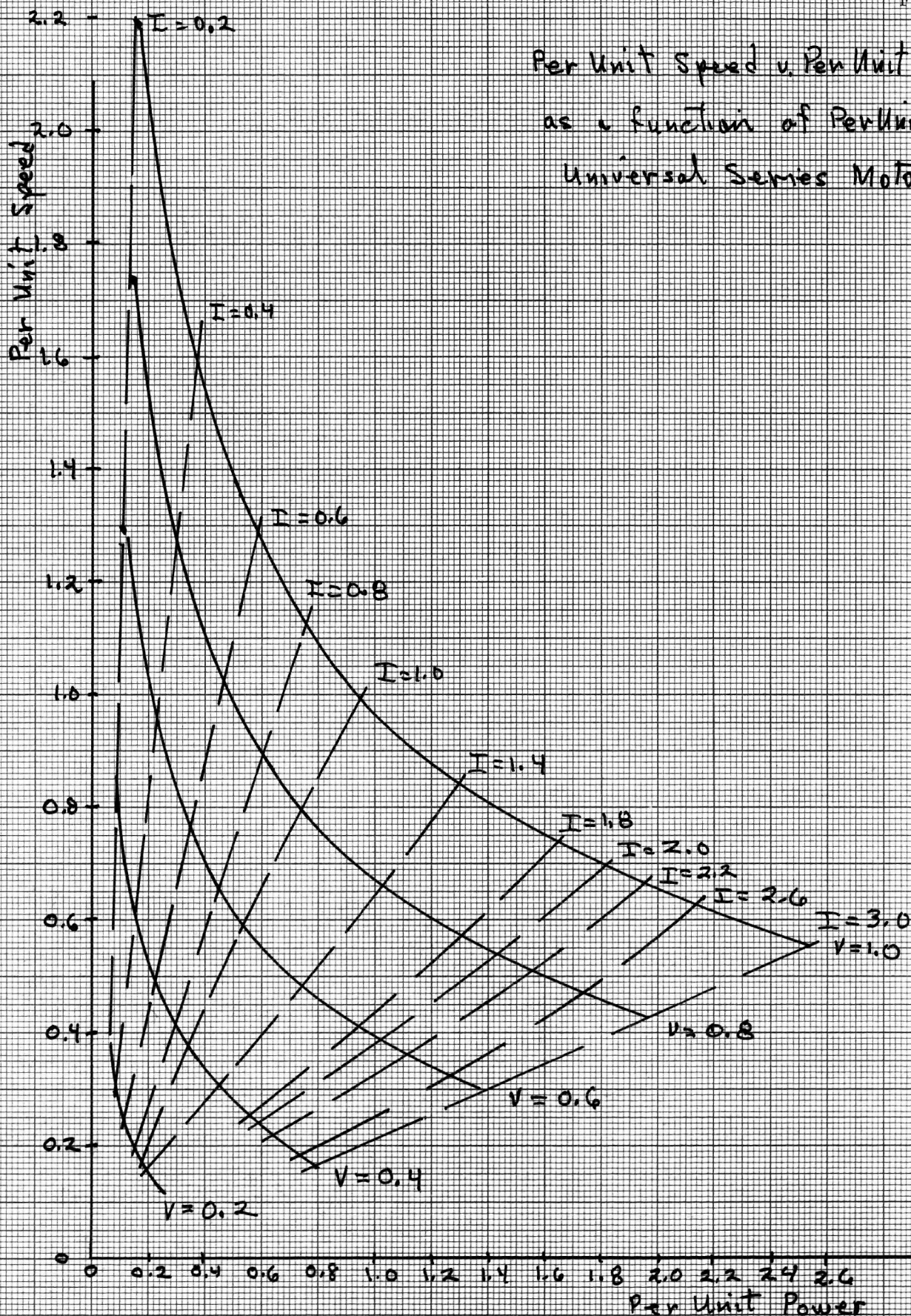


FIGURE F-10

Cruise: $N = 0.44$

$$P = \frac{6.51}{20} = 0.325$$

$$I = 0.8, V = 0.4$$

and for the maximum power during acceleration,

$$P = \frac{25.58}{20} = 1.28 \text{ at } N = 0.44$$

$$I = 2.1, V = 0.7$$

If top speed had been chosen as 1.0 per unit the operating conditions would be as follows:

Top Speed, $N = 1, V = 1.0 \quad P = 0.96$

$$\text{Motor size} = \frac{27.67}{.96} = 28.8 \sim 30 \text{ Kw}$$

$$\text{Grade climbing requires a per unit power of: } P = \frac{31.77}{30} = 1.06$$

at a speed of $(30/55)(1.0) = 0.55$ yielding $I = 1.6 \quad V = 0.73$

Cruise: $N = 0.55$

$$P = \frac{6.51}{30} = 0.22$$

$$I = 0.5 \quad V = 0.4$$

$$\text{Acceleration: } P = \frac{25.58}{30} = 0.85 \text{ at } N = 0.55$$

$$I = 1.4 \quad V = 0.68$$

If the EV is to use a 5.21/1 differential and 2 feet diameter tires, top speed of 55 MPH results in a motor speed of

$$N = (27.884) \left(\frac{G}{D} \right) (\text{MPH}) = 4000 \text{ rev/min}$$

For the 20 Kw motor, this is a per unit speed of 0.8. Therefore, the motor would be rated 20 Kw, $4000/0.8 = 5000 \text{ rev/m.}$ and must be capable of commutating 2.5 per unit current on grade climbing.

For the 30 Kw motor, its rated speed would be 4000 rev/m. but it need only have the capability of commutating 1.6 per unit current maximum.

In general, armature physical size is inversely proportion to speed. In the example above, the ability to commutate 2.5 per unit current permits selection of a 20 Kw motor, 5000 rev/m. which would be a smaller, lighter motor than would be required if commutation ability was limited to 1.6 per unit current requiring a 30 Kw, 4000 rev/m. selection. Another advantage in using the smaller motor is that at cruise, the motor power output is a higher percentage of its rated power than is the situation for the larger motor. Since the efficiency decreases at light loads on a motor, the use of the smaller motor results in increased efficiency during the cruise condition.

Ability to commutate high, short time overloads is discussed in Appendix G.

-CHOPPER CONSIDERATIONS-

The chopper thyristors must, of course, have a voltage and current capability exceeding the system voltage and maximum current which will be required.

In the above example, note that grade climbing (31.77 HP) occurs at $V = 0.7$ p.u. If a 15 HP motor was chosen, I_{pu} , for grade climbing would be:

$$I_{pu} = \frac{p}{V} = \frac{31.77}{(15)(0.7)} = 3.0 \text{ p.u.} \quad (F-6)$$

If a 120 volt system were used, and a 15 HP motor with, say, 75% efficiency was chosen, per unit current would be 125 amperes and the chopper thyristor current rating must be 375 amperes or greater. The chopper should have a current limit control feature, also.

For "soft" starts, it is desirable to start with a very low voltage, i.e. 0.03 - 0.05 per unit, requiring a ratio T_o/T of the same magnitude. In choppers which utilize the on time, T_o , for charging the force commutate capacitor, minimum T_o is fixed. If, for example, minimum on time is 0.001 seconds, and minimum desired voltage is 0.03 per unit, the maximum starting chopper frequency is, $f = \frac{1}{T} = \frac{0.030}{0.001} = 30 \text{ Hz}$. As shown in Chapter 3, the efficiency is quite dependent upon chopper frequency, increasing with frequency. Thus, the chopper control should have the ability to increase the frequency at which the chopper is operating to an upper limit as quickly as possible, subject, of course, to the minimum "on time" constraint imposed by the commutating capacitor charging scheme.

Motor circuit inductance is an important factor in the selection and application of a chopper controller thyristors have a maximum dI/dt rating. Since maximum rate of rise of current is determined by system voltage and

circuit inductance, these parameters must be controlled to a specified value. Chopper designs tend to be conservative with respect to operating conditions relative to thyristor allowable maximum ratings. Informal discussions with chopper designers indicate they prefer dI/dT to be less than 500 or 600 amperes per millisecond.

As shown in APPENDIX D, inductance decreases with frequency and care should be taken to evaluate dI/dt at the highest frequency the chopper will operate at.

Motor inductance can be controlled in the design of the motor.⁽¹⁶⁾ The important parameters which affect the inductance are as follows:

$$\text{Armature} \quad L = K_1 \frac{Z^2 \ell}{Qa^2 w} (d_2 + d_1) \quad (F-7)$$

where: z = armature inductors
 ℓ = stack length
 Q = number of slots
 a = number of parallel paths
 w = slot width
 d_1 = depth of copper in the slot
 d_2 = depth from top of the tooth to the top of the conductor

$$\text{Poles} \quad L = K_2 \frac{hn^2 \ell p}{ga^2} \quad (F-8)$$

where h = pole height
 n = number of turns
 p = number of poles
 g = air gap

ℓ = length of pole

a = number of parallel paths in pole windings

Reference 17 provides background information on motors and choppers.

Reference 18 presents an excellent discussion of the various chopper types and their advantages and disadvantages.

APPENDIX G - MOTOR DESIGN CONSIDERATIONS

The example used for preliminary selection of an EV motor power and speed rating in Appendix F dramatically points up the need for the EV motor to have the ability to commute, properly, short time overloads. The ratio of peak power to average power required by an EV varies from about 5/1 in heavy city traffic to 3/1 in suburban/rural driving situations. Thus, the motor design must be based on commutation limit as opposed to the traditional thermal constraint approach.

Because a motor for EV application must also carry its power supply, high efficiency over the entire operating range is a major design objective. Typically 1 Kwhr of lost energy requires carrying an additional battery weight on the order of 30 Kg (66 lbs).

Another objective not normally considered in design of motors for conventional industrial applications is that of achieving relatively high circuit inductance. Increasing inductance tends to suppress harmonic current magnitudes, thus increasing the efficiency. In addition, it tends to minimize chopper-motor interface problems in that it decreases the rate of rise of chopper current each cycle.

Because of the unavoidable electrical leakage paths that will develop in an EV environment, the electrical system voltage levels will probably be established at between 96 and 120 volts, which means a rather heavy current requirement for motors in the 15-30 Kw power range. In general, system voltage level does not appreciably affect the weight of the motor. However, this voltage range, for the power rating range does not indicate a clear choice of the use of a lap or wave winding. Yet a wave winding appears to offer advantages in that it does not need an equalizer winding.

In order to achieve ability to commutate relatively high short time overloads, the use of a laminated (thin) steel frame and interpoles are a must. In addition, the added cost of utilizing compensating (pole face) windings should be evaluated based on the reduction in motor size possible if high overloads can be accommodated.

It should be recognized that if compensating windings are used, they must be stranded to keep eddy current losses to a minimum.

The electromagnetic power developed in a DC motor armature is given by:

$$P = EI = \left(\frac{Z\phi PN}{60a} \right) I \quad (G-1)$$

where: Z = number of armature inductors

ϕ = flux/pole, webers

P = number of poles

N = rev/m.

I = armature current

a = parallel paths in the armature

defining the specific electrical loading, q , and the specific magnetic loading, B , as:

$$q = \frac{IZ}{a\pi d} \quad \text{ampere inductors/meter} \quad (G-2)$$

$$B = \frac{p\phi}{\pi D\ell} \quad (G-3)$$

where: ℓ = armature core length

$$\text{then } P = \pi^2 \frac{D^2 \ell N q B}{60} \quad (G-4)$$

It is important to note that, in EV applications, where the ratio of average to peak power is low, specific electrical loading can be quite high, relative to industrial type motor design and is realistically limited only by commutation capability and not thermal considerations.

High q permits a lower specific magnetic loading which in turn results in lower losses and higher efficiency. However, lower specific flux density should be obtained by larger diameter, rather than larger core length. Longer core length increases the cooling problem as well as introducing mechanical problems such as shaft deflection and overturning moment increase.

Studies ⁽²⁰⁾ have shown that high specific electrical loading, obtained with a wave winding, can result in substantial weight reductions for the motor. Figure G-1, reproduced from that reference shows the influence of specific loading and armature diameter on the weight of a 40 Kw shunt motor.

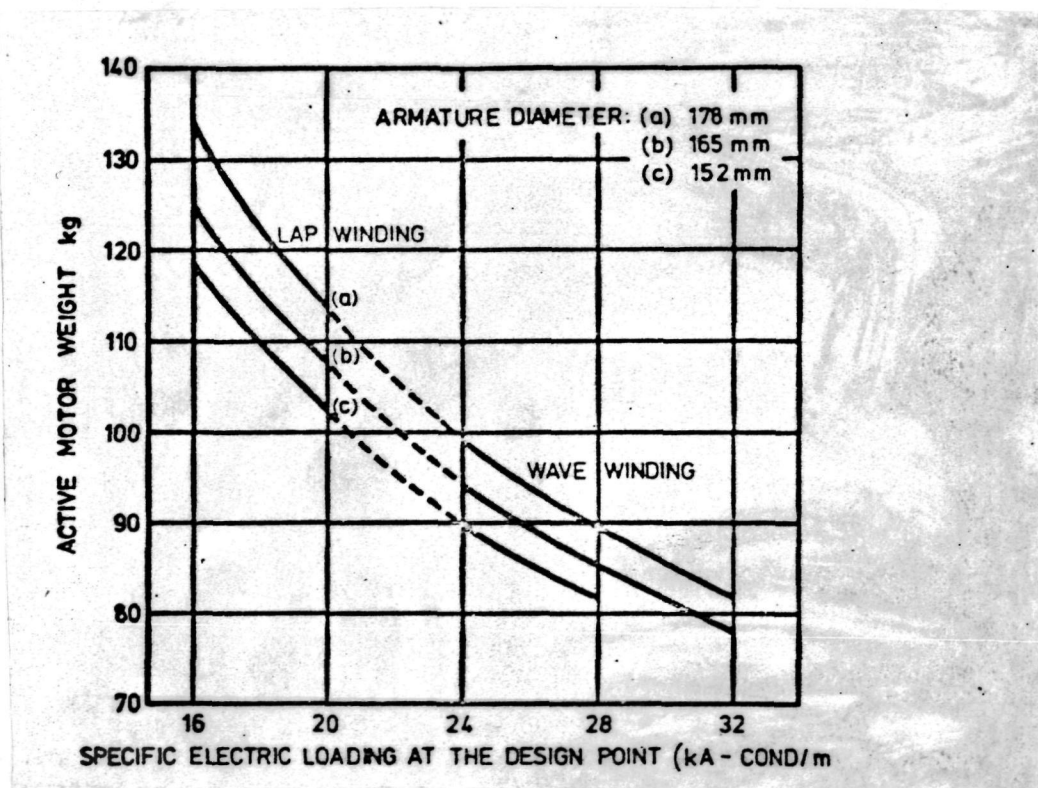


FIGURE G-1

The main considerations in ability to commute are the reactance emf in the coils being commutated and the presence of armature reaction. Interpoles can nullify the reactance emf. The actual reactance voltage is dependent upon slot permeance, conductor current, speed, and armature length. On the basis that the EV application stresses high speed and specific electrical loading,

the reactance can be decreased by a larger air gap and larger diameter (shorter length) armature. The larger air gap means more turns/pole for the field, which increases the circuit inductance. Only a compensating winding can eliminate armature reaction.

In order to increase the ability to commute, one tends to design the motor using the greatest number of commutator bars; yet using the lowest number of turns per coil (which yields the maximum slot space factor) which tends to increase the armature diameter. For a fixed brush width, this means more coils shorted during commutation which increases the losses.

Steps taken to increase the ability to commute (including the use of compensating windings) all tend to decrease armature inductance. However as noted above, a larger diameter armature results in more turns on the field which increases the circuit inductance. The field inductance (and number of turns) can also be increased by connecting all field windings in parallel, which requires p times as many turns than if the field windings were all in series.

From the Summary of Chapter 3, it can be seen that losses can be reduced by:

- i) reducing conductor height (armature)
- ii) using deeper slots
- iii) using more iron
- iv) using paralleled, small diameter conductors for both armature and field windings
- v) using a wave winding rather than lap type to eliminate the equalizer connection
- vi) using longer brushes (less width) to decrease the number of coils short circuited during commutation.
- vii) using low friction, low voltage drop brushes

viii) reduce the need for ventilation

ix) use of deep slots

The complexity of the design and the fact that a change in a variable can make one aspect more favorable but can have an adverse effect on another aspect (performance v. efficiency) seems to indicate that any motor design must be a compromise and that the power of the modern computer must be utilized in order to achieve a defined optimal design.